RP TU Rheinland-Pfälzische Technische Universität Kaiserslautern Landau

Dissecting the role of EPS15 and EPS15R in the mammalian brain

vom Fachbereich Biologie

der Rheinland-Pfälzischen Technischen Universität Kaiserslautern-Landau

zur Erlangung des akademischen Grades Dr. rer. nat. genehmigte

Dissertation

von

Jasmeet Kaur Shergill, M.Sc., geb. in Jamshedpur

Mündliche Prüfung: 18.12.2025

Dekan:	Prof. Dr. Stefan Kins
Promotionskommissionsvorsitzender:	Prof. Dr. Jan Pielage
Berichterstattende:	Prof. Dr. Tanja Maritzen
	Prof. Dr. Stefan Kins

D386

Summary

EPS15 and its paralog EPS15R are endocytic adaptor proteins best known for initiating clathrin-mediated endocytosis and facilitating the uptake of EGFR, yet their neuronal roles have remained unclear. This thesis establishes that both proteins are critical components for synaptic receptor regulation, neurodevelopment, and ventricular homeostasis, suggesting that their functions are closely integrated with broader processes essential for brain development and maintenance. Comprehensive analyses showed that EPS15 and EPS15R are broadly expressed across the brain but display a distinct regional enrichment and a progressive postnatal upregulation. Both localize to pre- and postsynaptic compartments, supporting a dual function in synaptic vesicle recycling and neurotransmitter receptor trafficking. Their interaction with the AMPA receptor subunit GluA1, and the resulting GluA1 surface accumulation upon loss of EPS15/EPS15R, identify them as key regulators of AMPAR endocytosis with a potential influence on excitatory balance. In contrast, transferrin receptor uptake remained unaffected, indicating that global clathrin-mediated endocytosis is preserved. Unbiased proteomic analysis defined the molecular networks through which EPS15 and EPS15R operate. Both interactomes were strongly enriched for canonical endocytic components, confirming their roles in vesicle formation and cargo selection. However, in addition, the EPS15R interactome revealed unique partners such as CALCOCO1 and SEC16A, implicating it in autophagy and ER-associated membrane trafficking. These findings suggest a non-canonical role for EPS15R as a scaffold linking endocytic, secretory, and degradative pathways.

At the organismal level, the forebrain-specific loss of EPS15 and EPS15R resulted in growth deficits, seizures, hind limb clasping, behavioral changes, alterations in brain anatomy, and reduced postnatal survival, highlighting their importance for overall brain function. Structural analyses revealed cortical and hippocampal lamination defects closely resembling those observed upon disruption of Reelin signaling. Supporting a mechanistic link, our biochemical analyses demonstrated that EPS15R physically associates with the Reelin receptor ApoER2, suggesting that it may participate in the trafficking or stabilization of Reelin receptor complexes, thereby influencing neuronal positioning and cortical layering during development. In addition, EPS15/15R knockout mice developed ventriculomegaly. Cell culture experiments revealed defective ependymal differentiation and multiciliogenesis as potential cause for this phenotype. Given that proper ependymal maturation requires controlled EGFR downregulation and Notch signaling modulation, the loss of EPS15/15R might disrupts these processes, thereby leading to impaired differentiation and compromised ventricular integrity.

Together, these findings identify EPS15 and EPS15R as multifaceted adaptors that integrate endocytic trafficking with neuronal signaling and brain morphogenesis. By ensuring proper receptor internalization, neuronal lamination, and ependymal differentiation, they safeguard both the synaptic and structural integrity of the brain.

Zusammenfassung

EPS15 und sein Paralog EPS15R sind endozytotische Adapterproteine, die vor allem für die Initiierung der Clathrin-vermittelten Endozytose und für die Internalisierung des EGF-Rezeptors bekannt sind, deren neuronale Funktionen jedoch bislang unklar geblieben sind. Diese Arbeit belegt, dass beide Proteine eine wichtige Rolle bei der Regulation synaptischer Rezeptoren, der neuronalen Entwicklung und der ventrikulären Homöostase spielen, was darauf hindeutet, dass ihre Funktionen eng mit umfassenderen Prozessen verbunden sind, die für die Entwicklung und Erhaltung des Gehirns unerlässlich sind. Umfassende Analysen haben ergeben, dass EPS15 und EPS15R im gesamten Gehirn weit exprimiert werden, jedoch eine deutliche regionale Anreicherung und eine progressive postnatale Zunahme zeigen. Beide lokalisieren in prä- und postsynaptischen Kompartimenten, passend zu einer dualen Funktion im synaptischen Vesikelrecycling und in der Internalisierung von Neurotransmitter-Rezeptoren. Ihre Interaktion mit der AMPA-Rezeptoruntereinheit GluA1 und die daraus resultierende Anreicherung von GluA1 an der Oberfläche bei Verlust von EPS15/15R identifizieren sie als wichtige Regulatoren der AMPAR-Endozytose mit einem möglichen Einfluss auf das exzitatorische Gleichgewicht. Im Gegensatz dazu ist die Transferrinrezeptoraufnahme unbeeinträchtigt, was darauf hindeutet, dass die globale Clathrin-vermittelte Endozytose intakt ist. Eine unvoreingenommene Proteomanalyse deckte die molekularen Netzwerke auf, über die EPS15 und EPS15R wirken. Beide Interaktome enthielten eine Vielzahl von endozytotischen Komponenten im Einklang mit einer Rolle von EPS15/15R bei der Vesikelbildung und der Auswahl der zu internalisierenden Proteine. Allerdings enthüllte das EPS15R-Interaktom auch nicht-endozytotische Partner wie CALCOCO1 und SEC16A, was auf eine Beteiligung von EPS15R an der Autophagie und dem ER-assoziierten Membrantransport hindeutet. Diese Ergebnisse sprechen für eine nicht-kanonische Rolle von EPS15R als Gerüstprotein, das endozytotische, sekretorische und degradative Wege verbinden könnte.

Auf organismischer Ebene führte der Verlust von EPS15 und EPS15R im Vorderhirn zu Wachstumsdefiziten, Krampfanfällen, Verhaltensänderungen, Veränderungen in der Gehirnanatomie und einer verminderten postnatalen Überlebensfähigkeit, was die Bedeutung von EPS15 und EPS15R für die Gehirnfunktion unterstreicht. Immunhistochemische Analysen ergaben Defekte in der Lamination des Kortex und des Hippocampus, die denen sehr ähnlich sind, die bei einer Störung der Reelin-Signalwegs beobachtet werden. Unsere biochemischen Analysen bestätigten einen mechanistischen Zusammenhang, indem sie zeigten, dass EPS15R mit dem Reelin-Rezeptor ApoER2 assoziiert ist. Dies deutet darauf hin, dass EPS15R am Transport oder

der Stabilisierung von Reelin-Rezeptorkomplexen beteiligt sein könnte und dadurch die neuronale Positionierung und die kortikale Schichtung während der Entwicklung beeinflusst. Darüber hinaus entwickelten EPS15/15R-Knockout-Mäuse eine Ventrikulomegalie. Unsere Zellkulturversuche sprechen dafür, dass eine gestörte Differenzierung und Multiziliogenese des Ependyms der Grund dafür sein könnten. Da eine korrekte Ependymreifung eine kontrollierte EGFR-Internalisierung und eine Modulation des Notch-Signalwegs erfordert, wäre es möglich, dass der Verlust von EPS15/15R diese Prozesse stört und so zu einer beeinträchtigten Ependym-Differenzierung und Ventrikelintegrität führt.

Zusammen genommen identifizieren diese Ergebnisse EPS15 und EPS15R als vielseitige Adapterproteine, die endozytotische Funktionen mit neuronaler Signalübertragung und der Morphogenese des Gehirns integrieren. Indem sie eine ordnungsgemäße Rezeptorinternalisierung, neuronale Lamination und ependymale Differenzierung sicherstellen, schützen sie sowohl die synaptische als auch die strukturelle Integrität des Gehirns.

Table of Contents

1 Introduction

The cell is enclosed by a lipid bilayer that restricts uncontrolled entry of macromolecules into the cytoplasm. Yet, to acquire essential nutrients and to adequately sense and respond to environmental changes, cells must remain in constant communication with their surroundings. This exchange is mediated largely by the plasma membrane, which serves as a critical component that separates a cell's interior from its external environment. The plasma membrane functions as a selectively permeable barrier that regulates the movement of ions, nutrients, and signaling molecules in and out of the cell. While the plasma membrane serves as a stable boundary, it remains highly dynamic owing to continuous exchange with intracellular compartments through tightly regulated trafficking pathways. For cells to acquire essential nutrients and appropriately respond to environmental cues, the activity and abundance of membrane proteins must be precisely regulated. Moreover, receptors activated by ligand binding and transmembrane proteins delivered via exocytosis must be retrieved from the plasma membrane to maintain homeostasis. Endocytosis represents a central mechanism for these processes, enabling the internalization of membrane regions together with associated proteins and extracellular cargo, thereby continuously reshaping the cell surface proteome.

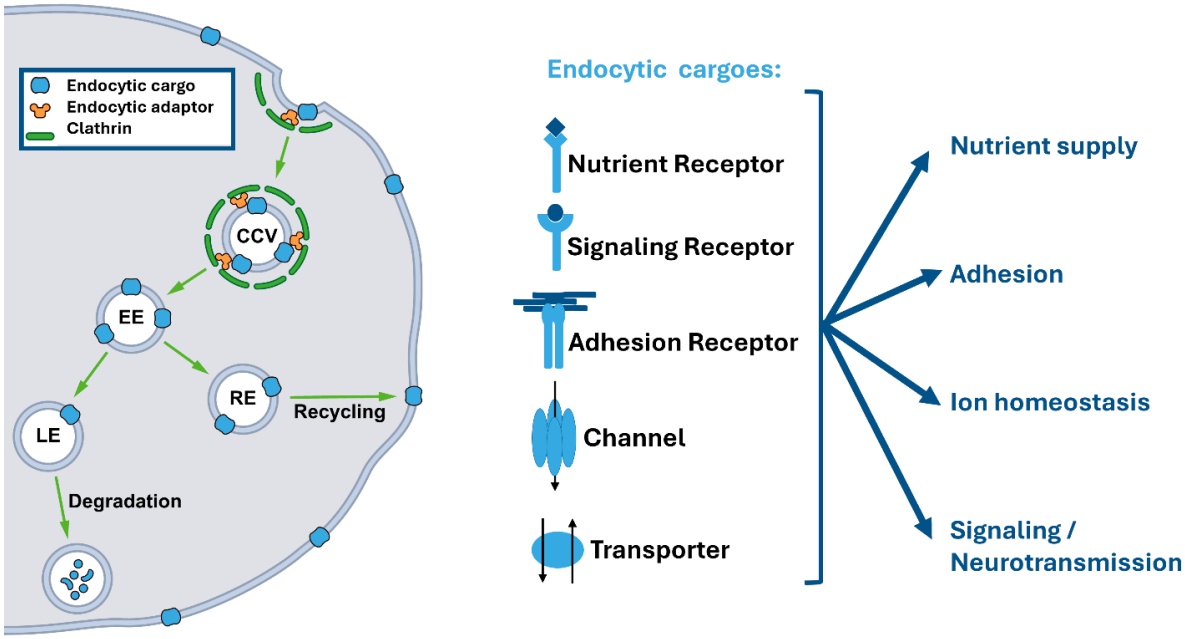

Figure 1.1. Schematic overview of endocytic trafficking and its cellular functions. The plasma membrane serves as a selectively permeable barrier that regulates the exchange of ions, nutrients, and signaling molecules between the intracellular and extracellular environments. Endocytosis provides a central mechanism to internalize membrane proteins and associated cargo, thereby continuously remodeling the cell surface proteome. Endocytic cargos are recruited into clathrin-coated vesicles (CCVs) with the help of adaptor proteins, trafficked through early endosomes (EE), and sorted for either recycling via recycling endosomes (RE) or degradation in late endosomes (LE) and lysosomes.

Through these pathways, endocytosis regulates diverse physiological processes, including nutrient supply, adhesion, ion homeostasis, and signaling including neurotransmission. Adapted from (López-Hernández et al., 2020).

Endocytosis constitutes a central hub through which cells regulate nutrient uptake, signaling, and interactions with their environment (Fig. 1.1). Classical examples for proteins regulated by endocytosis include the transferrin receptor (TfR), whose clathrin-mediated internalization is indispensable for iron acquisition and the generation of red blood cells (Dautry-Varsat, 1986; Mayle et al., 2012). In addition to nutrient uptake, endocytosis critically shapes intracellular signaling cascades. Epidermal growth factor receptor (EGFR) trafficking, for instance, not only drives proliferation, survival, and migration of cells but also terminates signaling by targeting receptors for degradation and sustains signaling cascades originating from endosomal compartments (Tomas et al., 2014; Vieira et al., 1996). Similarly, endocytosis also contributes to Reelin signaling, where internalization and trafficking of the Reelin receptors ApoER2 and VLDLR finetune pathway activity and influence neuronal migration and positioning during brain development (Chai & Frotscher, 2016; D'Arcangelo et al., 1999a). Notch signaling likewise depends on endocytosis, where Numb and Epsins regulate receptor and ligand trafficking to control cell fate decisions and differentiation during development (Cardano et al., 2019; Guo et al., 1996; Langridge & Struhl, 2017). Beyond nutrient and signaling pathways, the endocytic system regulates the availability of adhesion proteins such as integrins and cadherins, which is essential for processes like cell adhesion, polarity, and migration (Cadwell et al., 2016; Paul et al., 2015). Collectively, these examples highlight the multifaceted role of endocytosis in orchestrating key cellular processes that underpin tissue development and homeostasis and are therefore crucial for organismal health.

1.1 Mechanisms of endocytosis

Endocytosis, as already stated, enables cells to control both nutrient acquisition and the abundance of receptors at the plasma membrane. There are two general categories of endocytosis: one that depends on the coat protein clathrin, termed clathrin-mediated endocytosis (CME), and another that proceeds without clathrin, referred to as clathrin-independent endocytosis (CIE). Among these pathways, CME is the predominant route, accounting for the majority of endocytic flux (Bitsikas et al., 2014). Clathrin-independent endocytosis (CIE) provides alternative mechanisms for cargo entry.

1.1.1 Clathrin-mediated endocytosis

Clathrin-mediated endocytosis (CME) progresses through a highly ordered sequence of molecular events executed by more than 50 cytosolic proteins, in addition to clathrin, which together

orchestrate clathrin recruitment and coat assembly, cargo selection, membrane bending, vesicle scission, and subsequent uncoating (Fig. 1.2) to allow fusion of nascent endocytic vesicles with endosomes (Haucke & Kozlov, 2018; Kaksonen & Roux, 2018; McMahon & Boucrot, 2011).

The process of CME begins with nucleation, marked by the formation of shallow membrane invaginations called pits. This step is characterized by the assembly of a nucleation module consisting of early-acting endocytic proteins, such as FCHo1/2, EPS15, EPS15R, Epsins and Intersectins which establish endocytic sites (Henne et al., 2010a). These proteins recruit and activate the heterotetrameric adaptor complex AP-2 (composed of an α, β2, μ2, and σ2 subunit), a central hub that links membrane binding to cargo recognition (Collins et al., 2002). Indeed, cargo selection is mediated largely by AP-2, which recognizes canonical endocytic motifs in transmembrane proteins and engages a wide range of accessory adaptor proteins that expand cargo specificity (for example, EPS15 and Epsins for ubiquitylated receptors, β-arrestins for GPCRs, Dab2 and ARH for members of the LDL receptor family , CALM and AP180 for v-SNAREs such as VAMPs, and Stonin-2 for Synaptotagmins) (Azarnia Tehran et al., 2019). Together, they are involved in coupling cargo capture to the initiation of clathrin coat assembly.

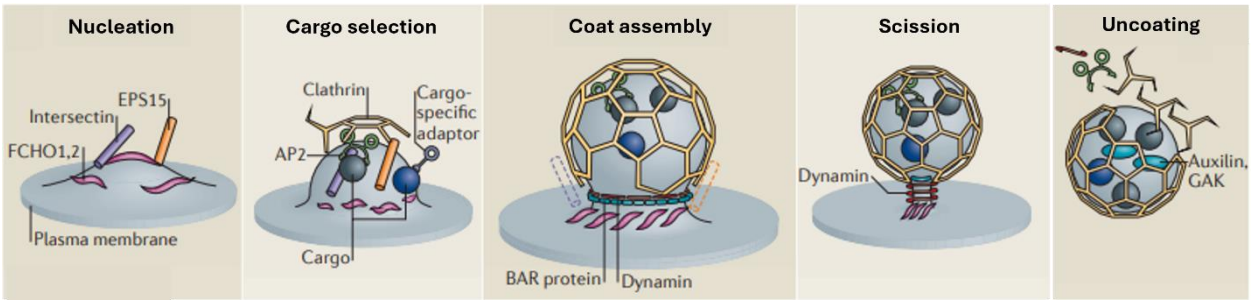

Figure 1.2. Stages of clathrin-mediated endocytosis (CME). CME proceeds through a series of well-defined steps involving nucleation, cargo selection, coat assembly, scission, and vesicle uncoating: (1) Nucleation, where early scaffolds and adaptors (FCHo1/2, EPS15s, Epsins, Intersectins) establish nascent endocytic sites and recruit AP-2. (2) Cargo selection mediated primarily by AP-2 and accessory adaptors. (3) Coat assembly through clathrin lattice formation and curvature-inducing BAR proteins (Epsins, CALM). (4) Scission mediated by dynamin through GTP hydrolysis. (5) Uncoating driven by Auxilin/GAK. This sequential pathway ensures selective cargo uptake and maintains plasma membrane homeostasis. Adapted from (McMahon & Boucrot, 2011).

Coat assembly is initiated by recruitment and polymerization of clathrin triskelia into a lattice that progressively bends the membrane into a pit. This growing coat stabilizes the invaginating pit, while membrane curvature is reinforced by amphipathic helix–containing adaptors (Epsins, CALM) and BAR domain proteins (FCHo1/2, Endophilin, Amphiphysin) that mold the neck region (Ford et al., 2002; Henne et al., 2007). As the coat matures and the pit deepens, Dynamin, a large GTPase, is recruited to the highly curved neck of the budding pit by BAR domain proteins

including Amphiphysin, Endophilin, and SNX9 (Ferguson et al., 2009). Dynamin then oligomerizes around the neck and through GTP hydrolysis catalyzes scission to release a clathrin-coated vesicle (Sweitzer & Hinshaw, 1998). Finally, the clathrin coat is disassembled by the ATPase Hsc70 in concert with Auxilin or GAK (in neuronal cells) (Schlossman et al., 1984; Ungewickell et al., 1995), enabling vesicle fusion with early endosomes. Collectively, this tightly choreographed sequence ensures the efficient and selective internalization of plasma membrane cargo and thereby helps to regulate signaling pathways and to maintain the steady-state composition of the plasma membrane.

1.1.2 Clathrin-independent endocytosis

Clathrin-independent endocytosis (CIE) encompasses a broad set of pathways that internalize cargo without reliance on the clathrin coat. Unlike clathrin-mediated endocytosis, which is supported by a well-defined machinery, CIE comprises multiple pathways that vary in their molecular requirements, cargo specificity, and physiological roles. These routes include both Dynamin-dependent and Dynamin-independent mechanisms (Mayor & Pagano, 2007). CIE mediates the uptake of diverse proteins including nutrient transporters, adhesion molecules, immune receptors, and growth factor receptors (Maldonado-Báez et al., 2013). Although initially considered a non-selective bulk process, it is now clear that CIE involves regulated cargo recognition and trafficking, with specialized pathways that feed into the early endosomal system for sorting and recycling.

Among the Dynamin-dependent pathways are caveolae-mediated endocytosis, which relies on Caveolin-1 and Cavin proteins and is sensitive to membrane cholesterol (Kiss & Botos, 2009), and fast endophilin-mediated endocytosis (FEME), in which the BAR-domain protein Endophilin drives rapid ligand-induced uptake of receptors like EGFR and β1-adrenergic receptors (Casamento & Boucrot, 2020). Other routes are dynamin-independent, including the clathrin-independent carriers/GPI-anchored protein-enriched compartments (CLIC/GEEC) pathway, regulated by CDC42 and ARF1, which internalizes GPI-anchored proteins, and the Arf6-dependent pathway, which mediates endocytosis of cargos such as MHC-I and Integrins (Mayor et al., 2014).

Interestingly, certain adaptors traditionally associated with CME, such as EPS15, EPS15R and Epsins, can also mediate CIE by coupling ubiquitinated receptors to clathrin-independent endocytic routes. An example for a receptor employing different uptake mechanisms is EGFR, which is primarily internalized by CME at low ligand concentrations but switches to CIE when ubiquitinated upon high ligand stimulation. This clathrin-independent route depends on proteins

harboring ubiquitin-interacting motifs, which act redundantly to couple ubiquitinated receptors to internalization (Sigismund et al., 2005).

Ultrafast endocytosis (UFE) which occurs at the presynapse is another recently discovered clathrin-independent endocytic mechanism. It mediates synaptic vesicle recycling within 50–100 ms at membrane sites adjacent to synaptic release zones in *C. elegans* neuromuscular junctions and mouse hippocampal neurons (Watanabe, Liu, et al., 2013; Watanabe, Rost, et al., 2013). It was shown that this pathway rapidly compensates for exocytosed membrane by internalizing a membrane area equal to four synaptic vesicles without using a clathrin coat. Since synaptic vesicles are thus not directly regenerated by UFE, clathrin is still needed downstream to generate synaptic vesicles from endosomes (Watanabe et al., 2014; Watanabe, Liu, et al., 2013; Watanabe, Rost, et al., 2013). UFE rapidly restores membrane surface area and tension, thereby maintaining synaptic transmission, and its disruption accelerates synaptic depression (Watanabe & Boucrot, 2017). Collectively, these pathways highlight the versatility of CIE as a group of endocytic mechanisms that complement CME in regulating nutrient uptake, receptor signaling, and plasma membrane homeostasis.

1.2 Endocytic adaptors in brain development and disease

Endocytosis is a fundamental process in the brain and is indispensable for neuronal development and communication. It sustains presynaptic vesicle recycling and enables the regulation of postsynaptic receptor abundance, processes that are fundamental for efficient neurotransmission and synaptic plasticity. At the presynapse, action potential–driven calcium influx triggers the fusion of synaptic vesicles with the plasma membrane, leading to neurotransmitter release. This fusion event depends on vesicular transmembrane proteins such as the calcium sensor Synaptotagmin1 and the SNARE protein Synaptobrevin/VAMP2 (Brunger et al., 2018). Following exocytosis, these proteins become embedded in the presynaptic membrane and must be efficiently retrieved by endocytosis and recycled into newly formed synaptic vesicles to sustain continuous neurotransmission (Azarnia Tehran et al., 2019). This retrieval process is essential to reverse membrane expansion at the active zone to maintain proper membrane tension, and to clear release sites of exocytosed material so that they remain available for subsequent rounds of fusion. It also enables the local recycling of vesicle proteins to replenish the vesicle pool, which is particularly critical given the long distance of synapses from the cell body (Kaempf & Maritzen, 2017). Postsynaptically, the precise regulation of neurotransmitter receptor numbers at the cell surface is critical, as their abundance directly determines the strength of synaptic responses. Endocytosis enables dynamic adjustments of receptor levels during synaptic plasticity (Carroll et al., 2001), a

process that forms the cellular basis of higher cognitive functions such as learning and memory. Given these broad cellular functions, defects in endocytosis have been implicated in psychiatric and neurodegenerative diseases, underlining the critical role of this process in health and disease (Azarnia Tehran et al., 2019). In this context, the following sections introduce key endocytic adaptor proteins and outline their specific roles in the brain, as well as the consequences of their loss or dysfunction.

1.2.1 AP2 in neuronal development and disease

Genetic studies highlight the essential role of AP-2 in mammalian development and neuronal health. Mice lacking the AP-2μ subunit die during early embryogenesis, whereas deletion of the AP-2β subunit results in perinatal lethality. In addition, loss of AP-2β has been associated with non-syndromic cleft palate and pronounced neurodegeneration in the thalamus and cortex, accompanied by reduced neuronal complexity (W. Li et al., 2010; Mitsunari et al., 2005). Mechanistic insights suggest that this phenotype reflects a non-canonical role of AP-2 in the retrograde trafficking of BDNF/TrkB-containing autophagosomes, which is critical for maintaining BDNF/TrkB signaling, neuronal branching, and survival (Kononenko et al., 2017). Impairments in AP-2–dependent sorting have also been proposed to contribute to neurological disorders such as epilepsy, as even subtle alterations in the efficiency of AP-2-mediated cargo handling appear to significantly affect neuronal excitability and increase seizure susceptibility (Helbig, Lopez-Hernandez, Shor, Galer, White, et al., 2019). Alterations in AP-2 have further been linked to neurodegenerative disease, as genome-wide association studies identified AP2A1 and AP2A2, as susceptibility loci for Alzheimer's disease, underscoring the contribution of trafficking pathways to disease pathogenesis (Raj et al., 2018). Collectively, these findings exemplify how dysfunction of endocytic adaptor proteins can underlie diverse developmental, neurological, and neurodegenerative disorders.

1.2.2 AP180 and CALM in synaptic vesicle trafficking and pathology

The monomeric adaptors AP180 and CALM are closely related proteins that play critical roles in endocytosis and neuronal function. AP180 expression is largely restricted to neurons, where it is localized to presynaptic terminals (Koo et al., 2015a), whereas CALM is more broadly expressed across tissues, including neurons, where it functions both pre- and postsynaptically (Yao et al., 2005). Investigations of knockout mouse models underscore their physiological relevance, showing that neurons lacking AP180 accumulate VAMP2 at the surface, a defect that is further aggravated by simultaneous CALM depletion, indicating a redundant role for these adaptors in VAMP2 sorting at the presynapse (Koo et al., 2015a). Consistent with the importance of VAMP2

in synaptic vesicle fusion, its mislocalization in AP180 knockout mice results in defective neurotransmission, epileptic seizures, and premature lethality (Koo et al., 2015a). CALM deficiency has also been shown to impair transferrin receptor trafficking in erythroid precursors, leading to defective transferrin uptake, anemia, and embryonic or early postnatal lethality in knockout mice (M. Suzuki et al., 2012). Beyond its role in vesicle trafficking, CALM has emerged as a genetic risk factor for Alzheimer's disease, where it facilitates amyloid-β (Aβ) clearance across the blood–brain barrier by mediating clathrin-dependent endocytosis and transcytosis of Aβ bound to LRP1 (Zhao et al., 2015). CALM is also known to regulate synaptic plasticity by controlling surface levels of calcium permeable-AMPARs. Specifically, CALM promotes the endocytosis of ubiquitinated AMPARs in a clathrin-independent manner, thereby influencing long-term potentiation and depression and ultimately modulating learning in vivo (Azarnia Tehran et al., 2022). Together, these findings highlight AP180 and CALM as essential adaptors whose dysfunction leads to severe neurological, hematopoietic, and neurodegenerative phenotypes.

1.2.3 Epsins in receptor endocytosis and neurodevelopment

The Epsin family (Epsin1–3) comprises ENTH-domain proteins that function as endocytic adaptors, with Epsin1 and Epsin2 expressed at high levels in the brain (H. Chen et al., 2009a). In addition to their ENTH domain, mammalian Epsins contain EH domains and one or more ubiquitin-interacting motifs (UIMs), which allow them to recognize ubiquitinated cargo proteins and couple them to the endocytic machinery (H. Chen et al., 1998; Shih et al., 2002). Through this mechanism, Epsins facilitate the internalization of ubiquitinated EGFR, thereby shaping receptor signaling and downregulation (Kazazic et al., 2009). A particularly critical role of Epsins is seen in the context of Notch signaling. The double knockout of Epsin1/2 results in embryonic lethality at E9.5–10 due to severe organogenesis defects resembling those caused by impaired Notch pathway activity, consistent with the downregulation of Notch target genes in these embryos (H. Chen et al., 2009b). Similarly, Epsin depletion in murine embryonic stem cells led to defective Notch signaling and abnormal neural differentiation, reminiscent of Notch loss-of-function (Cardano et al., 2019). Brain-specific deletion of all three Epsins further demonstrated their essential role in the nervous system, as animals displayed reduced survival, progressive motor dysfunction, and premature death before one month of age (Messa et al., 2014). Together, these findings establish Epsins as key endocytic adaptors whose UIM-mediated recognition of ubiquitinated cargo directly connects endocytosis to receptor signaling and neurodevelopmental integrity.

1.2.4 Numb and Numblike in neural cell fate and differentiation

Numb and its paralog Numblike (Numbl) are monomeric adaptor proteins with an N-terminal phosphotyrosine-binding (PTB) domain that mediates cargo recognition. Initially described in *Drosophila*, Numb was shown to regulate cell fate decisions during asymmetric cell division by modulating Notch signaling through endocytosis (Rhyu et al., 1994). Beyond internalization, Numb also contributes to postendocytic trafficking and degradation of Notch and its ligand Dll4 (McGill et al., 2009; Shao et al., 2017). In addition, Numb directly participates in the internalization and trafficking of EGFR, where it facilitates receptor redistribution from the apical to basolateral domains of radial glial progenitors (Fig. 1.3) (Abdi et al., 2019).

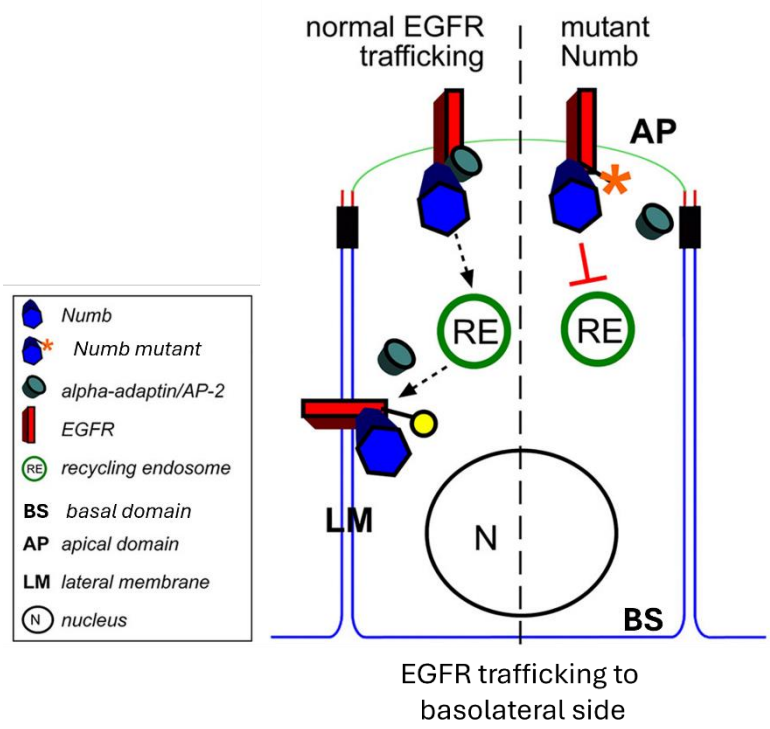

Figure 1.3 Numb in EGFR trafficking in radial progenitor cells. Under normal conditions (left), Numb directs EGFR trafficking from apical to basolateral domains via AP-2 and recycling endosomes, ensuring proper regulation of signaling. In Numb mutants (right), this redistribution fails, leading to persistent apical EGFR activity, impaired ependymal differentiation, and ventricular abnormalities. Adapted from (Abdi et al., 2019).

This spatial control of EGFR signaling is essential for the timely differentiation of multiciliated ependymal cells and the assembly of the neurogenic niche. Conditional deletion of Numb and Numbl in ependymal progenitors leads to defective EGFR downregulation, persistent receptor activation, and profound structural abnormalities, including impaired ciliogenesis, ventricular enlargement, glial scarring, and early lethality in mice (Abdi et al., 2019). In mammals, Numb and Numbl perform overlapping roles in neural development. Constitutive deletion of Numb has been shown to cause embryonic lethality around E11.5 with severe neural tube closure defects,

whereas Numbl knockout mice display no overt phenotype. However, combined loss of both proteins results in embryonic lethality by E9, confirming their redundancy (Gulino et al., 2010). Neuron-specific double knockout models show milder but functionally relevant phenotypes, including anxiety-like behavior when deleted in forebrain glutamatergic neurons (Qian et al., 2017). These findings underscore Numb's critical role in coordinating growth factor signaling and cell fate decisions during brain development, linking its adaptor function to both progenitor biology and ventricular homeostasis.

1.2.5 Intersectins in synaptic vesicle recycling and postsynaptic function

Intersectins (ITSNs) are multidomain scaffold proteins that coordinate endocytic events at synapses. In invertebrates, the ITSN ortholog Dap160 is essential for synaptic vesicle formation, with loss-of-function mutations leading to reduced vesicle numbers, abnormal morphology, and accumulation of endocytic intermediates (Koh et al., 2004; W. Wang et al., 2008). Mammals have two homologous Intersectin genes, ITSN1 and ITSN2 (Pucharcos et al., 2000) which give both rise to a long and a short isoform. While ITSN2 is broadly expressed across different human tissues, the long ITSN1 isoform is mainly expressed in neurons (Guipponi et al., 1998; Pucharcos et al., 2000). In mammals, ITSN1 appears less critical for synaptic vesicle endocytosis, though it supports vesicle replenishment and vesicle uncoating (Pechstein et al., 2015; S. Thomas et al., 2009). Beyond presynaptic functions, ITSN1 also contributes postsynaptically by regulating AMPAR and NMDAR trafficking (Glodowski et al., 2007; Nishimura et al., 2006) and by promoting dendritic spine development (S. Thomas et al., 2009). Thus, ITSN1 exerts both pre- and postsynaptic roles, linking endocytosis to vesicle cycling, receptor trafficking, and spine morphogenesis, although its precise contribution to mammalian brain physiology remains to be fully defined. ITSN1 has also emerged as a critical regulator of brain development through its involvement in the Reelin pathway (Fig. 1.4).

Mechanistically, ITSN1 acts as a scaffold linking VLDLR to Dab1, thereby facilitating Dab1 phosphorylation downstream of Reelin binding and ensuring proper radial glial organization and neuronal migration (Jakob et al., 2017a). Genetic interaction studies show that combined loss of ITSN1 and ApoER2 exacerbates cortical and hippocampal lamination defects, highlighting its importance in the VLDLR–Dab1 axis of Reelin signaling (Jakob et al., 2017a). In addition, ITSNs localizes to postsynaptic densities, where it associates with NMDA receptors and actin regulators to stabilize dendritic spines. Intersectin 1/2 double knockout mice exhibit reduced NMDA receptor levels, impaired cortico-striatal transmission, and stereotypic ASD/OCD-like behaviors,

linking ITSN dysfunction to neuropsychiatric disease (Vollweiter et al., 2023a). Collectively, these findings place ITSNs at the intersection of endocytosis, Reelin signaling, and synaptic plasticity, underscoring its essential role in neuronal development and behavioral regulation.

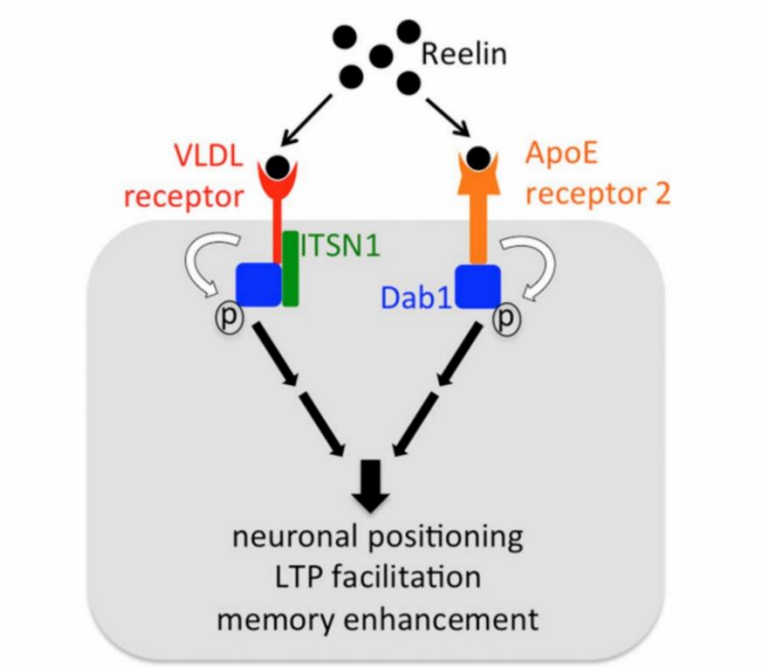

Figure 1.4 ITSN1 as a scaffold in the Reelin signaling cascade. Reelin binding to VLDLR and ApoER2 triggers Dab1 phosphorylation, which regulates neuronal positioning, synaptic plasticity, and memory. ITSN1 acts as a scaffold linking VLDLR to Dab1, thereby facilitating efficient Dab1 activation and downstream signaling. Adapted from (Jakob et al., 2017a).

1.3 EPS15 and EPS15R in Endocytosis and Beyond

Epidermal growth factor receptor substrate 15 (EPS15) and its mammalian-specific paralog EPS15R (also known as EPS15L1) are endocytic adaptor proteins with conserved roles in clathrin-mediated endocytosis. While EPS15 has been investigated in non-mammalian models, much less is known about the functions of either protein in the mammalian brain. Work in mammalian cell lines has suggested that the two proteins can substitute for one another in regulating endocytosis, yet it remains unclear to what extent their functions overlap in vivo. The uncertainty over whether EPS15 and EPS15R act redundantly or perform distinct roles in the mammalian brain, combined with their poorly defined functions in neurodevelopment and disease, makes them compelling candidates for study and the central focus of this thesis.

1.3.1 Structural organization of EPS15 and EPS15R

EPS15 was initially identified as a substrate phosphorylated by the epidermal growth factor receptor (EGFR) (Fazioli et al., 1993). During evolution, mammals acquired a second paralog, EPS15R , which shares 45% sequence identity and 61% similarity with EPS15 at the amino acid

level (Schumacher et al., 1995). Structurally, both proteins exhibit the features of multidomain scaffolding adaptors (Fig. 1.5). At their C-terminus, they contain three highly conserved EPS15 homology (EH) domains (Confalonieri & Di Fiore, 2002; Wong et al., 1995). These EH modules recognize the NPF (asparagine–proline–phenylalanine) motifs of partner proteins such as Numb, Stonin2, and Epsins (Polo et al., 2003; Rumpf et al., 2008; Salcini et al., 1997a). The central portion of the proteins is composed of heptad repeats forming a coiled-coil (CC) region, which enables homo- and heterodimerization of EPS15 and EPS15R and mediates binding to the endocytic scaffold proteins Intersectin1/2 (Sengar et al., 1999a; Tebar et al., 1997). Adjacent to these are proline-rich domain containing multiple DPF (aspartate–proline–phenylalanine) motifs required for high-affinity interaction with the adaptor complex AP-2 (Iannolo et al., 1997). At their N-terminus, are the ubiquitin-interacting motifs (UIMs) that mediate ubiquitin binding and monoubiquitination , linking EPS15/EPS15R to ubiquitin-dependent cargo sorting (Polo et al., 2002).Notably, EPS15R has also been shown to bind directly to the terminal domain of clathrin (Evergren et al., 2018). Through this modular architecture, EPS15 and EPS15R are able to assemble multi-protein complexes with AP-2, Clathrin, Dynamin, Intersectins, and Stonins, underscoring their function in endocytosis (Salcini et al., 1999) and positioning them as central adaptors within the clathrin-mediated endocytic machinery.

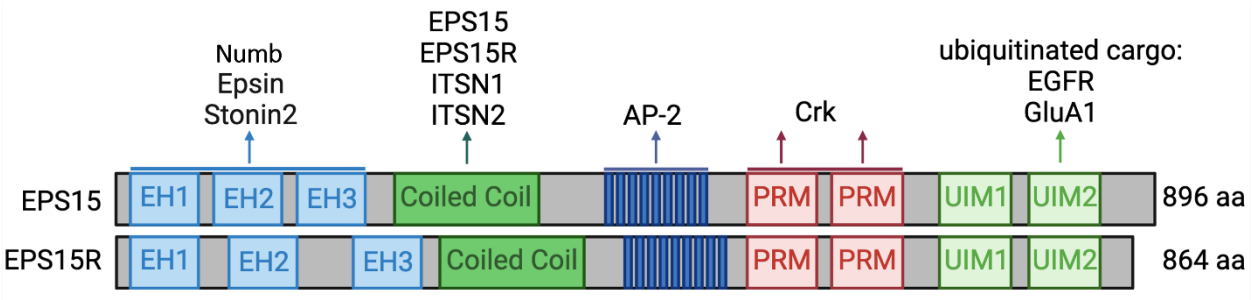

Figure 1.5. Domain architecture and interaction partners of EPS15 and EPS15R. Schematic representation of EPS15 and EPS15R protein domains. Both proteins contain three N-terminal EH domains that bind NPF-containing partners such as Numb, Epsins, and Stonin2. A central coiled-coil region that mediates homo-/heterodimerization and interaction with Intersectins, and a C-terminal proline-rich domain (PRM) that binds AP-2 and engages the SH3 domain of Crk. It also contains two C-terminal ubiquitin-interacting motifs (UIMs) which mediate recognition of ubiquitinated cargo such as EGFR and GluA1. This modular architecture enables EPS15/15R to assemble multi-protein complexes critical for clathrin-mediated endocytosis.

1.3.2 Canonical and cargo-specific functions of EPS15/15R in endocytosis

In vitro studies have shown that EPS15 and EPS15R act as largely redundant components of the endocytic machinery, as they share binding partners and jointly regulate clathrin-mediated endocytosis (van Bergen en Henegouwen, 2009). EPS15, together with FCHo1/2, functions as an

initiator of clathrin-mediated endocytosis by forming dynamic assemblies at the plasma membrane (Day et al., 2021). These assemblies, which are based on liquid-liquid phase separation (LLPS), rely on weak, liquid-like interactions that promote flexibility during vesicle budding. The EPS15-FCHo1/2 multivalent interaction is formed by the binding of the EH, CC and DPF motifs of EPS15 to the μ-homology domain of FCHo1/2, enabling their assembly into liquid-like protein droplets (Day et al., 2021). Disruption of this liquid-like state impairs endocytosis, highlighting the importance of EPS15-driven phase separation as a catalytic platform for vesicle formation (Witkowska & Haucke, 2021). EPS15s and Intersectins participate in this initiator network, supporting AP-2 recruitment and reinforcing redundancy within the early module (Henne et al., 2010a). Similar phase separation by Ede1, the yeast homolog of EPS15/EPS15R, underscores LLPS as a conserved mechanism for endocytic site nucleation (Kozak & Kaksonen, 2022a).

Functional studies in HeLa cells have shown that depletion of both proteins impairs CME of the transferrin receptor (TfR), a model for constitutive endocytosis, as well as the EGFR, a prototype of ligand-induced endocytosis (F. Huang et al., 2004). Consistent with their regulatory role, activation of EGFR triggers post-translational modifications of EPS15 and EPS15R, including tyrosine phosphorylation (Coda et al., 1998; Fazioli et al., 1993) and monoubiquitination (Delft et al., 1997; Woelk et al., 2006), which are required for efficient EGFR endocytosis (Confalonieri et al., 2000; Savio et al., 2016).

The functional relevance of EPS15/EPS15R for endocytosis appears to be determined by cargo specificity, with their contribution differing for individual receptors and global endocytic processes. While their depletion can interfere with the uptake of specific cargos like TfR and EGFR, a broader impairment of endocytosis is only observed when Intersectin1/2 are simultaneously removed (Henne et al., 2010b). This indicates that EPS15/15R act as critical adaptors for selected receptors but function mostly in a redundant manner with other endocytic adaptors during constitutive clathrin-mediated endocytosis (Carbone et al., 1997).

EPS15 and EPS15R, together with Epsin-1, have also been implicated in the clathrin-independent internalization of the epidermal growth factor receptor (EGFR) (Sigismund et al., 2005). Under conditions of high ligand stimulation, EGFR becomes ubiquitinated and is redirected from clathrin-mediated uptake toward a lipid raft–dependent, non-clathrin pathway. This process requires recognition of ubiquitin by Ub-interacting motif (UIM)–containing adaptors, and loss of EPS15, EPS15R, or Epsin impairs EGFR entry through this route, highlighting their essential role in coupling ubiquitinated cargo to clathrin-independent endocytosis (Fig. 1.6).

EPS15 has also been implicated as a specific adaptor for certain other ubiquitinated cargos, recognized through its UIM domains. These include connexin 43 (Cx43) and the AMPA receptor subunit GluA1. EPS15 interacts with ubiquitinated connexin 43 (Cx43) via its ubiquitin-interacting motif, and loss of EPS15 leads to Cx43 accumulation at the plasma membrane, indicating its role in its internalization (Girão et al., 2009). EPS15 also plays a pivotal role in the endocytosis of AMPA receptors by directly recognizing ubiquitinated GluA1 subunits through its ubiquitin-interacting motifs. This interaction, which depends on Nedd4-mediated ubiquitination of GluA1, facilitates receptor internalization and reduces surface AMPAR levels, and is thereby assumed to contribute to synaptic regulation and plasticity. Loss of EPS15 leads to impaired internalization of ubiquitinated GluA1 and altered receptor trafficking (Lin & Man, 2014). The physiological relevance of these cargo-specific interactions remains unclear, and it is not yet known whether EPS15R is involved. Together, these findings highlight EPS15 and EPS15R as multifunctional adaptors that not only initiate and support general clathrin-mediated endocytosis but also act as cargo-specific regulators, linking endocytic machinery to receptor trafficking, signaling pathways, and synaptic plasticity.

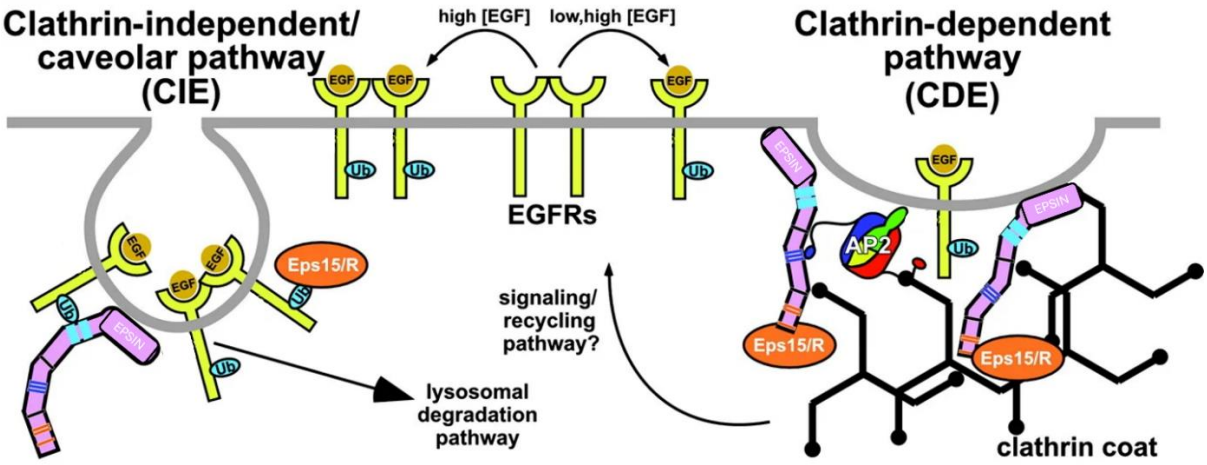

Figure 1.6 EPS15/EPS15R in clathrin-dependent and clathrin-independent EGFR endocytosis. EPS15/EPS15R and Epsins mediate EGFR uptake through both clathrin-dependent and clathrin-independent pathways. Under low ligand conditions, receptors enter via clathrin-coated pits, whereas high EGF stimulation promotes ubiquitin-dependent, non-clathrin internalization, linking EPS15/EPS15R to alternative trafficking and degradation routes. Adapted from *(Aguilar & Wendland, 2005)*.

1.3.3 Non-canonical functions of EPS15s

Beyond their established roles in endocytosis, EPS15 and EPS15R have also been implicated in the regulation of other pathways. Recent work published as preprint has uncovered a novel role for EPS15 and EPS15R in regulating clathrin-coated plaques, large flat clathrin lattices distinct from classical clathrin-coated pits (Bucher et al., 2018). These plaques arise following focal

adhesion mediated remodeling of the extracellular matrix (ECM), where localized ECM digestion creates topographical cues that recruit clathrin assemblies (Lampe et al., 2016). EPS15 and EPS15R were identified as key regulators of plaque formation, linking them directly to ECM sensing and cell migration. Loss of either protein disrupts the switch from focal adhesions to plaques, impairing the ability of cells to align migration with extracellular cues (Bucher et al., 2018). This highlights a role for EPS15 and EPS15R beyond endocytosis, positioning them as mediators of contact guidance and collective migration. Moreover, subcellular localization studies revealed EPS15 enrichment at endosomal and trans-Golgi network compartments (Chi et al., 2008; Kent et al., 2002), whereas a fraction of EPS15R resides in the nucleus (Poupon et al., 2002). These observations point to possible non-canonical functions of both proteins, though their biological relevance is yet to be clarified.

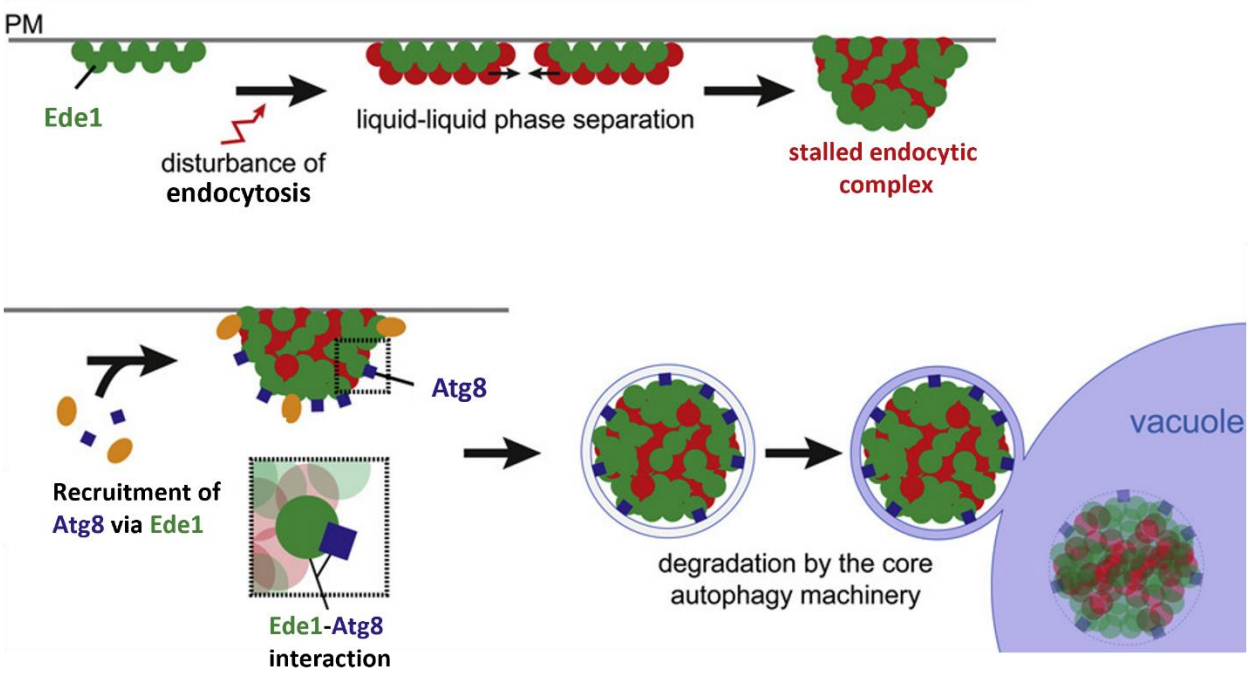

Figure 1.7. Ede1-dependent autophagic degradation of aberrant endocytic assemblies. The yeast EPS15 ortholog Ede1 functions as an intrinsic autophagy receptor and promotes liquid–liquid phase separation of stalled endocytic assemblies. These aberrant complexes are recognized through direct interaction of Ede1 with Atg8, enabling their recruitment to the core autophagy machinery and subsequent vacuolar degradation. This pathway highlights a non-canonical role of EPS15 family proteins in linking stalled endocytic complexes to autophagy. Adapted from *(Wilfling et al., 2020a)*.

In yeast, the EPS15 ortholog Ede1 has been identified as an intrinsic autophagy receptor, revealing an unexpected link between endocytic proteins and autophagic quality control (Fig. 1.7) (Wilfling et al., 2020a). Ede1 undergoes liquid–liquid phase separation to form condensates of aberrant clathrin-mediated endocytic assemblies, which are then selectively targeted for degradation. This process relies on distinct Ede1 domains that bind the autophagosomal protein Atg8 and connect

defective endocytic complexes to the core autophagy machinery. Structural studies further demonstrated the presence of Ede1-containing condensates both at the plasma membrane and within autophagic bodies, highlighting its role as a selective receptor that directs phase-separated protein assemblies into the autophagic pathway (Wilfling et al., 2020a). Given that mammalian EPS15 and EPS15R also undergo phase separation, these findings raise the possibility that similar, yet unexplored, mechanisms may exist in higher organisms, linking their endocytic quality control to autophagic degradation.

1.3.4 Insights from non-mammalian model organisms

Studies in non-mammalian models highlight the evolutionary importance of EPS15 family proteins in neuronal function. In *C. elegans*, the single ortholog EHS-1 is highly enriched at synapses and is essential for synaptic vesicle recycling. Its deletion leads to a severe reduction in synaptic vesicle numbers, causing impaired neurotransmission and locomotor defects. Genetic interaction with dynamin further supports a conserved role of EHS-1/EPS15 in presynaptic endocytosis (Salcini et al., 2001a). Similarly, studies in *D. melanogaster* have revealed a critical role for EPS15 in synaptic vesicle endocytosis and synapse development. Loss of EPS15 results in defective synaptic bouton formation and reduced synaptic vesicle recycling. A key binding partner of EPS15 in flies is Dap160, the ortholog of mammalian Intersectins, and double-mutant analyses indicate that these proteins cooperate to sustain efficient synaptic vesicle endocytosis (Koh et al., 2007). Mutant flies subjected to high-frequency stimulation also exhibit enlarged vesicles, reduced synaptic vesicle density, and a failure to maintain neurotransmission (Majumdar et al., 2006a).

1.3.5 Insights from mammalian model organisms

In mammals, gene duplication events have introduced additional complexity into the endocytic machinery, thereby providing functional redundancy that often mitigates the impact of losing individual components. This redundancy is evident in the case of EPS15, where EPS15 knockout mice are viable and fertile (Pozzi et al., 2012a). Primary embryonic fibroblasts from these animals show no defects in transferrin or EGFR uptake, suggesting compensation by EPS15R and/or other adaptors. The only phenotype reported so far in EPS15-deficient mice is a mild alteration in B cell development, with elevated marginal zone B cell numbers, though the mechanism remains unresolved (Pozzi et al., 2012a).

By contrast, loss of the brain-enriched paralog EPS15R causes much more severe consequences. EPS15R knockout mice display perinatal lethality, with >50% animals dying within two days (Fig. 1.8 A), likely due to impaired feeding and respiration. Surviving animals show growth retardation,

behavioral abnormalities, and premature death by two months of age (Milesi et al., 2019). The double knockout of EPS15 and EPS15R in mice results in embryonic lethality around E9.5, accompanied by pronounced morphological and vascular abnormalities, underscoring their essential and redundant roles during early development (Milesi et al., 2019). Conditional deletion of both proteins in the hematopoietic lineage further revealed their importance for red blood cell maturation, as mice developed anemia due to defective transferrin receptor endocytosis and consequent disturbances in iron homeostasis (Milesi et al., 2019). This phenotype closely parallels that observed in constitutive CALM knockout mice, where impaired TfR uptake similarly disrupts erythropoiesis (M. Suzuki et al., 2012). Mutations in the human EPS15R gene have also been associated with split-hand/split-foot malformation (SHFM) (Bens et al., 2011; Umair et al., 2018), further stating its crucial contribution to developmental processes.

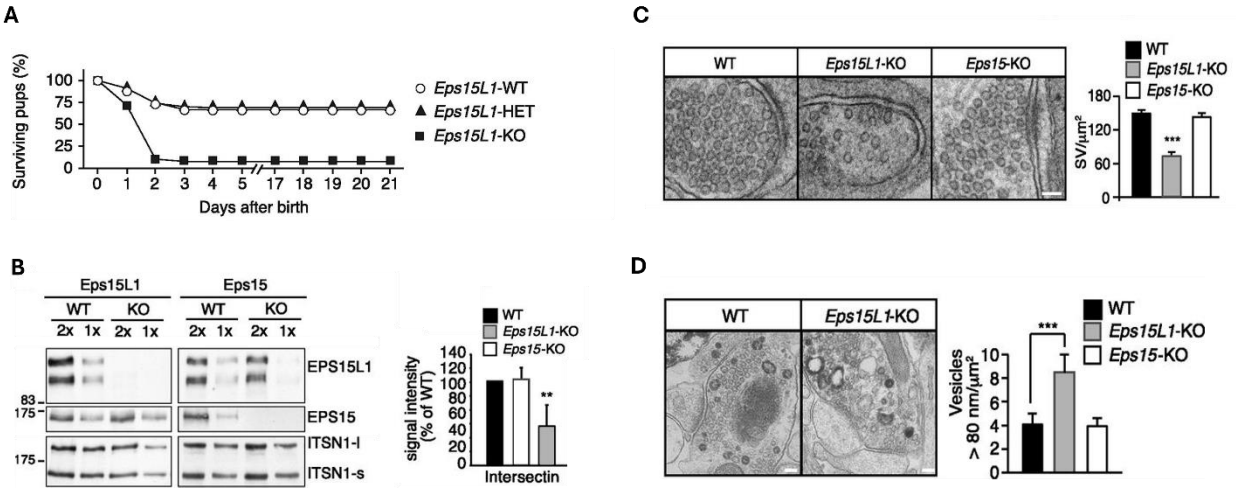

Figure 1.8. Synaptic and developmental phenotypes associated with EPS15R loss. **(A)** Survival curves reveal that EPS15R knockout mice exhibit perinatal lethality, with more than half of the animals dying within two days of birth. **(B)** Western blot analysis of brain lysates shows ~50% reduced Intersectin1 levels in EPS15R knockout mice. **(C)** Electron microscopy of hippocampal synapses demonstrates decreased synaptic vesicle density in the absence of EPS15R. **(D)** Upon strong stimulation, EPS15R-deficient neurons display accumulation of endosomal-like vacuoles. Findings from (Milesi et al., 2019).

Both EPS15 and EPS15R are expressed in neurons but exhibit distinct compartment-specific distributions. EPS15R shows strong co-localization with the presynaptic marker Synaptophysin and is enriched in synaptosomal fractions, supporting a primarily presynaptic localization (Milesi et al., 2019). In contrast, EPS15 forms prominent clusters along dendrites and partially co-localizes with PSD95, consistent with a postsynaptic enrichment (Lin & Man, 2014). Consistent with its presynaptic localization, hippocampal neurons from EPS15R-deficient animals exhibit reduced synaptic vesicle density (Fig. 1.8 C) and, under strong stimulation, accumulation of endosomal-like vacuoles (Fig. 1.8 D), partially paralleling the phenotypes observed in

invertebrate null mutants (Milesi et al., 2019). Interestingly, levels of Intersectin1 are diminished in EPS15R knockout brains (Fig. 1.8 B), whereas other endocytic and synaptic proteins remain unaffected (Milesi et al., 2019). This observation reinforces the strong functional link between EPS15s and Intersectins, reminiscent of the well-established interaction between EPS15 and its ortholog Dap160 in *Drosophila*, where their interaction is critical for efficient synaptic vesicle recycling (Koh et al., 2007). Together, these findings underscore the essential and partly overlapping roles of EPS15 and EPS15R, although further studies are needed to fully delineate their specific contributions to neuronal physiology.

1.4 Neurogenesis and brain development

Proper brain development relies on tightly regulated cellular and molecular mechanisms that coordinate neurogenesis, neuronal differentiation, and circuit assembly. As already discussed, (see 1.2), several adaptor proteins such as AP-2, CALM, Epsins, Numb, and Intersectins have already been implicated in diverse aspects of brain development, where they regulate receptor trafficking, intracellular signaling, and progenitor cell behavior. These findings highlight the critical contribution of endocytic adaptors to processes that shape neuronal development. In light of these precedents, EPS15 and EPS15R represent strong candidates for regulating similar developmental mechanisms. Indeed, as shown in later sections of this thesis, loss of EPS15/EPS15R leads to striking phenotypes affecting neurogenesis and brain architecture. To place these findings into context, the following section outlines key developmental programs, that will serve as a framework for interpreting the experimental results.

Neurogenesis is a central process in shaping the developing brain, as it generates neurons from neural stem and progenitor cells. Newly generated neurons subsequently undergo migration, differentiation, axon and dendrite formation, and synaptogenesis to establish functional networks. In the postnatal and adult brain, neurogenesis persists only in specialized niches. Within these regions, diverse neural stem cell (NSC) types, such as radial glial cells (RGCs), intermediate progenitors, or astrocyte-derived precursors, give rise to new neurons that integrate into existing circuits (Götz & Huttner, 2005; Hussain et al., 2023; Kempermann et al., 2015).

1.4.1 Mechanism of neocortical development

The functional complexity of the mammalian brain is largely attributed to the neocortex, which is characterized by its well-defined laminar organization. Cortical neurogenesis is a highly coordinated developmental program through which neural progenitors produce projection neurons that build the neocortical layers. During early brain development, neuroepithelial cells

(NECs) – the primary neural stem cells (NSCs) of the early neural tube – begin to transition into radial glial cells (RGCs).Neuroepithelial cells are a morphologically uniform, highly proliferative population of multipotent progenitors that generate the initial neural lineages of the developing brain (Cai et al., 2002). As neurogenesis begins, these progenitors acquire astroglial characteristics and transform into radial glial cells, which retain apico-basal polarity and exhibit broader lineage potential. RGCs are heterogeneous, encompassing both pluripotent and lineage-restricted progenitors capable of giving rise to neurons, astrocytes, and oligodendrocytes, while simultaneously providing a scaffold for the radial migration of newly born neurons (Malatesta et al., 2008; Rakic, 2009). At later embryonic and postnatal stages, subsets of radial glia persist as neural stem cells that sustain adult neurogenesis, thereby establishing a continuous stem cell lineage from the embryonic to the mature central nervous system. With the onset of corticogenesis (around E10.5) (Fig. 1.9) RGCs self-renew and generate neurons via intermediate progenitors (IPCs) or glia cells that populate the subventricular zone (SVZ) (Götz & Huttner, 2005). The earliest-born neurons migrate from the ventricular zone (VZ) to form a transient structure known as the preplate. As development proceeds, later-generated neurons migrate into the preplate and divide it into two layers – the superficial marginal zone and the deeper subplate – thereby establishing the cortical plate between them. Neurons subsequently added to the cortical plate migrate radially along RGC scaffolds in a temporally ordered sequence, expanding the plate in an "inside-out" manner to form the mature six-layered neocortex (Bayer & Altman, 1991; McEwan et al., 2023). Early born neurons migrate and settle into the deeper cortical layers. In contrast, later-born neurons first undergo a multipolar-to-bipolar transition before moving to more superficial layers of the cortex (Kriegstein & Noctor, 2004). Eventually all newly generated neurons migrate out of the ventricular zone (VZ) and subventricular zones (SVZ) toward the pial surface – the outer boundary of the developing cortex lined by the pia mater. Within the neocortex, deep-layer cortical neurons are marked by CTIP2 expression in layer V (Arlotta et al., 2005) and TBR1 in layer VI (Hevner et al., 2001), whereas upper-layer populations (layers II–IV) express SATB2 and CUX1. The marginal zone (MZ) at the cortical surface (layer I) lacks projection neurons and is instead populated by Cajal–Retzius cells (Schiffmann et al., 1997). This layered organization underpins the functional complexity of the mammalian cortex, and defects in these developmental programs are associated with diverse neurological disorders such as lissencephaly and polymicrogyria (Guerrini & Dobyns, 2014; Gupta et al., 2002).

The formation of the cortex critically depends on the Reelin signaling pathway. Reelin is a large, secreted glycoprotein produced by Cajal–Retzius cells located in the marginal zone (MZ), where it accumulates in the extracellular matrix and provides essential positional cues for migrating

neurons (D'Arcangelo et al., 1995a). Reelin binds to the receptors VLDLR and ApoER2 (D'Arcangelo et al., 1999a), which in turn recruit the cytoplasmic adaptor Dab1. This interaction promotes tyrosine phosphorylation of Dab1, a modification shown to be indispensable for Reelin signaling (Howell et al., 1999).

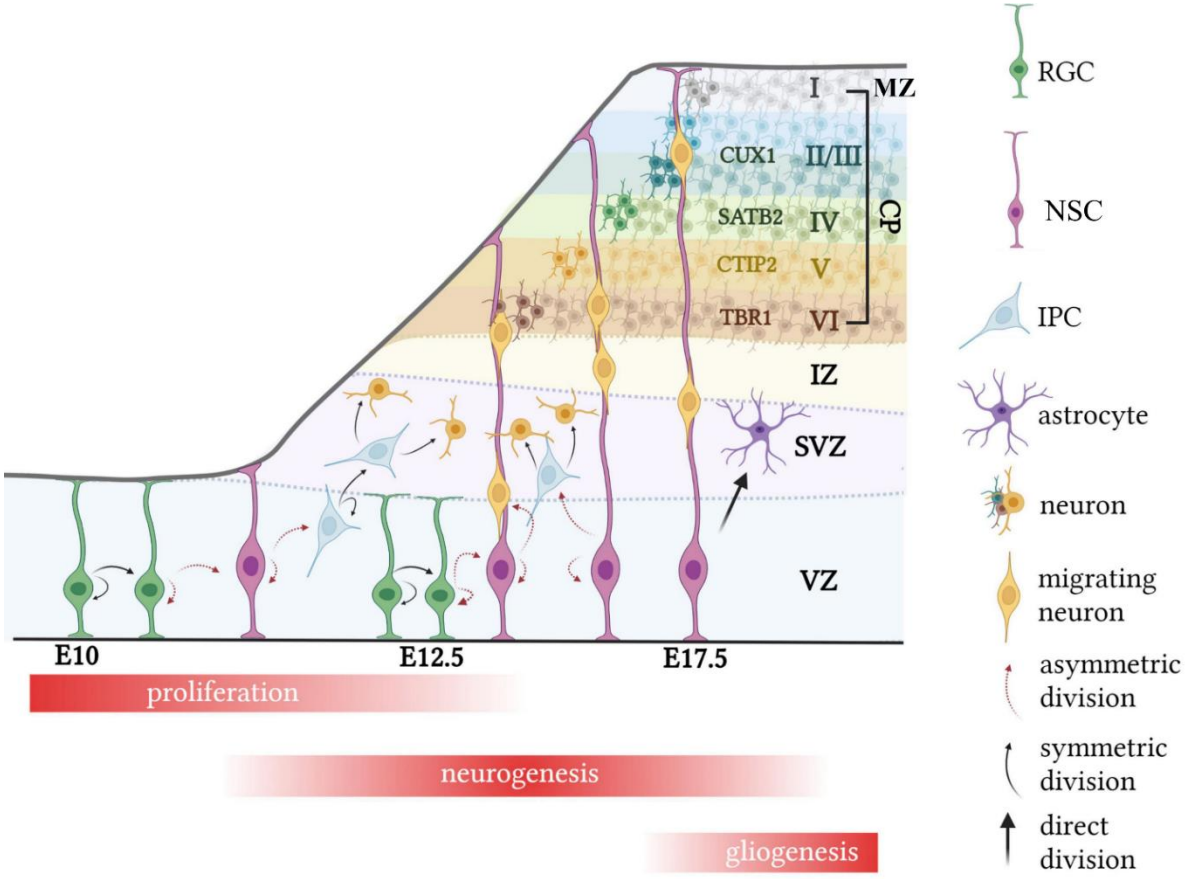

Figure 1.9. Stages of cortical neurogenesis and laminar organization. Schematic representation of corticogenesis in the developing rodent brain. At the onset of cortical development, neuroepithelial cells in the ventricular zone (VZ) transition into radial glial cells (RGCs), which act as neural stem cells (NSCs) capable of both self-renewal and generating neurons through intermediate progenitor cells (IPCs) in the subventricular zone (SVZ). Newly generated neurons migrate radially along RGC scaffolds toward the cortical plate (CP), with early-born neurons forming the deep layers ($CTIP2^+$ in layer V, $TBR1^+$ in layer VI) and later-born neurons populating the upper layers ($SATB2^+$ and $CUX1^+$ in layers II–IV). The marginal zone (MZ, layer I) at the cortical surface is populated by Cajal–Retzius cells. Between E11 and E18, successive waves of neuronal generation produce the six-layered neocortex in an "inside-out" manner. This temporal and spatial sequence shapes neocortical architecture and functional complexity. Adapted from *(McEwan et al., 2023)*.

Mutant mouse lines such as Reelin knockout (*reeler* mice), Dab1 knockout (*scrambler* / *yotari* mice) or VLDLR/ApoER2 double knockouts all display a characteristic inverted and disorganized cortical layering (D'Arcangelo et al., 1995a; Hirota et al., 2015; Ware et al., 1997) where defective radial neuronal migration leads to a failure of preplate splitting, causing neurons to occupy inappropriate positions and display abnormal orientation (Pinto-Lord et al., 1982). As a result, neurons fail to terminate migration at the marginal zone and instead accumulate beneath earlier-

born cells, leading to a loss of inside-out organization and an overall disruption of cortical lamination. However, the severity and extent of lamination defects vary among these models, reflecting the distinct roles of each component within the Reelin signaling pathway. Together, these findings demonstrate that the Reelin–VLDLR/ApoER2–Dab1 complex is essential for proper cortical lamination. Reelin signaling has been shown to also intersect with the Notch pathway during cortical development. In Reelin-deficient mice, levels of the cleaved Notch intracellular domain (Notch ICD) are reduced, leading to migration and morphological defects in neurons. Reelin prevents degradation of Notch ICD through Dab1, thereby sustaining Notch activity (Hashimoto-Torii et al., 2008). These insights highlight that the establishment of neocortical layers relies on the precise interplay of progenitor behavior, neuronal migration, and various signaling pathways, and that disturbances in these processes can result in severe developmental and neurological abnormalities.

1.4.2 Mechanism of hippocampal development

The hippocampus is a cortical structure located in the temporal lobe and is composed of the Cornu Ammonis (CA1–CA4) regions, which contain pyramidal neurons, as well as the dentate gyrus (DG) (Fig. 1.10). The principal connections within the hippocampus form the so-called trisynaptic circuit, a well-characterized pathway essential for information processing and memory formation. The DG receives its main input from the entorhinal cortex (EC) which is why the EC is considered a functional component of the hippocampus formation. Dentate granule cells, in turn, project to CA3 pyramidal neurons through the mossy fiber pathway. From there, CA3 pyramidal cells send axons, known as Schaffer collaterals, to pyramidal neurons in the CA1 region. The CA1 neurons then project to the subiculum and to deeper layers of the entorhinal cortex, thus completing the loop between the hippocampus and the neocortex. This organization ensures the bidirectional flow of information within the hippocampal formation(Patten et al., 2015). The DG itself consists of three distinct layers, the granule cell layer (GCL), molecular layer (ML), and hilus (Fig. 1.11). The development of the hippocampus, being a cortical structure, shares similarities with the formation of the neocortex (K. Hayashi et al., 2015). Both hippocampal and cortical neurons originate from progenitor cells located in the ventricular zones. In the hippocampus, radial glial cells within the ammonic and dentate neuroepithelium generate pyramidal and granule neurons, respectively (Altman & Bayer, 1990). Similar to cortical development, migration in the CA and dentate gyrus regions is regulated by Reelin secretion and signaling. With maturation, the neurogenic capacity of the DG becomes progressively confined to the subgranular zone (SGZ), located at the interface between the hilus and the granule cell layer (GCL), which serves as the lifelong hippocampal stem cell niche.

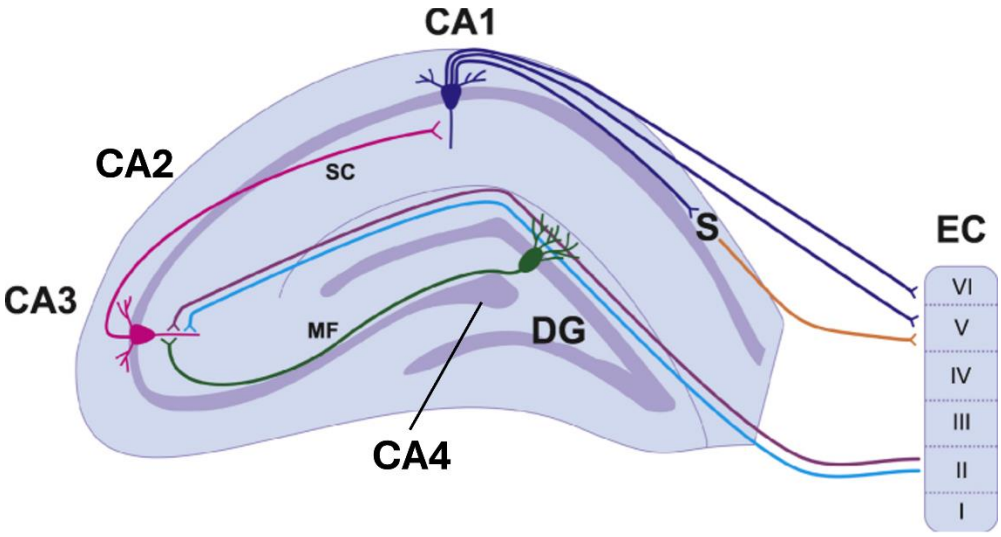

Figure 1.10 Simplified schematic of hippocampal circuitry. The hippocampus consists of the Cornu Ammonis (CA1–CA4) regions and the dentate gyrus (DG). Inputs from the entorhinal cortex (EC) reach DG granule cells. The granule cells project to CA3 via mossy fibers (MF), which connect to CA1 through Schaffer collaterals (SC). CA1 neurons then project to the subiculum (S) and back to the EC, forming the trisynaptic circuit. Adapted from (Patten et al., 2015).

In most brain regions, neurogenesis is largely confined to embryonic and early postnatal development, ceasing around birth (Kempermann et al., 2015). The dentate gyrus , however, is an exception, as it continues to generate neurons throughout adult life (Cameron et al., 1993a). In the adult DG, neural precursors reside within the subgranular zone, where type 1 cells represent multipotent progenitors with radial glia-like morphology (Seri et al., 2001, 2004). These cells display astrocytic features, expressing GFAP and stem cell markers such as Nestin and Sox2 (Filippov et al., 2003; Fukuda et al., 2003). Type 1 cells give rise to transiently amplifying type 2 progenitors, which proliferate actively. Type 2a cells retain glial characteristics, whereas type 2b cells begin to acquire neuronal traits, including the expression of Doublecortin (DCX) and NeuroD (Steiner et al., 2006). The type 2b cells transition into type 3 neuroblasts, which are DCX-positive and display limited proliferation. Following short-range migration into the granule cell layer, type 3 cells differentiate into mature granule neurons marked by NeuN and Calbindin, which integrate into hippocampal circuits within weeks (Fig. 1.11) (Toni & Schinder, 2016). The subventricular zone of the lateral ventricles represents the second major site of adult neurogenesis. Within this niche, slowly dividing stem-like cells expressing GFAP and Nestin give rise to transit-amplifying progenitors through asymmetric divisions (Doetsch et al., 1997, 1999). These progenitors subsequently generate DCX-positive neuroblasts, which migrate collectively through the rostral migratory stream toward the olfactory bulb (Lois & Alvarez-Buylla, 1994). This

continuous neuronal turnover is thought to be essential for olfactory processing in rodents (Gheusi et al., 2000), although its relevance for humans appears limited.

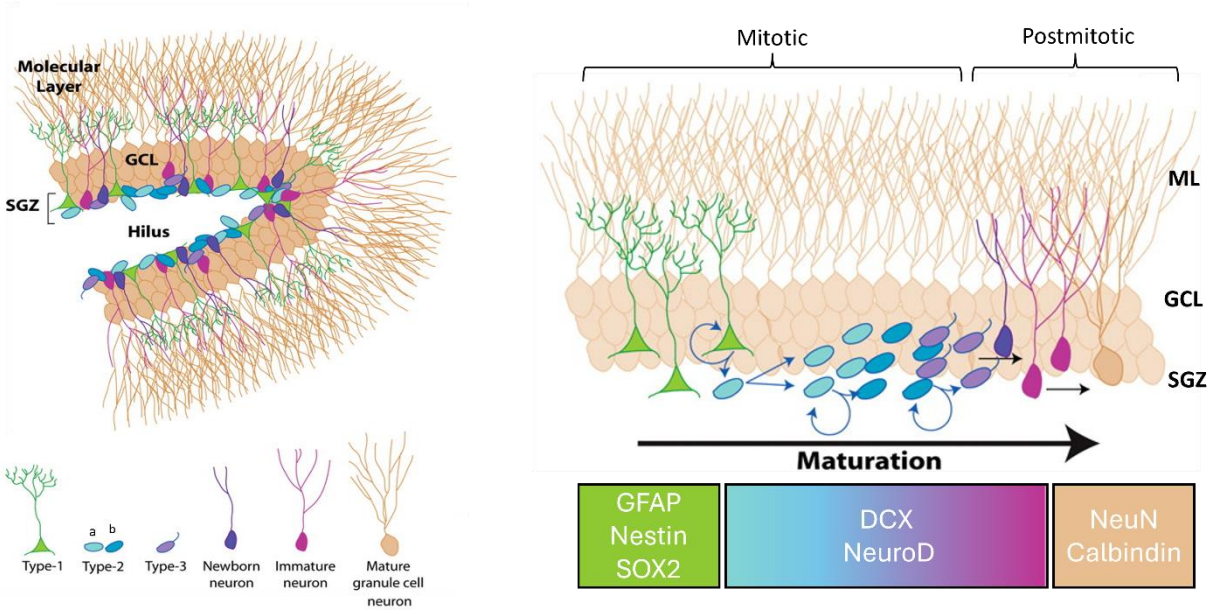

Figure 1.11 Stages of adult hippocampal neurogenesis. Left: Schematic representation of the hippocampal dentate gyrus (DG), showing its major layers: the molecular layer (ML), granule cell layer (GCL), hilus, and subgranular zone (SGZ), which together form a lifelong neurogenic niche. Right: Neural stem cells (type 1; green), characterized by radial glia-like morphology and expression of GFAP, Nestin, and Sox2, generate transiently amplifying type 2 progenitors (blue). Type 2a cells retain glial traits, while type 2b cells acquire neuronal features, including expression of DCX and NeuroD. These give rise to type 3 neuroblasts (purple), which undergo limited proliferation and migrate into the GCL, where they differentiate into immature neurons (magenta) and eventually mature granule cells expressing NeuN and Calbindin (orange). This sequence ensures the continuous generation and integration of new neurons into hippocampal circuits throughout life. Adapted from *(Eisch et al., 2008)*.

Reelin, as mentioned above is also essential for proper hippocampal organization (Frotscher, 1998). In *reeler* mice, defective Reelin signaling results in abnormal lamination, with pyramidal neurons in the CA regions and granule cells of the dentate gyrus appearing dispersed rather than forming compact layers (Hamburgh, 1963). In the DG, impaired Reelin signaling profoundly disrupts neurogenesis, as seen in *reeler* mice where radial glial scaffolds are disorganized and fail to orient radially, leading to abnormal DG layering (Förster et al., 2002; Weiss et al., 2003a). Consistently, conditional deletion of Dab1 in postnatal mice leads to ectopic accumulation of newborn neurons in the hilar region and impaired dendritic development, further emphasizing the essential role of the Reelin–Dab1 pathway in regulating neuronal migration and maturation (Teixeira et al., 2012). These findings firmly establish Reelin as a master regulator of neuronal migration and neurogenesis. Taken together, these insights highlight that hippocampal development and lifelong neurogenesis rely on the coordinated action of radial glial progenitors and Reelin signaling to ensure proper lamination and hippocampal circuit formation.

1.4.3 Mechanism of ventricular morphogenesis

The vertebrate central nervous system originates from the neural tube, whose inner cavity or lumen later expands to form the cerebrospinal fluid (CSF)-filled ventricular system. As neural progenitors proliferate, migrate, and differentiate, the anterior neural tube gives rise to the fore-, mid-, and hindbrain, while the posterior region develops into the spinal cord. The brain ventricles develop in parallel with these structures, resulting in the formation of four distinct cavities around birth (Eichele et al., 2019a). They are filled with CSF that is largely produced by the choroid plexus, a specialized secretory epithelium projecting into each ventricle (Cutler et al., 1968). Although their overall organization is conserved across vertebrates, ventricular morphology varies considerably among species, reflecting differences in brain anatomy (Nieuwenhuys et al., 1998).

In rodents (Fig. 1.12), the paired lateral ventricles (LV) within the forebrain connect via interventricular foramina to the narrow third ventricle (3V) of the diencephalon, which in turn links through the cerebral aqueduct to the fourth ventricle (4V) positioned between the mid- and hindbrain. The 4V is continuous with both the spinal canal and the subarachnoid space, from which CSF drains into the bloodstream through arachnoid granulations, specialized villous structures that mediate CSF absorption into the venous circulation (Hladky & Barrand, 2014).

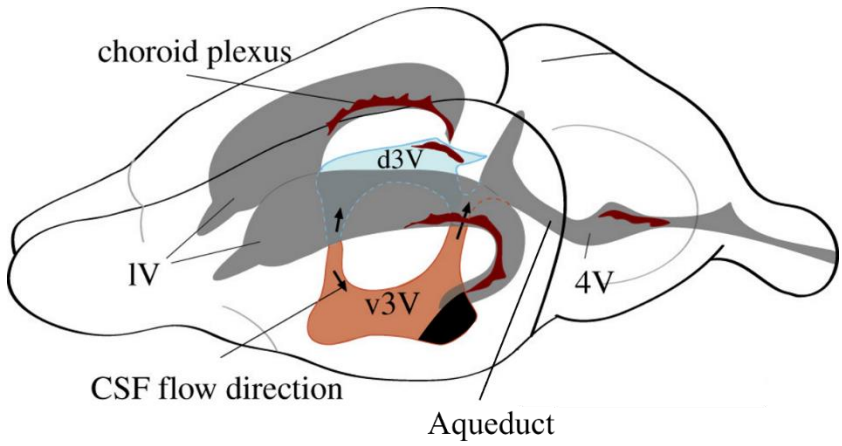

Figure 1.12 Schematic overview of the rodent ventricular system and cerebrospinal fluid (CSF) flow. The paired lateral ventricles (LV) connect to the third ventricle (3V), which extends through the cerebral aqueduct to the fourth ventricle (4V) between the midbrain and hindbrain. The choroid plexus (red) produces CSF that flows from the dorsal (d3V) to the ventral (v3V) third ventricle and onward into the 4V. Arrows indicate the direction of CSF circulation within the ventricular system. Adapted from (Eichele et al., 2019b).

The ventricular system is not only essential for CSF circulation, but it also serves as a neurogenic niche. Within the lateral ventricular wall, ventriculogenesis transforms the embryonic neuroepithelium into a postnatal epithelial layer composed of multiciliated ependymal cells (ECs)

and neural stem cells, ensuring both CSF homeostasis and neurogenic capacity. During embryonic development, the lateral ventricular wall is initially composed of a pseudostratified ventricular zone populated by radial glial cells, which serve as the primary neural stem cells of the developing brain (Merkle et al., 2004, 2007). As development progresses, the embryonic neuroepithelium gradually remodels into the postnatal ventricular–subventricular zone (V-SVZ), which consists of multiciliated ECs and a specialized subset of astroglial neural stem cells (Spassky et al., 2005; Tramontin et al., 2003). Lineage-tracing studies have demonstrated that embryonic radial glia contribute to both neural stem cells and ependymal cells, thereby coupling the generation of a multiciliated epithelium for the propulsion of the CSF with the establishment of the adult stem cell niche (Merkle et al., 2004; Spassky et al., 2005; Tramontin et al., 2003) (Fig. 1.13).

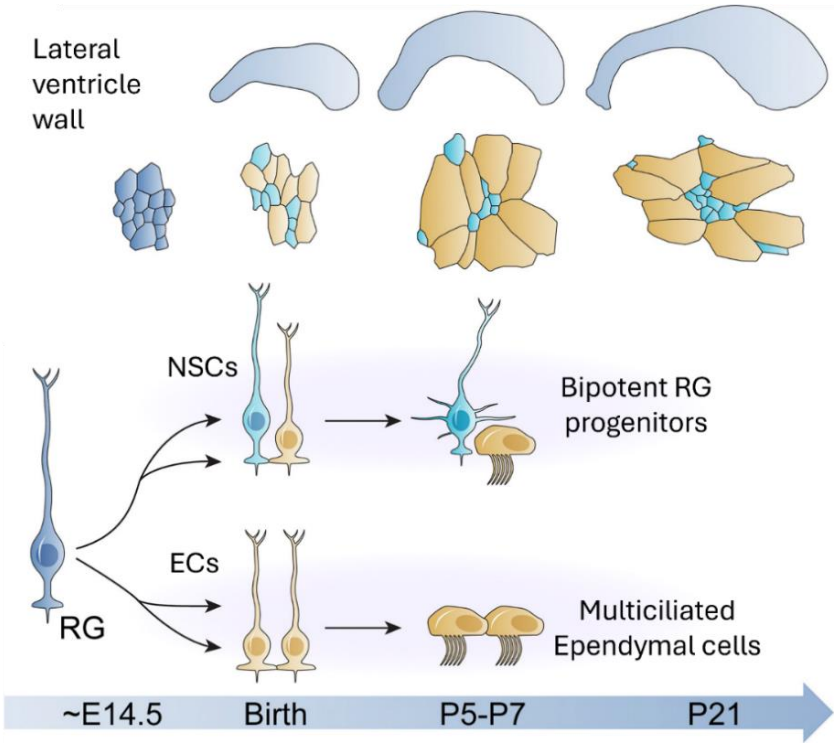

Figure 1.13 Radial glia lineage progression during ventriculogenesis. Schematic representation of ventricular wall maturation from embryonic day ~E14.5 to postnatal stages. Radial glial (RG) cells of the ventricular zone give rise to neural stem cells (NSCs) and ependymal cells (ECs). Postnatally, bipotent RG progenitors generate both NSCs and multiciliated ependymal cells, which acquire mature morphology around P5–P21. This transformation establishes the ventricular–subventricular zone (V-SVZ) niche, supporting lateral ventricle formation, and maintaining long-term neurogenic potential. Adapted from (Redmond et al., 2019).

Commitment to the ependymal lineage occurs during mid-fetal development, with most ECs generated between E14 and E16 (Spassky et al., 2005). These cells remain postmitotic, but only acquire their mature morphology postnatally, during the first week after birth, when ciliogenesis and apical surface expansion take place. The apical domains of differentiating ECs enlarge up to 11-fold between E17.5 and P21, allowing them to cover the expanding ventricular surface despite the loss of progenitors through consuming neurogenic divisions during juvenile stages (Redmond

et al., 2019). Multiciliation arises as radial glial cells, which initially bear a single primary cilium, begin to generate the numerous basal bodies required for motile cilia assembly. This process is initiated when the basal body of the primary cilium serves as a template for the formation of the deuterosome, a dense cytoplasmic structure that functions as nucleation center for centriole synthesis. The newly formed centrioles then mature into basal bodies and migrate toward the apical membrane, where they dock to initiate motile cilia assembly (Spassky et al., 2005). During late embryonic and early postnatal development, this process occurs in differentiating ependymal cells, derived from RGs, culminating in the formation of multiciliated ependymal cells that line the ventricles and drive cerebrospinal fluid flow. It follows a spatial gradient, with caudal and ventral regions of the ventricular wall maturing earlier than rostral and dorsal regions.

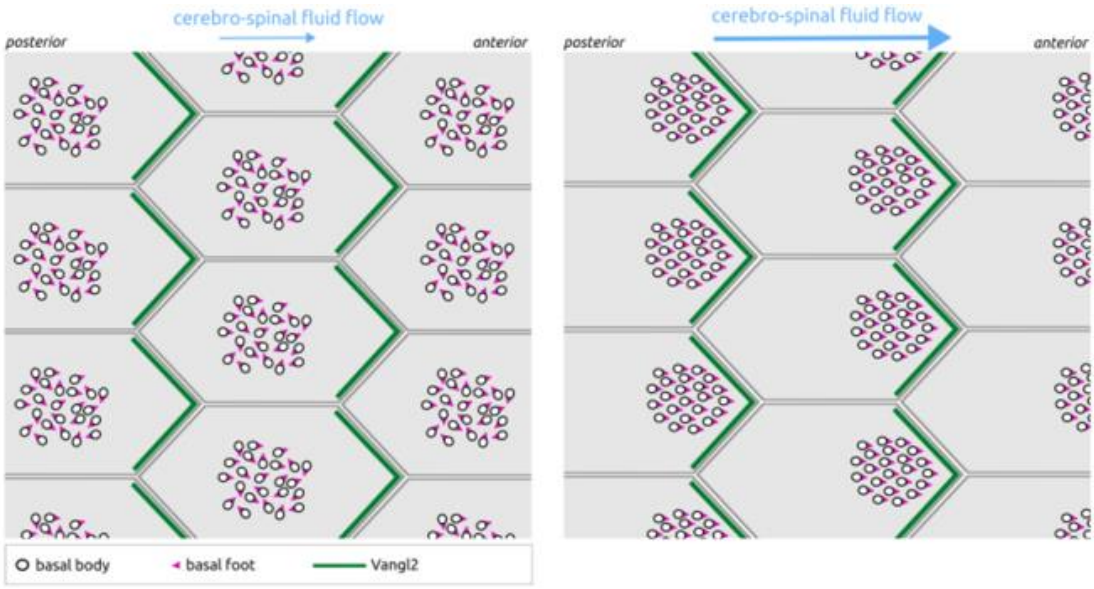

Figure 1.14 Establishment of planar cell polarity in ependymal cells. Schematic illustration showing the organization of basal bodies (black circles) and basal feet (magenta) in multiciliated ependymal cells. Rotational polarity (left) aligns basal feet uniformly in the direction of cerebrospinal fluid (CSF) flow, while translational polarity (right) positions basal body clusters anteriorly on the apical surface, ensuring synchronized ciliary beating an directional CSF movement. Both polarization types rely on core proteins such as Vangl2, whose asymmetric anterior localization is depicted in green.

As ECs expand and mature, they establish planar cell polarity, i.e. a coordinated alignment of cell polarity across the tissue plane with defined sets of cellular structures at distinct sides of the cells (Devenport, 2014). This depends on the RG primary cilium and hydrodynamic cues (Guirao et al., 2010; Mirzadeh et al., 2008, 2010). In addition, rotational polarity is established, which defines the uniform orientation of individual ciliary basal feet in the direction of the CSF flow, as well as translational polarity, which governs the collective positioning of basal body clusters off-centered towards the anterior side of the apical cell surface (Donati et al., 2024) (Fig. 1.14). Together, these features ensure correct cilia placement which is a prerequisite for synchronized ciliary beating and

directional CSF flow; and their disruption has been shown to result in ventriculomegaly or hydrocephalus (Foerster et al., 2017; Mirzadeh et al., 2010; Ohata, Nakatani, Herranz-Pérez, Cheng, Belinson, Inubushi, Snider, García-Verdugo, Wynshaw-Boris, & Álvarez-Buylla, 2014). Transcriptional regulators like GEMC1 act upstream to promote FOXJ1 expression, a key determinant of multiciliation and ependymal fate (Jacquet et al., 2009). Collectively, these developmental programs ensure that RG-derived ependymal cells establish a continuous, multiciliated epithelium, enabling the ventricles to mature into a functional cerebrospinal fluid conduit.

EGFR signaling plays a critical role in regulating the balance between neural stem cells and ependymal cells during the assembly of the lateral ventricular niche (Abdi et al., 2019). Postnatal radial glial progenitors that give rise to ependymal cells must suppress their EGFR activity, as persistent signaling inhibits their differentiation by blocking multiciliogenesis. This suppression is achieved through redistribution of EGFR away from the apical, CSF-contacting membrane. The endocytic adaptor Numb is central to this process, as it ensures proper EGFR relocation (Fig 1.3). Disruption of this mechanism prevents ependymal maturation, highlighting the importance of spatiotemporal control of EGFR signaling in establishing the adult neurogenic niche (Abdi et al., 2019). In parallel, Notch signaling also acts as a regulator of ependymal cell fate, where its downregulation is required for progenitors to exit the stem-like state and initiate the multiciliogenesis program (X. Wang et al., 2016). Disruption of endocytic control mechanisms, such as the loss of SNX27, results in aberrant Notch hyperactivation through increased γ-secretase–dependent cleavage, which blocks ependymal differentiation and causes severe hydrocephalus (X. Wang et al., 2016). Together, these findings underscore that precise temporal and spatial regulation of both EGFR and Notch signaling via endocytic trafficking is indispensable for proper ependymal maturation and CSF homeostasis. Overall, proper ventricular morphogenesis requires tightly coordinated radial glial differentiation, ciliogenesis, and signaling regulation.

1.5 Aim of thesis

The aim of this thesis is to elucidate the roles of the endocytic adaptor proteins EPS15 and EPS15R in the mammalian nervous system, with a particular focus on their contribution to brain development, synaptic function, and membrane trafficking. While both proteins have been well characterized as components of the endocytic machinery and in non-mammalian organisms, their in vivo functions within the mammalian brain remain largely unexplored. Previous genetic studies indicate that EPS15 and EPS15R are essential, as their combined loss causes embryonic lethality, yet the precise nature of their neuronal roles and the extent to which they act redundantly or diverge in function are not known.

To address these questions, the first part of this work is dedicated to the systematic characterization of EPS15 and EPS15R, including their developmental regulation, regional distribution, and subcellular localization. Their protein interaction networks will also be investigated to reveal both shared and unique partners, thereby identifying pathways through which they might exert canonical as well as non-canonical functions. The second part of the thesis employs conditional knockout strategies to interrogate the consequences of EPS15/15R loss in neuronal systems. An inducible knockout model provides an ex vivo platform to examine cell-autonomous effects on neuronal viability, endocytic activity, and receptor trafficking, while a forebrain-specific knockout model enables the analysis of developmental and structural phenotypes in vivo. Together, these complementary approaches allow for the evaluation of how EPS15 and EPS15R contribute to neuronal physiology at molecular, cellular, and organismal levels.

By integrating molecular characterization with targeted genetic models, this thesis seeks to define not only whether EPS15 and EPS15R act redundantly or possess distinct roles, but also what developmental, cellular, and behavioral phenotypes arise upon their loss. A particular emphasis is placed on uncovering how the absence of these adaptor proteins perturbs neuronal organization, synaptic receptor trafficking, and brain morphology, thereby linking molecular interactions to systems-level outcomes. Furthermore, by combining proteomic analyses with functional studies, this work aims to identify the mechanistic pathways through which EPS15 and EPS15R operate, from their classical role in clathrin-mediated endocytosis to potential non-canonical functions. In doing so, the thesis establishes a framework for understanding how adaptor proteins at the core of the endocytic machinery extend their influence into broader aspects of neuronal development and brain homeostasis.

2 Results

2.1 Characterization of endocytic proteins EPS15 and EPS15R

To gain a comprehensive understanding of the physiological relevance of EPS15 and EPS15R in the nervous system, we characterized their expression and localization in the mouse brain. Given their established roles as endocytic adaptor proteins, our analysis aimed to determine whether their distribution across brain regions and developmental stages might point to specialized or overlapping functions. Furthermore, by assessing their synaptic localization, we sought to clarify whether EPS15 and EPS15R act at pre- or postsynaptic sites, thereby providing a molecular basis for their potential involvement in neuronal communication and plasticity.

2.1.1 EPS15 and EPS15R are both expressed in the brain and exhibit developmental regulation

Based on previous findings indicating that EPS15R is predominantly expressed in the nervous system (Milesi et al., 2019), we further investigated the expression profiles of EPS15/15R across distinct brain regions to assess their spatial regulation. Quantitative analysis of immunoblots revealed region-specific expression patterns for both proteins (Fig. 2.1 A). EPS15 showed higher expression in the cerebellum than in any other tested brain region, whereas EPS15R was highly enriched in both cerebellum and cortex (Fig. 2.1 B,C), while it displayed significantly lower levels in the hind brain. Notably, both proteins were expressed in the hippocampus, suggesting potentially distinct synaptic roles in hippocampal circuits. The observed variation in expression profile provides additional evidence supporting non-redundant roles of EPS15 and EPS15R.

In addition to the region-specific expression profile, we examined the temporal dynamics of EPS15/15R expression. It has been previously shown that EPS15/15R double knockout (DKO) mice exhibit embryonic lethality around 9.5 days post coitum (Milesi et al., 2019), highlighting their indispensable roles during early development. To determine whether these proteins might also play a key role after birth, we analyzed their expression levels in postnatal brain tissue. Western blot analysis of mouse brain lysates from postnatal day 1 (P1) to 6 weeks old (P6w) mice revealed a progressive increase in the expression of both proteins (Fig. 2.1 D,E; S1), indicating that these endocytic adaptor proteins are developmentally regulated, similar to other endocytic adaptors such as AP2-α and Synaptotagmin1. These results suggest that, in addition to their essential function during embryogenesis, EPS15/15R likely continue to play important roles in the developing and maturing brain.

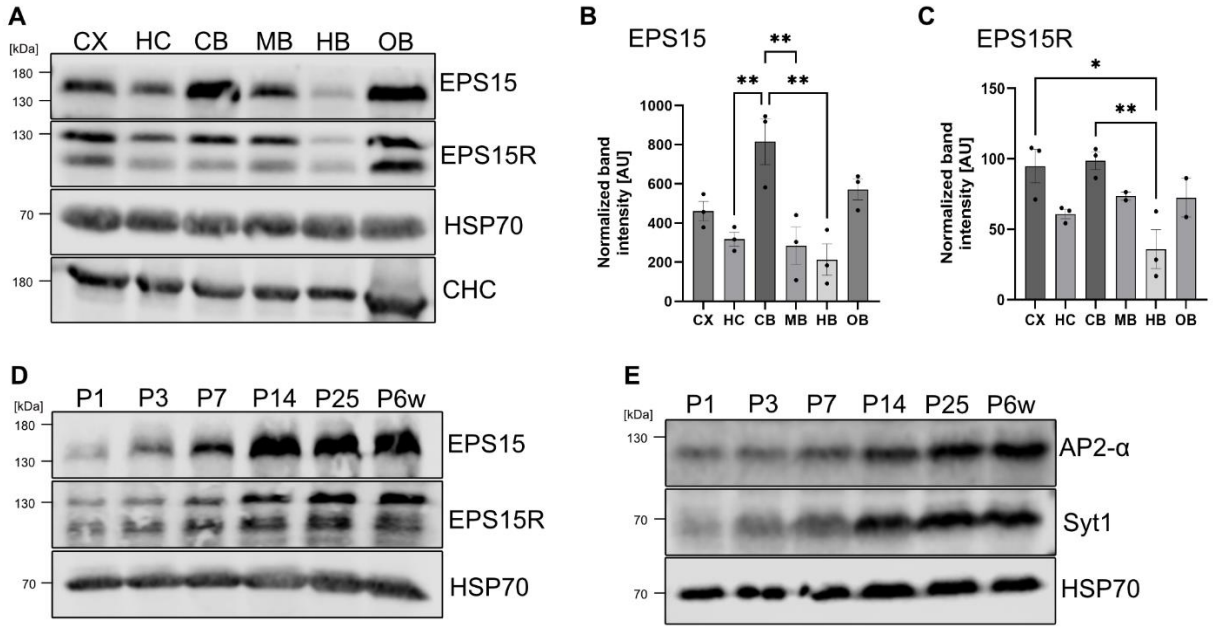

Figure 2.1 Spatial and developmental expression profiles of EPS15 and EPS15R. (A) Immunoblots of EPS15 and EPS15R across distinct brain regions (cortex (CX), hippocampus (HC), cerebellum (CB), midbrain (MB), hindbrain (HB), and olfactory bulb (OB)) to evaluate region-specific expression patterns. Mouse brain lysates (x µg) were blotted and probed with antibodies against the indicated proteins. HSP70 and CHC were detected as negative controls. **(B,C)** Quantification of EPS15 and EPS15R band intensities (EPS15 and EPS15R band intensities were normalized separately to HSP70 and Clathrin heavy chain (CHC), and the average of both normalized values was used for quantification). (n=3 independent experiments; one-way ANOVA test used to assess group differences, followed by Tukey's multiple comparison test; data are shown as individual data points with mean ± SEM; significance levels: *=p<0.05, **=p<0.01; non-significant data not marked). **(D,E)** Immunoblots from brain lysates of mice at the indicated postnatal (p) stages (1 day (p1) to 6 weeks (P6w)), showing increased expression of EPS15/15R over time. Mouse brain lysates (80 µg) were blotted and probed with antibodies against the indicated proteins. AP2-α and Synaptogmin1 (Syt1) served as reference endocytic markers; HSP70 was used as loading control (n=3 independent experiments; see Fig. S1 for quantification).

2.1.2 EPS15 and EPS15R localize to both pre- and post-synaptic sites

EPS15 has been shown to be enriched at synaptic sites in model organisms including *Caenorhabditis elegans* and *Drosophila melanogaster*, where it plays a crucial role in the nervous system by mediating synaptic vesicle recycling (Koh et al., 2007; Majumdar et al., 2006b; Salcini et al., 2001b). In mammals, EPS15R KO hippocampal neurons display a reduction in synaptic vesicle density, supporting its functional relevance at the synapse. In the adult mouse brain, both EPS15 and EPS15R are expressed in neurons, but both have been reported to show distinct subcellular localization patterns. EPS15R co-localizes with the presynaptic marker synaptophysin and is also enriched in the synaptosomal fraction compared to a postsynaptic density fraction, indicating a predominant presynaptic presence (Milesi et al., 2019). In contrast, EPS15 was shown to form intense clusters along dendrites in cultured hippocampal neurons and has been observed to partially co-localize with postsynaptic marker PSD95 (Lin & Man, 2014). In addition, EPS15 has been observed to partially co-localize with the postsynaptic marker PSD95 and is implicated

in the trafficking of the ubiquitinated AMPA receptor subunit GluA1, suggesting a potential post-synaptic role (Lin & Man, 2014). To investigate the precise localization of EPS15 and EPS15R in mammalian synapses, we performed a tryptic cleavage assay (Boyken et al., 2013; Shergill & Tehran, 2025). During synaptosome isolation, presynaptic proteins are protected due to resealing of the sheared off presynapse, whereas post-synaptic proteins remain exposed and are susceptible to proteolytic digestion by trypsin (Fig. 2.2 A). As expected, presynaptic markers such as SNAP25 and Synaptophysin remained intact after trypsin treatment, whereas the postsynaptic AMPA receptor subunits GluA1 and GluA2 displayed a reduced signal intensity. Interestingly, both EPS15 and EPS15R were partially sensitive to trypsin digestion and showed a significant reduction in signal intensity (EPS15/15R ~60% reduction) (Fig. 2.2 B,C), suggesting that they are not exclusively pre- or postsynaptic. This partial sensitivity to proteolysis indicates that EPS15 and EPS15R are present at both pre- and postsynaptic compartments within the synapse, similar to other endocytic adaptors like ITSN1 and CALM (Azarnia Tehran et al., 2022; Vollweiter et al., 2023b). These observations are in line with their proposed roles in regulating synaptic vesicle recycling and postsynaptic receptor trafficking. However, the precise compartment-specific functions of EPS15 and EPS15R at the mammalian synapse remain to be fully elucidated.

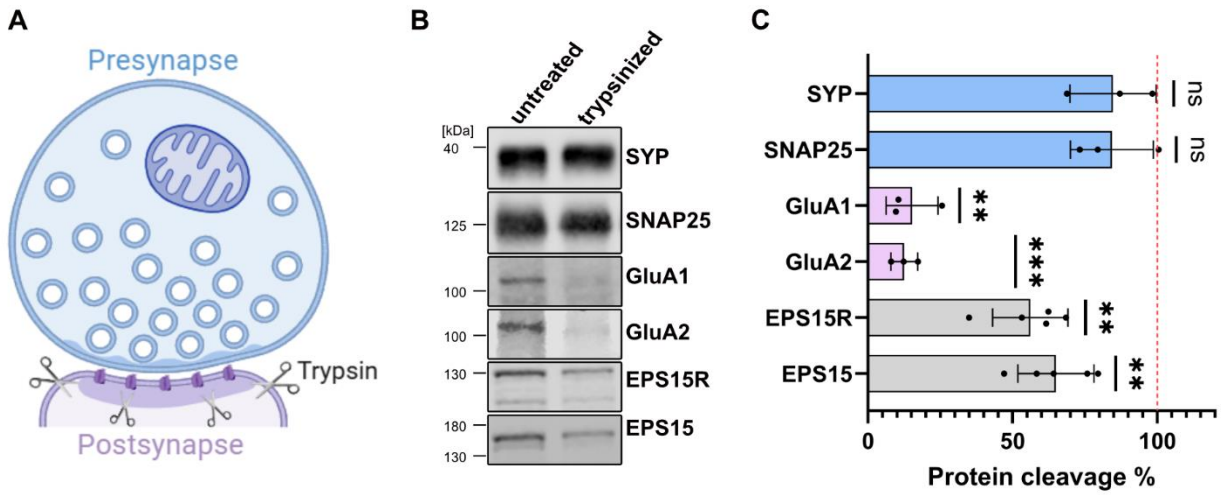

Figure 2.2 Trypsin cleavage assay reveals dual synaptic localization of EPS15 and EPS15R. (A) Schematic diagram of the tryptic cleavage assay on isolated synaptosomes. Presynaptic compartments reseal and are protected from proteolysis, whereas postsynaptic proteins remain exposed to trypsin and are cleaved. **(B)** Immunoblots showing levels of presynaptic (Synaptophysin (SYP), SNAP25), postsynaptic (GluA1, GluA2), and endocytic adaptor proteins EPS15 and EPS15R in untreated and trypsin-treated synaptosomes. Lysates of synaptosomes (x µg) were blotted and probed with antibodies against the indicated proteins. **(C)** Quantification of remaining protein after trypsin treatment. EPS15 and EPS15R exhibit partial cleavage (~60% remaining protein), indicating presence at both compartments. (n≥3 individual experiments; one-sample t-test performed for statistical analysis, with untreated samples normalized to 100%; data are shown as individual data points with mean ± SEM; significance levels: **=p<0.01, ***=p<0.001; ns, non-significant).

2.2 Mapping of EPS15 and EPS15R interaction networks

To uncover the molecular networks through which EPS15 and EPS15R exert their neuronal functions, we systematically mapped their protein interactomes using co-immunoprecipitation studies, in part coupled with mass-spectrometry. While EPS15 has been extensively studied in the context of endocytosis, comparatively little is known about EPS15R's specific binding partners and functions. Given their structural similarity but potentially distinct roles, we employed both targeted and unbiased strategies to characterize shared and unique interactors. This section outlines the rationale, methodology, and key findings of this interactome exploration, providing insights into canonical and non-canonical pathways linked to EPS15 and EPS15R.

2.2.1 Targeted investigation of EPS15R-GluA1 interactions

Given the partial sensitivity of both EPS15 and EPS15R to the tryptic digest of synaptosomes, our findings suggest that these adaptor proteins are present at both pre- and postsynaptic sites. As previously noted, EPS15 has been implicated in postsynaptic receptor trafficking through its interaction with the ubiquitinated AMPA receptor subunit GluA1 (Lin & Man, 2014). However, whether EPS15R shares this postsynaptic function remains unknown. Considering the high degree of sequence identity and structural similarity between EPS15 and EPS15R, as well as their overlapping subcellular localization pattern, we hypothesized that EPS15R may similarly interact with GluA1 at the postsynapse and thereby contribute to AMPA receptor regulation.

To investigate whether EPS15R interacts with GluA1, we performed co-immunoprecipitation (co-IP) experiments from adult mouse brain using three different biochemical preparations: whole brain lysates, crude synaptosome fractions, and purified synaptic membranes. This stepwise approach allowed us to assess the interaction across increasing levels of synaptic enrichment, as protein localization and complex formation may vary between compartments. EPS15R was successfully immunoprecipitated from all three fractions, and GluA1 was consistently co-immunoprecipitated, with the strongest signal observed in the synaptic membrane fraction, in line with the notion of EPS15R binding to postsynaptic plasma-membrane localized GluA1 to mediate its internalization. AP2-α a known endocytic interactor of EPS15R, was also robustly enriched in these co-IPs, whereas syntaxin1, a synaptic protein not expected to bind EPS15R, was absent indicating a high specificity of the co-IP (Fig. 2.3 A).

In parallel, we immunoprecipitated EPS15 from the same fractions under identical conditions to confirm its reported interaction with GluA1 and to validate our assay conditions. EPS15 also robustly co-precipitated GluA1, particularly in the synaptic membrane fractions, mirroring the

pattern observed for EPS15R. The successful co-IP of AP2-α and exclusion of Syntaxin1 from EPS15 IPs further confirmed the specificity and robustness of the experimental workflow (Fig. 2.3 B).

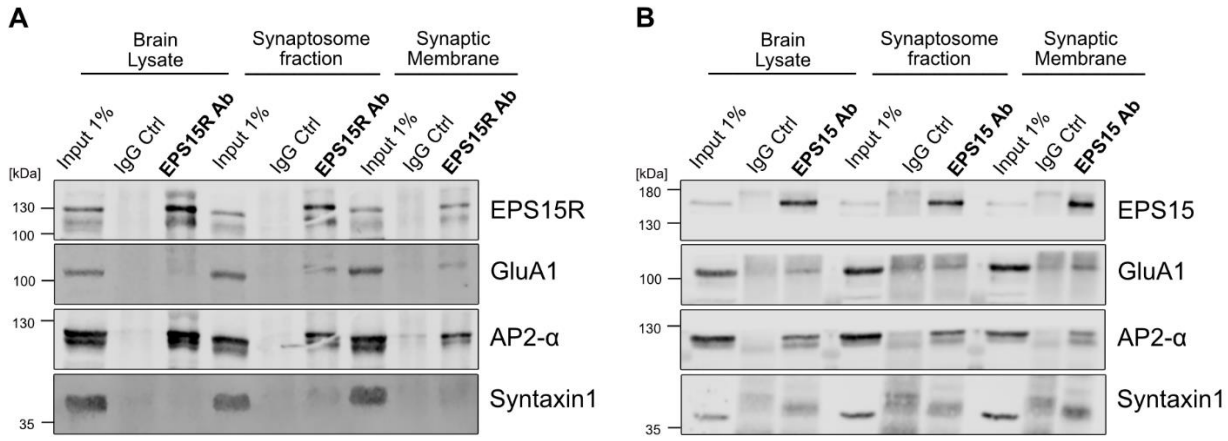

Figure 2.3 EPS15R and EPS15 form protein complexes with the AMPA receptor subunit GluA1 in synaptic brain fractions. (A) Representative immunoblots from co-immunoprecipitation (co-IP) experiments using an anti-EPS15R antibody on adult mouse brain lysate, a synaptosome fraction, and synaptic membranes. EPS15R efficiently co-precipitates GluA1 and AP2-alpha, but not Syntaxin1. **(B)** Parallel co-IP using an anti-EPS15 antibody under identical conditions confirms co-precipitation of GluA1 and AP2-alpha, but no detection of syntaxin1, indicating specificity of the interaction. (n=3 independent experiments).

Together these data demonstrate that EPS15R, like its paralog EPS15, is capable of associating with GluA1 in the brain, supporting a potential postsynaptic role in AMPA receptor regulation. EPS15 was shown to not just interact but also mediate the internalization of ubiquitinated AMPA receptors via its ubiquitin-interacting motif, and its knockdown impaired GluA1 internalization in a ubiquitin dependent manner (Lin & Man, 2014). Whether EPS15R also interacts with GluA1 via a ubiquitin-interacting motif and mediates AMPAR internalization in a similar manner remains to be investigated.

2.2.2 Unbiased proteomic identification of EPS15 and EPS15R interactors

While our targeted analyses provided evidence for EPS15R's interaction with GluA1, the broader landscape of proteins interacting with EPS15 and EPS15R in the brain remains poorly investigated. To uncover novel and potentially paralog-specific binding partners, we employed an unbiased proteomic approach. Co-immunoprecipitation was performed from adult mouse brain lysate using antibodies against either EPS15 or EPS15R, followed by mass spectrometry (MS) to identify associated proteins. This strategy aimed to define the synaptic interactome of both adaptor proteins and reveal candidate effectors involved in their diverse neuronal functions.

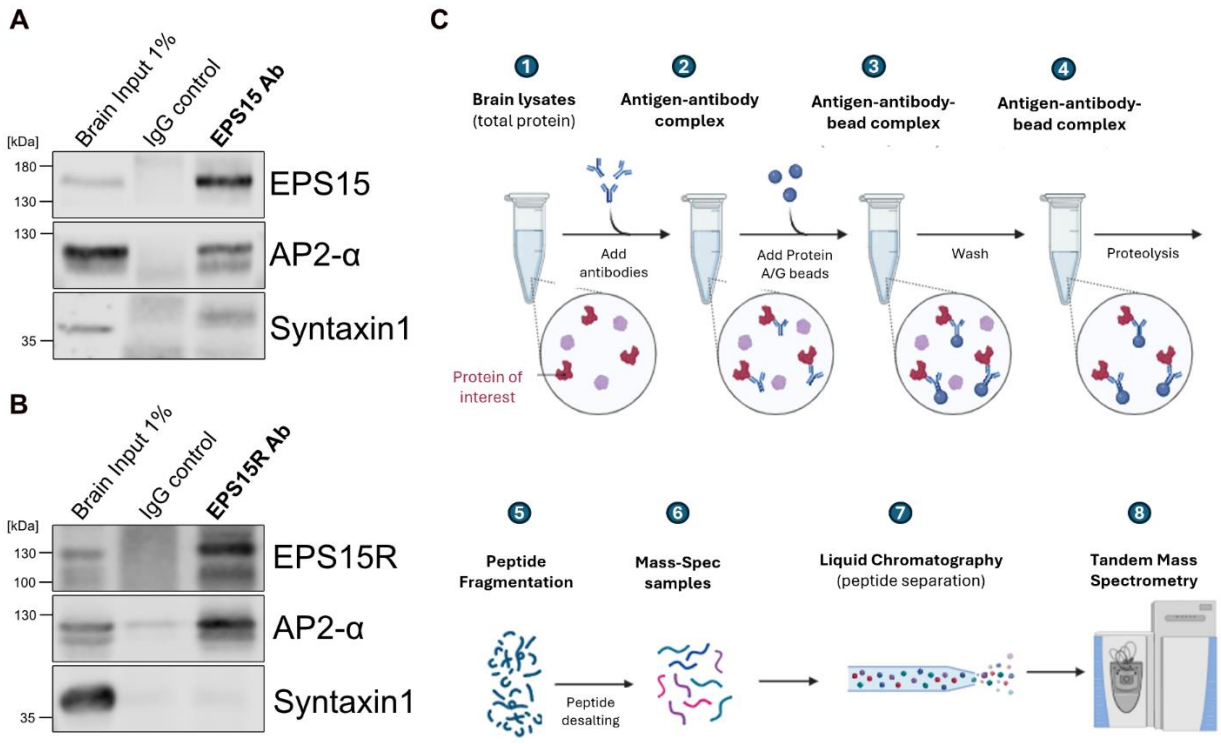

Figure 2.4 Workflow and validation of EPS15 and EPS15R co-immunoprecipitation for proteomic analysis. (A, B) Representative immunoblots showing validation of co-IP efficiency and specificity for EPS15 (A) and EPS15R (B) from adult brain lysates. Both antibodies successfully enriched the known interactor AP2-alpha, while syntaxin1 served as a negative control. Input represents 1% of total lysate. **(C)** Schematic overview of the co-IP coupled liquid chromatography (LC-MS/MS) workflow. Brain lysates from individual mice (n=4) were subjected to immunoprecipitation using antibodies against EPS15, EPS15R, or IgG as control. Protein complexes were isolated using magnetic protein A/G beads, followed by stringent washing and on-bead trypsin digestion, peptide cleanup, and LC-MS/MS analysis on a Q Exactive HF instrument.

To ensure the specificity and efficiency of the co-IP approach, the protocol was first optimized and validated using known interactors. As part of the initial validation, we demonstrated that antibodies against EPS15 and EPS15R successfully enriched the known binding partner AP2-α, while syntaxin1, a non-interacting protein, was absent from the co-precipitate (Fig. 2.4 A,B), confirming the specificity and reliability of the experimental conditions. For the mass spectrometry analysis, large scale co-IPs were performed using brain lysates from four individual mice (n = 4 biological replicates), using antibodies against EPS15, EPS15R, or IgG as a control. Protein complexes were captured using magnetic protein A/G beads, followed by a stringent washing protocol to minimize non-specific interactions. The bound proteins were digested on-bead with trypsin, and the resulting peptides were acidified, desalted using C18 stage tips, and vacuum-dried. Peptides were then reconstituted in a formic acid-containing buffer and analyzed using liquid chromatography – tandem mass spectrometry (LC-MS/MS) on a Q Exactive HF

instrument. This workflow (Fig. 2.4 C) enabled unbiased, high-sensitivity identification of protein interaction networks associated with EPS15 and EPS15R under near physiological conditions. The sample preparation for MS and subsequent proteomic data analysis were carried out with the support of Dr. Markus Räschle from the Department of Molecular Genetics at RPTU.

The resulting datasets were visualized using volcano plots to highlight significantly enriched proteins in EPS15 and EPS15R co-immunoprecipitates compared to IgG controls (Fig. 2.5 A,B). In these plots, the x-axis represents log2 fold changes in protein abundance between the specific co-IP and IgG control, indicating the degree of each enrichment, while the y-axis shows the -log10 p-value, reflecting the statistical significance of each enrichment. Proteins appearing in the upper right quadrant are therefore both highly enriched and statistically significant interactors.

As expected, both EPS15 and EPS15R were among the most strongly enriched proteins in their respective co-IP samples (highlighted in black), confirming their successful self-IP and assay robustness. Consistent with their established roles in clathrin-mediated endocytosis, both interactomes showed a significant enrichment for canonical endocytic machinery (highlighted in blue), including subunits of the AP2 complex (gene names: Ap2a1, Ap2a2, Ap2b1, Ap2s1), clathrin components (gene names: Clta, Cltb, Cltc), and other well-characterized key adaptor and scaffold proteins such as CALM, FCHo1/2, Stonin2 and Intersectins (gene names: ITSN1, ITSN2). These findings demonstrate the validity of the datasets and confirm that both EPS15 and EPS15R are central components of the endocytic protein network in the brain. Among the endocytic interactors, the strong enrichment of ITSN1 and ITSN2 is particularly noteworthy. Intersectins are well established interactors of EPS15-family proteins, functioning cooperatively in endocytic scaffolding and vesicle recycling. In Drosophila, EPS15 and its binding partner Dap160 (ITSN homolog) were shown to act together at synapses to enhance endocytic efficiency (Koh et al., 2007). In mammals, deletion of EPS15L1 results in reduced brain levels of ITSN1, suggesting mutual stabilization (Milesi et al., 2019). The robust co-enrichment of ITSNs in both EPS15 and EPS15R interactomes provides proteomic confirmation of this conserved interaction in the mammalian brain, reinforcing their central roles as coordinated scaffolds in endocytic complex assembly.

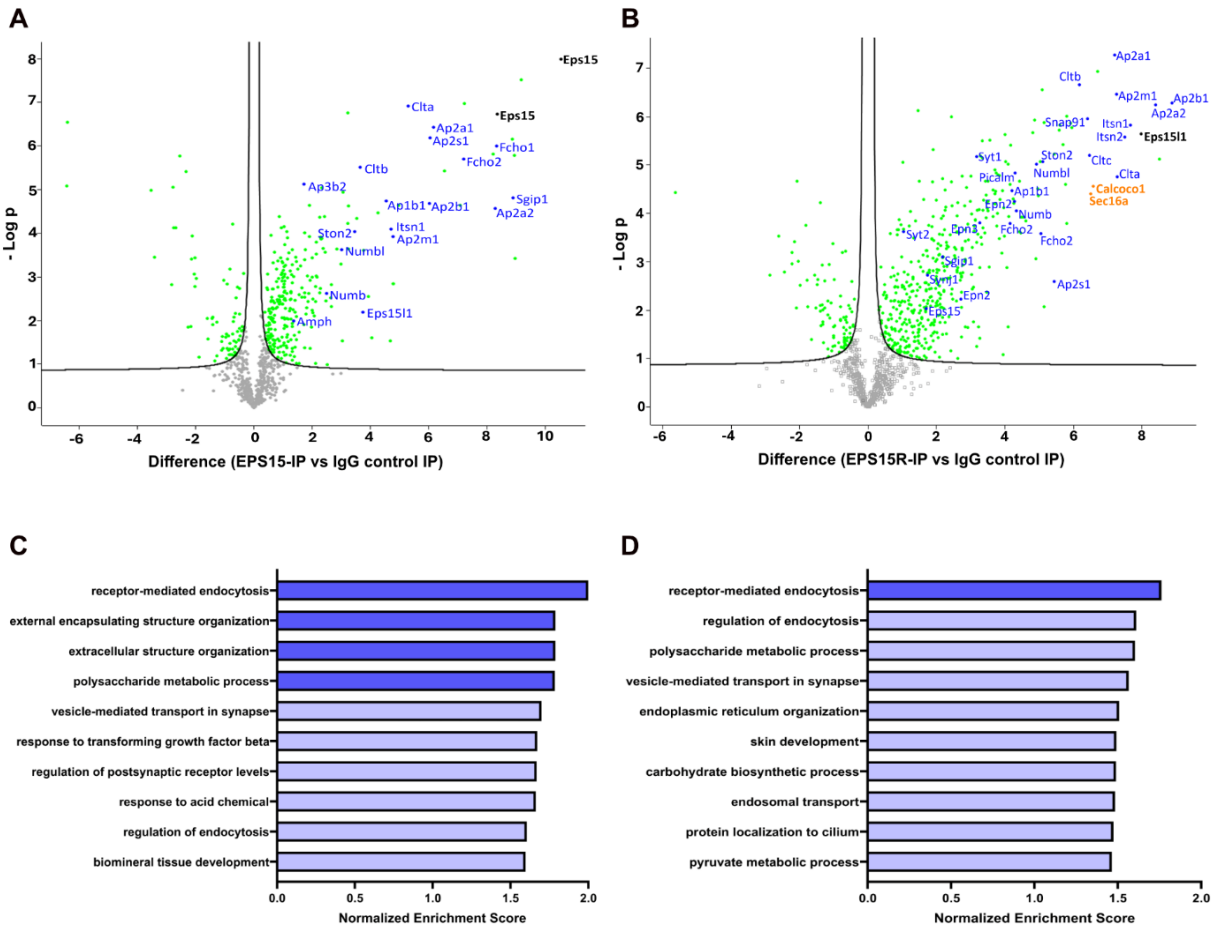

Figure 2.5 Comparative proteomic analysis of EPS15 and EPS15R interactomes reveals shared and isoform-specific protein networks. (A, B) Volcano plots depicting differential protein enrichment in EPS15 (A) and EPS15R (B) co-IPs versus IgG control co-IPs from adult mouse brain. Significantly enriched proteins ($p<0.05$, fold change>2) are shown in color. Known endocytic proteins are highlighted in blue, EPS15/15R in black, and selected novel EPS15R specific interactors in orange. **(C, D)** Gene Set Enrichment Analysis (GSEA) of significantly enriched proteins in EPS15 (C) and EPS15R (D) co-IPs using WebGestalt. Normalized enrichment scores are plotted for the top 10 enriched biological processes. Dark blue bars denote functional categories with FDR ≤0.05. While both interactomes converge on classical endocytic processes, the EPS15R dataset also shows enrichment in ER and endosomal transport pathway, suggesting broader roles in intracellular membrane dynamics.

To gain deeper insight into the functional landscape of the EPS15 and EPS1R interactomes, we performed a Gene Set Enrichment Analysis (GSEA) using the *WebGestalt* platform. This approach allowed us to identify biological processes and pathways that are statistically overrepresented among the proteins significantly enriched in each co-IP. The analysis confirmed that both EPS15 and EPS15R interactomes are strongly associated with clathrin-mediated endocytosis, synaptic vesicle trafficking, and related membrane transport processes (Fig. 2.5 C,D). Notably, endocytosis emerged as one of the top-enriched functional categories in both datasets, further supporting the core involvement of EPS15 and EPS15R in protein internalization. Among the enriched terms, those represented by darker blue bars corresponds to functional categories with an FDR (False

Discovery Rate) ≤ 0.05, indicating statistically significant enrichment after correction for multiple testing.

In the EPS15R dataset, in addition to endocytosis-related terms, several other enriched categories were linked to vesicle-mediated transport, endoplasmic reticulum and endosomal transport, supporting a broader role for EPS15R in dynamic membrane remodeling processes and intracellular transport dynamics. In contrast, the EPS15 interactome was more narrowly enriched for classical endocytosis processes, such as vesicle-mediated transport and receptor internalization, consistent with its well-established function. The additional enrichment observed in the EPS15R dataset raises the intriguing possibility that EPS15R may participate in specialized membrane trafficking pathways, potentially including roles in ER-Golgi transport or selective autophagy, as further supported by its specific novel interaction with CALCOCO1 and SEC16A shown on the volcano plot (highlighted in red) (Fig. 2.5 B, Table S1).

While these findings show a strong overlap in functional enrichment between EPS15 and EPS15R and their shared endocytic network, subtle differences hint at isoform-specific roles. These pathway-level insights complement the protein-level findings from the volcano plot analysis and provide functional validation of the proteomic dataset, particularly highlighting the functional architecture of EPS15/15R-centered interaction networks in the brain.

2.2.3 Novel EPS15R interactors suggest non-canonical roles

While both EPS15 and EPS15R are well-established components of the clathrin-mediated endocytic machinery, our proteomic screen revealed several EPS15R-specififc interactors that extend beyond classical endocytic roles. Among these, CALCOCO1 and SEC16A emerged as particularly intriguing candidates due to their strong enrichment in EPS15R co-IPs. These findings raise the possibility of a previously unrecognized link between EPS15R and alternative trafficking pathways, particularly those related to autophagy and endoplasmic reticulum (ER)-associated membrane dynamics.

CALCOCO1 is a selective autophagy receptor implicated in maintaining intracellular homeostasis by mediating the degradation of specific endomembrane compartments. It plays a critical role in ER-phagy and Golgiphagy, processes selectively targeting dysfunctional or excess portions of the ER and Golgi apparatus for lysosomal degradation (W. Chen et al., 2022; Nthiga et al., 2020a, 2021). CALCOCO1 engages with the core autophagy machinery by directly interacting with ATG8 family proteins via its LC3-interacting region (LIR), facilitating the recruitment of autophagosomal membranes to targeted ER and Golgi subdomains during selective autophagy

(Nthiga et al., 2020a). By engaging with the autophagic machinery, CALCOCO1 contributes to membrane turnover and organelle quality control, particularly under conditions of cellular stress (Nthiga et al., 2021). Through these functions it serves as a key regulator of membrane integrity and proteostasis in diverse physiological contexts, including neuronal systems (W. Chen et al., 2022).

SEC16A, on the other hand, is a large scaffold protein that plays an essential role in organizing ER exit sites (ERES) and facilitating COPII vesicle formation, thereby ensuring efficient trafficking from the ER to Golgi apparatus in the early secretory pathway (Connerly et al., 2005; Watson et al., 2006). Beyond its classical role in conventional secretion, emerging evidence has implicated SEC16A in broader membrane trafficking functions, particularly under cellular stress conditions. Under stress, SEC16A interacts with Golgi reassembly stacking proteins (GRASPs) and undergoes post-translational regulation by autophagy-initiating kinases (Joo et al., 2016, 2016; Piao et al., 2017). These findings indicate that SEC16A may function at the interface of secretory and autophagic pathways, potentially coordinating membrane dynamics during cellular stress responses.

The identification of both CALCOCO1 and SEC16A as EPS15R-specific interactors suggests that EPS15R may play an expanded role at the interface of membrane trafficking, autophagy, and ER homeostasis – potentially acting as a molecular bridge that coordinates endocytic and secretory-autophagic processes. To validate these mass-spectrometry findings, we performed co-immunoprecipitations followed by immunoblotting, confirming the physical association of EPS15R with both CALCOCO1 and SEC16A in mouse brain lysates. Antibodies against EPS15R successfully co-immunoprecipitated both CALCOCO1 and SEC16A, as visualized in the respective western blots (Fig. 2.6 A,B). In the CALCOCO co-IP blot (Fig. 2.6 A), a clear band corresponding to CALCOCO1 was detected exclusively in the EPS15R IP lane, but not in the IgG control, confirming the MS-identified interaction. AP2-α served as a positive control and was consistently enriched in EPS15R co-IPs, while syntaxin1, a membrane-associated synaptic protein not expected to bind EPS15R, was absent in the co-IP lanes, supporting the specificity of the assay. Similarly, the co-IP validation for SEC16A (Fig. 2.6 B) confirmed its presence in the EPS15R co-immunoprecipitates but not in the control co-IP. AP2-α again served as a positive control, whereas APPL1 was our negative control in this case. These results confirm that both CALCOCO1 and SEC16A are bona fide interaction partners of EPS15R in the brain and suggest a novel association of EPS15R with autophagy and ERES-related pathways.

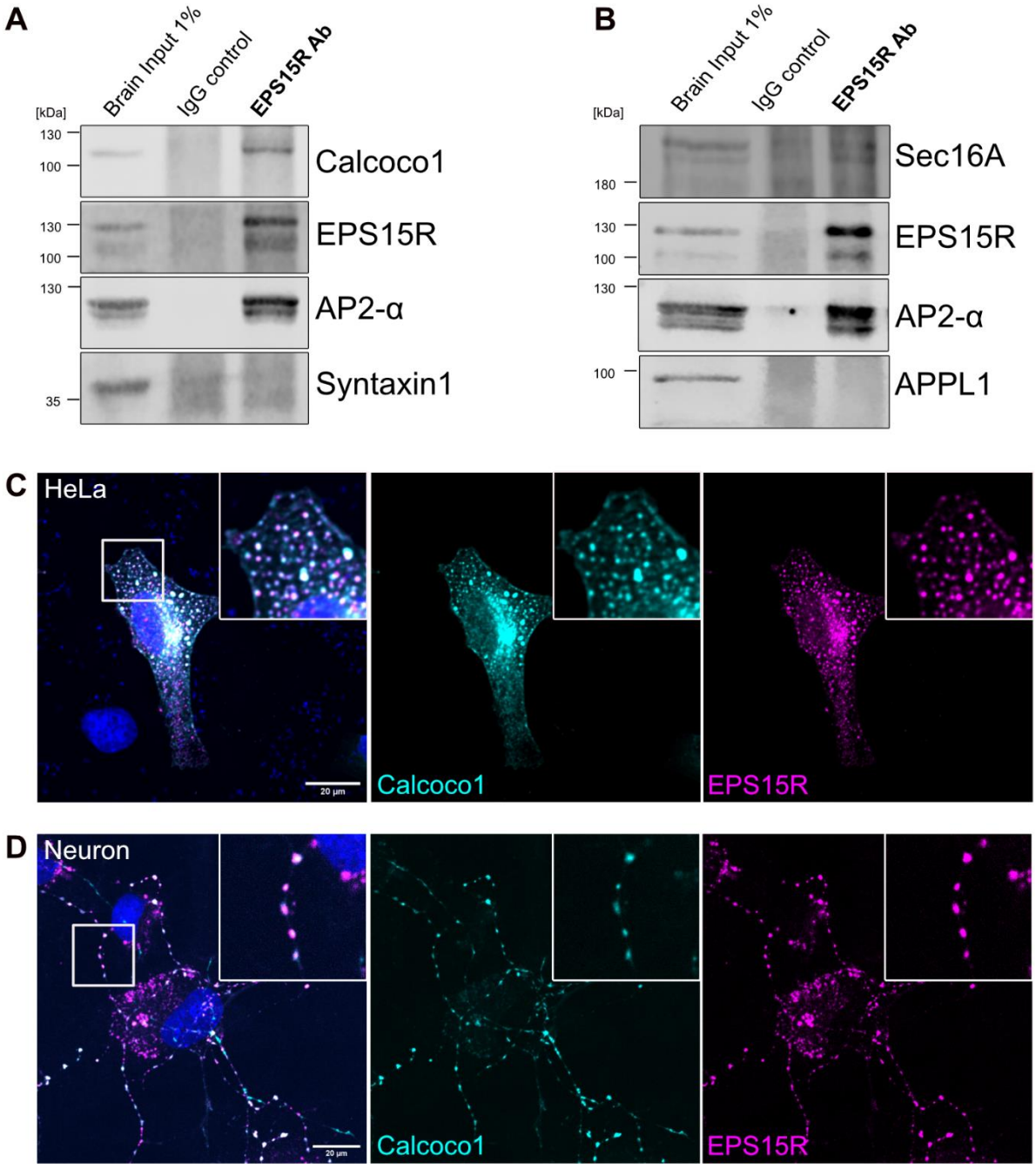

Figure 2.6 The non-canonical interactors CALCOCO1 and SEC16A potentially link EPS15R to autophagy and ER membrane dynamics. (A, B) Co-immunoprecipitation from adult mouse brain lysates using EPS15R-specific antibodies confirms the selective enrichment of CALCOCO1 (A) and SEC16A (B) in EPS15R co-IPs. AP2-alpha serves as a positive control, while syntaxin1 and APPL1 serve as negative controls, verifying specificity of these MS hits. **(C)** HeLa cells co-transfected with GFP-CALCOCO1 and RFP-EPS15R show strong co-localization of both proteins in punctate structures, indicating spatial association, as visualized by confocal microscopy. Scale bar: 20 µm. **(D)** A similar co-localization of GFP-CALCOCO1 and RFP-EPS15R puncta is observed in primary hippocampal neurons, supporting the physiological relevance of their interaction. Scale bar: 20µm. Insets show magnified views of boxed regions.

To further support the mass spectrometry and co-immunoprecipitation findings, we investigated whether EPS15R and CALCOCO1 spatially associate in cells. Since reliable antibodies for the

detection of endogenous EPS15R and CALCOCO1 by immunofluorescence were not available, we employed a co-transfection approach for expressing RFP-tagged EPS15R and GFP-tagged CALCOCO1 in HeLa cells and primary neurons. While CALCOCO1 expressed alone displayed a diffuse cytoplasmic distribution (Fig. S2), co-expression with EPS15R led to a striking redistribution into discrete punctate structures that overlapped with EPS15R (Fig 2.6 C,D). These structures resemble the liquid-liquid phase-separated condensates previously described for EPS15-family proteins, suggesting that CALCOCO1 may be actively recruited into EPS15R-positive condensates. Notably, this co-localization was not random, but rather occurred in discrete high-intensity regions, further supporting a specific and compartmentalized interaction between the two proteins. The consistent co-localization observed in both heterologous and neuronal contexts strengthens the evidence for a biologically relevant interaction. Due to the lack of a suitable plasmid, similar co-localization studies could not yet be performed for SEC16A. Together, these findings expand the functional landscape of EPS15R beyond its classical endocytic roles, positioning it as a potential integrator of membrane trafficking, autophagy, and ER-associated dynamics. The identification and validation of CALCOCO1 and SEC16A as EPS15R-specific interactors suggest novel, non-canonical roles for this adaptor protein in coordinating organelle homeostasis and stress-responsive trafficking pathways. These results open new avenues for exploring the involvement of EPS15R in neuronal quality control mechanisms and provide a foundation for future investigations into its potential contribution to autophagy-regulated neurophysiology.

2.3 Generation and characterization of EPS15 and EPS15R DKO mice

Previous studies in mammalian cell culture have suggested a neuronal role for EPS15, particularly in regulating the endocytosis of AMPA-type glutamate receptors composed of GluA1 subunits (Lin & Man, 2014). However, this observation has not been validated in vivo, thus, its physiological relevance in mammals remains unclear. In non-mammalian organisms the loss of EPS15 leads to severe neurological dysfunction (Koh et al., 2007; Majumdar et al., 2006b; Salcini et al., 2001b). While *C. elegans* mutants lacking their only EPS15 homolog EHS-1 are viable, the complete loss of EPS15 in *D. melanogaster* is lethal. Surprisingly, constitutive KO mice lacking EPS15 did not exhibit overt neurological phenotypes (Pozzi et al., 2012b), suggesting that EPS15 may not be essential for neurological function in mammals in vivo, or that its function may be compensated by a related protein such as the closely related EPS15R.

In contrast to EPS15, EPS15R appears to play a more prominent role in the mammalian nervous system. Mice lacking EPS15R are perinatally lethal dying shortly after birth (within 48 h). They also display notable neurological abnormalities, including a reduction in synaptic vesicle density and impaired nociceptive responses as assessed by tail flick assay (Milesi et al., 2019). Importantly, the simultaneous full-body deletion of both EPS15 and EPS15R results in embryonic lethality, accompanied by severe developmental defects. These findings indicate functional redundancy between the two proteins and underscore their essential role in development and an important function in the nervous system.

However, the early lethality observed in full-body DKO mouse models precludes investigations of EPS15 and EPS15R function in postnatal brain development and neuronal physiology. To overcome this limitation and to assess the roles of these endocytic adaptor proteins in the mammalian brain, we generated two different mouse models – a tissue-specific EPS15/15R DKO mouse model and an inducible EPS15/15R DKO mouse model.

2.3.1 Targeting strategy and validation of EPS15/15R dKO mice

For the generation of the DKO mouse model, exon 10 of the EPS15 gene and exon 1 of the *EPS15L1* gene were flanked by loxP sites through homologous recombination (Milesi et al., 2019). *The floxed mice were kindly provided to us by Dr. Sara Sigismund (University of Milan, Italy)*. In tissues expressing Cre recombinase, these flanked exons are excised, leading to disrupted gene expression and the loss of functional proteins. To drive Cre expression in a time- and tissue-specific manner, we used mouse lines expressing Cre under appropriate promoters.

For the tissue-specific model (eDKO), we utilized the promoter of the homeobox gene *Emx1*, which is predominantly expressed in the dorsal telencephalon of mice from embryonic stages into adulthood (Iwasato et al., 2000). To generate these mice, homozygous EPS15/15R floxed mice were crossed with Emx-1-Cre transgenic mice, resulting in selective deletion of both genes in Emx1-expressing regions (eDKO). This led to the targeted ablation of EPS15 and EPS15R in excitatory neurons of the forebrain and ependymal cells lining the brain ventricles (Fig. 2.7 A). This model system allowed us to assess the neuronal and developmental consequences of EPS15/15R loss in a region- and cell type-specific manner, without confounding effects of early embryonic lethality.

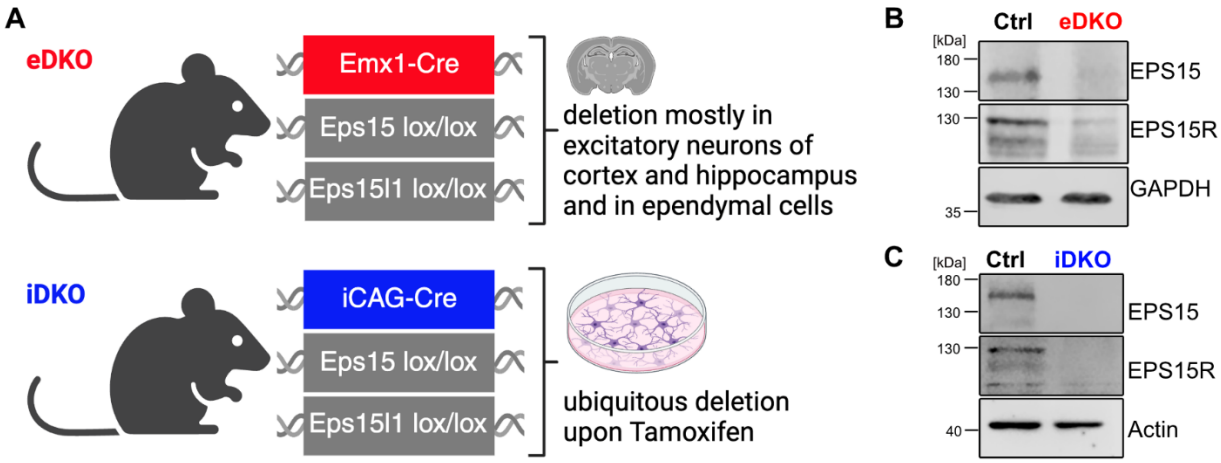

Figure 2.7 Generation and validation of EPS15/15R DKO mouse models. (A) Schematic representation of the conditional KO strategy: To allow for conditional deletion, EPS15/15R genes were flanked bx loxP sites. Tissue-specific deletion (eDKO) was accomplished by crossing floxed mice with Emx1-Cre transgenic mice, resulting in forebrain-specific recombination predominantly in excitatory neurons of the cortex, hippocampus and ependymal cells. For the generation of the inducible model (iDKO), floxed mice were crossed with iCAG-Cre mice, enabling ubiquitous EPS15/15R deletion upon tamoxifen administration in vitro. (B, C) Western blot validation of EPS15 and EPS15R deletion: (B) Immunoblot analysis of forebrain lysates from eDKO mice confirming the reduction in EPS15/15R protein levels compared to control mice (n=3). GAPDH served as loading control. (C) Immunoblot analysis of primary hippocampal cultures derived from iDKO mice and treated with tamoxifen demonstrates the efficient depletion of EPS15/15R proteins in culture. Actin served as loading control (n=4).

To generate an inducible DKO mouse model (iDKO) suitable for in vitro studies, the EPS15/15R floxed mice were crossed with iCAG-Cre transgenic mice (S. Hayashi & McMahon, 2002), expressing Cre recombinase fused to a mutated estrogen receptor under the control of the nearly ubiquitously active CAG promoter. This promoter constitutively expresses Cre recombinase which remains inactive until the addition of tamoxifen, which binds to the modified estrogen receptor, enabling nuclear translocation of Cre and subsequent recombination at loxP sites. This iDKO line

enabled culture-based studies, where primary neuronal or ependymal cell cultures derived from these mice could be induced to undergo recombination postnatally by treatment with tamoxifen (Fig. 2.7 A). This inducible system allowed us to study cell-autonomous effects of EPS15/15R loss in a controlled environment, independent of any organism-wide developmental abnormalities.

To confirm the effective deletion of EPS15 and EPS15R proteins in our DKO models, we performed immunoblot analysis. For the validation of the iDKO mouse model, primary hippocampal neurons were cultured from these mice and treated with tamoxifen to induce Cre-mediated recombination in vitro. Immunoblots of whole-cell lysates from these cultures confirmed the efficient depletion of EPS15 and EPS15R in the cultures (Fig. 2.7 C). For eDKO mice, EPS15/15R protein levels of forebrain lysates were evaluated by Western blotting. A substantial reduction of EPS15 and EPS15R levels was observed in eDKO mice compared to controls, confirming the successful in vivo deletion (Fig. 2.7 B). The residual signal detected may likely be attributed to potentially EPS15/15R expressing cell types not targeted by Emx1-Cre, such as astrocytes or interneurons, as well as potential imprecision in manual brain dissection. Nonetheless, the observed reduction in protein expression supports the successful Cre-mediated deletion of EPS15/15R in forebrain regions with active Emx1-promoter. Further validation using mass spectrometry analysis of eDKO brain tissue corroborated the loss of EPS15/15R, providing independent confirmation of their effective KO (Fig. S3).

2.3.2 In-vitro analysis of neuronal function upon EPS15/15R deletion

To explore the cell-intrinsic effects of EPS15 and EPS15R loss, we established primary neuron cultures from inducible knockout (iDKO) mice, in which gene deletion could be triggered in vitro by tamoxifen treatment. This approach enabled temporal control of EPS15/15R loss, allowing us to examine its cell autonomous effects during neuronal maturation in-vitro. By comparing control and iDKO cultures under identical conditions, we aimed to identify whether the absence of these adaptor proteins affects neuronal survival, and whether it leads to alterations in endocytic function. These in-vitro studies provided a controlled framework to investigate how neuronal physiology responds to the loss of EPS15/15R at the cellular level.

2.3.2.1 Assessment of neuronal viability in EPS15/15R iDKO cultures

Given the essential role of EPS15/15R in development and that complete loss of EPS15 and EPS15R leads to early embryonic lethality in mice, we sought to determine whether their loss in postmitotic neurons affects cell viability under homeostatic conditions. To evaluate potential changes in neuronal vulnerability to cell death, we performed a live-cell cytotoxicity assay with primary hippocampal neurons derived from EPS15/15R iDKO mice for this, we used Sytox green,

a membrane-impermeable dye that exclusively labels nuclei of dying or dead cells whose membrane is compromised, in combination with the membrane-permeable DNA dye Hoechst for general nuclei staining. This dual staining strategy enabled quantification of Sytox-positive dead cells relative to the total number of Hoechst-positive cells. Both, control and iDKO cultures, exhibited a large number of Hoechst-positive nuclei (magenta) and a lower amount of discrete Sytox signals (green) marking dead cells, with co-labelled nuclei appearing white in overlay images (Fig. 2.8 A). The proportion of Sytox-positive cells, calculated as fraction of total Hoechst-stained nuclei, was comparable between control and iDKO neuronal cultures (Fig. 2.8 B). Quantification showed no significant difference in Sytox-positive cells in iDKO cultures relative to controls. These findings suggest that EPS15/15R deletion does not impair neuronal viability these culture conditions.

2.3.2.2 Evaluating endocytic activity of EPS15/15R iDKO neurons via transferrin uptake

Given the established roles of EPS15 and EPS15R in clathrin-mediated endocytosis (CME), we sought to investigate whether their combined loss alters endocytic capacity in neurons. EPS15 family proteins have been previously implicated in transferrin receptor (TfR) uptake. However, transferrin receptor (TfR) internalization remains largely unaffected in EPS15 single knockout mouse embryonic fibroblasts (MEFs) (Pozzi et al., 2012c), likely due to functional compensation by EPS15L1. Indeed, the combined deletion of EPS15 and EPS15R in the hematopoietic system results in pronounced defects in TfR trafficking leading to aberrant retention of surface TfR and impaired erythrocyte maturation (Milesi et al., 2019). These observations highlight the redundant roles of EPS15 family proteins and prompted us to investigate whether transferrin receptor endocytosis displays a comparable dependence on EPS15/15R in neurons.

In addition, transferrin uptake is also widely used as a reliable proxy for clathrin-mediated endocytosis (CME) in general. Thus, a reduction in transferrin uptake upon loss of EPS15/15R could reflect a broad impairment of CME or a cargo-specific defect affecting TfR, while an unchanged uptake would argue against both a general CME defect and a TfR-specific uptake deficiency. We, therefore, examined transferrin uptake in control and iDKO neurons to determine whether EPS15/15R are required for efficient endocytosis of transferrin in the neuronal lineage.

Primary hippocampal neuron cultures from control and iDKO mice were incubated with fluorescently labelled transferrin at 37°C, to ensure standard uptake conditions. As a control, cells were also incubated at 4°C to prevent internalization, followed by an acid wash step to remove any

surface-bound transferrin. As expected, minimal to no fluorescence was detected at 4°C, confirming the effectiveness of surface stripping and the specificity of the assay for internalized

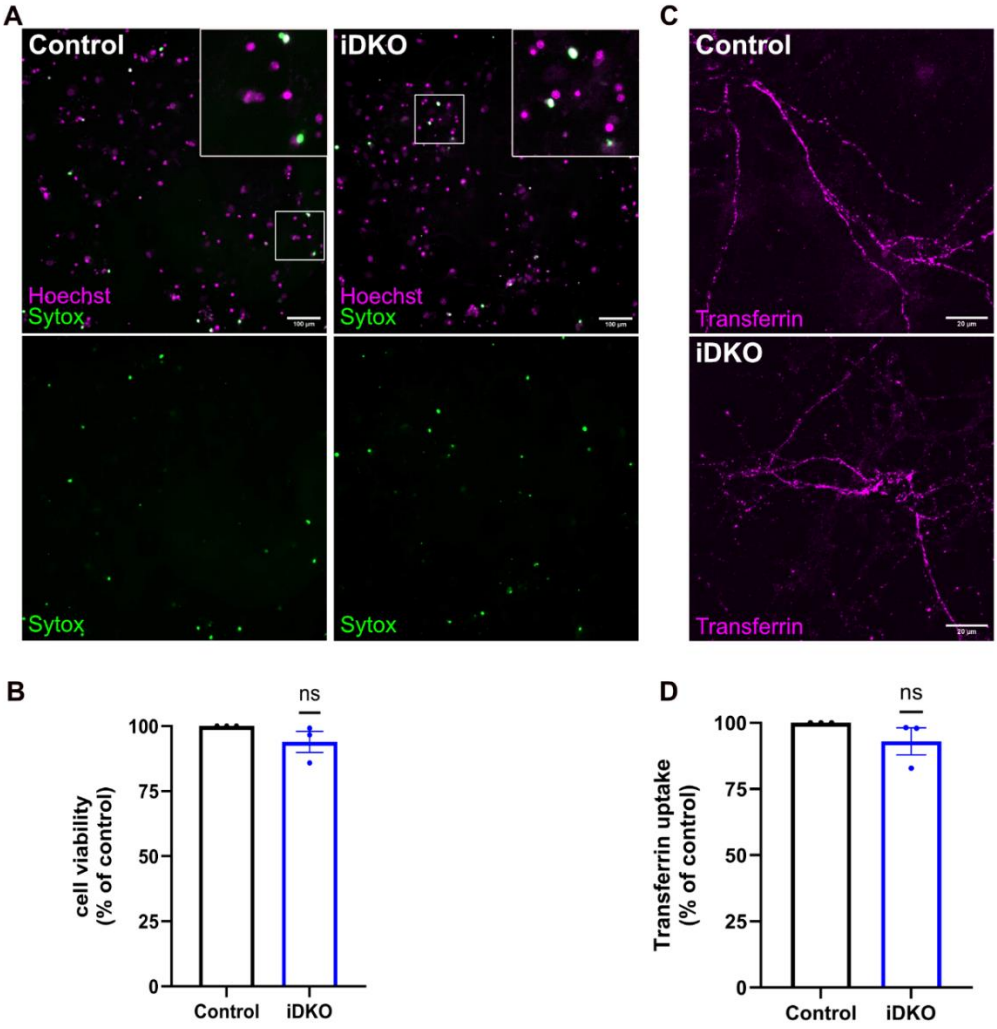

Figure 2.8 EPS15/15R deletion does not affect neuronal viability or transferrin uptake in hippocampal neurons (A) Representative live-cell images of control and EPS15/15R iDKO hippocampal neurons stained with Hoechst dye (magenta) to label all nuclei and Sytox dye (green) to mark nuclei of dead cells. The merged images (left panels) highlight co-labeled nuclei (Hoechst + Sytox) in white, indicating dying and dead cells. Insets show higher magnification of boxed regions. Scale bar: 100µm. **(B)** Quantification of Sytox-positive cells relative to Hoechst-stained cells shows no significant difference in neuronal viability between control and iDKO neurons (n=3 individual experiments; one-sample t-test performed for statistical analysis, control samples normalized to 100%) **(C)** Representative images of internalized fluorescently labeled transferrin in control and iDKO neurons following x min of incubation at 37°C. Scale bar: 20 µm. **(D)** Quantification of transferrin mean intensity normalized to control levels confirms that transferrin uptake is not significantly altered upon EPS15/15R deletion (n=3 individual experiments; one-sample t-test performed for statistical analysis, control samples normalized to 100%; data are shown as individual data points with mean ± SEM; significance levels: n.s.= non-significant).

cargo. In contrast, robust transferrin uptake was observed at 37°C in both control and iDKO neurons (Fig. 2.8 C). Our quantification of the mean intracellular fluorescence revealed no significant difference in transferrin uptake between genotypes. When normalized to control levels, iDKO neurons consistently displayed transferrin intensities close to 100% of control (Fig.

2.8 D). This indicates that EPS15/15R are not required for transferrin internalization in hippocampal neurons under basal conditions and suggests that clathrin-mediated endocytosis remains functionally intact. This observation is reminiscent of findings reported for the adaptor protein CALM, which is involved in transferrin endocytosis in erythroblasts but does not affect transferrin uptake in neurons (Azarnia Tehran et al., 2022). Such parallels highlight the cell-type specific roles of endocytic adaptor proteins and suggest that CME cargo internalization may be maintained through compensatory or redundant mechanisms in neurons.

2.3.2.3 Assessment of AMPAR endocytosis in EPS15/15R iDKO cultures

Our targeted biochemical analysis previously demonstrated (*see 2.2.1*) that EPS15R forms a protein complex with the AMPA-type glutamate receptor subunit GluA1 in adult mouse brain synaptosomes, supporting the hypothesis that EPS15R, like its paralog EPS15, may participate in postsynaptic AMPA receptor regulation. Given the reported role of EPS15 in mediating the internalization of ubiquitinated GluA1 via its ubiquitin interacting motif (UIM) (Lin & Man, 2014), and the structural and functional similarities between the two paralogs (Fig. 1.5), we sought to determine whether EPS15R similarly contributes to AMPAR endocytosis. To test this, we employed an established pHluorin-based live imaging approach to monitor surface versus internalized pools of superecliptic pHluorin (SEP)-tagged GluA1 in primary hippocampal neurons. This method relies on the pH-sensitive GFP variant pHluorin that is fluorescent at neutral extracellular pH indicating the surface pool, quenched upon acid exposure revealing background fluorescence, and unquenched by alkaline solution to reveal the total pool of tagged receptors (Fig 2.9 A). Using this assay, we assessed GluA1 trafficking dynamics in both control and EPS15/15R iDKO neurons to evaluate whether EPS15R loss alters constitutive AMPA receptor internalization. *This experiment, including imaging, data generation, and analysis, was kindly performed by Dr. Domenico A. Tehran*.

Live-cell imaging of SEP-GluA1 transfected hippocampal neurons revealed a significant increase in the surface pool of GluA1 in EPS15/15R iDKO cultures compared to controls (Fig. 2.9 B). In control neurons, approximately 35-40% of total GluA1 fluorescence was attributed to surface-localized receptors, consistent with ongoing internalization. In contrast, iDKO neurons exhibited markedly elevated surface GluA1 levels, exceeding 60% of the total signal, suggesting a decrease in basal GluA1 AMPA receptor endocytosis upon EPS15/15R loss. This phenotype is consistent with earlier findings that knockdown of EPS15 impairs GluA1 internalization (Lin & Man, 2014). Our data extend this observation by implicating EPS15R in the same trafficking process,

supported by our co-immunoprecipitation evidence showing an interaction between EPS15R and GluA1 in brain synaptosomes.

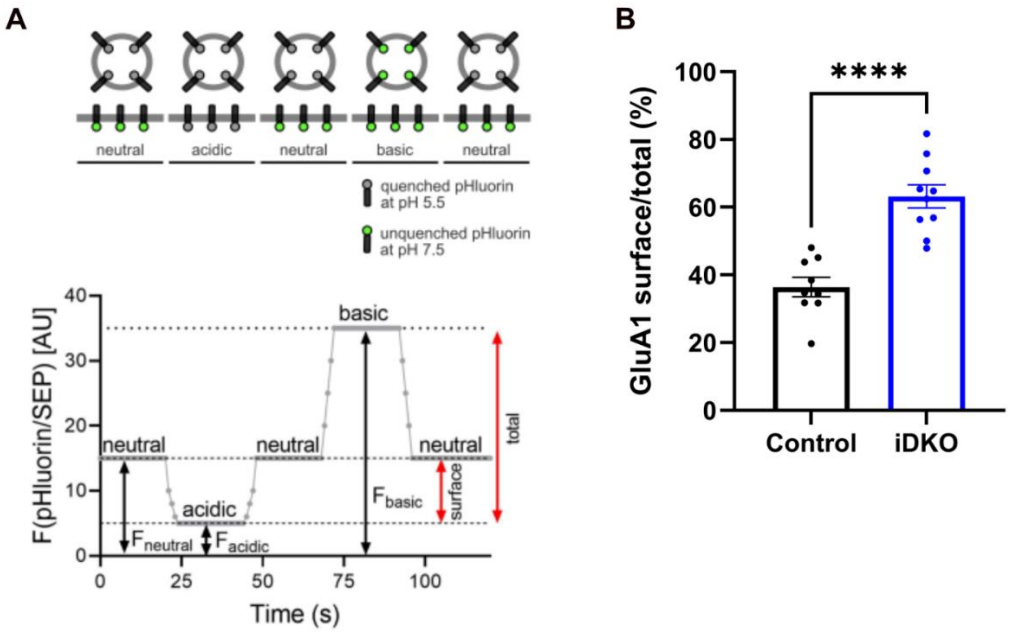

Figure 2.9 pHluorin imaging reveals defective AMPAR internalization in EPS15/15R-deficient hippocampal neurons. (A) Schematic representation of the acid–base quenching protocol used to assess SEP-tagged protein localization. At neutral pH, surface-exposed pHluorin remains fluorescent. Exposure to acidic buffer selectively quenches this surface signal. A neutral wash restores baseline conditions before a final basic buffer containing ammonium chloride is applied to reveal the full pHluorin-labeled receptor pool. Image adapted from (Azarnia Tehran et al., 2022). **(B)** Quantification of SEP-GluA1 surface-to-total ratio from live-cell pHluorin imaging reveals significantly increased surface GluA1 levels in EPS15/15R iDKO neurons compared to controls (control n=9, eDKO n=10 neurons; unpaired t-test was performed). (Data are shown as individual data points with mean ± SEM; significance level: ***=p< 0.001). *Data provided by Dr. Domenico A. Tehran.*

However, since our iDKO model involves the simultaneous deletion of both EPS15 and EPS15R, we cannot definitively attribute the observed defect to one paralog over the other. Very likely the two proteins perform redundant functions in regulating AMPAR endocytosis. Moreover, the role of ubiquitin in mediating GluA1 internalization in this context was not directly tested in the current assay. Further studies will be needed to determine whether, EPS15R, like EPS15, mediates AMPAR trafficking via its UIMs and to dissect the individual contribution of EPS15R and EPS15. Together, these findings support a role for EPS15 family proteins in controlling the internalization of GluA1-containing AMPARs and highlight potential mechanistic parallels in their regulation of postsynaptic receptor dynamics.

2.3.3 In vivo analysis of phenotypic consequences of EPS15/15R deletion

To investigate the broader physiological and developmental consequences of combined EPS15 and EPS15R loss, we employed an EMX1-Cre-based forebrain-specific knockout (eDKO) model in which gene deletion occurs during embryonic development in dorsal telencephalic regions (*see 2.3.1*). This in vivo approach allowed us to examine how the absence of these adaptor proteins affects forebrain development and function within an intact organismal context. By comparing control and eDKO animals, we aimed to assess the impact of EPS15/15R deletion across multiple levels of brain organization. These in vivo studies complement our in vitro findings and provide insights into how loss of EPS15/15R influences neuronal development at the morphological and behavioral level.

2.3.3.1 Growth deficits and early mortality of EPS15/15R eDKO mice

To assess the viability and inheritance pattern of the eDKO mouse line, we monitored the genotype distribution from heterozygous intercrosses. Our analysis of offspring revealed that mice of the different genotypes were born in ratios consistent with Mendelian inheritance. In this breeding scheme EPS15 is always floxed (lox/lox), while EPS15R is either heterozygously floxed (lox/-) or homozygously floxed (lox/lox) and their knockout is Cre-dependent. Based on this breeding scheme and the ratios predicted by the rules of Mendelian inheritance, 50% of the offspring were expected to be Cre-negative controls ($EPS15^{lox/lox}$ / $EPS15R^{lox/lox\ or\ lox/-}$ / Cre–), 25% EPS15 KO ($EPS15^{lox/lox}$ / $EPS15R^{lox/-}$ / Cre+), and 25% EPS15/15R double knockout ($EPS15^{lox/lox}$ / $EPS15R^{lox/lox}$ / Cre+). The observed distribution was 48% controls, 29.9% EPS15-KO and 21.9% eDKO (Fig. 2.10 A) with chi-square analysis showing no significant change, indicating that forebrain-specific deletion of EPS15/15R does not result in embryonic lethality. This contrasts with the early embryonic lethality seen in constitutive whole-body EPS15/15R DKO mice, demonstrating that forebrain-specific loss of these proteins is compatible with survival through embryogenesis.

Although eDKO mice were viable at birth and phenotypically indistinguishable from their littermates, they exhibited both increased postnatal mortality and growth impairments. Survival analysis revealed a marked reduction in survival probability in EPS15/15R dKO mice over the course of the first two postnatal months, with approximately 36% of eDKO mice dead by postnatal day 60 (P60) (Fig. 2.10 B,C), indicating a juvenile-onset lethality phenotype. In contrast, the EPS15 KO mice exhibited survival rates comparable to WT control littermates, with no significant mortality observed over the same period.

In addition to reduced survival, eDKO mice displayed growth impairments that became increasingly apparent over time (Fig. 2.10 D). At postnatal week 4, the body weight of eDKO mice was approximately 14% lower than that of their control littermates (Fig. 2.10 E). By week 8, this difference remained around 11%. However, the accuracy of this measurement may be negatively influenced by the reduced number of surviving eDKO mice at this point. Notably, EPS15 KO mice maintained a body weight similar to controls. These findings demonstrate that loss of EPS15R, but not EPS15, impairs postnatal growth and survival, highlighting the critical role for EPS15R in maintaining postnatal development and long-term survival.

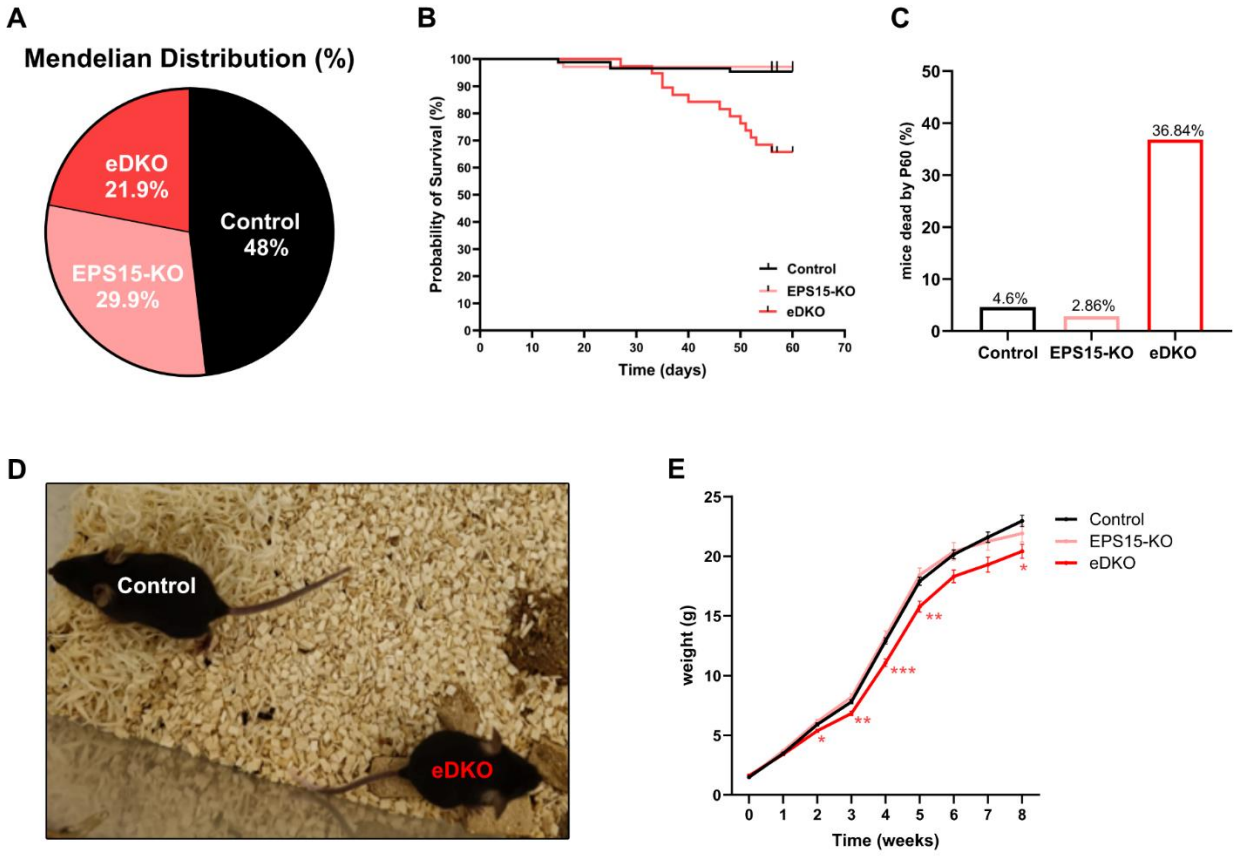

Figure 2.10 EPS15/15R eDKO mice show growth deficits and increased mortality. **(A)** The Mendelian distribution of genotypes from heterozygous intercrosses shows no significant deviation from expected ratios (statistical evaluation via χ^2 test: n.s = non-significant). **(B, C)** The analysis of the probability of survival and the quantification of mortality reveals juvenile-onset lethality in eDKO mice, with ~36% being dead by postnatal day 60 (P60), while the survival of EPS15 KO and control mice remains unaffected. (N: control=87, EPS15-KO=70, eDKO=38) **(D,E)** Representative image of two littermate mice of the indicated genotypes and growth curves demonstrate reduced postnatal weight gain in eDKO mice, with significantly lower body weight from week 2 onwards compared to control littermates (N at start: control=76, EPS15-KO=29, eDKO=31; N at end: control=36, EPS15-KO=16, eDKO=10; statistical evaluation via Two-way repeated measures ANOVA: mixed-effects model with REML and Geisser-Greenhouse correction and Šídák's multiple comparisons test) (significance levels: n.s.= non-significant, *=p<0.05, **=p<0.01, ***=p< 0.001).

2.3.3.2 Neurological and behavioral abnormalities in EPS15/15R eDKO mice

The eDKO mice were observed in their home cages post-weaning, i.e. at ~3-4 weeks of age, for behavioral and neurological abnormalities. A subset of mice (~30%) exhibited spontaneous epileptic seizures, including tonic-clonic convulsions (Fig. 2.11 A). Most of these episodes were transient with the mice resuming normal activity within a few minutes. However, it is plausible that more severe seizures might contribute to the increased mortality observed in the eDKO mice. Although this remains speculative. The direct cause of death in eDKO mice which were found dead without prior signs of ill health is yet to be determined and requires further investigation.

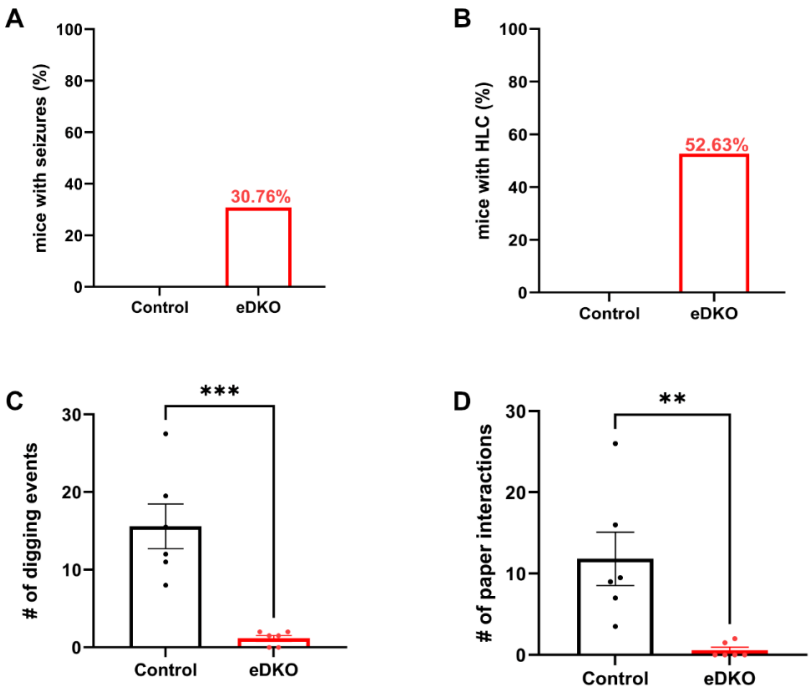

Figure 2.11 EPS15/15R eDKO mice exhibit neurological deficits. (A) Seizure frequency observed in eDKO mice indicates that ~30% of animals exhibit spontaneous tonic-clonic seizures post-weaning (control n=22, eDKO n=26, observation post-weaning at age ~P30). **(B)** Hindlimb clasping (HLC), a stereotypic neurological phenotype, is observed in ~52% of eDKO mice upon tail suspension at age P30, suggesting neurological deficits (control n=18, eDKO n=19). **(C, D)** Quantification of exploratory behaviors shows significant reduction in spontaneous digging events and paper interaction in eDKO mice compared to controls, indicating impaired motor function and/or motivation (control n=6, eDKO n=6; statistical evaluation by unpaired t-test; data are shown as individual data points with mean ± SEM; significance levels: **=p<0.01, ***=p< 0.001).

In addition to seizure activity, approximately 52% of eDKO mice exhibited hindlimb clasping when suspended by the tail – a stereotyped neurological phenotype characterized by inward limb retraction rather than normal extension reflex (Fig. 2.11 B, S4). Hindlimb clasping is commonly observed in various mouse models of neurodegeneration and neurodevelopmental disorders, including autism spectrum disorders (ASDs) and Alzheimer's disease (Chao et al., 2010; Gemelli et al., 2006; Schmeisser et al., 2012), and has also been reported in mice lacking the endocytic

adaptor AP180 (Koo et al., 2015b), suggesting shared pathological features. Behavioral alterations were also evident during routine cage observations. eDKO mice displayed reduced spontaneous activity, characterized by a decreased interaction with paper and decreased digging behavior (Fig. 2.11 C,D). These behaviors are commonly used as proxies for motor activity and exploratory drive in rodents. These findings suggest impairments in motor coordination and/or motivation, consistent with underlying neurological deficits.

2.3.3.3 EPS15/15R eDKO mice exhibit ventriculomegaly and signs of hydrocephalus

Given the observed neurological impairments and behavioral abnormalities, including the hindlimb clasping phenotype and seizures, we hypothesized that EPS15/15R might be critical for normal brain development and structural integrity. To assess brain-wide morphological consequences of EPS15/15R deletion, we performed a comparative analysis of Nissl-stained coronal brain sections from age-matched control and eDKO mice at postnatal day 30 (P30). This approach enabled the systematic evaluation of neuroanatomical changes across major brain regions following forebrain-specific loss of our endocytic adaptor proteins.

Nissl-stained coronal sections from P30 control and eDKO brains revealed a consistent enlargement of the lateral ventricles (LVs) in eDKO mice. For quantitative analysis, anatomically matched sections (Bregma 0.14 to 0.02 mm) were analyzed, demonstrating a notable increase in LV size in eDKO mice compared to controls. While control values ranged from 0.24mm^2 to 1.58 mm^2, LV areas in eDKO brains ranged from 1.00 mm^2 to 2.80 mm^2 (Fig. 2.12 A,B). Notably, the values varied more than sixfold across controls, whereas eDKO brains consistently exhibited larger ventricles with a relatively narrower range. Thus, despite inter-individual variation, it was evident that eDKO mice showed a robust enlargement of the lateral ventricles at this anatomical level. To determine whether this enlargement was regionally confined or reflected a global change, cumulative LV areas were calculated across matched sections along the rostro-caudal axis (Bregma -0.10 to 1.8 mm). In control animals, the summed LV area ranged from 0.86 mm^2 to 5.80 mm^2 (mean: 3.47 mm^2), whereas in eDKO mice it ranged from 2.57 mm^2 to 18.39 mm^2 (mean: 6.68mm^2). Despite notable inter-individual variability within the eDKO group, statistical analysis revealed a significant increase in cumulative LV area compared to controls (Fig. 2.12 C). These findings support the presence of ventriculomegaly in the absence of EPS15/15R, potentially indicative of an early or partial form of hydrocephalus. This interpretation is further supported by the occasional presence of dome-shaped cranial deformation in eDKO animals (Fig. 2.12 D), reminiscent of established hydrocephalus models. However, further analysis is required to confirm

the robustness of this observation and determine the frequency of dome-shaped heads in eDKO mice.

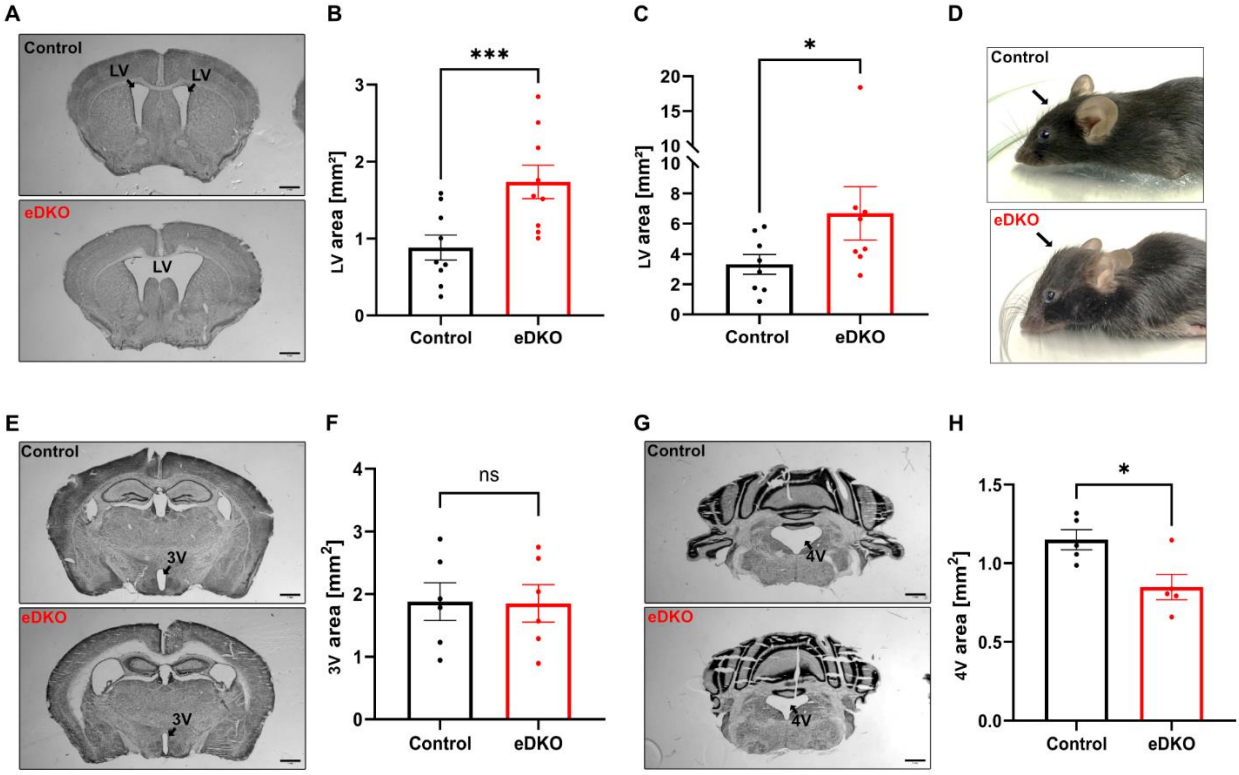

Figure 2.12 EPS15/15R loss causes gross morphological changes in brain and ventriculomegaly. (A) Representative Nissl-stained coronal sections from P30 control (top) and eDKO (bottom) brains showing marked dilation of the lateral ventricles (LV). **(B)** Quantification of LV area from anatomically matched coronal sections reveals significantly increased LV size in eDKO animals (n = 9 per genotype; paired t-test). **(C)** Cumulative LV area summed across matched sections along the rostro-caudal axis is also significantly increased in eDKO mice (n = 8 per genotype; Wilcoxon matched-pairs signed rank test) **(D)** Image of an eDKO mouse (bottom) displaying a dome-shaped skull (arrow), a phenotype commonly associated with hydrocephalus; control animal shown above. **(E)** Representative coronal sections showing comparable 3V morphology in control and eDKO brains. **(F)** Quantification of cumulative third ventricle (3V) area reveals no significant difference between genotypes (n = 6 per genotype; paired t-test). **(G)** Corresponding Nissl-stained sections showing 4V size difference between control and eDKO mice. **(H)** Fourth ventricle (4V) area from single matched sections at the cerebellar-hindbrain junction, is significantly reduced in eDKO mice (n = 6 per genotype; paired t-test; data are shown as individual data points with mean ± SEM; significance levels: ns= non-significant, *=p<0.05, ***=p< 0.001).

To assess whether ventricular enlargement in eDKO mice was restricted to the lateral ventricles or affected the entire ventricular system, we next examined the third ventricle (3V) and fourth ventricle (4V), given the anatomical continuity of the brain ventricular network. For 3V analysis, ventricle area was quantified from coronal sections within the third ventricle axis (Bregma -0.22 to -02.54 mm). For 4V analysis, a single matched section per animal was selected at the cerebellar-hindbrain junction. Quantitative analysis revealed no appreciable difference in the third ventricle size between genotypes: the control group exhibited a mean 3V area of 1.87 mm^2, while eDKO mice displayed a comparable mean of 1.85 mm^2, indicating that the third ventricle remains

unaffected (Fig. 2.12 E,F). In contrast, the fourth ventricle showed a modest but statistically significant reduction in eDKO animals (mean: 0.84 mm^2) compared to controls (mean: 1.15 mm^2) (Fig. 2.12 G,H). However, these results should be interpreted with caution as 4V measurements were derived from single matched slices, and cumulative volume estimates could not be obtained.

Together, these results demonstrate that EPS15/15R loss leads to alterations in the ventricular system comprising a ventricular enlargement of the lateral ventricles, while sparing the third ventricle, and a possible reduction of the fourth ventricle. This region-specific ventriculomegaly, coupled with dome-shaped cranial deformities in a subset of animals, is consistent with a form of obstructive or partial hydrocephalus. The absence of 3V enlargement argues against a communicating hydrocephalus. Instead, the increase of LV area and potential reduction in 4V size may suggest a localized impairment of CSF flow, potentially due to developmental alterations affecting the cilia-driven movement of the CSF or ventricular patency. These findings highlight a critical role for EPS15/15R in maintaining ventricular integrity and cerebrospinal fluid homeostasis, warranting further investigations into underlying mechanisms.

2.3.3.4 Impaired hippocampal lamination in eDKO mice

To evaluate the impact of EPS15/15R loss on hippocampal architecture, we first examined Nissl-stained coronal sections. The hippocampus in eDKO mice exhibited a visible structural disorganization with distorted overall morphology compared to controls. The cellular architecture of both, dentate gyrus (DG) and cornu ammonis (CA) regions, appeared disrupted, with neurons failing to form the densely packed, well laminated layers typically observed in control mice (Fig. 2.13 A). Instead, cells in these regions were more diffusely distributed, suggesting impaired hippocampal organization potentially due to underlying developmental defects.

To further assess the disrupted hippocampal architecture observed in Nissl-stained sections, we performed high-resolution immunohistochemical analysis using nuclear staining to visualize the layering pattern across hippocampal subregions. In control mice the DG and CA regions (CA1-CA3) exhibited the characteristic well-organized laminar structure, with tightly packed granule respectively pyramidal cell layers. In contrast, eDKO mice displayed pronounced lamination abnormalities across all examined hippocampal subfields. The DG displayed an altered morphology, characterized by less densely packed neurons and an irregular granular cell layer with less defined boundaries. Similarly, the CA1 region while still discernable exhibited loss of a sharply laminated pyramidal layer, with neurons appearing dispersed and misaligned. The disorganization became more pronounced in CA2 and CA3 subfields, where the pyramidal cell layer exhibited overt dispersion and loss of laminar integrity (Fig. 2.13 B).

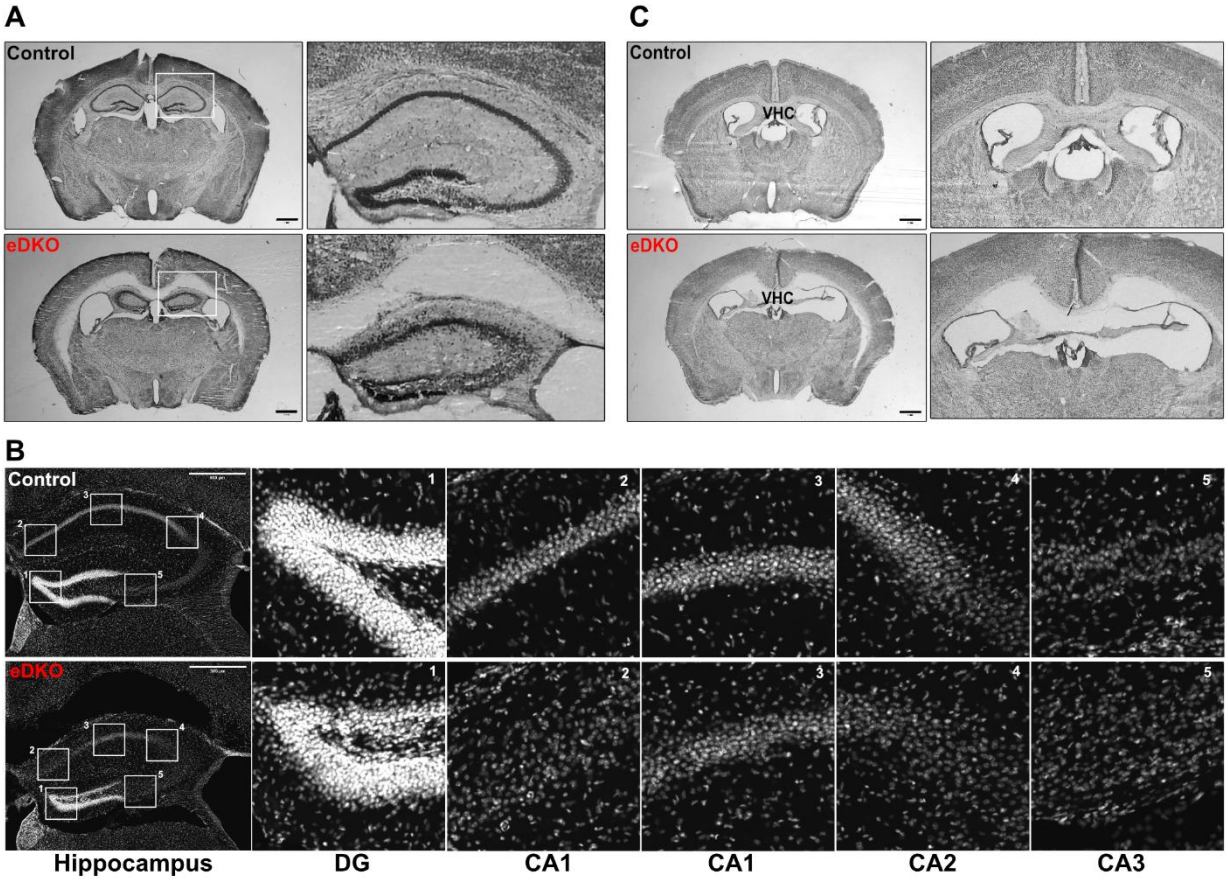

Figure 2.13 EPS15/15R loss disrupts hippocampal architecture and connectivity. (A) Representative Nissl-stained coronal brain sections from P30 control and eDKO mice showing overall brain morphology (left) and hippocampal structure at higher magnification (right). Hippocampal sections from eDKO mice display disrupted lamination indicative of underlying structural abnormalities. Scale bar, 50 µm. **(B)** DAPI-stained coronal hippocampal sections from p30 control and eDKO brains. Insets (1-5) show zoomed-in views of the dentate gyrus (DG) and CA1-CA3 subfields. While control mice display a well-defined laminar architecture, eDKO mice exhibit disorganized layering patterns with diffusely distributed neurons across all the subfields. Images were acquired using a 20x objective and stitched to reconstruct the full hippocampal structure. Scale bar, 500 µm. **(C)** Representative Nissl-stained coronal sections at the level of the ventral hippocampal commissure (VHC), with right panels showing magnified views of the VHC region. eDKO mice exhibit visibly reduced commissural structures in eDKO mice (see also Fig. S5). Scale bar, 50 µm.

We next assessed interhemispheric connectivity by analyzing the ventral hippocampal commissure (VHC), a major fiber tract connecting the bilateral hippocampi. In eDKO mice the VHC appeared visibly damaged (Fig. 2.13 C) or reduced (Fig. S5 A) in size compared to controls. Subsequent analysis and quantification of serially sectioned brain slices revealed a significant decrease in the cumulative area of the VHC in eDKO. While the mean VHC area in control animals was 2.99 mm^2, it was markedly decreased to 1.67mm^2 in eDKO mice (Fig. S5 B), indicating a partial loss of commissural projections. This suggests that EPS15/15R may play a role in the development or maintenance of long-range hippocampal connectivity. Together, the hippocampal lamination defects and VHC hypoplasia suggest that EPS15/15R might be required for the proper

positioning of hippocampal neurons as well as for the establishment or maintenance of long-range hippocampal connectivity, supporting a role for these endocytic adaptor proteins in brain development.

2.3.3.5 Cortical lamination defects in eDKO mice

To further investigate potential neuroanatomical changes resulting from loss of EPS15/15R, we extended our analysis to the neocortex, focusing on the organization of cortical layers. Given the observed laminar disorganization and layering defects in the hippocampus, we hypothesized that cortical development may also be perturbed in eDKO mice. To assess cortical lamination, we performed immunohistochemical analyses using layer-specific transcription factors as markers: CTIP2, which mostly labels deep layer V sub-cerebral projecting neurons (Arlotta et al., 2005), and TBR1, which preferentially marks layer VI corticothalamic neurons (Hevner et al., 2001). The superimposed labelling of CTIP2 and TBR1 enabled a comprehensive assessment of cortical layers since all layers except layers II-IV could thereby be differentiated from each other, allowing the simultaneous evaluation of laminar positioning and the relative distribution of distinct neuronal populations in age-matched P30 control and eDKO brains.

In control animals, TBR1 expression was most prominent in layer VI as expected, with reduced intensity in layer V and sparse signals in layer II-IV. CTIP2, by contrast, showed strong enrichment in layer V, weak expression in layer VI, and was virtually absent from upper layers. As expected, layer I was largely devoid of neuronal cell bodies. This combined staining approach facilitated a clear delineation of cortical laminae and enabled morphometric analyses (Fig. 2.14 A). Our quantification revealed that eDKO cortices exhibited layer-specific alterations in thickness: layer I was significantly thinner, whereas layer VI ($TBR1^+$) was significantly expanded compared to controls. No significant difference was observed in layer V ($CTIP^+$), while layers II-IV showed a tendency towards increased thickness in eDKO, which may reach statistical significance with a larger sample size (Fig. 2.14 B). Additionally, when the total thickness of the cortex (sum of all layers) was compared, eDKO cortices showed a non-significant trend toward increased overall thickness relative to controls, which might also become significant upon further sampling. These findings suggest that EPS15/15R is required for proper cortical layer formation, particularly influencing the organization of the outermost and innermost layers, potentially due to disrupted neuronal migration or impaired early neurogenesis.

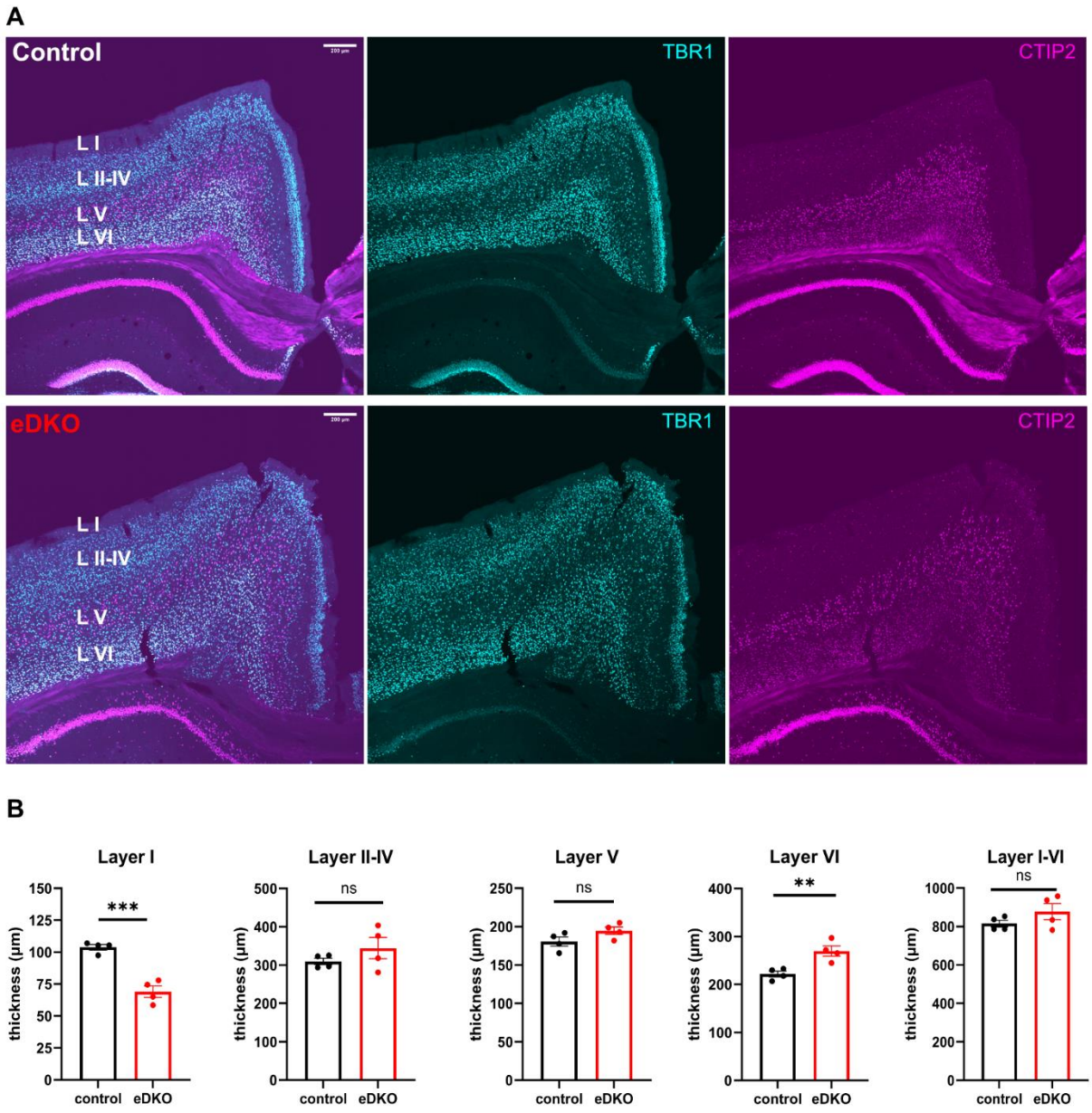

Figure 2.14 EPS15/15R loss alters cortical layers. (A) Immunofluorescent staining for CTIP2 (magenta, marker for layer V) and TBR1 (cyan, marker for layer VI) on coronal sections reveals differences in the thickness of cortical layers LI and LVI in eDKO brain compared to control brain. Whole images captured at 20x were stitched. Scale bar, 500 µm. **(B)** Quantification of cortical layer thickness. Layer I is significantly thinner and layer VI significantly thicker in eDKO mice. Layers II-IV and V show no significant differences. Total cortical thickness (LI-VI combined) shows a non-significant trend toward increased size in eDKO (n = 4 per genotype; paired t-test; data are shown as individual data points with mean ± SEM; significance levels: ns=non-significant, **=p<0.01, ***=p< 0.001).

2.4 Exploring mechanisms underlying EPS15/15R-driven brain pathologies

Following the identification of a spectrum of pronounced anatomical and neurological abnormalities in EPS15/15R eDKO mice – including ventriculomegaly, disrupted hippocampal and cortical organization, seizures, hindlimb clasping, and other behavioral changes – we next aimed to uncover the underlying mechanisms contributing to these phenotypes, focusing on the morphological brain alterations. To this end, we employed a multifaceted experimental approach combining histological, immunohistochemical, and biochemical analyses, alongside targeted anatomical and cellular investigations. These complementary strategies were designed to probe potential disruptions in key developmental and homeostatic processes, such as neuronal migration, neurogenesis, and ventricular integrity including ependymal cell differentiation and ciliogenesis. The following sections detail our efforts to dissect the cellular and molecular basis of the major phenotypes observed in EPS15/15R eDKO mice.

2.4.1 Mechanistic basis of lamination defects in eDKO brain

The pronounced disruption of hippocampal lamination and the alteration in cortical layering observed in EPS15/15R-deficient mice prompted us to further investigate the underlying cellular mechanisms. The presence of diffusely distributed neurons, the loss of compact laminar organization, and the abnormal thickness of specific cortical layers suggest perturbations in key neurodevelopmental processes in EPS15/15R-deficient mice. In particular, defects in neuronal layering can result from alterations in neurogenesis, impairments in neuronal migration, or disruption of the radial glial scaffold, which plays a critical dual role in progenitor maintenance and as a structural guide for migrating neurons. To elucidate the potential contribution of these processes to the lamination defects observed in eDKO mice, we conducted a targeted analysis of progenitor status, neuronal maturation, and laminar identity within the dentate gyrus. These analyses were aimed at determining whether abnormal neuronal positioning in eDKO mice reflects defects in cell generation, migratory capacity, or radial glial integrity – thereby providing mechanistic insights into the likely developmental origin of the observed structural abnormalities. In addition, we sought to explore whether specific signaling pathways known to regulate laminar organization and neuronal positioning might be affected in absence of EPS15/15R.

2.4.1.1 Disruption of radial glial scaffolding and neuronal maturation in the dentate gyrus

The establishment of proper hippocampal development relies on tightly regulated neurogenesis and the proper maturation and positioning of newly generated neurons based on a well-organized radial glial cell scaffold. The dentate gyrus (DG) is one of the few brain regions where neurogenesis and migration of immature neurons continues into postnatal adult life (Altman & Das, 1965; Cameron et al., 1993b; Kaplan & Hinds, 1977). In this region, radial glial cells (RGCs) located in the sub-granular zone (SGZ) serve dual roles as neural stem/progenitor cells and as structural scaffold for guiding migration of newborn neurons into the granule cell layer (GCL) (Palmer et al., 1997). This process not only depends on cell-intrinsic regulatory programs and extracellular signals, but also on the organization and polarity of RGCs. Any disruptions in either the proliferative behavior of progenitors or the integrity of the radial scaffold can result in lamination defects and long-lasting cytoarchitectural disorganization.

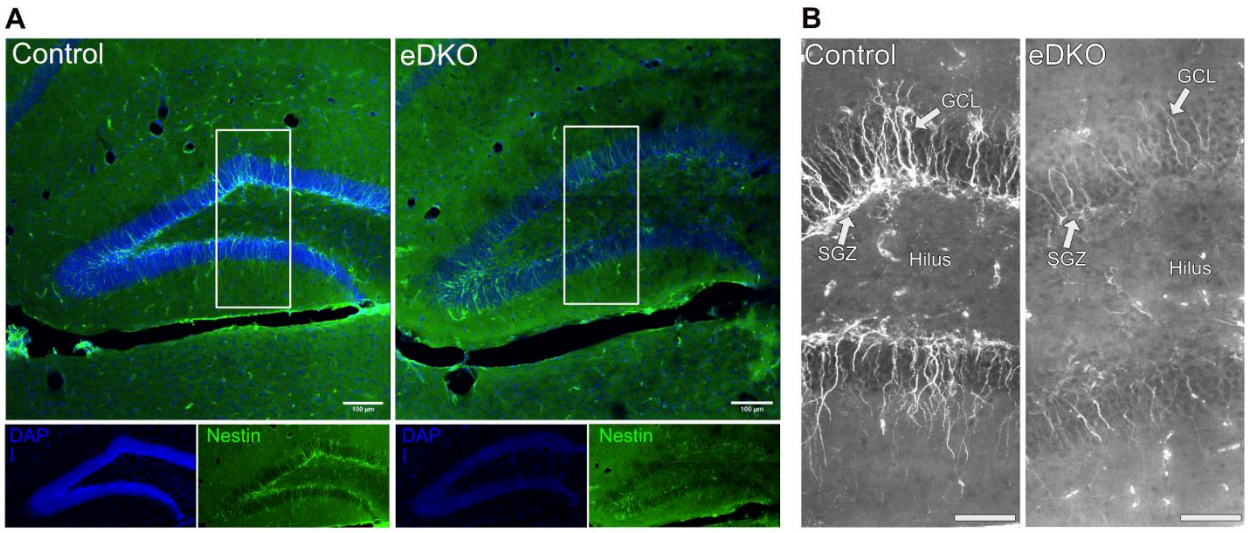

Figure 2.15 Disruption of radial glial scaffold organization in the dentate gyrus of EPS15/15R eDKO mice. **(A)** 40 µm thick coronal brain slices of 30 days old control and eDKO mice were stained with Nestin-specific antibodies and with the DNA stain DAPI. Representative confocal images of Nestin (green) and DAPI (blue) staining in the dentate gyrus of control and eDKO mice. In control animals, Nestin-positive processes are radially aligned and reach from the sub-granular zone (SGZ) to the granule cell layer (GCL). In eDKO mice, Nestin-positive processes appear disorganized and misaligned, with a less structured distribution across the dentate gyrus. Scale bar: 100 µm. **(B)** High-magnification inverted grayscale images of Nestin immunostaining from boxed regions in (A), showing radial glial fibers originating from the SGZ and projecting towards the GCL in control mice. In eDKO mice, Nestin-positive fibers appear shorter, less intense and less frequent. Scale bar: 50 µm. (n=4 per genotype).

To investigate whether altered scaffolding contributes to the lamination defects observed in eDKO mice, we analyzed marker proteins of progenitor cells and immature neurons in the postnatal DG. Nestin, a filament protein expressed in radial glia and undifferentiated neuronal precursors, revealed marked differences in radial glia architecture. In control animals, Nestin-positive

processes were clearly organized in parallel arrays extending from the sub-granular zone to granule cell layer, consistent with an intact and functional radial glial scaffold. In eDKO mice, however, Nestin-stained structures appeared markedly disorganized, with radial processes exhibiting a tangled, misaligned morphology and broader distributions across the DG (Fig. 2.15 A,B). These observations suggest both a potential persistence or expansion of an undifferentiated progenitor population and a disruption in the organization of radial glia scaffolding.

To further assess the downstream effects on neuronal maturation, we examined the expression of Doublecortin (DCX), a microtubule-associated protein expressed in migrating immature neuroblasts and early postmitotic neurons. In control mice DCX-positive cells were confined to sub-granular zone and inner granule cell layer, forming a sharply defined, radially aligned band of cell bodies reflecting the normal trajectory of granule neuron migration and integration. In eDKO mice, DCX expression was markedly increased and more broadly distributed across the granule cell layer, with DCX-positive cells appearing clustered and their processes irregularly oriented (Fig. 2.16 A,B). Notably, a considerable number of DCX-positive cells were observed in the hilus, a region where these cells are rarely found in control mice. Quantification of DCX fluorescence intensity within the hilar region (Fig. 2.16 C) confirmed a significant increase in DCX signal in eDKO mice, consistent with the presence of ectopic neuroblasts and aberrant neuronal positioning (Fig. 2.16 C). This ectopic localization suggests impaired migration or a failure of neuroblasts to integrate into the granule cell layer, likely due to disrupted guidance from radial glial fibers or delayed maturation.

Together, these findings indicate that loss of EPS15/15R perturbs the neurogenic environment of the hippocampus by disrupting radial glia scaffold integrity and impairing maturation and positioning of newly generated neurons. Notably, similar phenotypes have been described in Intersectin-1 (ITSN1) knockout mice, which exhibit disorganized radial glial scaffolding and ectopic accumulation of DCX-positive cells in the hilus (Jakob et al., 2017b). These parallels suggest that EPS15/15R and ITSN1 may converge on shared mechanisms that regulate the development and maintenance of the hippocampal neurogenic niche. The potential link between EPS15/15R and ITSN1 is further supported by our previously mentioned proteomic analysis, where we could confirm ITSN1 as a binding partner of both EPS15 and EPS15R (*see 2.2.2*). In parallel, eDKO mice revealed a reduction of ITSN1 expression levels (Fig. S3). Together, these findings indicate that EPS15/15R may regulate ITSN1 stability or expression, and that their coordinated function may be critical for maintaining radial glial architecture and proper neuronal development.

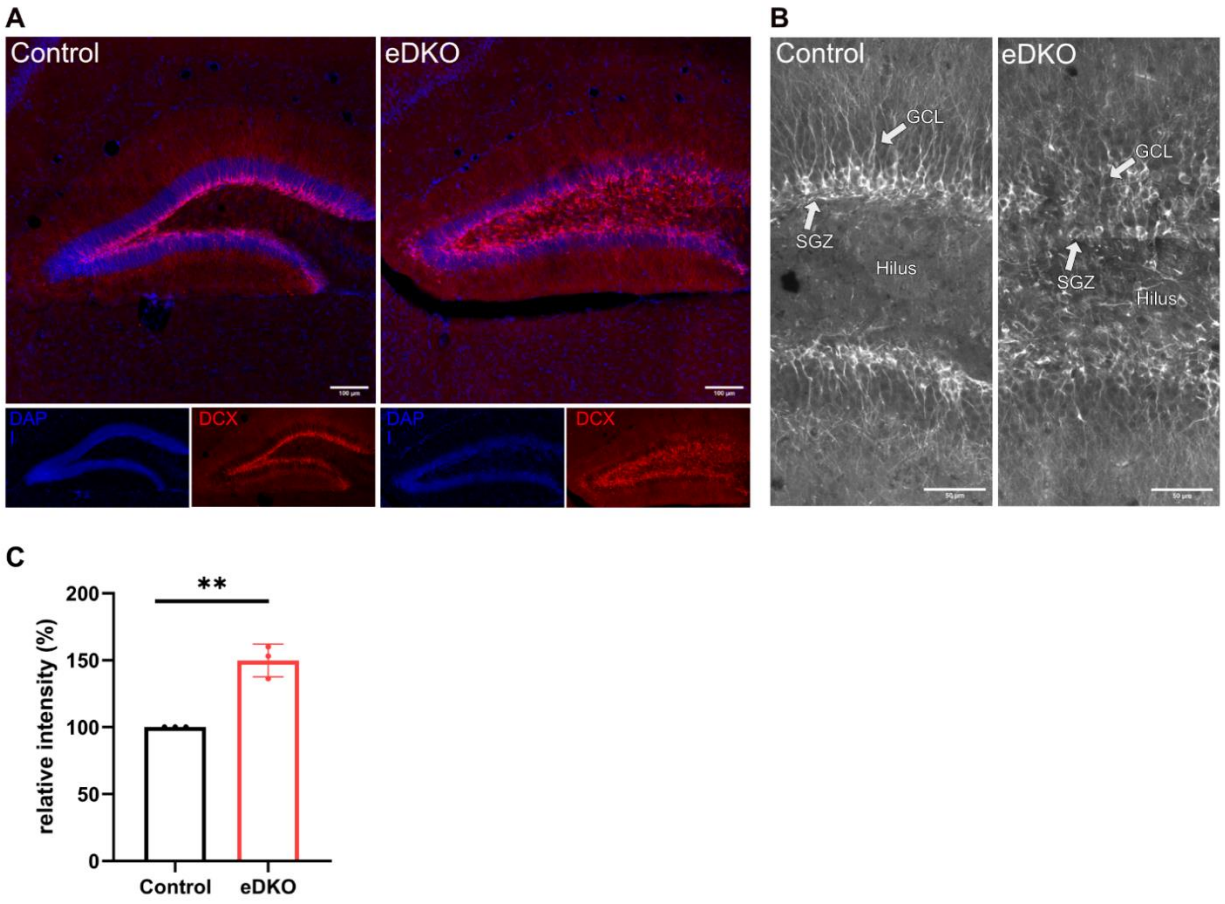

Figure 2.16 Impaired neuronal maturation visible via ectopic accumulation of Doublecortin-positive immature neurons in the dentate gyrus of EPS15/15R eDKO mice. (A) 40 µm thick coronal brain slices of 30 days old control and eDKO mice were stained with Doublecortin (DCX)-specific antibodies and with the DNA stain DAPI. Representative confocal images showing DCX (red) and DAPI (blue) staining in the dentate gyrus of control and eDKO mice. In the control brains, DCX-positive cells are confined to the SGZ and inner GCL, with their processes displaying radial alignment. In contrast, eDKO brains show an increased expression and a broader distribution of DCX, with DCX-positive cells not only spanning the entire GCL, but also residing throughout the hilus. Scale bar: 100µm. **(B)** High-magnification inverted grayscale images from boxed areas in (A), illustrating the altered distribution of immature neurons in eDKO mice. DCX-positive cells exhibit ectopic positioning and disorganized processes whose radial alignment is lost. Scale bar: 50µm. **(C)** Quantification of the DCX fluorescence intensity in the hilus of the dentate gyrus, normalized to control levels (n = 3 per genotype; paired t-test; data are shown as individual data points with mean ± SEM; significance levels: **=p<0.01).

2.4.1.2 Disrupted neuronal migration and fate specification in the dentate gyrus

Following the observed expansion of Nestin-positive progenitors and the accumulation of disorganized DCX-positive neurons in the dentate gyrus of EPS15/15R eDKO mice, we next sought to determine whether these early developmental disruptions were accompanied by defects in the subsequent stages of neuronal maturation – namely, laminar positioning and fate specification of postmitotic neurons. Proper laminar organization of the DG depends on timely

migration of newborn neurons from SGZ to GCL, where they adopt fate-specific gene expression programs and integrate into local hippocampal circuits.

To investigate whether EPS15/15R loss affects these later stages of development, we analyzed the expression of the previously mentioned two transcription factors, CTIP2 and TBR1, both of which are also expressed by postmitotic neurons in the DG apart from their expression in cortical layers. CTIP2 is expressed in developing and mature granule cells in the DG and is essential for the survival, differentiation, and synaptic integration of adult-born neurons (Simon et al., 2016). TBR1, on the other hand is also expressed in the postmitotic neurons of the hippocampus, but its precise role in hippocampal development and function remains unclear (T.-N. Huang & Hsueh, 2015).

In control animals CTIP2 and TBR1 expression was restricted to the granule cell layer of the dentate gyrus, consistent with their normal neuronal positioning. In contrast, eDKO mice displayed a pronounced ectopic localization of CTIP2+ and TBR1+ neurons (Fig. 2.17 A). Within the dentate gyrus, both CTIP2$^+$ and TBR1$^+$ cells were mis-localized to the hilus, indicating disrupted hippocampal positioning. In addition, substantial numbers of CTIP2$^+$ and TBR1$^+$ neurons were ectopically distributed within the molecular layer, i.e. outside the boundaries of the granule cell layer on the supragranular side. Our quantification confirmed a significant enrichment of ectopic CTIP2+ and TBR1+ neurons in the eDKO hippocampus (Fig. 2.17 B,C). The aberrant localization of CTIP2+ cells point to defective neuronal migration and may additionally reflect compromised granule cell maturation or survival, given the role of CTIP2 in these processes. The ectopic distribution and elevated number of TBR1+ cells in the hippocampus may similarly reflect migration defects, or potentially altered fate stabilization, especially if neurons inappropriately retain or adopt TBR1 expression outside its normal spatial context.

Taken together, these findings indicate that the loss of EPS15/15R leads to misplacement and/or potential identity disturbances in postmitotic neurons, as demonstrated by the ectopic distribution of CTIP2+ and TBR1+ cells in the DG. These defects point to a disrupted spatial guidance and molecular specification of granule cell development. Importantly, these abnormalities are preceded by earlier perturbations in progenitor behavior and neuronal maturation, as evidenced by the increased and disorganized populations of Nestin- and DCX-positive cells. This sequential disruption across developmental stages suggests that EPS15/15R play a critical role in maintaining the spatial, temporal, and molecular precision of neuronal development and migration required for proper hippocampal lamination.

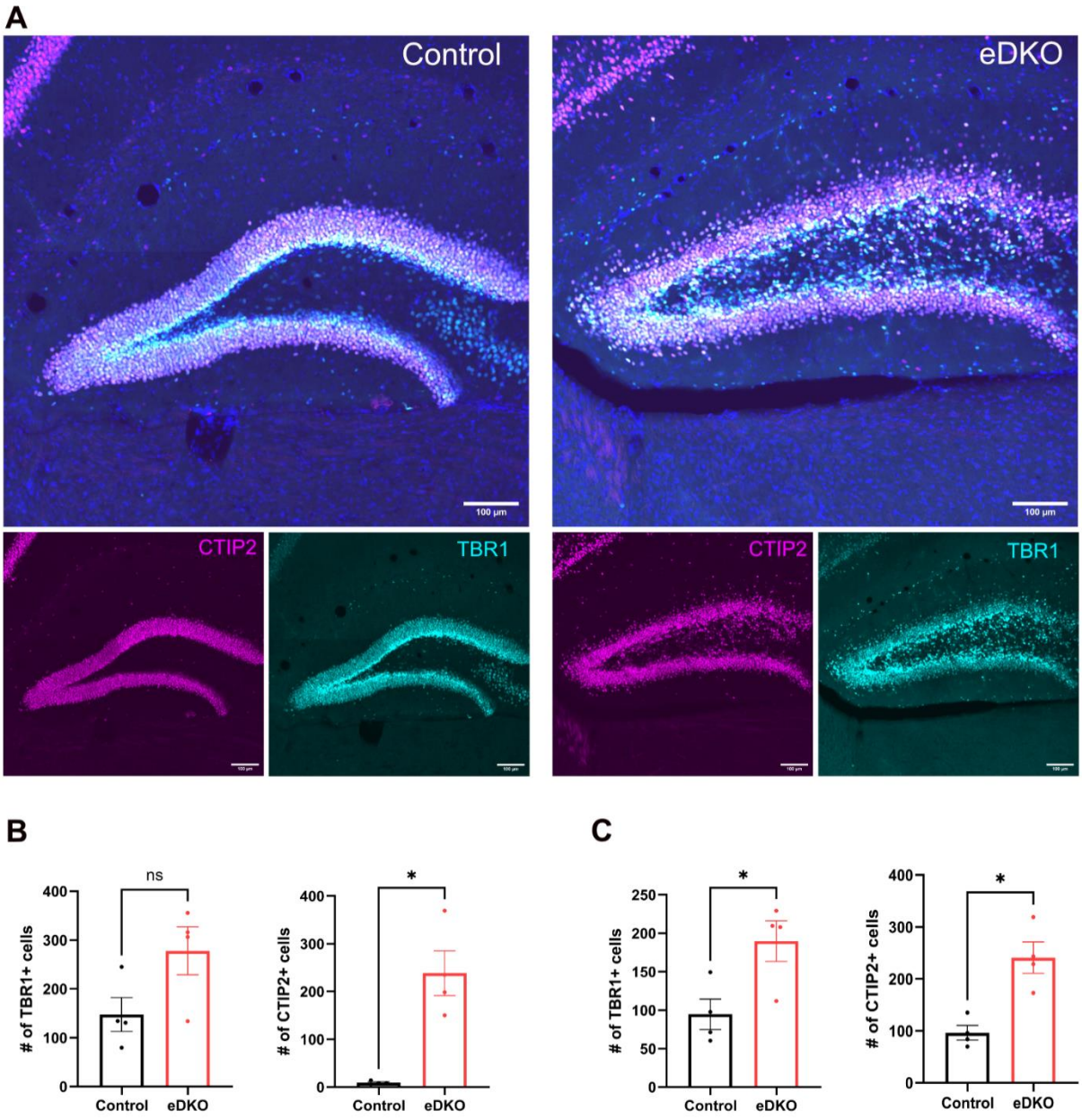

Figure 2.17 Ectopic localization of CTIP2- and TBR1-positive postmitotic neurons in the dentate gyrus of EPS15/15R eDKO mice. (A) 40 µm thick coronal brain slices of 30 days old control and eDKO mice were stained with CTIP2- and TBR1-specific antibodies and with the DNA stain DAPI. Representative confocal images showing CTIP2 (magenta), TBR1 (cyan), and DAPI (blue) staining in the dentate gyrus of control and eDKO mice. In control animals, CTIP2 and TBR1 expression are confined to the granule cell layer (GCL), consistent with the usual positioning of postmitotic neurons. In eDKO sections, both markers exhibit a broader distribution, reflecting the ectopic localization of CTIP2- and TBR1-positive cells to the hilus. Scale bar: 100µm. **(B)** Quantification of ectopic neuronal populations in the dentate gyrus hilus of hippocampus. The number of TBR1-positive cells in the hilar region remained comparable between control and eDKO mice, with a trend toward increased numbers in the eDKO group. CTIP2-positive neurons, however, were significantly more abundant in the eDKO hilus, suggesting aberrant localization (n=4 per genotype; Welch's unpaired t-test). **(C)** Quantification of mislocalized neurons in the molecular layer (supragranular side) of the dentate gyrus (DG) revealed a significant increase in both TBR1-positive and CTIP2-positive cells in eDKO mice compared to controls, indicating aberrant neuronal positioning (n=4 per genotype; Welch's unpaired t-test; data are shown as individual data points with mean ± SEM; significance levels: ns= non-significant, *=p<0.05).

2.4.1.3 SVZ neurogenesis remains preserved despite hippocampal defects

Given that the dentate gyrus (DG) is not the only site of neurogenesis in the postnatal brain, we extended our analysis to the subventricular zone (SVZ), another major neurogenic niche located along the lateral ventricles (Alvarez-Buylla & García-Verdugo, 2002). This region continuously generates neural progenitors that migrate along the rostro-migratory stream (RMS) towards the olfactory bulb. Since our earlier findings revealed significant neurogenic and structural abnormalities in the DG of EPS15/15R-deficient mice, we sought to determine whether similar perturbations extended to the SVZ. To assess whether EPS15/15R loss affected stem/progenitor populations beyond the hippocampus, we analyzed the expression of SOX2 and Nestin, canonical markers of neural stem and progenitor cells. This allowed us to determine whether the neurogenic abnormalities observed in the DG were part of a broader defect or restricted to specific brain regions.

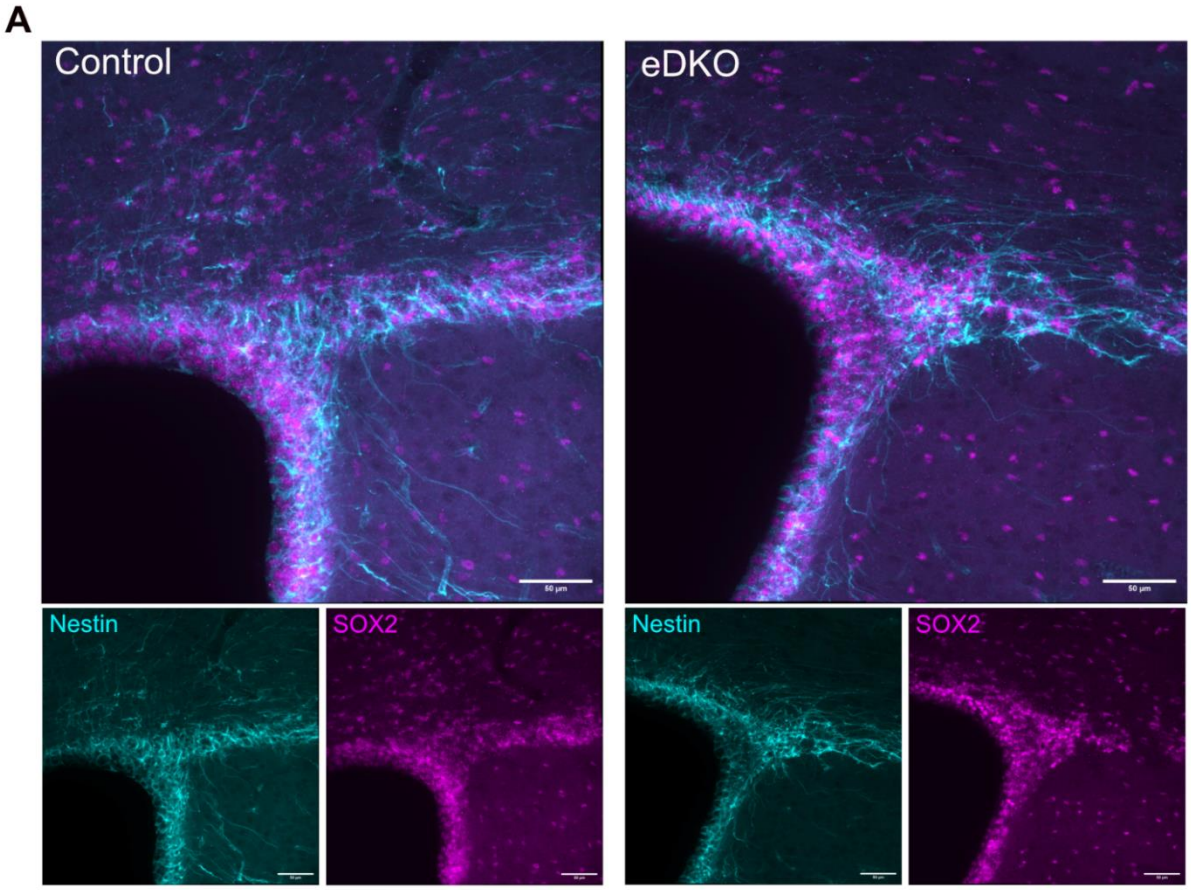

Figure 2.18 Neural stem cell and progenitor populations in the SVZ remain unaffected in EPS15/15R eDKO mice. (A) 40 µm thick coronal brain slices of 30 days old control and eDKO mice were stained with Nestin- and SOX2-specific antibodies. Representative confocal images showing Nestin (cyan) and SOX2 (magenta) staining in the subventricular zone (SVZ) along the lateral ventricles of control and eDKO mice. In both genotypes, SOX2-positive nuclei were densely localized within the SVZ, while Nestin-positive processes exhibited the typical radial orientation

and organization. No significant differences were observed between control and eDKO brains, indicating a preserved SVZ neural stem cell/progenitor niche. Scale bars: 50µm. (n=4 per genotype)

Immunofluorescence staining of coronal brain sections revealed strong SOX2+ nuclei and dense Nestin+ radial processes lining the lateral ventricles in both control and eDKO brains (Fig 2.18 A). The distribution, density, and morphology of SOX2- and Nestin-positive cells appeared comparable across genotypes, with no evidence of depletion, disorganization, or mislocalization in the SVZ. SOX2 signals remained robustly restricted to the ventricular lining, while Nestin-positive fibers extended radially in a pattern typical of SVZ progenitor scaffolding.

Together, these findings suggest that SVZ stem/progenitor populations are preserved in the absence of EPS15/15R. In contrast to the DG, where increased Nestin and DCX expression, radial glial disarray, and ectopic localization of postmitotic neurons were observed, the SVZ does not show any overt changes in stem cell architecture. This points to a region-specific requirement for EPS15/15R in neurogenesis and supports the idea that its developmental functions are more critical within the hippocampal neurogenic niche than in the SVZ. Notably, similar region-selective effects were reported in ITSN1 knockout mice, where the SVZ-RMS neurogenesis remained intact despite hippocampal defects, again supporting the idea that EPS15/15R and ITSN1 may converge on hippocampus-specific developmental pathways.

2.4.1.4 Involvement of the Reelin pathway in EPS15R-dependent neuronal development

The widespread abnormalities in neurogenesis, neuronal migration, and laminar organization observed in EPS15/15R-deficient mice suggest a disruption of key signaling pathways required for proper neuronal development. We focused our investigation of potential molecular mechanisms on the Reelin signaling pathway, a central regulator of neuronal positioning and cortical and hippocampal lamination (Curran & D'Arcangelo, 1998; D'Arcangelo et al., 1995b). This pathway is known to influence radial glial organization, neuronal migration, and postmitotic identity stabilization – processes disrupted in the eDKO brain. Our interest in Reelin signaling was further supported by prior studies showing that ITSN1, whose expression is reduced in eDKO mice, and which interacts with EPS15/15R, functions as a component of the Reelin pathway. These phenotypic and molecular parallels led us to hypothesize that EPS15 and EPS15R may contribute to neurodevelopmental integrity in part by regulating the Reelin signaling cascade.

Reelin signaling has been implicated in regulating hippocampal neurogenesis and laminar patterning through its main receptors, ApoER2 and VLDLR (D'Arcangelo et al., 1999b; Hiesberger et al., 1999; Trommsdorff et al., 1999a). To better understand how EPS15/15R may interface with

this pathway, we revisited the role of ITSN1 in supporting Reelin receptor signaling. Using GST-pulldown assays from mouse brain lysates, ITSN1 was previously shown to associate with the intracellular domain of VLDLR, whereas no interaction with ApoER2 could be detected (Jakob et al., 2017b). This receptor specificity suggested a distinct molecular role for ITSN1 within the Reelin cascade and raised the question of whether EPS15 and EPS15R might engage the pathway through a similar receptor interaction. To explore this, we assessed whether EPS15/15R physically interacts with either the ApoER2 or VLDLR intracellular tail, using a similar pulldown approach as Jakob et al. to identity a potential receptor-specific interaction.

We performed GST-pulldown assays using the intracellular domains of ApoER2 and VLDLR fused to GST and incubated them with mouse brain lysates. Surprisingly, the immunoblotting revealed that EPS15R, in contrast to ITSN1, selectively associated with ApoER2, while no interaction was observed with VLDLR (Fig. 2.19 A) arguing against an EPS15R/ITSN1 complex functioning concertedly in Reelin signaling. This receptor-specific interaction was consistently detected across replicate experiments and was absent in GST-only controls. Importantly, pulldown efficiency was validated by Ponceau staining which revealed distinct GST fusion protein bands on the membrane, thereby confirming that the GST-tagged bait proteins were successfully captured and recovered during the assay. In parallel, the absence of GAPDH signal in the lanes of the pulldown samples confirmed the specificity of the experiment. Interestingly, only EPS15R, but not EPS15 bound to the ApoER2 tail underlining the greater importance of EPS15R for brain function (Fig. 2.19 B). Quantification of the immunoblots across four independent pulldown experiments further substantiated this observation. EPS15R showed significantly enriched binding to ApoER2 compared to GST and VLDLR (Fig. 2.19 C), whereas EPS15 did not show any significant interaction with either receptor (Fig. 2.19 D). These findings suggest a distinct molecular role for EPS15R in modulating Reelin signaling via ApoER2, independent of its paralog EPS15 and its interactor ITSN1. The discovered EPS15R-ApoER2 interaction supports a model in which EPS15R contributes to neuronal migration and lamination through the selective regulation of Reelin receptor-mediated developmental signaling.

Given this specific interaction, it is conceivable that EPS15R may fulfill the same function for ApoER2 which ITSN1 fulfills for VLDLR: facilitating the recruitment of the adaptor protein Dab1, a key effector of Reelin signaling, for subsequent phosphorylation. Its selective binding to ApoER2 also raises the possibility that EPS15R could contribute to the receptor's internalization and trafficking. These potential mechanisms warrant further investigation to clarify the functional role of EPS15R within the Reelin cascade.

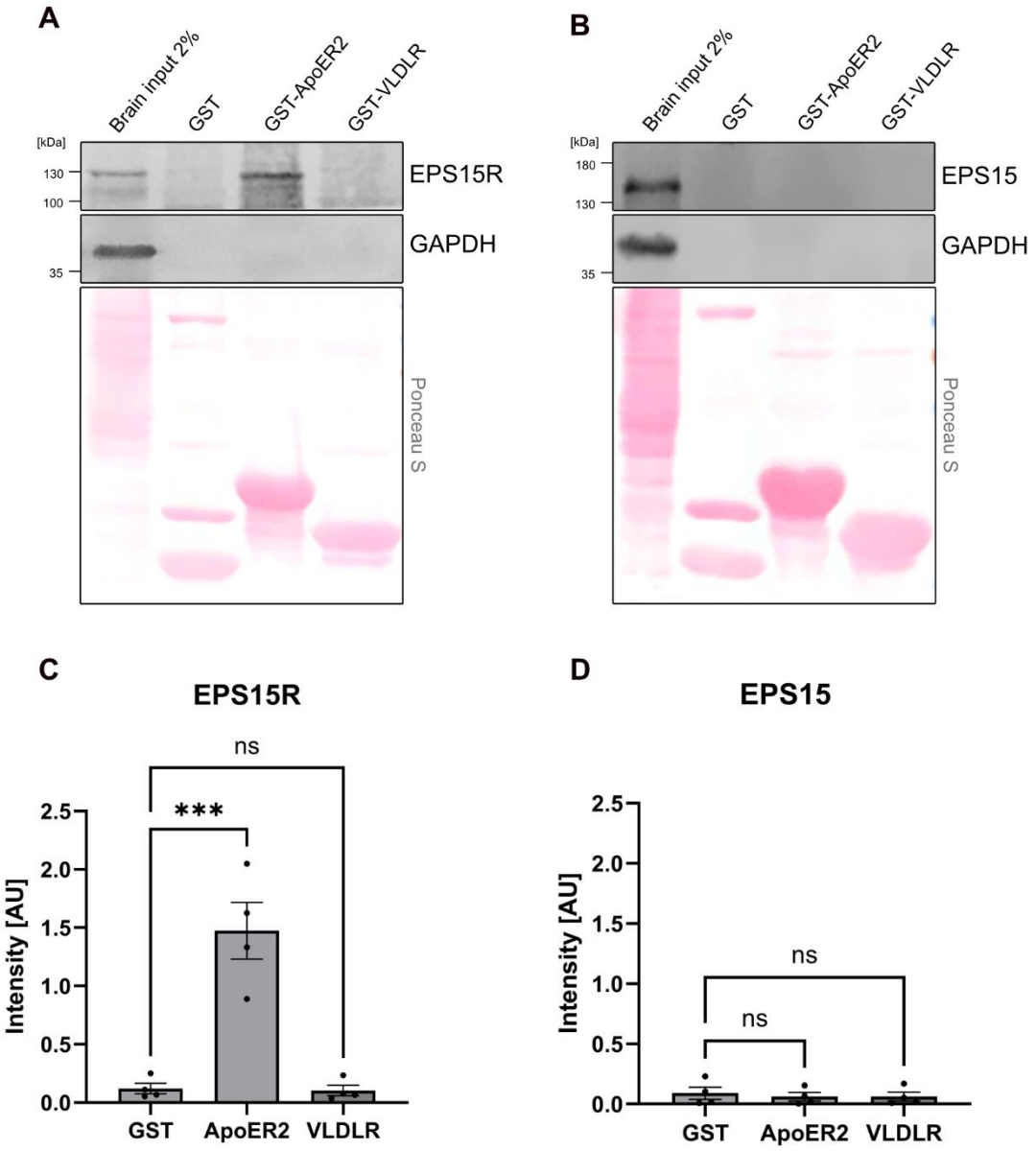

Figure 2.19 EPS15R selectively associates with the intracellular domain of ApoER2. (A, B) Immunoblots of GST-pulldown assays using GST-tagged intracellular domains of ApoER2 and VLDLR incubated with mouse brain lysates reveal that EPS15R, but not EPS15, selectively binds to ApoER2. No interaction was observed with VLDLR or in GST-only controls. GAPDH was absent in pulldown lanes, confirming specificity. Ponceau S staining below each blot confirms comparable loading and recovery of GST-fusion proteins. **(C, D)** Quantification of band intensities show a significant enrichment of EPS15R binding to ApoER2 compared to GST and VLDLR controls, while EPS15 does not show significant interaction with either receptor. These results highlight a receptor-specific interaction of EPS15R with ApoER2, implicating it in selective regulation of Reelin receptor signaling (n = 4 independent experiments; ordinary one-way ANOVA with Dunnett's multiple comparisons test; data are shown as individual data points with mean ± SEM; significance levels: ns= not significant, ***=$p < 0.001$),

2.4.2 Mechanistic insights into the development of hydrocephalus in eDKO mice

The pronounced enlargement of the lateral ventricles in EPS15/15R eDKO mice strongly implicates hydrocephalus as a key neuroanatomical phenotype. To better understand its etiology, we investigated both its temporal onset and the potential underlying mechanism contributing to ventricular dilation. Hydrocephalus may arise from a variety of causes including aberrant CSF dynamics, due to impaired CSF flow or clearance, often linked to underlying structural or cellular abnormalities such as congenital malformations of the ventricular system, defective ependymal cells lining the ventricles, dysfunctional cilia, or impaired cell adhesion. To address these possibilities, we first examined the developmental onset of hydrocephalus, and based on this timing, subsequently investigated different candidate molecular and cellular mechanisms that could account for the phenotype.

2.4.2.1 Early-onset ventricular enlargement in eDKO mice

To identify the developmental window most relevant for investigating the molecular basis of hydrocephalus in eDKO mice, it was essential to first determine when ventricular abnormalities begin to emerge. Knowing whether the phenotype emerges during early developmental stages or arises later during postnatal maturation was essential for narrowing down the candidate processes and time points for mechanistic exploration. Therefore, we examined brain sections from early postnatal stages (P5) to assess the timing of ventricular expansion and clarify whether hydrocephalus in the EPS15/15R-deficient model reflects an early-onset or a rather progressive condition.

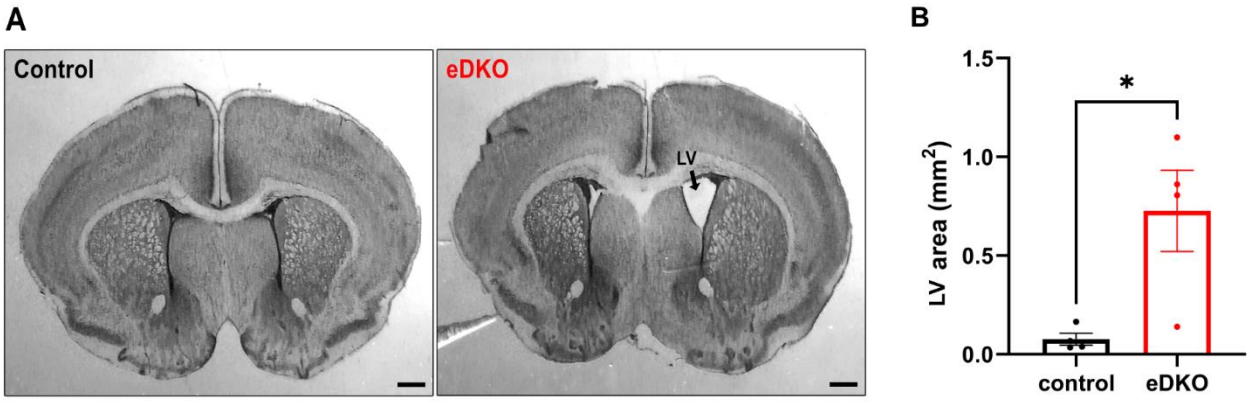

Figure 2.20 Early-onset ventricular enlargement in EPS15/15R-deficient (eDKO) mice. (A) Representative Nissl-stained coronal brain sections from P5 control (top) and eDKO (bottom) mice, highlighting the lateral ventricles (LV). eDKO brains show marked ventricular enlargement already at this early postnatal stage. Scale bar: 500 µm. **(B)** Quantification of summed lateral ventricle (LV) cross-sectional area reveals a significant increase in eDKO mice compared to controls (n=4 per genotype; unpaired Welch's t-test; data are shown as individual data points with mean ± SEM; significance level: *=$p < 0.05$).

Notably, we already observed a clear enlargement of the lateral ventricles in the eDKO mice at P5, indicating that hydrocephalus begins to manifest during early postnatal development (Fig. 2.20 A,B). The identification of ventricular enlargement as early as P5 and given the close temporal association with the ventricle expansion (Redmond et al., 2019), strongly suggests that hydrocephalus in EPS15/15R-deficient mice is a developmental defect rather than a secondary consequence of later-stage pathology. This early onset highlights the need to examine upstream cellular and molecular processes critical for ventricular morphogenesis. It prompted us to investigate both upstream and downstream processes that govern ventricular morphogenesis. Specifically, we examined whether defects in early neuronal determinants such as the cell adhesion molecule L1CAM or alterations in primary cilia, known to regulate progenitor behavior might contribute to the observed phenotype. In parallel, we assessed differentiation of radial glial cells into ependymal cells, focusing on structural and molecular features essential for establishing the multiciliated ependymal layer that drives cerebrospinal fluid dynamics.

2.4.2.2 Surface expression of L1CAM is unaltered in iDKO neurons

To explore potential molecular contributors to the observed hydrocephalus upon loss of EPS15/15R, we assessed the surface levels of the neuronal cell adhesion molecule L1CAM. Its critical role in progenitor differentiation and neurogenesis during early brain development made it an ideal candidate for investigation (Grońska-Pęski et al., 2020). L1CAM is a transmembrane glycoprotein that plays a central role in brain development, particularly in neuronal migration, axon pathfinding, and the formation of commissural tracts (Schmid & Maness, 2008). Importantly, mutations in the human *L1CAM* gene cause a spectrum of X-linked neurological disorders, collectively known as L1 syndrome, which includes hydrocephalus due to stenosis of the aqueduct of Sylvius (HSAS) (Jouet et al., 1994). In mouse models, L1CAM deficiency leads to phenotypes ranging from agenesis of major axonal tracts to variable degrees of lateral ventricle enlargement, depending on the genetic background (Dahme et al., 1997; Demyanenko et al., 1999; Jouet et al., 1994). In our eDKO mice, we observed a marked reduction in the size of the ventral hippocampal commissure (Fig. 2.13 C), further raising the possibility that L1CAM-related processes might be disrupted. Besides, L1CAM is known to undergo endocytosis (Kamiguchi et al., 1998) and therefore a potential cargo of endocytic adaptors like EPS15/15R.

To investigate whether L1CAM surface abundance is affected in the EPS15/15R-deficient context, we performed a surface biotinylation on primary cortical neuron cultures derived from control and iDKO mice. This method allows the selective labeling and isolation of surface-exposed proteins and can be followed by immunoblotting to quantify the level of plasma membrane-

localized L1CAM. By comparing surface levels between genotypes, we aimed to determine whether altered endocytic trafficking in the absence of EPS15/15R affects L1CAM surface expression, potentially contributing to the ventricular abnormalities observed in the eDKO mice. However, our analysis revealed no detectable difference in surface L1CAM levels between control and iDKO cultured neurons (Fig. 2.21 A), indicating that L1CAM internalization from the plasma membrane remains intact in the absence of EPS15/15R. These findings suggest that L1CAM dysregulation is unlikely to underlie the observed hydrocephalus or commissural defects in the eDKO.

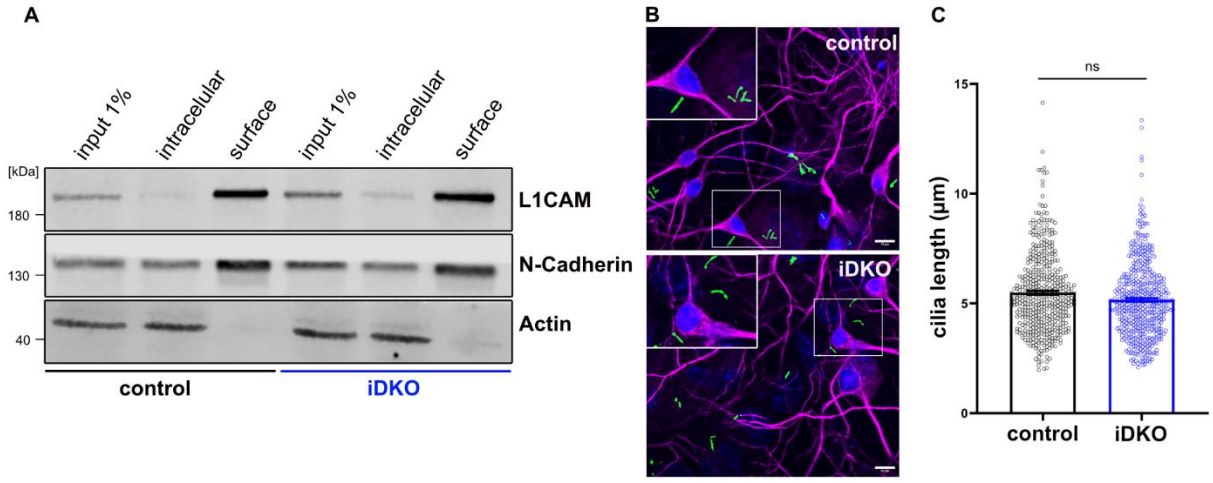

Figure 2.21 L1CAM surface levels and primary cilia length are unaffected in EPS15/15R-deficient neurons. (A) Surface biotinylation of DIV14 primary cortical neurons derived from control and iDKO neurons, followed by immunoblotting for the indicated proteins. The surface fractions show comparable levels of L1CAM between genotypes, indicating unaltered internalization in iDKO neurons. N-Cadherin served as a membrane marker, and actin was used as a loading control and to show the absence of intracellular proteins in the surface fraction. N=1 experiment. **(B)** Immunofluorescence images of DIV14 hippocampal neurons stained with MAP2 (magenta) to mark the neuronal somatodendritic compartments and Arl13b (green) to label primary cilia. Insets show zoom-in views of selected regions highlighting individual cilia. No clear differences in cilia morphology or abundance were observed between control and iDKO neurons. Scale bars, 10 µm. **(C)** Quantification of primary cilia length in control and iDKO neurons. No significant difference in cilia length was detected (N: control=356, iDKO=354 cilia from 2 independent experiments; unpaired t-test;). (Data are shown as individual data points with mean ± SEM; significance level: ns= not significant).

2.4.2.3 Unaltered primary cilia integrity in EPS15/15R-deficient neurons

There is growing evidence that primary (non-motile) cilia play a crucial role in brain development, particularly in regulating the behavior of neural progenitor cells and thereby potentially maintaining ventricular architecture (Youn & Han, 2018). These microtubule-based organelles serve as signaling hubs that coordinate pathways such as Sonic Hedgehog (Shh), Wnt, and mTOR-dependent signaling, all of which are essential for apicobasal polarity, proliferation control, and tissue organization (Foerster et al., 2017; Mill et al., 2023). Disruption of primary cilia formation in radial glial progenitors, through conditional deletion of genes such as Kif3a, Ift88, or B9d2, has

been shown to result in ventriculomegaly and hydrocephalus (Foerster et al., 2017; Town et al., 2008). These studies collectively highlight that primary cilia are not only essential for cell-intrinsic signaling but are also crucial for proper ventricular morphogenesis and prevention of hydrocephalus.

In light of these findings and the role of EPS15/15R in membrane trafficking and signaling, we hypothesized that their loss might impair primary cilia structure or stability. To explore this possibility, we assessed primary cilia length in DIV14 hippocampal neuron cultures derived from control and iDKO mice. Although postmitotic neurons do not fully recapitulate the progenitor state, they retain structurally intact primary cilia and serve as a useful proxy to examine potential defects in ciliogenesis. Our quantitative analysis revealed no significant difference in cilia length between control and iDKO neurons, suggesting that primary cilia formation and elongation are not overtly affected under these conditions (Fig. 2.21 B,C). These results indicate that altered primary cilia are unlikely to underlie the ventricular enlargement phenotype observed in EPS15/15R-deficient mice.

2.4.2.4 Cell-intrinsic defects in ependymal maturation in absence of EPS15/15R

To further investigate the cellular basis of hydrocephalus in absence of EPS15/15R, we next sought to determine whether intrinsic defects in ependymal cell differentiation could underlie the ventricular abnormalities observed in vivo in eDKO mice. Given that ependymal cells arise through a defined postnatal maturation process from radial glial progenitors and are responsible for establishing the multiciliated ventricular lining essential for CSF flow, impairments in their differentiation may directly impact ventricular structure and function. Since the ventricular enlargement was already evident at postnatal day 5 (P5), a stage when radial glial progenitors have largely differentiated into ependymal cells and expanded their apical domains to shape the lateral ventricles (Redmond et al., 2019), this timing suggested a possible link to defective ependymal differentiation, as it represents a developmental window where the ventricular system is on the way to functional maturity.

To this end we employed primary ependymal cell cultures as an ex vivo system to probe potential deficits in this lineage. Since our lab did not have prior expertise with this system, I visited the laboratory of Nathalie Spassky at IBENS-ENS, Paris, to learn how to isolate and differentiate ependymal cells from postnatal mouse brains. This approach enabled us to monitor the differentiation capacity of progenitor cells isolated from control and iDKO brains under controlled conditions, with a focus on quantifiable morphological parameters. Primary ependymal cell cultures were established by dissecting the telencephalon containing the lateral ventricular wall

of postnatal mouse brains. Following dissection, (1) progenitor cells were isolated and expanded in culture for several days, and (2) subsequently reseeded, where differentiation was induced by serum starvation (Delgehyr et al., 2015). Under these conditions, the progenitors progressively matured into multiciliated ependymal cells, providing an ex vivo system to study their differentiation in a controlled environment.

We first wanted to determine whether EPS15 and EPS15R are expressed in ependymal cells, as no published information was available. Since suitable antibodies for immunohistochemistry or immunofluorescence staining were lacking, we addressed this question by performing immunoblotting on lysates from primary ependymal cell cultures. Samples were collected at different stages of differentiation (DIV0, DIV7, and DIV14) to assess both expression and potential changes over time. In our ependymal cultures, both EPS15 and EPS15R levels were barely detectable at DIV0 but increased strongly by DIV7 and remained elevated at DIV14, suggesting an upregulation during ependymal differentiation (Fig. 2.22 B). Next, we aimed to test whether conditional deletion of EPS15 and EPS15R could be achieved in primary cultures by adding tamoxifen. The treatment with tamoxifen effectively depleted both proteins, confirming the efficacy of the inducible deletion system (Fig. 2.22 C). With this validated system in place, we set out to functionally interrogate the cultures in order to identify cellular mechanisms that might underlie the hydrocephalus phenotype.

The differentiation of radial glial cells (RGCs) into ependymal cells (ECs) is a tightly regulated process involving centriole amplification, apical migration of centrioles, and the formation of motile cilia bundles. This transition is initiated by the inhibition of Notch signaling in progenitor cells and the subsequent activation of the coiled-coil domain proteins GEMC1 and Multicilin, which in turn promote the expression of the transcription factor FOXJ1 (Spassky & Meunier, 2017) (Fig. 2.22 A). FOXJ1 drives the expression of genes essential for the formation of motile cilia, including steps such as basal body docking and axoneme assembly (Yu et al., 2008), thereby enabling the differentiated ependymal cell layer to generate a directed CSF flow. Therefore, we examined the level of FOXJ1, the master regulator of multiciliogenesis, to assess whether EPS15/15R loss affects ependymal differentiation upstream of FOXJ1 expression. Western blot analysis was performed on lysates from DIV14 primary ependymal cell cultures derived from control and iDKO mice. As expected, the expression of both EPS15 and EPS15R was strongly reduced in iDKO cultures, confirming the efficacy of the inducible deletion system. Notably, we observed a marked reduction in FOXJ1 protein levels in the iDKO samples compared to the controls, indicating that indeed events upstream of FOXJ1 expression must be disturbed leading to a downregulation of the transcriptional program required for motile cilia formation. Our

quantification revealed that FOXJ1 expression was decreased to approximately 40% of control levels (Fig 2.22 C,D), suggesting that loss of EPS15/15R compromises the induction or stability of FOXJ1 during ependymal differentiation. This finding points towards a potential mechanistic link between EPS15/15R-dependent pathways and the regulation of transcriptional programs essential for ependymal cell maturation.

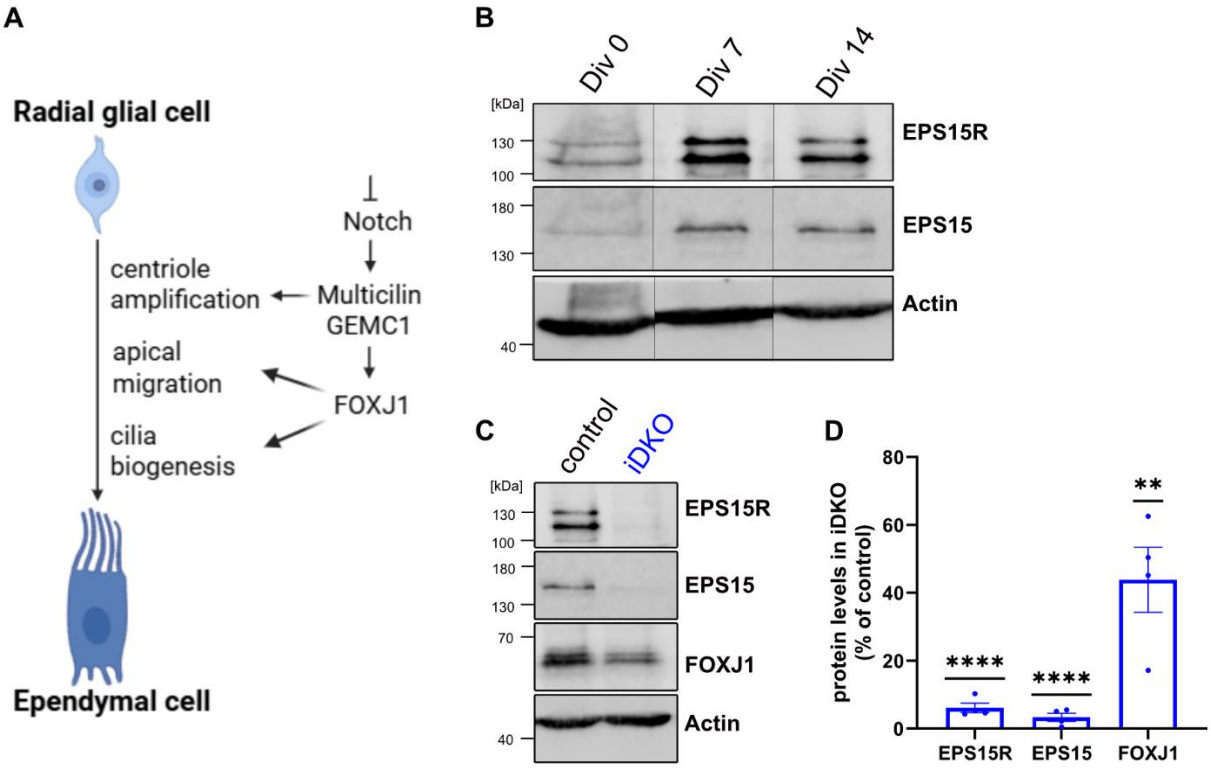

Figure 2.22 Loss of EPS15/EPS15R impairs ependymal cell differentiation and FOXJ1 expression. **(A)** Schematic representation of the molecular cascade regulating radial glial cell differentiation into multiciliated ependymal cells. Key events include centriole amplification, apical centriole migration, and cilia biogenesis, with FOXJ1 acting downstream of GEMC1 and Multicilin to drive the motile ciliogenesis pathway. **(B)** Representative Western blot analysis showing the temporal expression of EPS15R and EPS15 in primary ependymal cultures derived from control mice at DIV0, DIV7, and DIV14. Actin serves as a loading control. **(C)** Representative Western blot of EPS15, EPS15R, and FOXJ1 expression in DIV14 primary ependymal cultures derived from control and iDKO mice. Actin was used as a loading control. **(D)** Quantification of protein expression levels in iDKO cultures relative to control. Expression of EPS15R and EPS15 is significantly reduced, confirming knockout efficiency. FOXJ1 levels are also significantly decreased in iDKO cultures, suggesting impaired ependymal maturation (n = 4 independent experiments; one-sample t-test). (Data are shown as individual data points with mean ± SEM; significance level: **=p<0.01, ***=p< 0.001).

To evaluate whether the observed deficits in ependymal differentiation extend to defects in ciliogenesis, we next analyzed the ciliary profiles of ependymal cells using immunostaining for the cilia membrane marker Arl13b (Fig. 2.23 A,B). In control cultures we observed a progressive increase in the proportion of cells bearing mature cilia bundles from DIV5 to DIV14, consistent with the expected timeline of ependymal multiciliogenesis. By DIV14, the majority of control ependymal cells exhibited cilia bundles, indicating successful transition into a fully differentiated,

multiciliated state. In contrast, EPS15/15R iDKO cultures showed a markedly attenuated increase in cilia bundle formation over time. At each time point examined, the percentage of multiciliated cells in iDKO cultures was significantly lower than in controls, with the largest disparity observed at DIV14 (Fig 2.23 C). Notably, a greater proportion of iDKO cells retained a single primary cilium at DIV7 and DIV14 compared to controls (Fig. 2.23 D), indicating a failure to achieve the multiciliated phenotype characteristic of terminally differentiated ependymal cells. While the proportion of cells completely lacking cilia remained low across all groups, it was consistently higher in the iDKO cultures compared to controls, particularly at DIV14, further supporting maturation deficits (Fig. 2.23 E). These findings suggest that EPS15 and EPS15R are required for the terminal differentiation of ependymal cells, particularly the formation of multiciliated structures. Their absence may compromise CSF flow dynamics, thereby contributing to the development hydrocephalus.

To further assess the impact of EPS15/15R loss on ependymal cell maturation, we next examined basic cellular characteristics such as morphology, cell number, and density across different stages of differentiation. Analysis of ependymal cell morphology across DIV5, DIV7 and DIV14 revealed a progressive increase in cell area in both control and iDKO cultures, with iDKO cells appearing larger than controls at each time point (Fig 2.23 F). Despite this trend, these differences did not reach statistical significance. In contrast, the number of ependymal cells showed opposing trajectories: control cultures exhibited a gradual increase over time, whereas iDKO cultures showed a decline from DIV5 to DIV7, followed by only a partial recovery by DIV14. These changes were paralleled by a reduction in the number of nuclei per field in iDKO cultures compared to controls, with significant reductions observed on DIV7 and DIV14 (Fig.2.23 G, H). Together, these data suggest that loss of EPS15 and EPS15R leads to progressive deficits in ependymal cell area and density during in vitro maturation, which may reflect impaired differentiation capacity and/or reduced cell survival.

Given the noticeable reduction in cell numbers in EPS15/15R iDKO cultures, we considered the possibility that the increased cell area and impaired multiciliogenesis might be, at least in part, a consequence of an influence of reduced cell density on the differentiation process. A low density of cultured cells can lead to an altered cell morphology due to the greater available area for cell spreading and may compromise any contact-dependent signals critical for efficient multiciliogenesis.

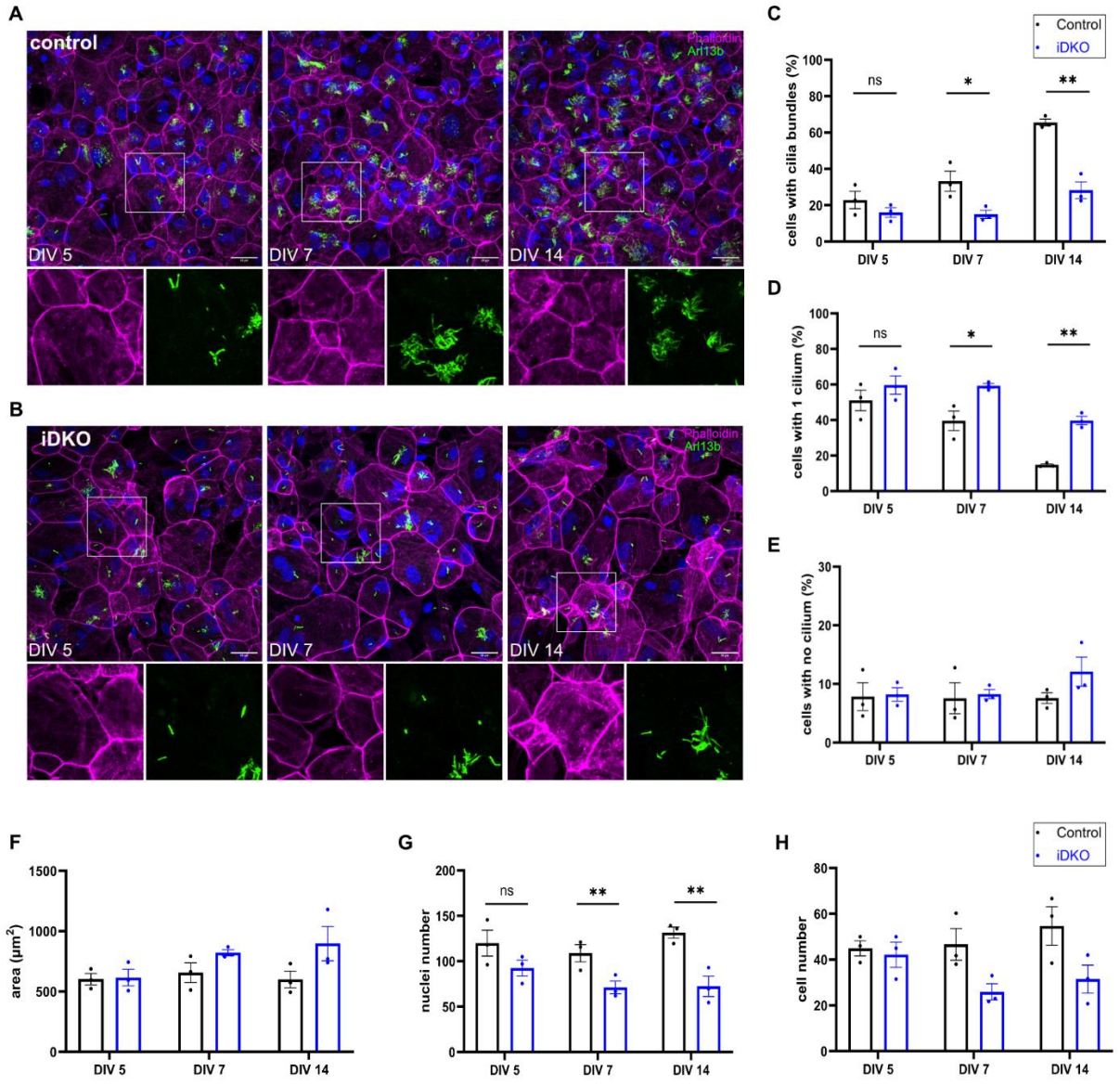

Figure 2.23 EPS15/15R are essential for proper ependymal cell maturation and multiciliogenesis in vitro. (A-B) Representative confocal images of primary ependymal cell cultures derived from control **(A)** and EPS15/15R iDKO **(B)** mice at DIV5, DIV7, and DIV14. Cultures were stained for Arl13b (green) to mark cilia, Phalloidin (magenta) to label F-actin, and DAPI (blue) for nuclei. Insets show zoom-in views of cells and cilia bundles. Scale bar: 10 µm. **(C-E)** Quantification of ciliation profiles over time. iDKO cultures contained significantly fewer cells with cilia bundles **(C)** and increased proportions of cells with only a single cilium **(D)** or no cilia **(E)**, particularly at DIV14. **(F-H)** Quantification of average cell arear **(F)**, total nuclei per field **(G)**, and cell number **(H)** across the culture period. While cell area gradually increased in both groups, cell number and nuclei count significantly declined in iDKO cultures from DIV5 to DIV14 (n=3 individual experiments; unpaired t-test). (Data are shown as individual data points with mean ± SEM; significance levels: ns= non-significant, *=p<0.05, **=p<0.01).

To examine, whether the observed phenotypes were secondary to alterations in cell density rather than acutely triggered by EPS15/15R loss, we used two different approaches: a) At the reseeding/serum starvation step iDKO cells were plated at twice the usual density to compensate for their later lower cell numbers (iDKO-2x). b) We modified the timing of gene deletion by adding

tamoxifen only at the onset of ependymal differentiation (i.e. at the reseeding/serum starvation step), instead of during the earlier progenitor expansion phase (iDKO-late). For comparison, the original protocol in which tamoxifen was added from the beginning of the culture period, i.e. to progenitor cells before expansion, is hereafter referred to as iDKO-early.

Our quantification (Fig. 2.24) at DIV14 showed a consistent reduction in nuclei and total cell numbers across all iDKO conditions relative to controls. The decrease was most pronounced in iDKO-early cultures, whereas both delayed induction (iDKO-late) and increased plating density (iDKO-2x) partially alleviated this reduction, although cell and nuclei numbers at the end of differentiation remained below control levels (Fig. 2.24 A,B). In contrast, mean cell area was markedly enlarged in all iDKO conditions, indicating that the increase in cell size represents a robust phenotype independent of culture density or timing of gene deletion (Fig. 2.24 C). Quantification of multiciliated bundles revealed the strongest loss in iDKO-early cultures, while both iDKO-late and iDKO-2x cultures displayed higher but variable values. Despite this upward trend, cilia-bundle numbers remained below control levels, even though the decrease did not reach statistical significance (Fig. 2.24 D). Given the substantial variability observed across replicates, additional experiments with increased sample size will be required to draw a definitive conclusion regarding the extent of ciliation recovery.

Although modifying cell density or the timing of gene deletion attenuated the severity of the phenotype, neither approach was sufficient to completely restore normal cell morphology and ciliation. The persistence of increased cell size and the tendency to impaired cilia bundle formation indicates that these defects are not solely attributable to reduced cell density, but instead reflect cell-intrinsic consequences of EPS15/15R loss. The stronger phenotype observed in iDKO-early compared to iDKO-late cultures demonstrates that deletion during the progenitor expansion phase leads to more pronounced defects than deletion initiated at the onset of differentiation, pointing to a requirement for EPS15/15R not only during terminal ependymal maturation but already during earlier stages of progenitor maintenance and expansion. Notably, even when iDKO cells were plated at twice the normal density (iDKO-2x), total cell and nuclei numbers at the end of differentiation remained lower than in controls, suggesting that reduced cell yield cannot be compensated by a higher initial seeding density. This continued decline implies that EPS15/15R loss may compromise progenitor viability, proliferative capacity, or differentiation efficiency. The more pronounced deficits observed upon early deletion further support a model in which EPS15/15R function is required during the proliferative phase to sustain progenitor integrity and ensure proper transition into the multiciliated ependymal state. This

possibility warrants further investigation to fully define stage-specific requirements for EPS15/15R in the progenitor and ependymal cells.

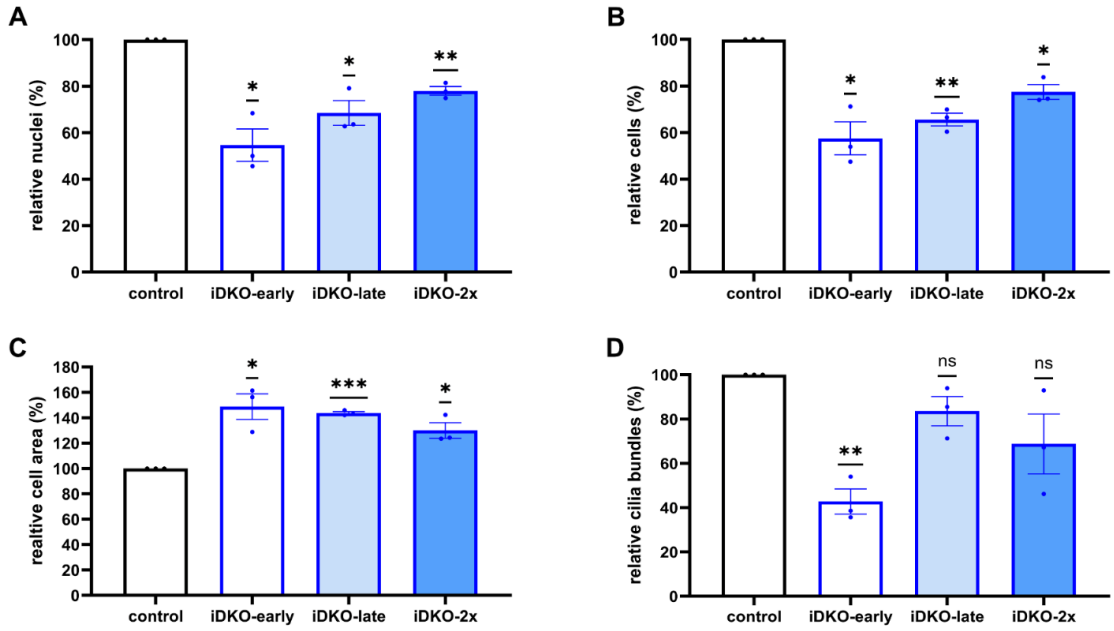

Figure 2.24 Increased plating density or delayed gene deletion partially alleviate but do not fully rescue multiciliation and cell density defects in EPS15/15R iDKO cultures. (A–D) Quantification of relative nuclei number **(A)**, cell number **(B)**, mean cell area **(C)**, and number of cilia bundles **(D)** at DIV14 in control, iDKO-early, iDKO-late, and iDKO-2x cultures. In iDKO-early cultures, early tamoxifen application caused the strongest reduction in nuclei and overall cell numbers, accompanied by enlarged cell areas and a marked loss of multiciliated bundles. Delaying tamoxifen induction (iDKO-late) or increasing initial plating density (iDKO-2x) partially improved nuclei and cell numbers, but values remained below control levels. Cell area enlargement persisted across all iDKO conditions, and cilia bundle numbers showed high variability and partial recovery compared to iDKO-early (n=3 individual experiments; one-sample t-test; data are shown as individual data points with mean ± SEM; significance levels: ns=non-significant, *=p<0.05, **=p<0.01, ***=p < 0.001).

Collectively, these findings indicate that EPS15 and EPS15R are critical for proper ependymal cell maturation, likely by influencing (signaling) processes affecting FOXJ1 expression and thereby multiciliogenesis. The persistence of reduced cell numbers, enlarged cell areas, and a tendency to impaired ciliation in iDKO cultures, despite increased seeding density or delayed deletion, indicates that these defects reflect cell intrinsic effects of EPS15/15R loss rather than secondary consequences of culture conditions. As these observations are based on in vitro analyses, future studies employing dissections and whole mount staining of lateral ventricular walls will be critical to validate these findings and assess the integrity of the ependymal layer in vivo in its native tissue context. The observed early onset of hydrocephalus at P5, coinciding with ependymal maturation, further underscores the importance of EPS15 family proteins in regulating terminal ependymal differentiation, with their loss potentially disrupting cerebrospinal fluid dynamics and contributing to the pathogenesis of hydrocephalus.

3 Discussion

The mammalian brain is built through a highly orchestrated sequence of events, where new neurons are born and migrate to their destinations, and subsequently wire into networks that ultimately support thought, memory, and behavior. Each of these developmental steps depends on cells being able to constantly adjust how they interact with their environment, whether that means responding to guidance cues, remodeling adhesion sites, or tuning the strength of emerging synapses. Such flexibility is not achieved by alterations in gene expression alone but relies on rapid and reversible mechanisms, that function within shorter timescales. Endocytosis represents one such mechanism. By continuously internalizing receptors, transporters, and adhesion molecules, it ensures that neurons can fine-tune their responsiveness to signals, recycle the machinery required for neurotransmitter release, and remodel connections as circuits mature. In this context, endocytosis emerges not just as a background process but as a central mechanism that enables neurons to adapt to their developmental and functional demands.

At synapses, the stakes are especially high, since the presynaptic terminals must recycle vesicles with every round of neurotransmission, while postsynaptic sites must constantly regulate receptor abundance to enable synaptic plasticity. To carry out these tasks with precision, neurons rely on a diverse set of endocytic adaptor proteins. These adaptors act as the molecular interface between cargo and the endocytic machinery, ensuring that specific receptors, transporters, or adhesion molecules are selectively internalized at the right time and place. Over the past decades, many such adaptors have been identified (*see section 1.2*). Their importance in the brain has become clear from the phenotypes that arise when they are disrupted, ranging from failures in synaptic vesicle recycling (Koo et al., 2015b; Pechstein et al., 2015) to profound developmental defects (Abdi et al., 2019; Jakob et al., 2017b; W. Li et al., 2010; Mitsunari et al., 2005) Among the many adaptor proteins that contribute to these processes, EPS15 and its paralog EPS15R remain relatively little explored in the context of the mammalian brain. In this thesis, we demonstrate that EPS15 and EPS15R play important roles in the mammalian brain, not only consistent with their canonical functions as endocytic adaptors but also suggesting broader contributions that extend beyond endocytosis and influence neurogenesis and brain development.

3.1 EPS15 and EPS15R as endocytic adaptors in the brain and synapse

Much of what is known about the function of EPS15 and EPS15R in brain stems from studies in non-mammalian systems, where orthologs of EPS15 have been shown to be indispensable for synaptic vesicle recycling and efficient neurotransmission (Koh et al., 2007; Salcini et al., 2001b). In mammalian cell lines, both proteins have been established as scaffolding adaptors that initiate clathrin-mediated endocytosis and mediate the uptake of classical cargos such as the transferrin receptor and EGFR (Carbone et al., 1997; F. Huang et al., 2004). Yet, despite their clear involvement in endocytic pathways, their specific roles in the brain and in synaptic organization have remained poorly defined. It is still not understood to what extent EPS15 and EPS15R act redundantly or carry distinct functions in neurons, nor how their adaptor activities influence neuronal signaling.

It had been previously shown that both EPS15 and EPS15R are expressed in the brain, with EPS15R being preferentially enriched compared to its paralog (Milesi et al., 2019). Our results expand on this observation by revealing that the two proteins follow distinct regional expression patterns in the brain (Fig. 2.1 A,B,C). EPS15 is particularly abundant in the cerebellum, whereas EPS15R shows strong enrichment in both cerebellum and cortex but is relatively low in the hindbrain. The presence of both proteins in the hippocampus suggests that they may contribute to hippocampal function. Importantly, we also find that EPS15 and EPS15R expression is dynamic as it increases progressively throughout postnatal development (Fig. 2.1 D, S1). This temporal regulation mirrors that of other endocytic adaptors such as AP2-α, and synaptic vesicle proteins such as Synaptotagmins and Synaptophysin (Fig. 2.1 E) (Berton et al., 1997; Knaus et al., 1986; Koo et al., 2015b). Notably, these upregulations coincide with key developmental transitions such as synaptogenesis, activity-dependent synaptic remodeling, and the onset of experience-driven plasticity, all of which require a functional synaptic vesicle pool and efficient endocytosis for vesicle recycling and receptor turnover (Camblor-Perujo & Kononenko, 2022; Lohmann & Kessels, 2014). In addition, the increase in AP-2 expression during postnatal development likely also contributes to dendritogenesis (Koscielny et al., 2018). The postnatal increase in Synaptophysin most likely is related to synaptogenesis with which it coincides, and might be involved in activity-dependent synapse formation (Knaus et al., 1986; Tarsa & Goda, 2002). Similarly, Synaptotagmins such as Syt1, II, III, and IV are strongly upregulated postnatally, coinciding with the onset of activity-dependent neurotransmission (Berton et al., 1997; Kochubey et al., 2016). In line with these trajectories, the progressive increase of EPS15 and EPS15R expression likely reflects a

comparable requirement for enhanced endocytic capacity to sustain vesicle recycling, receptor turnover, and synaptic plasticity in the maturing nervous system.

While expression analyses highlight that EPS15 and EPS15R are developmentally regulated and regionally enriched, understanding their contribution to neuronal function also requires knowledge of their synaptic expression and precise subcellular localization. Neurons are uniquely polarized, and adaptor proteins may exert distinct functions depending on whether they operate at presynaptic terminals, where vesicle recycling is critical, or at postsynaptic sites, where receptor trafficking shapes synaptic strength. Determining where EPS15 and EPS15R reside within the synapse was therefore essential to connect their adaptor roles with the mechanisms of neurotransmission and plasticity. Previous studies have provided initial insights into where these two paralogs may be located within the synapse. EPS15R was reported to co-localize with the presynaptic marker synaptophysin and was also enriched in synaptosomal fractions in comparison to postsynaptic density fraction, indicating a predominantly presynaptic presence (Milesi et al., 2019). By contrast, EPS15 has been observed to partially co-localize with the postsynaptic marker PSD95, while forming dense clusters along dendrites in hippocampal neurons, suggesting an enriched presence at the postsynapse. Supporting this notion, EPS15's participation in the trafficking of GluA1, also points towards a role at the postsynapse (Lin & Man, 2014). These earlier studies place EPS15R at presynaptic terminals and EPS15 at postsynaptic sites, but our data indicate that this division is too simplistic. We employed the tryptic cleavage assay to distinguish protected presynaptic proteins from exposed postsynaptic components (Fig. 2.2 A). While canonical presynaptic markers such as SNAP25 and synaptophysin were resistant to trypsin mediated digestion, postsynaptic receptors like GluA1 and GluA2 were efficiently cleaved. Surprisingly, EPS15 and EPS15R were only partially degraded, exhibiting about 60% protein cleavage (Fig. 2.2 B,C). This partial sensitivity points to a distribution across both sides, pre- and post- of the synapse rather than a strict compartmentalization. This phenotype is reminiscent of other endocytic adaptors, ITSN1 and CALM (Azarnia Tehran et al., 2022; Vollweiter et al., 2023b). This similarity is unlikely to be coincidental, since ITSN1 is a known interactor of EPS15 family proteins (Koh et al., 2007; Milesi et al., 2019), and CALM, like EPS15, has been implicated in the trafficking of GluA1 (Azarnia Tehran et al., 2022). It is therefore plausible that EPS15/15R might share functional parallels with CALM and its close interactor ITSN1. These findings suggest that EPS15 and EPS15R are versatile components of the synaptic endocytic machinery, acting possibly in both presynaptic vesicle recycling and postsynaptic receptor turnover, thereby contributing to the overall plasticity and adaptability of synapses. The trypsin cleavage assay primarily informs on protein localization based on protein accessibility to trypsin and provides quantitative insight into

their relative abundance at either site, but to resolve a protein´s synaptic localization at nanoscale level, complementary methods like STED microscopy will be required in the future. STED offers the spatial precision to not only distinguish a protein´s distribution at pre- versus postsynaptic sites but can visualize adaptor proteins within synaptic nanodomains. Currently, we could not attempt this as no reliable antibodies for EPS15 or EPS15R immunostaining were available. An alternative strategy would be to use CRISPR/Cas9 for endogenous tagging of EPS15 and EPS15R directly in primary neurons, for example using the ORANGE system (Willems et al., 2020). This strategy enables the insertion of small epitope or fluorescent tags at endogenous loci in cultured neurons, which would allow live-cell imaging of EPS15 and EPS15R at native expression levels and facilitate nanoscale mapping of their distribution when combined with super-resolution techniques.

3.1.1 EPS15 and EPS15R as players in AMPAR endocytosis

Multiple endocytic adaptor proteins have been implicated in AMPAR internalization during synaptic plasticity. The μ2 subunit of AP-2 directly binds GluA2 and GluA3, a mechanism required for NMDAR-dependent synaptic plasticity (Kastning et al., 2007; Lee et al., 2002). PICK1 associates both with GluA2 and the α-adaptin subunit of AP-2, and its disruption impairs constitutive and activity-dependent AMPAR endocytosis (Fiuza et al., 2017; Hanley & Henley, 2005). CALM regulates ubiquitinated GluA1-containing calcium-permeable AMPARs by promoting their endocytosis via its ANTH domain, thereby shaping synaptic plasticity (Azarnia Tehran et al., 2022). Similarly, it was shown that EPS15 interacts with the ubiquitinated AMPA receptor subunit GluA1 and promotes its internalization (Lin & Man, 2014), but whether this property is conserved in EPS15R had not been addressed. With this study we have now shown that EPS15R also contributes to the regulation of GluA1 containing AMPARs.

We examined EPS15R-GluA1 interactions in the brain using co-immunoprecipitation from brain enriched synaptic fractions (Fig. 2.3 A). Strikingly, GluA1 was consistently detected in EPS15R complexes, with the interaction strongest in purified synaptic membranes, a compartment where receptor internalization is expected to occur. Parallel experiments with EPS15 confirmed its robust association with GluA1 under identical conditions, validating both our experimental strategy and the idea that the two paralogs can converge on similar postsynaptic targets (Fig. 2.3 B). Together, these findings argue that EPS15R, like EPS15, is able to engage GluA1 in the brain and may therefore participate in AMPAR endocytosis. Our data opens the possibility that both paralogs act in parallel to regulate postsynaptic receptor trafficking, thereby broadening the repertoire of adaptors implicated in AMPAR regulation.

Building on this evidence for a biochemical association, an important consideration was whether the interaction between EPS15 family proteins and GluA1 had functional consequences for AMPAR trafficking. Previous studies had already shown that knockdown of EPS15 impairs the internalization of ubiquitinated GluA1 (Lin & Man, 2014), pointing to a postsynaptic role in receptor turnover. Consistent with this, SEP-GluA1 imaging revealed that loss of EPS15 and EPS15R caused a strong accumulation of surface receptors, indicative of reduced basal AMPAR endocytosis (Fig. 2.9 B). With this finding we not only confirmed the reported role of EPS15 but also established that EPS15R participates in the same pathway. At the same time, the use of a double knockout limited our ability to disentangle paralog-specific contributions. To better resolve the degree of redundancy between EPS15 and EPS15R in AMPAR trafficking, one approach would be to compare the surface GluA1 accumulation in neurons lacking either paralog individually. In addition, rescue experiments in the double knockout background could test whether re-expression of EPS15 or EPS15R is sufficient to reverse the surface accumulation phenotype. It is also important to note that EPS15/15R are unlikely to act as the sole adaptors for GluA1 endocytosis. We previously showed that, in addition to CALM which selectively regulates calcium-permeable AMPARs, both HIP1 and HIP1R can bind and internalize ubiquitinated GluA1 (Azarnia Tehran et al., 2022). This raises the possibility of compensatory mechanisms in the absence of EPS15/EPS15R. Evaluating CALM and HIP1/HIP1R levels in our iDKO neurons, and testing whether their co-depletion further increases GluA1 surface accumulation or whether their overexpression can restore normal surface levels, will be important to clarify the extent of redundancy versus specificity among these adaptor proteins. The apparent multiplicity of adaptors acting on AMPARs may reflect the need for context-dependent regulation, allowing neurons to fine-tune receptor trafficking across distinct subcellular compartments, developmental stages, or activity states. Such modularity could ensure robust control of synaptic strength under varying physiological or stress conditions, while maintaining resilience against the loss or dysfunction of individual adaptor proteins.

Another important question is whether EPS15R, like EPS15, also relies on ubiquitin-interacting motifs (UIMs) to mediate GluA1 internalization (Lin & Man, 2014). Ubiquitination is a critical sorting signal that directs GluA1 away from constitutive AP2-mediated recycling and toward activity-dependent endocytosis and degradation (Schwarz et al., 2010). Under high activity, such as triggered by AMPA stimulation, GluA1 ubiquitination is induced and serves as the trigger for its internalization and subsequent degradation. For EPS15 to facilitate GluA1 endocytosis, Nedd4-mediated ubiquitination of GluA1 and recognition through its UIMs is required (Lin & Man, 2014), while CALM similarly relies on ubiquitin binding via its ANTH domain to internalize

GluA1 (Azarnia Tehran et al., 2022). To determine whether EPS15R acts in the same pathway, rescue experiments in iDKO neurons with EPS15R mutants lacking UIMs would directly test the requirement for ubiquitin binding. Complementary approaches could involve mutating GluA1 at K868 to prevent its ubiquitination, and combining this with wild-type EPS15R re-expression, which would clarify whether EPS15R function depends on receptor ubiquitination, as has been shown for EPS15 and CALM. Together, such experiments would establish whether EPS15R shares the ubiquitin-dependent mechanism characterized for EPS15 and CALM, or whether it fulfills a distinct role in regulating GluA1 trafficking.

As a complementary validation, GluA1 surface levels should be quantified by biotinylation-based isolation of surface proteins performed on EPS15/15R iDKO neurons or eDKO brain tissue. In addition, STED super-resolution microscopy could be used to test whether EPS15 and EPS15R are required for the recruitment of AMPAR subunits to endocytic sites, as their loss may reduce the co-localization of AMPAR subunits with endocytic markers such as clathrin. To directly assess their role in AMPAR internalization, endocytic uptake can be examined using an antibody feeding assay in which live neurons are labeled with antibodies recognizing the extracellular domain of GluA1, followed by controlled internalization and acid stripping to visualize the internalized receptor pool. This approach could further be complemented by live imaging of pHluorin-tagged AMPARs to dynamically monitor receptor trafficking and endocytic events in real time. To assess the specificity of EPS15 and EPS15R in receptor sorting, surface and total levels of all other AMPAR subunits (GluA1–4) as well as NMDAR subunits (GluN1, GluN2A/B) should be analyzed. This can be achieved by immunofluorescence labeling of control and iDKO neurons under non-permeabilized conditions to detect surface receptors and detergent-permeabilized conditions to measure total pools, using antibodies against extracellular domains of these subunits. Quantifying surface-to-total ratios for different neurotransmitter receptors would reveal whether EPS15/EPS15R act selectively on GluA1 or more broadly across glutamate receptor subtypes.

AMPAR trafficking is central to the two major forms of synaptic plasticity: long term potentiation (LTP), that strengthens synaptic transmission through activity-driven exocytic delivery of AMPARs into the postsynaptic membrane and long term depression (LTD), that weakens synapses by AMPAR endocytosis and removal from the surface (Diering & Huganir, 2018). In CALM knockout mice we observed impaired LTD, consistent with a chronic surface accumulation of GluA1 (Azarnia Tehran et al., 2022). To gain insight into whether EPS15/EPS15R may play a complementary role in regulating neurotransmission and synaptic plasticity, electrophysiological approaches should be employed. Measuring LTD in EPS15 and EPS15R deficient neurons would reveal whether their loss interferes with these receptor trafficking processes. Such experiments

would provide valuable insight into how EPS15 and EPS15R shape neurotransmission and plasticity and may ultimately influence learning and memory in the brain. Nevertheless, our study already positions the EPS15 family as critical endocytic adaptors in postsynaptic GluA1 AMPAR trafficking, underscoring their importance in maintaining receptor homeostasis and synaptic plasticity.

3.1.2 EPS15/15R are dispensable for TfR endocytosis in neurons

Having established a role for EPS15 family proteins in AMPAR regulation, we next asked whether their function extends to other cargos. Apart from GluA1, another receptor that has been repeatedly implicated as an EPS15/15R cargo is the transferrin receptor (TfR) (F. Huang et al., 2004; Milesi et al., 2019). Initial studies in HeLa cells have shown that simultaneous depletion of EPS15 and EPS15R disrupts TfR uptake, pointing to an essential role for these adaptors in ligand-induced endocytosis of TfR (F. Huang et al., 2004). In the mammalian hematopoietic system, combined deletion of both paralogs also severely impaired TfR trafficking, ultimately leading to iron imbalance and defective red blood cell maturation (Milesi et al., 2019). In primary fibroblasts, loss of EPS15 alone did not affect TfR internalization, suggesting that EPS15R or other adaptor proteins can compensate in this context (Pozzi et al., 2012b). Given the unique endocytic demands of neurons, ranging from synaptic vesicle recycling to receptor turnover, it remained unclear whether loss of both paralogs would compromise TfR uptake or whether compensatory mechanisms would preserve TfR internalization. Additionally, mice lacking TfR in neural progenitors develop lethal seizures associated with excessive AMPAR surface expression (K. Liu et al., 2016), a phenotype that closely resembles the seizures observed in EPS15/15R eDKO mice. Hence, it was important to assess whether defective TfR endocytosis might underlie this phenotype. However, with this study, we could confirm that transferrin uptake in hippocampal neurons remains unaffected, as iDKO cultures internalized fluorescently labeled transferrin to the same extent as controls (Fig. 2.8 C,D). This indicates that the observed neurological phenotype is unlikely to result from impaired TfR internalization. Thus, despite the established role of EPS15 family proteins in TfR trafficking in other cell types, they appear dispensable for transferrin internalization in the neuronal context. Instead, clathrin-mediated endocytosis of TfR remains functionally preserved, suggesting that alternative adaptor proteins can substitute for EPS15 and EPS15R in supporting this canonical pathway. Moreover, since TfR is a bona fide clathrin-mediated endocytosis cargo, the unaltered uptake further indicates that global CME function is intact in neurons lacking both paralogs. Interestingly, this mirrors observations made for the adaptor protein CALM, which is indispensable for transferrin uptake in erythroblasts (M. Suzuki et al., 2012) but dispensable in neurons (Azarnia Tehran et al., 2022). Together, these findings

underscore that adaptor requirements are strongly shaped by cellular context. For neurons, the ability to maintain transferrin uptake independently of EPS15 family proteins may reflect the high prioritization of nutrient acquisition via redundant adaptors which can facilitate the uptake of TfR.

In this regard, it is notable that the transferrin receptor itself has also been implicated in AMPAR trafficking, linking iron uptake pathways to synaptic regulation. TfR regulates AMPAR trafficking by promoting AP2–GluA2 binding (K. Liu et al., 2016). Its loss disrupts AMPAR internalization, causes surface accumulation of GluA1/2 and leads to impaired synaptic scaling. TfR uptake itself remained unchanged in our system but the way it regulates AMPAR trafficking resembles the function of EPS15/15R. While TfR modulates AP2–cargo interactions, EPS15/15R act as adaptors linking ubiquitinated receptors to the endocytic machinery. These findings raise the possibility that TfR and EPS15/15R converge on overlapping steps of the endocytic process, but through distinct molecular routes. Whether these mechanisms cooperate, compensate, or operate independently in neurons remains an important open question, and future work dissecting their interplay may clarify how multiple regulatory layers shape AMPAR trafficking and synaptic plasticity. Viewed together, these findings draw a coherent picture of EPS15 and EPS15R in the neuronal endocytic machinery. Their region-specific enrichment and developmental upregulation point to sustained importance throughout brain maturation. At the synapse, their distribution to both pre- and postsynaptic compartments suggests that they are required at both terminals, supporting vesicle recycling presynaptically while also regulating receptor trafficking postsynaptically. Consistent with this, we demonstrate that both paralogs converge on AMPAR trafficking, where their loss disrupts receptor internalization. By contrast, transferrin uptake remains intact in iDKO neurons, underscoring that nutrient acquisition is safeguarded by redundancy, while EPS15 family proteins are dedicated to more specialized, brain-specific cargos. Taken together, EPS15 and EPS15R emerge not only as canonical adaptors within clathrin-mediated endocytosis but also as possible regulators of synaptic and developmental processes in the mammalian brain.

3.2 Novel interactors of EPS15R

One of the key advances of this study was to move beyond candidate-based approaches and instead ask, in an unbiased manner, which proteins actually associate with EPS15 and/or EPS15R in the murine brain. While classical endocytic partners such as AP2, ITSNs, Epsins and various others are well established, little was known about the broader synaptic interaction landscape of these adaptors, and whether they may also engage with proteins outside the canonical endocytic machinery. To address this, we turned to co-immunoprecipitation from brain lysates combined with mass spectrometry, reasoning that such a proteomic screen would allow us to capture both established and unexpected binding partners of EPS15/15R in brain under near-physiological conditions. The experimental strategy was carefully validated by using antibodies, which reliably enriched known interactors while excluding non-specific proteins, ensuring that the subsequent large-scale analysis would yield meaningful data (Fig. 2.4 A,B). Following this validation, co-immunoprecipitated complexes were subjected to mass spectrometry, including sample preparation, peptide generation, and subsequent LC-MS/MS analysis (Fig. 2.4 C). With this foundation, the proteomic screen aimed to provide a global snapshot of the molecular environment of EPS15 and EPS15R in the adult brain, revealing not only shared interactors but also candidates that appeared to be enriched in a paralog-specific fashion. The proteomic analysis yielded a rich set of interaction partners selectively enriched in EPS15 or EPS15R complexes (Fig. 2.5 A,B). As anticipated, both adaptors were enriched in their respective immunoprecipitates, confirming the robustness of the assay. Beyond this expected validation, the datasets prominently featured a suite of expected classical endocytic proteins. This pattern not only reinforces the established roles of EPS15 and EPS15R as integral parts of the endocytic machinery but also provides confidence that the approach captured biologically meaningful interactions rather than experimental noise.

EPS15s along with FCHo1/2 and Epsins have long been recognized as early endocytic adaptors that orchestrate the initiation of clathrin-mediated endocytosis (CME) (Henne et al., 2010a). Hence, the strong enrichment of these endocytic proteins along with clathrin light and heavy chains in our co-immunoprecipitates was expected and confirmed the reliability of the dataset. Another important confirmation of the dataset came from the enrichment of the adaptor protein complex AP-2. This complex is a well-established partner of EPS15s, and their association has been shown to be critical for receptor-mediated endocytosis (Benmerah et al., 1998; Collins et al., 2002). Our co-immunoprecipitates also contained all subunits of AP-2, providing strong evidence that the interaction was captured comprehensively. The strong enrichment of ITSN1 and ITSN2 stands out as particularly meaningful, as Intersectins have long been recognized as important

binding partners of EPS15-family proteins (Koh et al., 2007; Sengar et al., 1999b), which cooperate to organize endocytic scaffolds and promote efficient vesicle recycling. This relationship is evolutionarily conserved in *Drosophila*, where EPS15 and its homologous partner Dap160 (ITSN homolog) act together at synapses and enhance endocytic efficiency, underscoring their synergistic role in vesicle turnover (Koh et al., 2007). Evidence from mammalian systems further supports this interdependence, as the loss of EPS15 and EPS15R was shown to reduce ITSN1 levels in the brain (Fig. 1.8 B), suggesting that these proteins not only interact but also stabilize one another at the molecular level (Milesi et al., 2019). Our finding that both ITSN1 and ITSN2 were robustly co-enriched with EPS15 and EPS15R in the mammalian brain therefore provides additional proteomic confirmation of this interaction under physiological conditions. Alongside these, other endocytic proteins like Numb, CALM, Stonin2, Synaptojanin1 were also enriched, confirming their already published interactions (Haffner et al., 1997; Martina et al., 2001; Morgan et al., 2003; Salcini et al., 1997b). To complement the analysis, we also applied gene set enrichment analysis, which allowed us to move beyond single interactors and instead assess which cellular processes were statistically overrepresented in the datasets. The outcome was strikingly consistent with the known functions of EPS15-family proteins as both interactomes showed strong enrichment for pathways related to clathrin-mediated endocytosis, synaptic vesicle trafficking, and other membrane transport processes (Fig. 2.5 C,D). Endocytosis ranked among the most significantly enriched categories, confirming that the proteomic approach captured the canonical endocytic machinery. This pathway-level view confirms that the proteomic screen reliably captured the established endocytic roles of EPS15 and EPS15R, thereby lending confidence to the identification of more unconventional or previously unrecognized binding partners. The gene enrichment analysis also revealed an interesting divergence between the two paralogs. The EPS15 interactome aligned closely with classical endocytic functions, emphasizing vesicle-mediated uptake and receptor internalization, consistent with its established role in clathrin-mediated endocytosis. In contrast, the EPS15R dataset showed a broader spectrum of categories, extending into processes such as endoplasmic reticulum and endosomal transport. This difference suggests that EPS15R may not be confined to endocytosis alone but could contribute to more specialized pathways of membrane remodeling and intracellular transport. Such a shift is particularly intriguing, as it raises the possibility that EPS15R is potentially linked to ER–Golgi dynamics or even autophagy. In line with this, several candidate interactors emerged from the proteomic screen that point directly to these extended functions, most notably CALCOCO1, a receptor involved in selective autophagy, and SEC16A, a critical organizer of ER exit sites and ER–Golgi trafficking.

3.2.1 EPS15R interaction with CALCOCO1 points to Endocytosis–Autophagy crosstalk

CALCOCO1 emerged as one of the top hits in our co-immunoprecipitation mass spectrometry analysis, showing a level of enrichment comparable to well-established endocytic adaptors (Fig. 2.5 B, Table S1), which gave us confidence to examine this interactor more closely and follow up on its potential significance. CALCOCO1 is a known, rather recently discovered, selective autophagy receptor that safeguards intracellular homeostasis by directing dysfunctional or excess endomembrane compartments to degradation (W. Chen et al., 2022; Nthiga et al., 2020b, 2021). In particular, it has been implicated in ER-phagy (Nthiga et al., 2020b) and Golgiphagy (Nthiga et al., 2021), processes that target specific domains of the ER and Golgi apparatus for lysosomal clearance. Mechanistically, CALCOCO1 connects these organelles to the autophagic machinery through direct binding to ATG8 family proteins via its LC3-interacting region (Nthiga et al., 2020b), thereby recruiting autophagosomal membranes to ER and Golgi subdomains during selective autophagy. In doing so, it contributes to organelle quality control, membrane remodeling, and proteostasis, functions that become especially important under stress conditions. Its established relevance in autophagy makes its strong co-enrichment with EPS15R particularly intriguing, raising the possibility that EPS15R could influence selective autophagy and/or ER–Golgi turnover through a direct association with CALCOCO1. In order to validate this mass spectrometry finding, we first performed a co-immunoprecipitation experiment and confirmed that EPS15R indeed could successfully pull down CALCOCO1, thereby reinforcing the proteomic data (Fig. 2.6 A). To further confirm this interaction, we performed co-transfection experiments with EPS15R and CALCOCO1 plasmids in both HeLa cells and primary neurons. Under these conditions, CALCOCO1 was strongly recruited into EPS15R-positive puncta (Fig. 2.6 C,D), presumably EPS15R condensates, whereas when expressed on its own it appeared more diffusely distributed (Fig. S2), suggesting that EPS15R promotes CALCOCO1 localization within EPS15R-induced liquid–liquid phase-separated assemblies.

The potential interaction between EPS15R and CALCOCO1 opens up intriguing physiological possibilities. One speculative scenario is that EPS15R, in concert with CALCOCO1, could act as a molecular link between endocytosis and selective autophagy under conditions of membrane or trafficking stress. A parallel can be drawn to the yeast adaptor Ede1, the functional homolog of EPS15, which has been shown to safeguard the endocytic machinery during stress conditions by redirecting defective or stalled endocytic assemblies to autophagic clearance (Wilfling et al., 2020a). Ede1 undergoes liquid–liquid phase separation, forming condensates of aberrant

clathrin-mediated endocytic assemblies, which are subsequently cleared through selective autophagy. This process is mediated by its ability to engage ATG8, thereby marking defective endocytic complexes for degradation (Wilfling et al., 2020a). Mammalian EPS15 and EPS15R are also known to undergo liquid–liquid phase separation (Day et al., 2021), raising the possibility that mechanisms analogous to those described for Ede1 in yeast may exist in higher organisms. Interestingly, our proteomic screen did not detect core autophagy proteins such as ATG family members or LC3, suggesting that EPS15R does not directly engage the autophagic machinery. Instead, CALCOCO1 may provide the missing link by bridging EPS15R to autophagosomes, as it directly binds ATG8 family proteins through its LC3-interacting region (Nthiga et al., 2020b). In this way, CALCOCO1 could act as an adaptor that connects phase-separated endocytic assemblies induced by EPS15R to the autophagy pathway, thereby enabling selective turnover of defective endocytic complexes or remodeling of endomembrane compartments. This interpretation aligns well with the yeast paradigm while at the same time offering a plausible explanation for how such a function might be executed in the mammalian system. This observation suggests that CALCOCO1 may be actively recruited into EPS15R condensates, positioning it to link these assemblies to the autophagic machinery. And CALCOCO1, with its established role in ER-phagy and Golgiphagy, could serve a similar quality-control function in mammalian cells by targeting dysfunctional endomembrane domains for degradation. EPS15R, just like Ede1 in this context might enable the recognition and turnover of endocytic or trafficking intermediates that fail to progress, thereby maintaining homeostasis of the endomembrane system. Such a mechanism would be particularly relevant in neurons, where the balance between efficient receptor trafficking and the clearance of defective membrane compartments is essential for long-term synaptic function. While direct evidence is still lacking, the CALCOCO1–EPS15R association identified here raises the possibility that EPS15R extends its role beyond endocytosis to contribute to autophagy-mediated quality control of the neuronal membrane system.

In order to test this hypothesis, it will be important to probe whether other endocytic proteins co-reside within EPS15R–CALCOCO1 assemblies and whether their localization depends on EPS15R. We also would need to confirm whether these puncta display properties of liquid-like condensates, using FRAP experiments to monitor their recovery time or by acute disruption of LLPS with chemicals like 1,6-hexanediol which dissolve liquid-like assemblies (Wilfling et al., 2020b). Simultaneously, functional assays are needed to determine whether EPS15R contributes to the autophagic clearance of aberrant endocytic assemblies, for instance induced by stalled clathrin-coated pits through Pitstop (clathrin inhibitor) treatment (von Kleist et al., 2011) or Dynasore (dynamin inhibitor) treatment (Macia et al., 2006). The lifetime and turnover of these

stalled intermediates could be monitored by live-cell TIRF imaging of fluorescently tagged endocytic components under control versus autophagy-deficient conditions, thereby directly probing whether autophagy supports their resolution. In parallel, high-resolution imaging can be applied to examine whether core autophagy components, such as ATG8/LC3 proteins, are recruited to stalled endocytic intermediates. Moreover, a potential impact of EPS15R deletion on CALCOCO1 function should be examined to clarify whether CALCOCO1's role in selective autophagy depends on EPS15R. Finally, an important aspect to fully uncover and support this hypothesis is understanding how EPS15R and CALCOCO1 interact at the domain level. Both yeast Ede1 and mammalian EPS15 rely on their coiled-coil domains for phase separation, enabling the formation of liquid-like protein assemblies (Day et al., 2021; Kozak & Kaksonen, 2022b). Since CALCOCO1 itself contains a coiled-coil region (Fig. S2) (Nthiga et al., 2020b), this represents the most likely interface for interaction with EPS15R, though whether these regions indeed mediate CALCOCO1 recruitment remains to be determined. Together, these approaches will clarify whether EPS15R and CALCOCO1 form a functional module connecting endocytosis with selective autophagy, thereby extending the classical role of EPS15-family proteins into broader pathways of membrane maintenance and cellular homeostasis.

3.2.2 The ER exit site scaffold SEC16A as a novel EPS15R interactor

SEC16A also emerged as another highly enriched interactor in our proteomic screen (Fig. 2.5 B, Table S1), with levels of enrichment comparable to classical endocytic adaptors, similar to CALCOCO1. SEC16A is a large scaffold protein best known for its role in organizing endoplasmic reticulum exit sites and enabling the formation of COPII-coated vesicles, thereby driving cargo trafficking from the ER to the Golgi in the early secretory pathway (Connerly et al., 2005; Watson et al., 2006). While this canonical function in secretion is well established, more recent work has expanded its significance to broader aspects of membrane trafficking, particularly under conditions of cellular stress. In such contexts, SEC16A has been shown to associate with Golgi reassembly stacking proteins (GRASPs) and to undergo regulation by autophagy-initiating kinases, highlighting its potential role at the interface of secretory and autophagic pathways (Joo et al., 2016; Piao et al., 2017). The enrichment of SEC16A in the EPS15R interactome therefore suggests that EPS15R may influence also early secretory and stress-responsive membrane dynamics, raising intriguing questions about how these pathways may intersect in neurons. To validate this mass spectrometry finding, we performed co-immunoprecipitation experiments and were able to confirm that EPS15R was able to co-precipitate SEC16A (Fig. 2.6 B), thereby reinforcing the proteomic data and establishing SEC16A as a bona fide interactor of EPS15R.

However, we were unable to verify their co-localization in cells, as suitable antibodies and plasmids for reliable detection of SEC16A were not available.

What the interaction between EPS15R and SEC16A means in a physiological context remains an open question that we need to address. In addition to SEC16A, our proteomic screen also identified other components of the COPII machinery, including SEC23 and SEC24, although these were not as highly enriched. This raises the possibility that EPS15R may associate more broadly with elements of the secretory pathway. However, since CALCOCO1 is an established autophagy receptor (Nthiga et al., 2020b, 2021) and SEC16A itself has been reported to undergo post-translational regulation by autophagy-initiating kinases (Joo et al., 2016) and to contribute to autophagosome-related membrane remodeling under stress (Piao et al., 2017), it is conceivable that SEC16A participates in the same autophagy-related pathway as CALCOCO1 and EPS15R. In such a model SEC16A, as shown in yeast, might generate a specialized subset of COPII vesicles that are redirected toward forming autophagosomes (Lemus & Goder, 2016). EPS15R could function as a scaffold protein by first assembling condensates with stalled endocytic machinery and then linking these to CALCOCO1 while also stabilizing SEC16A at modified ER exit sites. CALCOCO1 would provide the selective recruitment of cargo and mediate LC3 engagement, whereas SEC16A would supply the membrane platform required for autophagosome initiation. Interestingly, ultrastructural studies of Ede1 condensates in yeast revealed that these assemblies are frequently wrapped by ER membranes, creating a ribosome-free microenvironment at the plasma membrane–ER interface (Wilfling et al., 2020b). This spatial coupling between endocytic condensates and ER domains provides a precedent for how endocytic adaptors could integrate with secretory membranes. Thus, the parallel recovery of CALCOCO1 and SEC16A in our immunoprecipitates may indicate a functional convergence in which endocytic adaptors, autophagy receptors and secretory scaffolds cooperate to redirect ER exit site activity away from secretion and toward autophagosome biogenesis under stress. To test this hypothesis, several complementary experimental strategies can be applied. Co-expression and imaging of SEC16A, EPS15R, and CALCOCO1 would allow us to visualize whether these proteins come together, particularly under stress conditions like nutrient starvation or by inducing aberrant endocytic assembly formation (with Pitstop or Dynasore). We would also need to determine whether these proteins colocalize with early autophagy markers such LC3. Loss-of-function approaches, such as knockdown or acute depletion of each component, would clarify whether they are required for efficient autophagosome formation and flux, which can be measured by LC3 puncta accumulation and p62 degradation (Kuijpers et al., 2021). In parallel, secretion and autophagy could be measured within the same cellular context, for instance by combining a secretion reporter such as

the RUSH system (Boncompain et al., 2012) with LC3 flux measurements, to determine whether the activity of this triad mediates a switch from secretion to autophagy during stress. Additionally, co-immunoprecipitation experiments could be performed under normal and autophagy-inducing conditions to determine whether the interaction between EPS15R, SEC16A, and CALCOCO1 is strengthened during stress, thereby supporting a functional link in autophagy. Finally, membrane-tracing experiments could help establish whether ER- or Golgi-derived membranes contribute to autophagosomes in a SEC16A-dependent manner, and electron microscopy could provide ultrastructural evidence for the same. Together, these approaches would offer a straightforward means to evaluate whether SEC16A, EPS15R, and CALCOCO1 cooperate functionally to redirect secretory trafficking machinery toward autophagosome biogenesis.

Taken together, the identification of CALCOCO1 and SEC16A as highly enriched EPS15R interactors highlights an unexpected expansion of the EPS15R interaction landscape beyond classical endocytic adaptors. Their selective enrichment in EPS15R, but not EPS15, argues for non-redundant functions of the two paralogs. While CALCOCO1 points toward a potential link between endocytosis and selective autophagy, SEC16A suggests a connection with ER exit site organization. Although the precise physiological relevance of these interactions remains to be established, their recovery alongside canonical endocytic proteins argues that EPS15R may act as a versatile scaffold at the interface of multiple membrane trafficking pathways. Future experiments will define the molecular details of these associations and determine whether EPS15R coordinates endocytosis, secretion, and autophagy in a context-dependent manner, particularly in neurons where tight regulation of membrane turnover is essential for long-term function.

3.3 Consequences of EPS15/15R loss on development and behavior

Having established EPS15 and EPS15R as canonical adaptors in endocytosis and uncovered non-canonical functions of EPS15R in processes such as autophagy and secretion, we next asked how their loss impacts the brain at the organismal level. Understanding their role in shaping postnatal growth, development, and neural function required a model system that allows controlled perturbation of both proteins in vivo, thereby enabling us to connect molecular functions with physiological outcomes. Past studies have revealed that the constitutive EPS15 knockout mice show no overt neurological impairments (Pozzi et al., 2012a), likely due to compensation by its paralog EPS15R, which proves more critical, since its absence leads to perinatal lethality with synaptic and sensory defects (Milesi et al., 2019). Combined deletion of both paralogs causes embryonic lethality, highlighting their shared yet non-redundant roles in development, but preventing insight into their functions in the postnatal brain. Against this background, our study provides an important extension: by generating a tissue-specific mouse model targeting both genes in the brain, we were able to bypass embryonal lethality and directly assess how their loss impacts postnatal development, neuronal function, and behavior. The forebrain-specific double knockout (eDKO) enabled us to assess developmental and organismal consequences in vivo. In addition, to minimize animal suffering, we established an inducible double knockout (iDKO) for cell culture experiments, that allowed temporal control of gene deletion in primary neuronal and ependymal cultures (Fig. 2.7 A). Our validation experiments confirmed that both systems functioned as intended (Fig. 2.7 B), providing robust models for the subsequent analyses of neuronal, developmental, and behavioral phenotypes. In addition, we also performed a proteomic analysis of forebrain tissue from control and eDKO mice (Fig. S3) in collaboration with Dr. Markus Räschle. This analysis revealed a marked depletion of EPS15R together with its major interaction partners, the Intersectins (ITSN1 and ITSN2), further confirming the efficient deletion of EPS15R in the eDKO brains.

3.3.1 EPS15R is essential for postnatal development and viability

Since the complete loss of EPS15 and EPS15R was shown to be lethal (Milesi et al., 2019), we first turned to the inducible knockout (iDKO) model to examine whether their deletion is compatible with neuronal survival. Using a Sytox assay, we found no significant reduction in the viability of cultured neurons lacking both proteins (Fig. 2.8 A,B). Having established that neuronal viability per se was not impaired in vitro, we investigated the consequences of neuronal loss of function at the organismal level using the forebrain-specific EPS15/15R knockout model. Our analysis of

revealed that eDKO mice were born in accordance with Mendelian ratios (Fig. 2.10 A). This demonstrates that the restricted deletion in the forebrain is not embryonically lethal and provides an opportunity to investigate the postnatal consequences of EPS15/EPS15R loss. Comparable findings have been reported for other endocytic adaptor proteins. For example, the forebrain-specific deletion of CALM also yielded offspring at Mendelian frequencies (Azarnia Tehran et al., 2022). In contrast, constitutive ITSN1/2 double knockout mice were viable but born at sub-Mendelian frequencies (Gerth et al., 2017). Together, these observations suggest that while the complete organismal loss of EPS15/15R disrupts early development too severely for viability, their forebrain-restricted deletion does not prevent the birth of viable pubs, thereby establishing this mouse model as a useful framework for studying later neurological outcomes.

Having established the forebrain-specific EPS15/15R knockout model, we next examined postnatal development and survival. Although eDKO mice were viable at birth and initially indistinguishable from their littermates, they displayed clear impairments as they matured (Fig. 2.10 D,E) and also. a progressive decline in viability, with roughly one third of eDKO mice dying within the first two months of life (Fig. 2.10 B,C). Notably, such deficits were absent in EPS15 single knockout mice, which developed normally in terms of both body weight and survival. These findings suggest that EPS15R is the main determinant of the postnatal lethality and growth impairment observed in the double knockout. Interestingly, this phenotype of the eDKO mice resembles that of AP180 knockout mice, which also show reduced weight gain and a steep decline in viability within the first postnatal month (Koo et al., 2015b). This similarity becomes even more striking when considering the neurological manifestations of both models. Approximately one third of the eDKO mice exhibited spontaneous epileptic seizures (Fig. 2.11 A), often presenting as tonic–clonic convulsions, with most observed episodes being short and transient (< 1 min) and followed by a return to normal activity after a few minutes. A comparable phenotype has been described for AP180 knockout mice, where a similar fraction of animals also suffered from spontaneous seizures (Koo et al., 2015b). While many episodes were mild, some AP180-KO mice progressed to fatal tonic extensions, which provided a direct explanation for the sharp decline in their postnatal survival. Taken together, these parallels suggest that seizures may also have contributed to the postnatal mortality of our eDKO mice, similar to what has been reported for AP180-KO, even though we did not directly observe fatal episodes in our own cohort. Consistent with this interpretation, seizure phenotypes have also been reported in other genetic models targeting presynaptic and endocytic regulators, including Synapsins, Amphiphysin, and Syndapin, further linking disturbances in vesicle trafficking machinery to epileptic activity (Di Paolo et al., 2002; Koch et al., 2011; Rosahl et al., 1995). Mutations in the endocytic adaptor

AP2M1 have also been linked to epileptic encephalopathies in humans (Helbig, Lopez-Hernandez, Shor, Galer, Ganesan, et al., 2019). Together, these findings point to seizures as a recurrent consequence of disrupting key components of the endocytic and synaptic vesicle machinery, highlighting that it is primarily presynaptic disturbances that critically impact network excitability and synaptic balance.

How these seizures arise in the context of adaptor protein loss remains an important mechanistic question. Epilepsy is broadly considered to result from an imbalance between excitatory and inhibitory neurotransmission, and perturbations of endocytic regulators can shift this balance in multiple ways. In the case of AP180 knockout mice, seizures have been attributed to presynaptic defects in synaptic vesicle recycling. Loss of AP180 prevents proper retrieval of Synaptobrevin-2, leading to its depletion from vesicles and a disproportionate reduction of inhibitory over excitatory transmission, as inhibitory terminals rely on high-frequency, tonic activity and therefore require more frequent vesicle recycling. Consequently, defects in synaptic vesicle reformation more strongly impair inhibitory neurotransmission, causing an excitatory/inhibitory imbalance which shifts hippocampal networks toward hyperexcitability, resulting in spontaneous seizures (Koo et al., 2015b). In our EPS15/15R eDKO model, the deletion is restricted to excitatory neurons of the forebrain, suggesting a different mechanism. Loss of EPS15 family proteins in invertebrates has been shown to cause vesicle depletion (Majumdar et al., 2006a; Salcini et al., 2001b), while EPS15R knockout mice show reduced vesicle density (Milesi et al., 2019). These findings point to an essential role of EPS15 family proteins in vesicle recycling, but it remains unclear how their deletion in mammalian neurons affects the sorting of specific vesicle proteins and the functional integrity of the vesicle pool. Unlike the AP180 model, where selective vulnerability of inhibitory synapses explains the seizures, in our case it may instead stem from defective vesicle recycling at excitatory terminals, potentially altering release probability or vesicle replenishment. However, direct evidence that a selective impairment of vesicle recycling at excitatory terminals causes hyperexcitability is lacking, and mechanistically it is difficult to envision how such a defect would directly trigger seizure activity. Therefore, more likely, secondary network-level adaptations or compensatory plasticity in response to impaired presynaptic function might contribute to the emergence of hyperexcitability.

Whether defects in EPS15/15R-deficient neurons also lead to an imbalance in neurotransmission, and thereby seizures, remains to be determined. To address this, it will be important to directly examine synaptic vesicle recycling in EPS15/15R-deficient neurons. Using pHluorin-tagged SV proteins such as Synaptotagmin1, Synaptophysin or Synaptobrevin2 in hippocampal neurons from iDKO mice, we can quantify surface-to-vesicular ratios and track exo–endocytic kinetics

under defined stimulation paradigms. Complementary assays to study SV protein retrieval using pH-sensitive antibody labeling of endogenous SV proteins will help validate these results. In addition, VGLUT and VGAT labeling will allow discrimination between excitatory and inhibitory terminals. As already discussed, impaired SV turnover could also compromise basal neurotransmission and disturb the excitation–inhibition balance, making it essential to measure basal synaptic transmission as well as the amplitudes of excitatory and inhibitory evoked currents (EPSCs and IPSCs) in eDKO neurons. In parallel, acute slice recordings under ictogenic conditions will provide information on seizure threshold and duration, offering direct insight into how EPS15/15R deficiency alters network excitability. Together, these experiments will clarify whether defective SV recycling and excitatory neurotransmission converge on a common pathway that drives hyperexcitability and seizure activity in our model.

Previous works have also demonstrated that dysregulation of AMPAR can trigger epileptic phenotypes. For instance, deletion of the transferrin receptor in neural progenitors causes lethal seizures in young mice, which were directly associated with an abnormal increase in AMPAR and accompanied by hindlimb clasping and early postnatal lethality (K. Liu et al., 2016). Similarly, our EPS15/15R knockout mice exhibit comparable neurological symptoms and early postnatal lethality, suggesting a shared underlying mechanism with the TfR knockout model. In our model, however, transferrin uptake is preserved, whereas GluA1 trafficking is impaired. Given that EPS15 and EPS15R interact with GluA1 and regulate its endocytosis, their loss in excitatory forebrain neurons may specifically disrupt AMPAR turnover, resulting in elevated surface expression which may enhance excitatory drive. Moreover, extensive basic and clinical studies support AMPAR as a molecular target in epilepsy therapy (Rogawski, 2013). These mechanisms together provide a plausible explanation for the seizures observed in our eDKO mice. To test this hypothesis, we would need to measure basal AMPAR-mediated synaptic transmission by recording field excitatory postsynaptic potentials (fEPSPs), alongside LTP and LTD recordings in eDKO mice. Changes in baseline synaptic strength or in the magnitude and stability of LTP/LTD would indicate altered GluA1 trafficking and support its role in driving hyperexcitability. In addition, applying a GluA1-selective inhibitor like IEM-1460 would help determine whether these effects are indeed driven by excessive GluA1 activity. However, it is important to note that forebrain-specific CALM knockouts, which are also implicated in AMPAR endocytosis, show impaired GluA1 trafficking with increased surface GluA1, enhanced LTP, and reduced LTD, yet display no deficits in viability or seizure activity (Azarnia Tehran et al., 2022). In the CALM knockout, surface levels of GluA1 are moderately increased (~1.3-fold), while GluA2 remains unchanged. In contrast, the TfR knockout shows a broader and more pronounced increase in both GluA1 and

GluA2 surface expression (~1.5-fold) (K. Liu et al., 2016). In EPS15/15R-deficient neurons, the GluA1 surface fraction rises even more strongly (~1.7-fold) (Fig. 2.9 B), indicating a more severe impairment of receptor internalization, although it remains to be determined whether GluA2 trafficking is similarly affected. These comparisons suggest that phenotype severity depends on both the extent and specificity of AMPAR accumulation. While modest, GluA1-restricted increases in the CALM knockout mainly affect plasticity, broader elevations involving multiple subunits, as in the TfR knockout, can provoke hyperexcitability. The pronounced GluA1 surface increase in EPS15/15R-deficient neurons may similarly enhance excitatory drive and contribute to seizure susceptibility, especially if GluA2 is also affected. Overall, whether excessive AMPAR surface accumulation directly contributes to the seizures and eventually the lethality observed in EPS15/15R-deficient mice remains to be determined.

3.3.2 EPS15R loss causes neurological and behavioral deficits

Beyond seizures, our eDKO mice also displayed additional neurological deficits, most notably hindlimb clasping reflex. In healthy mice, tail suspension triggers an outward extension of the hindlimbs, but in affected mutants this response is replaced by an abnormal inward folding of the legs, and sometimes also fore limbs, a behavior widely recognized as a marker of neurological impairment. Limb clasping had previously been noted in the constitutive EPS15R knockout mice (4 weeks old), although the sample size in that study was very limited, with only one out of four surviving KO mice showing clasping behavior (Milesi et al., 2019). Our findings now support this initial observation and confirm that loss of EPS15/15R is associated with the clasping behavior (Fig. 2.11 B, S4). In some mice, this abnormal reflex extended beyond the hindlimbs, with both hind- and forelimbs folding inward into a bat-like posture during tail suspension. Various mouse models of neurodegeneration and neurodevelopmental disorders, including autism spectrum disorders (ASDs) and Alzheimer's disease (Chao et al., 2010; Gemelli et al., 2006; Schmeisser et al., 2012) display this phenotype. This reflex involves not only sensory pathways, but also spinal motor circuits that normally coordinate fore- and hindlimb movements. The presence of hindlimb clasping in our model indicates that loss of EPS15 and EPS15R compromises motor or coordination-related pathways, extending the spectrum of deficits beyond seizures alone. Limb clasping has been linked to dysfunction across multiple brain regions, including the cerebellum, neocortex, and basal ganglia, and is thought to arise from disturbances in motor coordination pathways and neuromodulatory systems such as serotonin and noradrenaline (Lalonde & Strazielle, 2011). Similar to seizures, this phenotype has also been reported in AP180 knockout mice (Koo et al., 2015b), further pointing to shared pathological consequences of endocytic adaptor loss. Mice with altered NMDAR signaling also show hindlimb clasping (N. Suzuki et al.,

2024), raising the possibility that changes in glutamate receptor regulation contribute to this phenotype. EPS15/15R are established regulators of AMPAR, but their role in NMDAR trafficking is unknown. If such an interaction exists, it could provide an alternative explanation for the clasping observed in our eDKO mice. Impaired autophagy is another cause of clasping (Komatsu et al., 2006), and given the interaction of EPS15R with CALCOCO1, a link to autophagy-related protein quality control is also conceivable. These possibilities should be addressed in future studies of our model. Ultimately, however, limb clasping is a rather nonspecific phenotype that can result from diverse deficits across multiple pathways and brain regions, and therefore should be interpreted with caution in terms of mechanistic conclusions.

In addition to seizures and hindlimb clasping, our eDKO mice also showed clear behavioral alterations during routine cage observations. They displayed reduced spontaneous activity, reflected by decreased digging behavior and diminished interaction with paper (Fig. 2.11 C,D). Such behaviors are widely used as proxies for exploratory drive (de Brouwer et al., 2019) and motor activity in rodents (Dudek et al., 1983; Latham & Mason, 2004), and have been employed as a measure to assess aspects of neurological and psychiatric conditions, including anxiety, autism spectrum disorder (ASD), and obsessive–compulsive disorder (OCD) (Pond et al., 2021). An increase in digging behavior has been interpreted as a repetitive response associated with anxiety or compulsive tendencies (Broekkamp et al., 1986; A. Thomas et al., 2009). Conversely, a reduction in digging can indicate diminished exploratory drive or impaired motivation, reflecting underlying neurological dysfunction.

It is important to note that the reduced digging and spontaneous activity we observed were based on general cage behavior and not on standardized assays. While such observations provide valuable first insights, they do not allow conclusions about the underlying causes of these deficits. Standardized behavioral tests, however, can better disentangle specific behavioral components and will be required in future studies. Building on behavioral paradigms that have yielded conclusive results in our past studies of AP180 and ITSN knockout mice (Koo et al., 2015b; Vollweiter et al., 2023b), a comprehensive battery of behavioral assays will better reveal the deficits in eDKO mice. Nest-building ability can be assessed as a measure of motivation and motor coordination, since this behavior is often impaired in neuropsychiatric disease models and was also altered in AP180 and ITSN1 knockouts. In addition, repetitive or compulsive-like behaviors can be tested with the marble-burying assay, a paradigm previously applied in related knockout models. Exploration- and anxiety-related behaviors can be evaluated using the Open Field and Elevated Plus Maze (EPM), which probe the balance between curiosity and anxiety that is frequently shifted in endocytic mutants and mouse models of neuropsychiatric disorders.

Cognitive performance may be addressed with the object exploration test, which measures recognition memory by assessing the ability to discriminate between familiar and novel objects. Together, these experiments would provide a structured framework to link the observed cage behaviors to defined behavioral domains and clarify the contribution of EPS15/15R to motor, cognitive, and affective functions.

3.4 Consequences of EPS15/15R loss on brain architecture

The brain represents one of the most complex networks in biology, capable of continuously integrating cues through the coordinated activity of diverse neuronal populations. Its architecture is organized according to the principles of segregation and integration, which allow specialized regions to process distinct types of information while simultaneously contributing to coherent global states essential for cognition and behavior (Sporns et al., 2004). This intricate organization is not present at birth but gradually emerges through tightly regulated developmental programs, with structural and morphometric changes shaping the maturation of neuronal circuits across the lifespan (J. Li et al., 2024). Importantly, the establishment of these networks provides the substrate not only for higher-order cognitive functions but also for vulnerability to developmental and neuropsychiatric disorders.

While much of brain plasticity in adulthood relies on synaptic remodeling and circuit-level reorganization (Forrest et al., 2018), certain regions such as the hippocampus and sub-ventricular zone retain the unique capacity to generate new neurons throughout life, termed adult neurogenesis (Kempermann et al., 2015; Lim & Alvarez-Buylla, 2016). This continued plasticity highlights how structural development and lifelong adaptability are fundamentally intertwined. Given that both developmental patterning and neurogenic processes depend on the precise action of signaling pathways and molecular regulators, it is not surprising that a growing number of genes and proteins have been identified as critical determinants of brain development, shaping not only laminar organization and neuronal positioning, but also overall brain organization and neurogenic niche maintenance. In line with this, many adaptor proteins classically known for their roles in endocytosis as already discussed (*see section 1.2*), have also emerged as important regulators in brain development. With this study, we now add EPS15 and EPS15R to this expanding repertoire, uncovering a previously undescribed role for these adaptors in the developmental shaping of cortical and hippocampal architecture, ventricular organization, and in sustaining neurogenesis-dependent plasticity.

3.4.1 EPS15/15R is essential for hippocampal and cortical layering

Among the different brain regions examined, the hippocampus stood out as one of the most vulnerable to EPS15/15R loss. In the healthy brain, its architecture is defined by the orderly lamination of granule cells in the dentate gyrus and pyramidal neurons across the CA fields, forming compact and sharply delineated layers. This organization was clearly disrupted in eDKO animals, where the normally crisp boundaries were blurred, and neuronal distributions appeared irregular (Fig. 2.13 A,B). The dentate gyrus in particular lost its compact granule cell band, while

in the cornu ammonis the disruption was graded wherein CA1 retained some recognizable structure, but its pyramidal layer was broadened and misaligned, and these defects became progressively more severe in CA2 and CA3, where overt dispersion of neurons was observed. Such a phenotype immediately raises the possibility of underlying developmental disturbances. Interestingly, this widespread laminar disorganization strongly echoes the defects described earlier for the EPS15/15R interactor ITSN1. ITSN1-deficient mice display nearly identical hippocampal abnormalities (Jakob et al., 2017b). Similar to ITSN1 knockout mice, the overall shape of the dentate gyrus was also altered in our model, further emphasizing structural disruption at the level of hippocampal architecture. But the lamination defects in EPS15/15R-deficient mice were more severe than those described for ITSN1 knockouts. In ITSN1-deficient hippocampi, pyramidal neurons in the CA regions were less densely packed, with dispersion most pronounced in CA3 and extending into CA1, and in some cases the pyramidal layer appeared split into two layers (Jakob et al., 2017b). By comparison, the EPS15/15R phenotype was more extensive, as pyramidal neurons showed diffuse disorganization across multiple CA subfields, with the normally discernable layering and transitions between CA regions largely lost. In addition, the dentate gyrus displayed a striking accumulation of ectopic neurons within the hilus. This added severity suggests that the underlying molecular mechanisms in EPS15/15R-deficient mice may differ from those driving the phenotype in ITSN1 knockouts.

In the case of ITSN1-deficient mice, follow-up studies revealed that these hippocampal defects arise from impaired Reelin signaling. ITSN1 was shown to associate with the Reelin receptor VLDLR and its downstream adaptor Dab1, thereby facilitating Reelin-induced Dab1 phosphorylation (Jakob et al., 2017). Because ITSN1-driven defects were traced back to a failure in Reelin signaling, it was natural to wonder whether a similar mechanism might underlie the abnormalities we observed in EPS15/15R-deficient mice. *Reeler* mice, which completely lack Reelin, and knockouts of its core signaling components such as VLDLR, ApoER2, or Dab1, all show striking lamination defects that have long served as benchmarks for understanding this pathway (D'Arcangelo, 2005). We therefore turned to these models as a point of reference, asking whether our phenotype resembled any of them closely enough to suggest that EPS15/15R might converge on the same signaling cascade. When placed side by side, some clear parallels emerged. Like *reeler* and Dab1 mutants, our eDKO mice displayed diffuse dispersion of CA pyramidal neurons and an abnormal distribution of granule cells in the dentate gyrus, accompanied by ectopic accumulation of immature neurons in the hilus (D'Arcangelo, 2005; Stanfield & Cowan, 1979; Trommsdorff et al., 1999b). However, the defects in our model were not as catastrophic as in *reeler* or Dab1 knockouts. At the same time, they were more pronounced than in VLDLR knockouts, where the

hippocampal phenotype is generally milder with only a subtle neuronal dispersion. Instead, the degree and character of the abnormalities most closely resembled receptor ApoER2 knockout mice, which exhibit a pronounced CA1–CA3 dispersion and dentate gyrus defects without complete architectural loss (Trommsdorff et al., 1999b) (Fig. S7).

Reelin, however, is not only indispensable for hippocampal organization but also plays a central role in establishing the layered architecture of the neocortex. However, in ITSN1 knockout mice, the alterations were largely confined to the hippocampus, as cortical lamination appeared grossly preserved without major inversion or disorganization. Layer I remained largely devoid of neurons, consistent with controls, and ectopic accumulations were not observed unless ITSN1 loss was combined with ApoER2 deficiency (Jakob et al., 2017b). Such an ectopic accumulation of neurons in layer I has also been described for VLDLR/ApoER2 DKO mice (Trommsdorff et al., 1999b). The loss of EPS15/15R also produced some laminar abnormalities in the neocortex. While the overall six-layered structure was preserved, layer I was significantly reduced in thickness and layer VI expanded, with trends toward thickening of the other layers (Fig. 2.14 A,B) . Unlike the inverted cortex and ectopic neurons in layer I seen in *Reeler*, Dab1, or ApoER2/VLDLR double mutants, our eDKO mice resembled the subtler phenotypes of single receptor knockouts. VLDLR mutants show relatively mild cortical changes, with layer 1 remaining cell-free as in wild type, but the remaining layers no longer clearly separated, and neurons arranged in an abnormal radial pattern. In contrast, the lamination defect in ApoER2 knockouts was more pronounced with a poor separation of layers and neurons appearing to be packed into dense horizontal bands (Trommsdorff et al., 1999c). The latter pattern aligns more closely with the alterations we observed, since horizontal cortical layers were visible in our eDKO mice. The reduction of layer I together with the expansion of layer VI observed in our eDKO mice is particularly noteworthy, as it indicates that neurons do not overshoot into the marginal zone, as in severe Reelin mutants, but instead deeper layers maybe expand at the expense of the marginal zone. Overall, the cortical phenotype in EPS15/15R-deficient mice was milder than the hippocampal defects, suggesting that EPS15/15R play a more critical role in hippocampal than in cortical lamination. Altogether, with this study we were able to identify EPS15/15R as critical regulators of brain lamination, whose loss produces hippocampal defects closely resembling ApoER2 deficiency while causing only subtle cortical alterations. This highlights a region-specific requirement for EPS15/15R, with a particularly pronounced role in shaping hippocampal architecture. To better understand this mislayering, laminar fate mapping approaches would be highly informative. For example, timed BrdU/EdU pulse–labeling at embryonic stages combined with laminar markers such as TBR1 (layer VI), CTIP2 (layer V), RORB (layer IV), and SATB2 (layers II/III) could reveal whether

neurons are generated in appropriate numbers but mispositioned, or whether altered neurogenesis contributes to the phenotype.

3.4.2 EPS15/15R is important for radial glial scaffold integrity and neuronal migration

Radial glial cells fulfill dual roles in the developing brain, acting as multipotent progenitors that give rise to neurons and glia while also providing a scaffold for glial-guided neuronal migration (Campbell & Götz, 2002). Importantly, they express key components of the Reelin signaling cascade (Förster et al., 2002; Hartfuss et al., 2003; Luque et al., 2003), which are indispensable for proper neuronal positioning. The Reelin pathway is essential for establishing a proper radial glial scaffold in the dentate gyrus, earlier studies have shown that this structure is profoundly disrupted in not only *reeler* and *scrambler* mice, but, as well in ApoER2/VLDLR DKO mice, where secondary radial glial cells fail to align and instead adopt disorganized or stellate morphologies (Trommsdorff et al., 1999b). Even in single receptor mutants, such as VLDLR or ApoER2 knockouts, a graded impairment of scaffold formation is observed (Weiss et al., 2003b), emphasizing that Reelin signaling dosage critically shapes glial organization. Because malformation of the radial glial scaffold is thought to contribute directly to the neuronal migration defects observed in these models, we next extended our investigation to EPS15/15R-deficient mice. Given the pronounced hippocampal lamination defects in the eDKO, we reasoned that abnormalities in scaffold organization might underlie or exacerbate the ectopic positioning of granule cells and the dispersion of pyramidal neurons in CA regions.

In line with this hypothesis, our analyses revealed striking alterations in both radial glial architecture and neuronal maturation in the eDKO dentate gyrus. Nestin staining, which marks radial glia and undifferentiated progenitors, revealed that unlike the orderly parallel arrays of radial glia in controls, eDKO mice displayed tangled, misaligned processes with a broader distribution across the DG (Fig. 2.15 A,B). These abnormalities were accompanied by defects in neuronal maturation. DCX labeling, which highlights migrating immature neurons, revealed that in controls DCX-positive neuroblasts were confined to the SGZ and inner GCL, reflecting normal migration. However, in eDKO mice, DCX expression was markedly increased, dispersed across the GCL, and notably included ectopic cells in the hilus (Fig. 2.16 A-C). Such features closely resemble Reelin pathway mutants, where scaffold disruption leads to granule cell mispositioning (Brunne et al., 2013; Drakew et al., 2002). The parallels highlight that EPS15/15R deficiency compromises hippocampal development through mechanisms converging on the regulation of radial glia and neurogenesis. Interestingly, similar defects were also reported in ITSN1 knockout mice, which

exhibit both scaffold disorganization and ectopic accumulation of DCX-positive cells (Jakob et al., 2017b).

Building on these early disruptions, we next asked whether the misorganization of progenitors and immature neurons in the eDKO dentate gyrus was accompanied by defects at later stages of neuronal development. Since proper hippocampal lamination relies not only on scaffold integrity and neuroblast migration but also on the accurate positioning and fate specification of postmitotic neurons, we examined the distribution of CTIP2- and TBR1-expressing cells as markers of granule cell maturation and identity. Analysis of CTIP2 and TBR1 showed that EPS15/15R loss affects later stages of neuronal development as well. Unlike controls, where both markers were confined to the granule cell layer, eDKO mice displayed numerous ectopic neurons in the hilus and molecular layer, pointing to defects in migration and fate stabilization (Fig. 2.17 A-C). These findings extend previous observations from Reelin and ITSN1 mutants by showing that EPS15/15R loss disrupts not only scaffold organization and neuroblast migration, but also the spatial stabilization of postmitotic granule cell identity.

While our data indicate that EPS15/15R deficiency perturbs the organization and migration of newborn neurons in the dentate gyrus, pointing to a disrupted neurogenic niche, it remains unclear whether the overall output of neurogenesis is quantitatively altered. In ITSN1 knockouts, the scaffold disruption was indeed accompanied by increased proliferation, which compensated to preserve granule cell numbers despite ectopic positioning of newborn neurons (Jakob et al., 2017b). Whether this is the case for our eDKO mice will need to be tested. To address this, targeted experiments are needed, for example, proliferation can be assessed with BrdU/EdU incorporation and Ki67/PH3 staining to quantify dividing progenitors and map their location. Survival of newborn neurons can be tested using cleaved caspase-3 or TUNEL assay on birth-dated cohorts. Neuronal maturation can be evaluated by quantifying $NeuN^+$/$Calbindin^+$ granule cells and tracking BrdU/EdU-labeled cells as they transition from DCX^+ to mature stages. Together, these approaches will clarify whether EPS15/15R loss alters the overall production of granule neurons or whether, as in ITSN1 deficiency, compensatory mechanisms maintain neuronal cell population despite severe disorganization.

3.4.3 EPS15R is a component of Reelin-ApoER2 pathway

As already mentioned, ITSN1 supports Reelin signaling through its interaction with VLDLR and Dab1, ensuring proper phosphorylation and migration control. This led us to ask whether EPS15 and EPS15R might support this pathway in a similar way. To test this, we examined potential interactions with the two main Reelin receptors – VLDLR and ApoER2. In contrast to ITSN1,

which binds VLDLR, our assays revealed that EPS15R selectively associated with ApoER2, whereas no interaction with VLDLR was detected (Fig. 2.19 A,C). Notably, EPS15 showed no detectable binding to either receptor (Fig. 2.19 B,D). This points out that, consistent with the developmental and behavioral phenotypes, the laminar organization defects in our model are also primarily driven by EPS15R. Importantly, EPS15R bound specifically to ApoER2 but not to VLDLR, and the fact that our eDKO lamination defects most closely resembled those of ApoER2 knockout mice lends further support to this conclusion. This interpretation is further supported by expression patterns, as ApoER2 is more abundant than VLDLR in the forebrain and is often considered the dominant Reelin receptor in this region (D'Arcangelo, 2005). Since our conditional knockout is restricted to the forebrain, this aligns well with the phenotypic overlap between ApoER2 and EPS15R deficiency and may also underlie the stronger severity of defects in our model compared with ITSN1 loss. It is also worth noting that VLDLR deficiency primarily manifests as defects in the cerebellum, whereas ApoER2 loss predominantly affects the neocortex, further reinforcing the mechanistic link between ApoER2 and EPS15R (Trommsdorff et al., 1999b). To assess further similarities between ApoER2 KO and EPS15R KO, MAP2 staining can be used to examine the radial arrangement of apical dendrites in the neocortex. In ApoER2 knockout mice this pattern is poorly developed, and detecting a comparable defect in eDKO mice would further strengthen the link between the two models.

Therefore, with this study we identify a receptor-specific role of EPS15R in modulating Reelin signaling via ApoER2, in contrast to ITSN1, which supports the pathway through interacting with VLDLR. While it had remained unclear in the ITSN1 study why no interaction with ApoER2 was detected, our findings now suggest a model in which EPS15R and ITSN1 act through distinct Reelin receptors, with EPS15R engaging ApoER2 and ITSN1 engaging VLDLR. To further clarify how EPS15R contributes to Reelin signaling, it will be important to determine whether its role resembles that of ITSN1 or represents a distinct mechanism. In the case of ITSN1, it was proposed that it functions primarily as a signaling scaffold, facilitating the association and co-clustering of VLDLR with Dab1 and thereby promoting efficient Dab1 phosphorylation, rather than acting as a classical endocytic adaptor (Jakob et al., 2017b). Whether EPS15R similarly operates as a scaffold for ApoER2 and its downstream partner Dab1, or instead contributes through its canonical role in endocytosis, remains an open question that our ongoing work aims to answer.

To address this, the next step will be to test whether loss of EPS15R alters ApoER2 trafficking. Following the strategy used in the ITSN1 study (Jakob et al., 2017b), this can be examined by employing cell surface biotinylation to quantify ApoER2 surface levels in our control vs iDKO neuronal cultures. In addition, given antibodies which recognize extracellular domains of

ApoER2, receptor distribution can be assessed by immunofluorescence staining under non-permeabilizing conditions, which will help visualize ApoER2 specifically at the cell surface. Internalization dynamics can be directly measured through antibody uptake assays in neurons expressing tagged ApoER2 constructs. These experiments will allow us to determine whether EPS15R contributes to Reelin signaling through its canonical role in receptor internalization or, like ITSN1, acts independently of endocytosis as a signaling scaffold. To test the scaffolding hypothesis, we next plan to investigate whether EPS15R physically interacts with Dab1 and whether this interaction is required for efficient signaling. Similar to the strategy used for ITSN1, pulldown assays and complementary co-immunoprecipitation experiments will be performed to assess whether EPS15R associates with Dab1 in neuronal tissue. Beyond binding, it will also be important to examine whether the absence of EPS15R affects the activation status of Dab1. For this, Dab1 co-immunoprecipitation from hippocampal lysates of control and eDKO mice should be performed, and the precipitates should be probed with phospho-tyrosine-specific antibodies to determine relative levels of phosphorylated Dab1. In parallel, it would also be beneficial to assess the overall expression of Reelin pathway components by immunoblotting cortical and hippocampal lysates, since changes in receptor abundance or Reelin expression could indirectly account for the observed defects. In ITSN1-deficient mice, phosphorylated Dab1 was reduced, whereas protein levels of VLDLR, ApoER2, and Dab1 remained unchanged, and only Reelin levels showed a modest increase detectable both by immunoblotting and immunohistochemistry (Jakob et al., 2017b). Replicating these analyses in the EPS15/15R eDKO will therefore be essential to establish whether reduced Dab1 activation, rather than altered receptor expression, accounts for the lamination defects. Together, these experiments will help clarify whether EPS15R serves as a molecular scaffold in the Reelin cascade, similar to ITSN1, or whether its role is fundamentally different and rooted in endocytic regulation of ApoER2.

Beyond structural lamination defects, it will also be critical to assess whether loss of EPS15R impacts the functional arm of Reelin signaling. A well-established role of Reelin in the postnatal hippocampus is the enhancement of synaptic plasticity, in particular long-term potentiation (LTP) in acute hippocampal slices (Beffert et al., 2005; Weeber et al., 2002). This effect requires both ApoER2 and VLDLR, since genetic ablation of either receptor abolishes Reelin-induced LTP enhancement. Given our evidence that EPS15R associates with ApoER2, it will be important to test whether this interaction is also required for the plasticity-promoting functions of Reelin. Specifically, LTP induction can be measured in hippocampal slices from control and EPS15/15R-deficient mice under baseline conditions and following Reelin application. If EPS15R loss diminishes or abolishes the Reelin-dependent augmentation of LTP, this would not only provide

functional confirmation of its role in ApoER2 signaling, but also establish a direct link between the developmental migration defects and later impairments in synaptic plasticity.

3.4.4 EPS15/15R loss also disrupts hippocampal commissural integrity

In our EPS15/15R eDKO mice, we also detected a marked disruption of the ventral hippocampal commissure (VHC) (Fig. 2.13 C, S5). Given the close developmental relationship between the VHC and the corpus callosum, which both cross the commissural plate and depend on shared midline glial scaffolds and axon guidance cues, this finding is particularly relevant (Lindwall et al., 2007; Moldrich et al., 2010). Defective Eph/ephrin signaling is known to cause commissural malformations such as callosal agenesis (Mendes et al., 2006). Interestingly, ITSN1 has also been implicated in commissure formation, and callosal defects were reported (Sengar et al., 2013), however, in previous studies from our and the Haucke laboratory on the ITSN1 KO model, EphB-mediated forward signaling remained intact and corpus callosum formation appeared unaffected (Jakob et al., 2017b). Notably, EphrinB/EphB and Reelin signaling pathways interact closely (Bouché et al., 2013; Sentürk et al., 2011), suggesting that their potential dysregulation in our model could contribute to VHC damage. At the same time, this phenotype is not fully recapitulated in Reelin pathway mutants, indicating that additional or distinct mechanisms downstream of EPS15/15R may contribute to its occurence. In light of the frequent co-occurrence of hippocampal commissure and corpus callosum anomalies, it will be important to examine whether the corpus callosum is likewise compromised in EPS15/15R-deficient mice.

3.5 Consequences of EPS15/15R loss on brain ventricle development

The mammalian brain is organized around a central ventricular system, a network of interconnected cavities filled with cerebrospinal fluid (CSF). Far from being a passive reservoir, this system is essential for maintaining intracranial pressure, clearing metabolic waste, and distributing signaling molecules across distant brain regions. Proper formation of the ventricle system and a tight regulation of the CSF pressure is essential for CNS development, as its disruption causes severe neurological defects (Bothwell et al., 2019; Lowery & Sive, 2009; Zhang et al., 2017). Hydrocephalus is one such pathological condition, characterized by abnormal accumulation of CSF leading to ventricular enlargement and increased intracranial pressure. It may be congenital or acquired and can result from a variety of pathological causes. It is further classified into distinct subtypes based on the underlying mechanism (as discussed later), reflecting the diverse and still incompletely understood pathways leading to ventricular enlargement (Koleva & De Jesus, 2025). It is within this complex and still unresolved landscape that our study identifies a new player. We find that the loss of the endocytic adaptor proteins EPS15/15R produces pronounced ventriculomegaly consistent with hydrocephalus, revealing a previously unrecognized molecular pathway that safeguards ventricular integrity.

3.5.1 EPS15/15R loss causes early-onset hydrocephalus

Our study revealed that loss of EPS15/15R produces clear alterations in ventricular morphology. Nissl-stained coronal brain sections at postnatal day 30 showed a robust enlargement of the lateral ventricles in eDKO mice compared to controls (Fig. 2.12 A-C), establishing ventriculomegaly as a consistent feature of EPS15/15R deficiency. Interestingly, while the lateral ventricles were markedly affected, the cumulative third ventricle area appeared unchanged, and the fourth ventricle displayed a modest reduction in size (Fig. 2.12 E-H). This region-specific phenotype points to a selective disruption of parts of the ventricular system rather than a global defect. Notably, such abnormalities were absent in single EPS15 knockout mice, suggesting that EPS15R may play the dominant role in safeguarding ventricular integrity. In addition, dome-shaped cranial deformities were occasionally observed in eDKO mice (Fig. 2.12 D), a feature that is strongly indicative of elevated intracranial pressure and classically associated with hydrocephalus.

Similar ventricular changes have been described in other genetic models of hydrocephalus, such as Mdnah5 knockout mice, in which immotile ependymal cilia lead to severe ventricular expansion, cortical thinning, and perinatal lethality (Ibañez-Tallon et al., 2002), Similarly, Mpdz knockout mice develop aqueductal stenosis due to progressive ependymal loss, leading to massive

CSF accumulation, dome-shaped skulls, and death within the first postnatal weeks (Feldner et al., 2017a). In both Mdnah5 and Mpdz KO mice, hydrocephalus develops rapidly, with dome-shaped skull deformities already evident by postnatal day 3–5 and progressing to severe ventricular enlargement and early lethality. By contrast, in EPS15/15R-deficient mice such cranial deformities were only observed occasionally and typically at one month of age or later, indicating a milder and more slowly progressing phenotype. Nevertheless, the presence of dome-shaped skulls, even if infrequent, supports the interpretation that the ventriculomegaly in eDKO mice reflects an impaired CSF homeostasis, rather than a secondary ventricular dilation due to parenchymal atrophy or other causes.

Hydrocephalus can arise in an acquired form, developing postnatally as a consequence of insults such as trauma, infection, or hemorrhage (Bramall et al., 2022). Or it can also be congenital, originating from abnormal brain development or genetic mutations that disrupt ventricular morphogenesis or CSF regulation flow, as observed in L1CAM or Celsr2/3 mutants. (Jouet et al., 1994; Tissir et al., 2010). In such cases, defects in CSF-producing structures or in pathways controlling ventricular integrity lead to excessive fluid accumulation or distorted architecture from the outset (Munch et al., 2012). Given these distinctions, we also sought to determine the timing of ventricular enlargement in our eDKO mice to clarify whether their phenotype emerges during development. In our model, ventriculomegaly is evident by P30, but to assess whether its onset is early or progressive we examined brains as early as P5. Embryonic stages could not be analyzed due to permit restrictions. The analysis at P5 revealed a clear enlargement of the lateral ventricles (Fig. 2.20), indicating that ventricular abnormalities in the eDKO mice arise very early in postnatal life rather than gradually during later maturation. This early onset is significant, as already mentioned, P5 represents a critical window of ventricular expansion and ependymal maturation (Redmond et al., 2019). The presence of ventriculomegaly at this stage therefore argues that hydrocephalus in EPS15/15R-deficient mice reflects a developmental defect rather than a secondary consequence of subsequent pathology. These observations underscore the importance of investigating early cellular and molecular events that shape ventricular morphogenesis, as disruptions during this narrow postnatal window are likely to set the stage for the hydrocephalus phenotype we observe later in life.

Hydrocephalus can be broadly classified based on cerebrospinal fluid (CSF) flow dynamics into obstructive (non-communicating) and non-obstructive (communicating) forms. In obstructive hydrocephalus, the problem lies in impaired CSF drainage, often caused by narrowing or blockage of the ventricular pathways that normally allow fluid to circulate (Tully & Dobyns, 2014). In non-obstructive hydrocephalus, intracranial pressure can be normal or even low (Pang & Altschuler,

1994), and ventriculomegaly may persist with poor outcomes despite successful CSF diversion (Riva-Cambrin et al., 2022). The combination of enlarged lateral ventricles, preserved third ventricle size, and a potentially smaller fourth ventricle in our eDKO mice, does not fit with a communicating (non-obstructive) hydrocephalus, which typically presents with uniform enlargement of the entire ventricular system (Saigal et al., 2018). Instead, this pattern raises the possibility of an obstructive or partial form of hydrocephalus, where CSF flow may be locally impaired. In particular, the mild reduction observed in the fourth ventricle points toward a potential disturbance at the level of the cerebral aqueduct, though this possibility will need to be investigated in greater detail. These ventricular changes in our eDKO mice resemble those seen in other models of impaired CSF flow caused by ependymal or ciliary dysfunction (Abdelhamed et al., 2018; Neupane et al., 2021; Zou et al., 2020), which also display LV-predominant ventriculomegaly and to varying degrees, the third and fourth ventricle, despite an open aqueduct.

For instance, the loss of Rsph9, a radial spoke head protein essential for regulating motile cilia, disrupts the coordinated beating of ependymal cilia bundles which leads to impaired CSF circulation causing hydrocephalus with enlarged lateral and third ventricles, a milder dilation of the fourth ventricle, and a structurally open aqueduct (Zou et al., 2020). Similarly, the loss of Ccdc39, an axonemal protein leads to immotile ependymal cilia, resulting in perinatal-onset hydrocephalus with severe enlargement of the lateral and third ventricles, and an only modest fourth ventricle dilation, while the aqueduct remains patent despite poor CSF flow (Abdelhamed et al., 2018). In contrast, B3glct is not a structural ciliary protein but an endoplasmic reticulum glycosyltransferase, and its loss disrupts ependymal polarity which compromises CSF flow, producing a high-frequency hydrocephalus characterized by enlarged lateral and third ventricles, variable fourth ventricle dilation, and an unoccluded aqueduct (Neupane et al., 2021). However, in EPS15/15R-deficient mice we consistently observed LV enlargement, but not obvious dilation of the third ventricle—a pattern not typically reported in these other hydrocephalus models. This selective LV phenotype raises the question whether subtle 3V changes similar to the mild 4V involvement may have escaped detection in our standard histological sections. More sensitive approaches such as MRI will be required to clarify whether subtle 3V alterations are present. While the aqueduct appeared structurally normal on inspection in eDKO mice, quantification will be needed to conclusively verify its patency. To more precisely classify the type of hydrocephalus in our model, another useful approach will be to inject Evans blue dye into the ventricles of eDKO mice and monitor how far it travels through the ventricular system (Neupane et al., 2021), hereby revealing whether CSF flow is obstructed at the aqueduct or more broadly impaired throughout the ventricular network. A common aspect across Rsph9, Ccdc39, and B3glct mutants is that the

underlying defect resides in ependymal cells which display either impaired ciliary motility (Rsph9 and Ccdc39) or disrupted cell polarity (B3glct). This convergence strongly suggests that ependymal cell dysfunction is a central driver of lateral ventricle enlargement, making it plausible that ependymal cells are also compromised in EPS15/15R-deficient mice.

Although we previously considered seizures as a likely contributor to the early lethality observed in our mice, we cannot entirely rule out hydrocephalus and its associated complications. In other mouse models, severe hydrocephalus alone has been sufficient to drive premature death, whether through inefficient CSF circulation (Zou et al., 2020), aqueductal obstruction leading to rapid intracranial pressure buildup (Borit & Sidman, 1972), or massive ventriculomegaly with cortical thinning (Wyss et al., 2012). By contrast, the hydrocephalus in our eDKO mice appears less severe, with cranial deformities due to CSF build-up only occasionally observed and lacking the intensity seen in these established models (Feldner et al., 2017b; Ibañez-Tallon et al., 2002). Thus, while hydrocephalus may contribute to mortality in EPS15/15R deficient mice, it is unlikely to be the predominant cause, making seizures the more probable driver of early death.

3.5.2 No evidence for adhesion proteins as drivers of hydrocephalus in eDKO mice

To begin addressing the cellular and molecular mechanisms that might underlie the hydrocephalus phenotype in our model, we focused first on candidate genes previously linked to congenital hydrocephalus that potentially could be endocytically regulated by EPS15/15R. Among these, L1CAM, a cell-surface glycoprotein on axons of postmitotic neurons, stood out as a particularly compelling candidate. In humans, loss of L1CAM causes X-linked hydrocephalus due to stenosis of the aqueduct of sylvius (HSAS), characterized by corpus callosum agenesis, intellectual disability, spasticity, and ventricular enlargement (Jouet et al., 1994). Consistent with this, L1CAM mutant mice display ventricular expansion together with a smaller hippocampus, defective pyramidal neurons, and abnormalities in major axonal tracts such as the corpus callosum and corticospinal tract (Dahme et al., 1997; Demyanenko et al., 1999; Jouet et al., 1994). Beyond these gross malformations, L1CAM is also critical for neuronal migration, neurite outgrowth, and dendritic organization, with undulating apical dendrites in layer V cortical neurons that fail to reach layer I (Grońska-Pęski et al., 2020). Since our EPS15/15R-deficient mice also exhibited neuronal migration and lamination defects, this made L1CAM an especially relevant candidate to investigate in this context. Moreover, as a cell-surface glycoprotein, L1CAM is well positioned to be regulated by endocytic adaptor proteins like EPS15/15R, since it is known to undergo endocytosis (Kamiguchi et al., 1998). Through receptor internalization and trafficking,

EPS15/15R could potentially influence the surface availability of L1CAM, thereby impacting its developmental functions. These considerations led us to specifically examine whether L1CAM surface levels are altered in EPS15/15R-deficient neurons as a potential mechanism contributing to the observed ventriculomegaly. To test this, we quantified L1CAM surface levels by surface biotinylation in primary cortical neurons from control and iDKO mice and immunoblotted for plasma membrane L1CAM. Surface L1CAM levels were comparable between genotypes (Fig. 2.21 A), indicating that L1CAM steady state surface levels are preserved without EPS15/15R. This makes L1CAM dysregulation an unlikely primary driver of the hydrocephalus or commissural defects in our model.

L1CAM is not the only cell–cell adhesion molecule that has been linked to hydrocephalus. Junctional adhesion molecule 3 (JAM-3), which localizes to intercellular contacts, has also been implicated, as JAM-3 knockout mice develop severe hydrocephalus with massively enlarged lateral ventricles, cortical thinning, lamination defects, and astrogliosis, accompanied by obstructed CSF flow (Wyss et al., 2012). Interestingly, in our mass spectrometry dataset comparing control and eDKO forebrain lysates (Fig. S3 A), JAM-3 appeared mildly downregulated by fourfold in the eDKO brain. However, when we sought to validate this result by western blotting of forebrain lysates, no difference in JAM-3 expression was detected between genotypes (Fig. S3 C,D). Given this discrepancy and the absence of a clear reduction at the protein level, we did not pursue JAM-3 further in the context of our study. Nevertheless, differences in sensitivity between mass spectrometry and immunoblotting mean that subtle changes cannot be completely excluded, and this remains an avenue that could be still explored in future work.

3.5.3 EPS15/15R are essential for ependymal cell differentiation

Our finding that ventriculomegaly is already present at P5 suggests that the hydrocephalus phenotype arises during the early developmental period critical for ventricular morphogenesis (Redmond et al., 2019). Around this time, the embryonic radial glial epithelium is undergoing major remodeling to establish both the neural stem cell pool and the multiciliated ependymal lining that drives CSF circulation. Proper proliferation and differentiation of radial glial cells are therefore essential for securing ventricular integrity. Importantly, these progenitors are equipped with primary cilia that function as signaling hubs for pathways such as Sonic Hedgehog, Wnt, and mTOR, which regulate polarity, proliferation, and tissue organization (Foerster et al., 2017; Mill et al., 2023). Disruption of ciliary function in radial glia has been shown to cause ventriculomegaly and hydrocephalus, underscoring their importance for ventricular development (Foerster et al., 2017; Town et al., 2008). Against this background, we asked whether defects in radial glial cell

primary cilia might contribute to the ventricular abnormalities observed in EPS15/15R-deficient mice. Using hippocampal neuron cultures as a proxy system, we compared primary cilia length between control and iDKO cells. No significant differences were observed, indicating that gross ciliogenesis of primary cilia and their elongation are preserved in the absence of EPS15/15R (Fig. 2.21 B,C). Since we previously observed a reduced cilia length in ITSN1/2-deficient neurons (unpublished data from Dennis Vollweiter), we anticipated a similar phenotype in the EPS15/15R-deficient context, however, no such defects were detected. These findings argue against structural defects in radial glia primary cilia as a major contributor to the hydrocephalus phenotype.

Since defects in radial glial cilia did not account for the ventricular abnormalities in our model, we turned to ependymal cells, one of the most critical cell types for maintaining ventricular homeostasis. These multiciliated epithelial cells arise from radial glial progenitors during mid-fetal development but only acquire their mature features postnatally, coinciding with the period in which we observed ventriculomegaly in our mice. Their differentiation involves a dramatic apical surface expansion and the assembly of 30 to 50 motile cilia per cell, which beat in a coordinated, polarity-dependent manner to drive directional CSF flow (Redmond et al., 2019). The disruption of this process has been repeatedly linked to ventriculomegaly and hydrocephalus, and numerous mouse models highlight this vulnerability (Abdi et al., 2019; Lavado & Oliver, 2011; X. Wang et al., 2016). This underscores the importance of proper ependymal cell maturation for ventricular integrity. In this context, we asked whether loss of EPS15/15R interferes with ependymal cell differentiation or multiciliogenesis, thereby contributing to the hydrocephalus phenotype observed in our mice.

To address whether EPS15/15R influence ependymal cell development, we turned to an ex vivo differentiation system using primary ependymal cell cultures. This approach allowed us to monitor the maturation of progenitors isolated from the lateral ventricular wall under controlled conditions. Using this system, we first asked whether EPS15 and EPS15R are even expressed in ependymal cells, as this had not been documented before. Indeed, both proteins showed a low expression in progenitors but became strongly upregulated during differentiation, consistent with a role in this lineage (Fig. 2.22 B). Importantly, the inducible deletion by tamoxifen efficiently depleted EPS15/15R in culture, validating the system for functional interrogation (Fig. 2.22 C,D). Having established that EPS15/15R are upregulated during ependymal maturation, we next asked whether their loss impacts the transcriptional program that drives differentiation and multiciliogenesis of ependymal cells. Central to this process is FOXJ1, the master regulator which orchestrates basal body docking and axoneme assembly to generate motile cilia (Fig. 2.22 A). When we examined FOXJ1 protein levels in differentiated ependymal cultures, we found them to

be markedly reduced in iDKO cells (Fig. 2.22 C,D), suggesting that EPS15/15R are required to sustain the signaling required for proper induction or stability of FOXJ1, thereby positioning them upstream of the transcriptional machinery that governs ependymal cell differentiation. Interestingly, the reduction of FOXJ1 in our EPS15/15R-deficient cultures is consistent with phenotypes described in FOXJ1 KO models, where failure to establish a mature multiciliated epithelium leaves the ventricular wall covered by immature radial glia or astrocyte-like cells and leads to severe hydrocephalus (Hou et al., 2023). While our iDKO does not represent a complete loss of FOXJ1, the partial downregulation we observe suggests that similar pathways of impaired ependymal maturation may be at play, potentially contributing to the ventriculomegaly seen in our mice. We also detected increased astrocytes in the SVZ and ventricular lining of eDKO brains, though this phenotype appeared restricted to specific regions in sectional analysis and was quite variable, highlighting the need for a more comprehensive evaluation (Fig. S6). To test defects in ependymal differentiation more directly, future studies should examine the ventricular wall in vivo using whole-mount preparations to assess the persistence of radial glia or astrocytic coverage. A similar convergence can be seen in Ulk4 mutant mice, where loss of Ulk4 leads to disorganized ependymal cilia, aqueductal obstruction, and impaired CSF flow (M. Liu et al., 2016). Mechanistically, Ulk4 regulates the FOXJ1 pathway by modulating its expression and the transcription of its downstream ciliogenesis genes. Ulk4 acts as a scaffold protein that coordinates ciliogenesis and ciliary beating, and its loss results in hydrocephalus through defective ependymal ciliogenesis. Although EPS15/15R are not classical ciliogenesis factors, the reduction of FOXJ1 we observe suggests a comparable mechanism, whereby impaired activation of the FOXJ1 program destabilizes ependymal maturation and contributes to ventricular pathology. It will be important to examine downstream Foxj1 targets, since genes essential for ciliogenesis and axoneme function are altered in Ulk4 mutants and may likewise contribute to the ependymal defects in EPS15/15R-deficient mice.

Given the reduction in FOXJ1, we next asked whether this translated into defects in ependymal maturation and multiciliogenesis. Consistent with expectations, control cultures progressively acquired multicilia bundles, with most cells reaching a fully differentiated state by DIV14. In contrast, EPS15/15R-deficient cultures showed a clear impairment: fewer cells developed cilia bundles, while many retained only a single primary cilium even at late stages (Fig. 2.23 A-E). A small but consistently higher fraction of cells also lacked cilia altogether. These findings indicate that without EPS15/15R, progenitors fail to complete the transition into fully multiciliated ependymal cells, a defect that would be predicted to compromise CSF flow and contribute directly to the hydrocephalus phenotype. This failure to complete multiciliogenesis is reminiscent of

defects seen when upstream regulators of the ciliogenic program, such as GEMC1 or Multicilin (Mcidas), are lost (Kyrousi et al., 2015). In those mutants, centriole amplification is blocked, leaving cells arrested with only a primary cilium (Lu et al., 2019; Terré et al., 2016). The persistence of single cilia and reduced numbers of multiciliated cells in our iDKO cultures suggest that EPS15/15R deficiency may similarly interfere with basal body production or apical migration, pointing to defects upstream of FOXJ1. To address this possibility more directly, it will be important to assess GEMC1 and Multicilin levels in our cultures, as well as to perform basal body and centriole staining using markers such as FOP1 or Centrin, alongside deuterosome markers like Deup1. Such experiments would clarify whether centriole amplification itself is impaired, or whether basal bodies are normally generated but fail to assemble cilia.

While our data point to impaired multiciliation as a key defect in EPS15/15R-deficient ependymal cells, it remains possible that additional abnormalities in ciliary motility or polarity contribute to the hydrocephalus phenotype. Several models illustrate how ventriculomegaly can arise even when cilia are successfully generated but fail to beat effectively or to orient correctly. For example, Kif6 and Mdnah5 knockouts produce structurally abnormal or immotile cilia due to the loss of the central pair or dynein arms (Ibañez-Tallon et al., 2002, 2004; Takagishi et al., 2024), while Rsph9 and Ccdc39 mutants assemble cilia that exhibit aberrant waveforms, all leading to impaired CSF flow (Abdelhamed et al., 2018; Zou et al., 2020). Similarly, hydrocephalus in Celsr2/3 or Dishevelled mutants arises from defective planar cell polarity, which causes basal bodies to misalign and cilia to beat in uncoordinated directions despite normal ciliogenesis (Ohata, Nakatani, Herranz-Pérez, Cheng, Belinson, Inubushi, Snider, García-Verdugo, Wynshaw-Boris, & Alvarez-Buylla, 2014; Tissir et al., 2010). These examples highlight that even when ependymal cells become multiciliated, hydrocephalus can still arise if the cilia fail to function properly. Future studies using high-speed video microscopy to analyze beat frequency using the movement of added fluorescent beads as indicator of efficient fluid propulsion and also test for planar and rotational polarity using markers such as Vangl2 and Frizzled to assess coordinated flow will be important to test this possibility in our model.

Beyond ciliogenesis, we also examined whether EPS15/15R loss affects more general aspects of ependymal cell development. While both control and iDKO cultures showed the expected increase in cell area as differentiation progressed, iDKO cells tended to be larger at each stage (Fig. 2.23 F). More striking were changes in cell number and density, where control cultures expanded over time but iDKO cultures declined between DIV5 and DIV7 and only partially recovered by DIV14 (Fig. 2.23 G). This was accompanied by fewer nuclei per imaging field, indicating a reduction in overall cell density (Fig. 2.23 H). These findings suggest that loss of EPS15/15R

compromises ependymal maturation not only through defective multiciliation but also by affecting cell survival, proliferation and/or differentiation efficiency, which could further weaken ventricular integrity.

To test whether the abnormal cell morphology and the multiciliation impairment in iDKO cultures were simply secondary to a lower density during culturing rather than a direct effect of EPS15/15R loss on the differentiation program, we adjusted either cell seeding density or the timing of gene deletion. Increasing the plating density partially alleviated the lower cell number in mature cultures but did not normalize cell area or restore multiciliation completely (Fig. 2.24), while delaying the induction of EPS15/15R deletion until the onset of differentiation produced milder defects than the early deletion but still failed to rescue the phenotype. These findings indicate that the enlarged cell size and impaired multiciliogenesis in iDKO cells are not just byproducts of reduced cell density but reflect cell-intrinsic consequences of EPS15/15R deficiency on the differentiation process. The stronger deficits upon early DKO induction further suggest that EPS15/15R are already required during the progenitor expansion phase to secure cell viability and differentiation potential, with their loss compromising both progenitor maintenance and subsequent ependymal maturation. To dissect these possibilities more directly, future experiments could include BrdU incorporation to assess proliferation, cleaved caspase-3 immunostaining to measure apoptosis, and Sytox-based live/dead assays to monitor cell survival in culture.

Our finding that EPS15/15R loss reduces ependymal cell density and disrupts their differentiation resonates with other hydrocephalus models where defects in progenitor proliferation, survival, or fate commitment undermine the formation of a proper ventricular lining. SIX3 (homeobox transcription factor) conditional KO mice fail to fully suppress radial glial identity, resulting in fewer differentiated ependymal cells and the persistence of immature progenitors leading to a defective lateral ventricular wall, abnormal neuroblast migration and differentiation, and the development of hydrocephalus (Lavado & Oliver, 2011). Similarly, in the case of SNX27, an endosomal trafficking adaptor, its loss in mice impairs ependymal differentiation, producing hydrocephalus without detectable increases in apoptosis, suggesting that a shift in proliferation and differentiation balance is sufficient to trigger pathology. This defect is accompanied by elevated NICD and Hes1 expression, indicating that Notch hyperactivation contributes to the failure of ependymal maturation and subsequent ventricular dilation (X. Wang et al., 2016). Notch signaling is already known to act as a key negative regulator of multiciliogenesis (Spassky & Meunier, 2017). Thus, excessive Notch activity, as observed in SNX27-deficient mice, likely interferes with FOXJ1-mediated ependymal differentiation, contributing to defective

multiciliation and hydrocephalus. Together, these examples underscore that impaired progenitor expansion, survival, or differentiation represents a common route to hydrocephalus, placing our EPS15/15R-deficient phenotype within this broader category of ventricular pathologies driven by defects in ependymal lineage development.

Out of all existing models, Numb conditional KO mice stand out as a particularly relevant comparison. Numb and its paralog Numblike (Numbl) are adaptor proteins initially identified as determinants of asymmetric cell division via Notch endocytosis (Rhyu et al., 1994), Numb has since been shown to regulate multiple pathways, including EGFR. In radial glial progenitors, Numb directs the internalization and redistribution of EGFR away from the apical, CSF-contacting surface, a process required for timely progenitor differentiation into multiciliated ependymal cells (Fig. 1.3) (Abdi et al., 2019). Similarly, conditional loss of Numb and Numbl in the postnatal SVZ results in ventricular enlargement accompanied by partial loss of the ependymal lining, underscoring their essential role in maintaining ventricular wall integrity (Kuo et al., 2006). It is known that Numb negatively regulates Notch signaling (Cayouette & Raff, 2002), but in the ventricular system its loss causes ependymal defects independently of NICD activity. NICD overexpression failed to rescue the loss of ependymal adhesion or ventricular integrity (Kuo et al., 2006), and NICD levels remained unchanged in lateral ventricle whole mounts from Numb/Numbl-deficient mice (Abdi et al., 2019). In contrast to Numb deficiency, SNX27 loss is associated with increased NICD expression, indicating that Notch hyperactivation underlies the defective ependymal differentiation observed in these mutants (X. Wang et al., 2016).

Since EPS15 and EPS15R are endocytic adaptor proteins that, like Numb, participate in EGFR internalization and trafficking, their loss may similarly disrupt receptor turnover and downstream signaling required for ependymal differentiation. The strong phenotypic parallels with Numb and Numbl mutants, including impaired multiciliation, ventricular enlargement, and early lethality, suggest that defective regulation of EGFR signaling could underlie the ventricular pathology observed in EPS15/15R-deficient mice. At the same time, EPS15 and EPS15R also interact with Epsins, which are key mediators of Notch receptor endocytosis (Cardano et al., 2019; H. Chen et al., 2009b; Henne et al., 2007), raising the possibility that altered Notch signaling may also contribute. Since inhibition of Notch activity is required for GEMC1- and Multicilin-dependent induction of FOXJ1 and subsequent multiciliogenesis (Fig. 2.22 A), sustained Notch activation—as seen in SNX27 knockout mice—can hinder ependymal differentiation and lead to defective cilia formation (Spassky & Meunier, 2017; X. Wang et al., 2016). Therefore, EPS15 and EPS15R may potentially safeguard ventricular integrity by coordinating the endocytic regulation of both EGFR and Notch pathways during ependymal maturation.

A key question now is whether the differentiation and multiciliogenesis defects observed in EPS15/15R-deficient ependymal cells reflect indeed a misregulated endocytosis of critical signaling receptors EGFR or Notch. To probe this, future work should directly assess receptor trafficking and signaling activity in iDKO cultures, by measuring EGFR phosphorylation dynamics, Notch intracellular domain levels, and receptor distribution at the apical surface, alongside endocytosis assays using ligand uptake or surface biotinylation. Pharmacological approaches could complement these analyses, such as testing whether inhibition of EGFR (e.g., via the inhibitor erlotinib) or Notch (e.g., via the inhibitor DAPT) can normalize FOXJ1 expression or restore multiciliation, thereby revealing whether excessive signaling contributes to the phenotype. In parallel, genetic rescue experiments with EPS15/EPS15R constructs deficient in specific domains, such as ubiquitin-binding (ΔUIM), membrane bending (ΔEH), or phase separation (ΔCC), would help delineate which adaptor functions are essential for ependymal maturation. Finally, co-immunoprecipitation or surface proteomics in differentiating ependymal cultures could help uncover cell-type specific EPS15/15R interactors and cargo proteins, highlighting whether Notch, EGFR, or additional pathways are directly affected. Together, such experiments would establish whether the hydrocephalus phenotype of EPS15/15R-deficient mice is driven by a failure to properly regulate receptor signaling, thereby linking endocytic adaptor function to the transcriptional and structural programs of ventricular development.

3.6 Conclusions and open questions

This study establishes EPS15 and EPS15R as critical endocytic adaptor proteins with roles that extend from neurotransmitter receptor regulation to broader aspects of brain development and ventricular integrity. At the synapse, both proteins appear to be required for AMPAR endocytosis, with their loss leading to GluA1 surface accumulation. This reveals that EPS15/15R safeguard excitatory balance by ensuring proper receptor trafficking, placing them at the heart of mechanisms that control synaptic plasticity and potentially seizure susceptibility. Unlike transferrin receptor uptake, which remains intact in their absence, AMPAR trafficking depends specifically on these adaptors, emphasizing their selective yet essential function in neuronal cargo sorting.

Beyond canonical endocytic pathways, our proteomic analyses uncovered novel interactors such as CALCOCO1 and SEC16A, pointing to unexpected roles for EPS15R at the intersection of endocytosis, autophagy, and the secretory system. These findings suggest that EPS15R may act as scaffold linking membrane trafficking and stress-responsive pathways, thereby expanding its influence beyond clathrin-mediated endocytosis. Whether these interactions represent specialized neuronal adaptations or broader cellular functions remains an open question.

EPS15/15R deficiency also translates into defects in brain development and behavior. Forebrain-specific DKO mice exhibit seizures, clasping reflexes, and reduced exploratory drive, underlining the importance of these adaptors for network stability and motor-cognitive function. At the architectural level, their loss leads to lamination defects in cortex and hippocampus, reminiscent of phenotypes observed in models with disrupted Reelin signaling. EPS15R's potential interaction with the Reelin receptor ApoER2 suggests that it may influence not only endocytosis but also provide scaffolding within the Reelin cascade, raising the possibility that adaptor proteins also in this manner can help fine-tune developmental signaling pathways. Whether EPS15/15R help coordinate Reelin receptor trafficking and downstream Dab1 signaling is an open question that could provide insight into how adaptor proteins shape large-scale brain architecture.

Perhaps the most striking phenotype is the development of ventriculomegaly, potentially caused by impaired ependymal differentiation. Our study revealed that EPS15/15R-deficient ependymal cells exhibit reduced density, enlarged morphology, and impaired multiciliogenesis, reminiscent of phenotypes described in Numb conditional KO mice where disrupted EGFR blocks ependymal differentiation (Abdi et al., 2019). This parallel suggests that EPS15/15R may act through similar pathways, raising the critical question of whether hydrocephalus in our model stems from sustained EGFR signaling or other signaling imbalance affecting ependymal maturation, such as

that involving Notch. The concomitant reduction of FOXJ1 further implicates upstream ciliogenesis regulators such as GEMC1 and Multicilin. The persistence of primary cilia and reduced multiciliation point to defects in centriole amplification or basal body migration upstream of FOXJ1 induction. Future work should therefore examine upstream regulators of multiciliogenesis and the structural components of basal body and centriole assembly to determine whether EPS15/15R loss primarily disrupts signaling processes governing transcriptional control or the machinery required for ciliogenesis.

Taken together, our findings identify EPS15 and EPS15R as integrators of endocytic trafficking, neuronal signaling, and ventricular homeostasis. Beyond establishing their necessity for AMPAR regulation and ependymal maturation, this work also opens up broader conceptual avenues. EPS15/15R emerge not just as adaptors at the plasma membrane, but as potential coordinators of how cells balance internalization, signaling, and secretory outputs in a developmental context. This raises the exciting possibility that defects in these proteins could represent a common molecular thread linking synaptic dysfunction, lamination defects, and hydrocephalus. Exploring this integrative role may reveal principles of brain organization that extend well beyond EPS15/15R, providing insight into how trafficking proteins safeguard neural development and resilience against disease.

4 Materials and Methods

4.1 Materials

4.1.1 Mouse lines

Experiments were performed on male and female C57BL/6N wildtype (WT) mice or EPS15/EPS15R double knock-out (dKO) mice generated using either forebrain specific constitutive Emx1-Cre (Iwasato et al., 2000) or on primary neurons/ependymal cells obtained from tamoxifen-inducible CAG-CreERT2 mice (S. Hayashi & McMahon, 2002). Floxed EPS15 and EPS15R mice, originally generated and described by (Milesi et al., 2019) were a kind gift to us by Dr. Sara Sigismund (IEO, Milan, Italy) and subsequently bred into the mentioned Cre-driver lines in our facility.

For the constitutive neuron-specific dKO line, EPS15 $^{LOX/LOX}$ / EPS15R $^{LOX/LOX}$ / Emx1 Cre^{-} mice were bred with EPS15 $^{LOX/LOX}$ / EPS15R $^{-/LOX}$ / Emx1 Cre^{+} mice, generating Cre-positive and Cre-negative animals. EPS15 $^{LOX/LOX}$ / EPS15R $^{LOX/LOX}$ / Emx1 Cre^{+} mice were used as dKO mice for experimental studies and Cre-negative littermates as controls. For the inducible line, EPS15 $^{LOX/LOX}$ / EPS15R $^{LOX/LOX}$ mice were bred with CAG Cre^{+} mice to obtain Cre-positive and Cre-negative littermates. Cre-positive cultures were induced to generate EPS15/15R double knockouts (dKO), while Cre-negative cultures were used as controls.

All animals were bred in accordance with the German law for conducting animal experiments and kept in a light and dark cycle of 12 h with food and water *ad libitum* at the animal facility of the RPTU Kaiserslautern-Landau. The constitutive dKO mice were bred under a special permit (G21-2-072).

4.1.2 Chemicals and reagents

General chemicals and reagents were purchased from standard suppliers including Bio & Sell (Germany), Biozym Scientific (Germany), Carl Roth (Germany), Merck (Germany), Sigma-Aldrich (USA), Thermo Fisher Scientific (USA), VWR international LLC (USA) or from the chemical supply of the RPTU. To ensure reproducibility, certain key critical reagents were purchased from specific suppliers only (Table 4.1)

Table 4.1 Key chemicals and reagents

Chemicals / Reagents	Manufacturer
1-β-D-Arabinofuranosyl-cytosine-hydrochloride (Ara-C)	Sigma-Aldrich, USA
Acrylamide Mix 30%, ROTIPHORESE®	Carl Roth, Germany
B27 supplement (50x)	Thermo Fisher Scientific, USA
Bradford reagent	Bio-Rad, USA
c0mplete® Protease inhibitor tablet, Mini, EDTA-free	Merck, Germany
DAPI 98% (4',6-Diamidino-2-phenylindol)	Carl Roth, Germany
Desoxyribonuclease (DNase) I, from bovine pancreas, Type IV	Sigma-Aldrich, USA
Dulbecco's modified Eagle's medium (DMEM), high glucose	Sigma-Aldrich, USA
Dulbecco's Phosphate Buffered Saline (DPBS)	Sigma-Aldrich, USA
Entellan ™	VWR International LLC, USA
FastDigest buffer (10x)	Thermo Fisher Scientific, USA
Fetal bovine serum (FBS)	Thermo Fisher Scientific, USA
FBS Superior Stabil *(for primary neuron culture)*	Bio & Sell, Germany
Gelatin, from porcine skin gel strength 300, Type A	Sigma-Aldrich, USA
GeneRuler™ DNA ladder mix	Thermo Fisher Scientific, USA
Goat serum	Thermo Fisher Scientific, USA
Hanks' Balanced Salt Solution (HBSS)	Thermo Fisher Scientific, USA
HEPES (1M)	Thermo Fisher Scientific, USA
ImmuMount ™	Epredia, USA
Insulin (human recombinant)	Sigma-Aldrich, USA
Isopropyl-ß-D-thiogalactopyranosid (IPTG)	Carl Roth, Germany
Ketamine (KETASET)	Zoetis, Germany
L-cysteine	Sigma-Aldrich, USA
L-glutamine, GlutaMAX™ (100X)	Thermo Fisher Scientific, USA
LI-COR Intercept® blocking buffer	LI-COR Biosciences, USA
Minimum Essential Medium (MEM) with Earle's salt	Thermo Fisher Scientific, USA
Neurobasal-A medium (NBA)	Thermo Fisher Scientific, USA
Nuclease free water, DEPC treated, sterile	Carl Roth, Germany
PageRuler™ Pre-stained protein ladder	Thermo Fisher Scientific, USA
Papain (2x crystalline suspension)	Worthington, USA
Penicillin-Streptomycin (Pen/Strep), 10.000 U/ml	Thermo Fisher Scientific, USA
Phenylmethylsulfonylfluoride (PMSF)	Carl Roth, Germany
Phusion™ High-Fidelity DNA Polymerase	Thermo Fisher Scientific, USA
Pierce® Glutathione agarose beads	Thermo Fisher Scientific, USA
Pierce® Protein A/G magnetic beads	Thermo Fisher Scientific, USA
Poly-L-Lysine	Sigma-Aldrich, USA
Protease inhibitor complex (PIC)	Sigma-Aldrich, USA
Restriction enzymes, FastDigest	Thermo Fisher Scientific, USA
Sodium bicarbonate (0.075%)	Thermo Fisher Scientific, USA
T4 Ligase	Thermo Fisher Scientific, USA
T4 ligase buffer, 10x	Thermo Fisher Scientific, USA
Taq Polymerase (5 U/µl)	Bio & Sell, Germany

TEMED (N,N,N,N-Tetramethylethylendiamin)	Carl Roth, Germany
Transferrin Holo Bovine Plasma	Merck, Germany
Trypan blue solution, 0.4%	Carl Roth, Germany
TrypLE™ Express, with Phenol Red	Thermo Fisher Scientific, USA
Trypsin-EDTA (0.05%)	Thermo Fisher Scientific, USA
Trypsin, from bovine pancreas, Type XI, Lyophilized powder	Sigma-Aldrich, USA
Trypsin Inhibitor (from chicken egg white)	Merck, Germany
Xylazine (Rompun 2%)	Elanco, Germany
Xylazine (Rompun 2%)	Elanco, Germany

4.1.3 Consumables

General consumables were purchased from standard suppliers including Biozym Scientific (Germany), Carl Roth (Germany), Corning (USA), Epredia (USA), SARSTEDT (Germany), Starlab (Germany) and VWR International LLC (USA). To ensure reproducibility, certain key consumables were purchased from specific suppliers only (Table 4.2)

Table 4.2 Key consumsables

Consumables	Manufacturer
Cell culture dishes	SARSTEDT, Germany
Cell culture well plates	Corning, USA
Dissection tools	Fine Science Tools, Germany
Graduated glass pipettes (SILBERBRAND-ETERNA)	Brand, Germany
Immersion oil Type F	Nikon, Japan
Kimtech precision wipes	Kimberly Clark, USA
Microscope cover glasses (Round, ø18 and 25 mm)	Marienfeld, Germany
Nitrocellulose blotting membrane (Amersham)	Cytiva, USA
Superfrost™ Plus slides	Epredia, USA

4.1.4 Kits

Commercial kits were used wherever stated in accordance with manufacturer's protocols (Table 4.3)

Table 4.3 Commercial kits used

Kit	Manufacturer
JetPrime transfection kit	Polyplus, France
Nucleobond plasmid midi kit	Machery-Nagel, Germany
Nucleospin plasmid mini kit	Machery-Nagel, Germany
Nucleospin gel and PCR cleanup kit	Machery-Nagel, Germany
Pierce ® BCA protein assay kit	Thermo Fisher Scientific, USA
ProFection Mammalian transfection system	Promega Corporation, USA

4.1.5 Antibodies and fluorescent reagents

Table 4.4 List of primary antibodies

Antigen	Species	Dilution	Use	ID	Company
Actin	mouse	1:2000	WB	A5441	Sigma-Aldrich, USA
Arl13b	mouse	1:200	IF	857602	BioLegend, USA
AP2-α	mouse	1:1000	WB	610502	BD Transduction, USA
APPL1	rabbit	1:500	WB	3276	Cell signaling, USA
Calcoco1	mouse	1:500	WB	sc-515670	Santa Cruz Biotechnology, USA
Clathrin	rabbit	1:100	WB	ab21679	Abcam, UK
CTIP2	rat	1:400	IHC	ab18465	Abcam, UK
Doublecortin	mouse	1:50	IHC	sc-271390	Santa Cruz Biotechnology, USA
EPS15	mouse	1:250	WB	610806	BD Transduction, USA
EPS15R	rabbit	1:300	WB	-	Gift from Sara Sigismund lab
EPS15R	rabbit	1.5 µg	IP	ab76004	Abcam, UK
FOXJ1	mouse	1:500	WB	14-9965-82	Invitrogen, USA
GAPDH	mouse	1:1000	WB	G8795	Sigma-Aldrich, USA
GluA1	mouse	1:500	WB	MAB2263	Merck, Germany
GluA2	mouse	1:500	WB	MAB397	Merck, Germany
HSP70	mouse	1:2000	WB	MA3006	Thermo Fisher Scientific, USA
IgG Isotype	mouse	3 µg	IP	31903	Thermo Fisher Scientific, USA
ITNS1	mouse	1:200	WB	sc-136242	Santa Cruz Biotechnology, USA
L1CAM	mouse	1:500	WB	-	Gift from AG Kins
N-Cadherin	mouse	1:1000	WB	610920	BD Transduction, USA
Nestin	mouse	1:100	IHC	MA1-81819	Invitrogen, USA
Sec16a	rabbit	1:500	WB	20025-1-AP	Proteintech, USA
Snap25	mouse	1:250	WB	111011	Synaptic Systems, Germany
SOX2	rabbit	1:200	IHC	14962	Cell signaling, USA
Synaptophysin	mouse	1:500	WB	101011	Synaptic Systems, Germany
Synaptotagmin1	rabbit	1:500	WB	105103	Synaptic Systems, Germany
Syntaxin1	mouse	1:500	WB	110111	Synaptic Systems, Germany
TBR1	rabbit	1:400	IHC	ab183032	Abcam, UK

Table 4.5 List of secondary antibodies

Antigen	Species	Dilution	Use	ID	Company
anti-mouse IRDye© 680RD	goat	1:10000	WB	926-68070	LI-COR, USA
anti-rabbit IRDye© 680RD	goat	1:10000	WB	926-68071	LI-COR, USA

anti-mouse IRDye© 800CW	goat	1:10000	WB	926-32210	LI-COR, USA
anti-rabbit IRDye© 800CW	goat	1:10000	WB	926-32211	LI-COR, USA
anti-guinea pig Alexa Fluor 647	goat	1:200	IF	A21450	Invitrogen, USA
anti-rabbit AlexaFluor 567	goat	1:400	IHC	A11029	Invitrogen, USA
anti-rat AlexaFluor 647	goat	1:400	IHC	A11036	Invitrogen, USA
anti-mouse AlexaFluor 488	goat	1:200 1:400	IF IHC	712-605-153	Jackson Immuno-Research, USA

Table 4.6 List of fluorescent reagents

Dye	Concentration	ID	Company
DAPI	1 µg/ml	6335.1	Carl Roth, Germany
Hoechst (siR700-DNA)	0.5 µM	SC015	SPIROCHROME, Switzerland
Phalloidin STAR RED	1:1000	STRED-0100	Abberior, Germany
Sytox™ Green	0.1 µM	S7020	Invitrogen, USA
Transferrin AlexaFluor 647	25 µg/ml	T23366	Invitrogen, USA

4.1.6 Plasmids

Table 4.7 List of plasmids

Construct	Insert species	Backbone	Tag	Internal number	Origin
RFP-EPS15R	mouse	pmRFP	RFP	#M44	Cloned by Celine Schuster
GFP-Calcoco1	human	pDest	eGFP	#M37	Gift from Prof. Terje Johansen, Norway
GST	-	pGex4T-1	GST	#2112	Amersham
GST-ApoER2-ICR	mouse	pGex4T-1	GST	#3754	Gift from Prof. Volker Haucke, Berlin
GST-VLDLR-ICR	mouse	pGex4T-1	GST	#3761	Gift from Prof. Volker Haucke, Berlin

4.1.7 Primers

Table 4.8 List of primers used for genotyping

Primer	Sequence (5'-3')	Expected size (bp)
EPS15L1 forward	AGGAGTCCAAGGGCATCTTCAGC	WT : 218 bp LOX : 279 bp
EPS15L1 reverse	CAGCCATCCAGACACAGCACACA	
EPS15 forward	GTGCTCCTTAGGTCCTGTGG	WT : 754 bp LOX : 900 bp
EPS15 reverse	AAATGTGGGCTAGCAAGGCA	
CAG CRE forward	CCGGGCTGCCACGACCAA	WT : no band CRE : 400 bp
CAG CRE reverse	GGCGCGGCAACACCATTTTT	

4.1.8 Devices and equipment

The most relevant instruments for the experimental procedures in this thesis are summarized below (Table 4.9)

Table 4.9 List of essential instruments

Device	Model	Company
Absorbance plate reader	SpectroStar® Nano	BMG Labtech, Germany
Binocular	Stemi 508	Carl Zeiss, Germany
Blotting chamber	Criterion® Blotter	BIO-RAD, USA
CO_2 incubator	CB 170	Binder, Germany
Counting chamber	Neubauer Improved, 0.1 mm	Marienfeld Superior, Germany
Cryotome	Leica CM3050 S	Leica Biosystems, Germany
Electrophoresis chamber for agarose gels	Mini-Sub® Cell GT Cell	BIO-RAD, USA
Electrophoresis chamber for SDS-PAGE	Mini-PROTEAN® Tetra Cell	BIO-RAD, USA
Epifluorescence microscope	Eclipse Ti2-E	NIKON, Japan
Fluorescence microscope	Spinning Disk Confocal	NIKON, Japan
Gel imaging system	E-BOX	Vilber, France
Homogenizer	Hei-Torque Core	Heidolph Instruments, Germany
Immunoblot imaging system	Odysses® Fc Model 2800	LI-COR Biosciences, USA
Inverted microscope	Axio Vert.A1	Zeiss, Germany
Mini centrifuge	MiniStar	VWR International LLC, USA
Peristaltic pump	Pump-head: YZ1515x	Longer Pump, China
pH meter	FiveEasy	Mettler Toledo, USA
Sonifier	SFX 250, 5mm tip	Branson, USA
Table-top centrifuges	MICRO STAR 17R MICRO STAR 17	VWR International LLC, USA
Table-top centrifuges	5804R 5910 Ri	Eppendorf, Germany
Thermocyclers	peqSTAR 2x peq Start 2x Gradient	PEQLAB Biotechnologie, Germany

4.1.9 Software and online tools

The software programs and online resources used for data analysis, visualization and other aspects of the thesis are summarized below (Table 4.10)

Table 4.10 List of software and online tools

Software / Online tools	Application	Source
Affinity designer	Image editing and figure design	Serif Europe Limited, UK
Biorender	Generation of illustrations	https://app.biorender.com/

NCBI Homepage	DNA sequence alignment (BLAST)	https://blast.ncbi.nlm.nih.gov
Cellpose 3.0	Cell segmentation (ependymal cells only)	https://www.cellpose.org/ Carsen Stringer & Marius Pachitariu
ChatGPT 5 (OpenAI)	Paraphrasing and grammar check	https://chatgpt.com/
Fiji/ImageJ	Image processing, analysis and quantification	NIH, USA
GraphPad Prism	Statistics and graph design	GraphPad Software, USA
Image Studio v6.0	Immunoblot imaging and analysis	LI-COR Biosciences, USA
MaxQuant Perseus v1.6.15.0	Mass spectrometry data analysis and visualization	MPI Biochemistry, Germany
Microsoft Office	Generation of text, spreadsheets and presentations	Microsoft Office, USA
SnapGene viewer	Design of cloning strategy and DNA sequence analysis	GSL Biotech LLC, USA
QuillBot	Paraphrasing and grammar check	https://quillbot.com/
Uniprot	Protein sequence check	https://www.uniprot.org/
WebGestalt	Gene set enrichment analysis	https://www.webgestalt.org/
Zotero	Reference management tool	https://www.zotero.org/

4.2 Biochemical methods

4.2.1 Mouse brain extract preparation

For analysis of protein expression levels and protein-protein interactions, whole brains or dissected brain regions of interest were collected and lysed. Brain lysis buffer (20 mM HEPES pH 7.4, 2 mM $MgCl_2$, 100 mM KCl, 1 mM PMSF, 1% Triton X-100) containing protease and phosphatase inhibitors was freshly prepared. Mouse brains were homogenized in ice-cold lysis buffer (1.5 ml lysis buffer per 100 mg tissue) using a glass homogenizer with 12 strokes at 900 rpm. The homogenates were rotated for 15 min at 4°C to ensure complete lysis and subsequently centrifuged at 900 x g for 10 min at 4°C to remove large debris and nuclei (pellet P1). The resulting supernatant (S1) was collected, and the protein concentration was determined using BCA or Bradford assay.

4.2.2 Synaptosome preparation

Mouse brains were homogenized in 8 ml ice-cold sucrose buffer (0.32 M sucrose, 5 mM HEPES, pH 8) per brain using a glass homogenizer with 12 strokes at 900 rpm. The homogenate was centrifuged at 900 x g for 10 min at 4°C to precipitate large cellular debris and nuclei (pellet P1), and the supernatant (S1) was collected. S1 was further centrifuged at 10000 x g for 15 min at 4°C to separate the supernatant (S2) containing soluble proteins from the pellet (P2) enriched in crude synaptosomes. P2 was resuspended in 2 ml of ice-cold sucrose buffer, diluted with additional 6

ml of ice-cold sucrose buffer, and centrifuged again at 15000 x g for 15 min at 4°C. The resulting washed crude synaptosome pellet (P2') was resuspended in 2 ml of ice-cold sucrose buffer, and the protein amount was determined using BCA or Bradford assay.

4.2.3 Synaptic membrane preparation

For isolating synaptic membranes, the procedure was continued after obtaining the crude synaptosomal fraction (pellet P2'). P2' was resuspended in 4 ml of ice-cold double distilled water (ddH_2O) and homogenized by hand with three strokes using a glass potter homogenizer. The buffer was rapidly adjusted to a final concentration of 4 mM HEPES. The lysate was rotated for 30 min at 4°C to promote osmotic lysis of synaptosomes and subsequently centrifuged at 25000 x g for 25 min at 4°C. This centrifugation separated the synaptosomal cytosolic fraction (S3) from the membrane enriched pellet (P3). The resulting P3 fraction, corresponding to purified synaptic membrane, was resuspended in 1 ml of lysis buffer (20 mM HEPES pH 7.4, 2 mM $MgCl_2$, 100 mM KCl, 1 mM PMSF, 1% Triton X-100)for subsequent biochemical applications.

4.2.4 Preparation of total cell lysate from eukaryotic cells

Total cell lysates from eukaryotic cell lines or primary cells were prepared using RIPA lysis buffer (50mM Tris-HCl pH 7.4, 150mM NaCl, 1mM EDTA, 1% Triton X-100, 0.5% Sodium Deoxycholate, 0.1% SDS in H_2O). Cells grown on a 10 cm plastic culture dish were washed once with ice-cold PBS, and residual buffer was aspirated completely. Dishes were immediately transferred to ice, and 250-500 µl of RIPA buffer were added directly, and lysates were harvested using a cell scraper. The lysates were collected into pre-chilled microcentrifuge tubes, and to ensure complete lysis, samples were incubated for 10-15 min on a rotating wheel at 4°C. Lysates were clarified by centrifugation for 15 min at maximum speed in a tabletop cooling centrifuge (≈ 17000 x g, 4°C). The resulting supernatant was collected, and the protein concentration was determined using Bradford or BCA assay.

4.2.5 Protein quantification by Bradford or BCA assay

Protein concentrations were determined using either Bradford (Coomassie G250) or the Bicinchoninic acid (BCA) assay, with bovine serum albumin (BSA) serving as the standard. A BSA stock solution was serially diluted to generate a standard curve (0-2 mg/ml). For the Bradford assay, 2 µl of sample or standard were mixed with 200 µl of commercial Bradford reagent in a 96-well plate and incubated for 5 min at room temperature. Then its absorbance was measured at 595 nm using the *SpectroStar* instrument. Similarly for the BCA assay, 2 µl of sample or standard were incubated with 200 µl of freshly prepared BCA working reagent (Reagent A: Reagent B, 50:1)

for 30 min at 37°C, and absorbance was measured at 562 nm. In both cases, the concentrations were calculated from the standard curve by linear regression corrected for sample dilution.

4.2.6 Trypsin cleavage assay

For the tryptic digestion assay, crude synaptosomes were prepared from mouse brains as described before. A trypsin stock solution (0.1 mg/ml) was prepared, and varying volumes of the stock solution (1250 µl, 500 µl, 250 µl, 125 µl) were added to 3-5 mg of synaptosome lysate, ensuring that all the reaction volumes were equal in the end. The mixture was incubated for 10 min at 30°C in a water-bath with gentle agitation and swirling, and then centrifuged at 8700 x g for 3 min at 4°C. The resulting pellet was resuspended in 1x Laemmli sample buffer (LSB) (6x LSB: 375 mM Tris pH 6.8, 50% glycerin, 10% β-mercaptoethanol, 10% SDS, 0.03% bromophenol blue) and denatured at 93°C for 10 min. Proteins were separated by SDS-PAGE and analyzed by immunoblotting. Blots were imaged using Odyssey Fc Imaging System (Li-COR Biosciences), and quantitative analysis of band intensities was performed with Image Studio Software. The optimal trypsin concentration for a specific post-synaptic protein cleavage was determined empirically by assessing pre- and postsynaptic protein digestion.

4.2.7 Immunoprecipitation

Co-immunoprecipitation experiments were performed using protein extracts derived from the brain fraction of interest (brain lysates, crude synaptosomes, synaptic membrane preparations) depending on the experimental requirements. For each reaction, 4-5 mg of protein were incubated with 1.5-3 µg of the respective primary antibody or species-matched IgG control in IP lysis buffer (50 mM Tris HCl, 100 mM NaCl, 1% Triton X-100, protease inhibitor tablet EDTA free, phosphatase inhibitors cocktail 1 and 2). The mixture was rotated for 1 h at 4°C to allow antibody binding. Subsequently, 30 µl of pre-equilibrated Protein A/G magnetic beads were added to the mixture and incubated for an additional 2 h at 4°C on a rotating wheel to facilitate immune complex formation. After incubation, the beads were collected using a magnetic support and washed three times with 1 ml of ice-cold washing buffer (50 mM Tris HCl, 100 mM NaCl, 1% Triton X -100). Each wash was performed on rotation for 10 min at 4°C. Following the final wash, residual buffer was carefully aspirated and immunoprecipitated proteins were eluted by adding 20 µl of 1x LSB (6x LSB: 375 mM Tris pH 6.8, 50% glycerin, 10% β-mercaptoethanol, 10% SDS, 0.03% bromophenol blue). Samples were denatured at 95°C for 15 min and then briefly centrifuged. The supernatant, containing the eluted protein complexes, was subjected to SDS-PAGE and immunoblotting.

4.2.8 Mass Spectrometry

For proteomic analysis, immunocomplexes captured on Protein A/G magnetic beads (see 4.1.7) were processed on-bead for LC-MS/MS. Beads were collected on a magnetic rack and subjected to a graded wash series of 10 mins each to remove detergents and non-specific binders while preserving complexes: 2x 500 µl wash buffer I (WB-I : 50 mM Tris-HCl, 100 mM NaCl, 1% Triton X-100, pH 7.5), followed by 1x 500 µl wash buffer II (WB-II : 50 mM Tris-HCl, 100 mM NaCl, 0.05% Triton X-100, 5% glycerol, pH 7.5). A final wash was performed with 500 µl wash buffer II without Triton X-100, and beads were then transferred to a fresh low-bind tube.

For on-bead proteolysis, 50 µl of Elution/Digestion buffer I (EB-I: 2 M urea, 50 mM Tris-HCl pH 7.5, 1 mM DTT, 5 ng/µl trypsin) were added, and samples were incubated for 30 min at room temperature. Beads were magnetically cleared, and the peptide-containing supernatant was retained. Beads were then rinsed again with 100 µl of Elution/Digestion buffer II (EB-II: 2 M urea, 50 mM Tris-HCl pH 7.5, 5 mM chloroacetamide), and the supernatant was combined with the EB-I supernatant: the pooled eluate was incubated overnight at room temperature to complete digestion and alkylation of peptides. Peptides were then stabilized by acidification with 15 µl of 10% trifluoracetic acid (TFA), ensuring the pH dropped below 2 (using pH indicator paper). Samples were then desalted using three-layer C18 StageTips and dried in a SpeedVac for 20 min at room temperature. The dried peptides were subsequently reconstituted in 8 µl of buffer A (0.1% formic acid) and adjusted with 1 µl of buffer A* (0.1% TFA, 2% acetonitrile) prior to injection. For LC-MS/MS, 4 µl of the peptide solution were loaded onto a nano-LC system coupled to a high-resolution mass spectrometer and analyzed using a 90 min gradient (all reagents were prepared in MS-grade H_2O). Data analysis was performed with *MaxQuant Perseus V1.6.15.0* software with help of Dr. Markus Räschle.

4.2.9 Surface Biotinylation

To selectively isolate surface-exposed proteins from cortical neuronal cultures, a biotinylation assay was employed at DIV14-16. Cultures were grown in 6-well plates at a density of at least 1.2 x 10^6 neurons per well, and for each experimental condition (control and iDKO) at least three wells were used. Cells were placed on ice to inhibit endocytosis and quickly washed with ice-cold PBS^{2+} buffer (137 mM NaCl, 2.7 mM KCl, 10 mM Na_2HPO_4, 1.8 mM KH_2PO_4, 1mM $CaCl_2$, and 0.5 mM $MgCl_2$; pH 7.4). The cells were then incubated with freshly prepared non-membrane-permeant, cleavable biotin derivative, sulfo-NHS-SS-biotin (0.5 mg/ml in PBS^{2+}) for 20 min at 4°C under gentle shaking. After biotinylation, the unreacted biotin was quenched by two sequential washes with PBS^{2+} containing 50 mM glycine for 2 min each. Following quenching, neurons were

lysed by scraping in RIPA lysis buffer (50mM Tris-HCl pH 7.4, 150mM NaCl, 1mM EDTA, 1% Triton X-100, 0.5% Sodium Deoxycholate, 0.1% SDS in H_2O) supplemented with protease and phosphatase inhibitors. Lysates were incubated on rotation for 15 min at 4°C, clarified by centrifugation at maximum speed for 15 min, and supernatants were collected. Protein concentrations were determined using BCA assay, and aliquots of total lysates were reserved as input controls. Equal protein amounts were incubated with 50-100 µl of streptavidin agarose beads at 4°C for 2 h on rotation. Following incubation, beads were centrifuged, and supernatants were collected as the intracellular fraction. Beads were subsequently washed three times with RIPA buffer (without inhibitors), and bound proteins were eluted by boiling for 10-15 min in 30 µl 1x LSB (6x LSB: 375 mM Tris pH 6.8, 50% glycerin, 10% β-mercaptoethanol, 10% SDS, 0.03% bromophenol blue). The resulting biotinylated (surface) protein fraction, together with reserved input from total and intracellular lysates, was subjected to SDS-PAGE and immunoblot analysis.

4.2.10 Expression and affinity purification of GST-fusion proteins

To produce GST-tagged fusion proteins, the E. coli expression strain BL21 was used. An overnight starter culture of 50 ml was prepared in LB medium containing 50 µg/ml of antibiotics and grown at 37°C in an incubator shaking at 180 rpm. The following day, 500 ml of 2x YT medium supplemented with 50 µg/ml of antibiotics were inoculated with the overnight starter culture and cultivated at 37°C with shaking at 180 rpm. Once the cultures reached an optical density of 0.7-0.8 at 600 nm, the temperature was reduced to 30°C and protein expression was induced with 0.5 mM IPTG. Cells were harvested after 4 h of induction at 30°C and collected by centrifugation at 4000 x g for 15 min at 4°C. The resulting bacterial pellet was resuspended in 20 ml ice-cold 1x PBS, and aliquots of the suspension were stored at -20°C until further processing.

For protein purification, 10 ml of frozen bacterial pellets were thawed at room temperature and supplemented with 1 mM PMSF, 125 units of benzonase, and a small amount of lysozyme. After incubation on ice for 15 min, cells were disrupted by sonication at 30% amplitude/power for 1 min using a digital sonifier, while keeping the cells on ice throughout. Following sonication, Triton X-100 was added to a final concentration of 1% (v/v), and lysis was continued for another 15 min on rotation at 4°C. Cell debris was removed by centrifugation at 22000 x g for 15 min at 4°C, and the cleared supernatant was incubated with 250 - 500 µl of pre-washed GST-bead resin for 1-2 h at 4°C with continuous rotation. The beads were then washed three times with ice-cold PBS, and the bound GST-fusion proteins were finally resuspended in 1 ml of PBS. Protein concentration was determined using Bradford or BCA assay and validated by visual inspection after performing SDS-PAGE followed by Coomassie staining.

4.2.11 GST Pulldown assay

GST pulldown assays were carried out to investigate protein-protein interactions. For each reaction, 100 µg of purified GST-fusion protein bound to glutathione resin were incubated with freshly prepared brain lysates. Prior to incubation, brain extracts were clarified by ultracentrifugation to remove insoluble material. The mixture was incubated for 2-4 h on rotation at 4°C. Following incubation, the beads were washed three times with ice-cold brain lysis buffer (20 mM HEPES pH 7.4, 2 mM $MgCl_2$, 100 mM KCl, 1 mM PMSF, 1% Triton X-100) containing Triton X-100 to remove unbound proteins, followed by a final wash without any detergent. The residual wash buffer was carefully removed, and bound proteins were eluted by resuspending the beads in 40 µl of 1x LSB (6x LSB: 375 mM Tris pH 6.8, 50% glycerin, 10% β-mercaptoethanol, 10% SDS, 0.03% bromophenol blue), followed by heating at 95°C for 10 min. After a brief centrifugation, the supernatant containing the interacting proteins were collected and subjected to SDS-PAGE and immunoblot analysis.

4.2.12 SDS-PAGE

Proteins were separated according to their molecular weight using sodium dodecyl sulfate-polyacrylamide gel electrophoresis (SDS-PAGE) using Tris-glycine-based buffers. Gels were cast in glass plates assembled in a casting frame, consisting of a stacking gel (3.8%) layered on top of a separating gel (4-14%) depending on the size of the proteins of interest (Table 4.11). The electrophoresis chamber was filled with 1x running buffer (25 mM Tris base, 192 mM glycine, 0.1% SDS, pH 8.4), and protein samples prepared in 1xLSB (6x LSB: 375 mM Tris pH 6.8, 50% glycerin, 10% β-mercaptoethanol, 10% SDS, 0.03% bromophenol blue), were loaded alongside a molecular weight marker. Electrophoresis was initiated at constant voltage of 80 V to allow stacking of proteins, followed by separation in the separating gel at 120-150 V until the dye front reached the bottom of the gel. Following electrophoresis, proteins were either transferred to nitrocellulose membrane for immunoblotting or directly visualized by Coomassie staining.

Table 4.11 Composition of separating and stacking polyacrylamide gels for SDS-PAGE

Separating gel (15 ml for 2 gels)	6%	8 %	10%	12 %
ddH_2O	8 ml	7 ml	6 ml	5 ml
1.5 M Tris-HCl (pH 8.8) + 0.4% SDS	3.75 ml	3.75 ml	3.75 ml	3.75 ml
30% bis-acrylamide mix	3 ml	4 ml	5 ml	6 ml
10% APS	150 µl	150 µl	150 µl	150 µl

TEMED	15 µl	15 µl	15 µl	15 µl

Stacking gel (5 ml for 2 gels)	**3.8 %**
ddH_2O	8 ml
1 M Tris-HCl (pH 6.8)	3.75 ml
30% bis-acrylamide mix	3 ml
10% APS	150 µl
TEMED	15 µl

4.2.13 Coomassie staining

Proteins separated by SDS-PAGE were visualized by Coomassie Brilliant Blue R-250 staining. Polyacrylamide gels were incubated in staining solution (0.1% Coomassie dye, 40% methanol, 10% acetic acid in ddH_2O) for 2 h at room temperature with gentle shaking to allow dye binding. Excess stain was removed by incubation in destaining solution (40% methanol, 10% acetic acid, in ddH_2O) overnight, resulting in visualization of protein bands against a clear background.

4.2.14 Immunoblotting

Proteins separated by SDS-PAGE were transferred onto nitrocellulose membranes (0.2 µm) using a wet transfer system. Transfer was performed at constant voltage in ice-cold 1x transfer buffer (25 mM Tris base, 192 mM glycine, 20% methanol, pH 8.3) at 110 V for 90 min. After transfer, membranes were briefly rinsed and stained with Ponceau stain (0.5% Ponceau S dye, 1% acetic acid) to confirm efficient protein transfer and equal loading. The stain was subsequently removed by repeated washes in TBST (1x TBS with 0.1% Tween-20). Membranes were blocked in Li-COR commercial blocking solution for 30-60 min at room temperature to prevent nonspecific binding. Membranes were then incubated with primary antibodies diluted in TBST containing blocking solution (1:1) overnight at 4°C. The following day, membranes were washed three times in TBST and incubated with species appropriate IR Dye-conjugated secondary antibodies (1:10000, Li-COR) for 45-60 min at room temperature. Excess antibody was removed by several washes in TBST followed by a wash in TBS. Fluorescent signals were detected using the Li-COR Odyssey imaging system, and band intensities were quantified using Image Studio software.

4.3 Cell biological methods

4.3.1 Cell culture

Cell lines (HeLa, HEK293) were maintained in complete growth medium composed of Dulbecco's modified eagle medium (DMEM) supplemented with 10% fetal bovine serum (FBS) and 1% Penicillin/Streptomycin (Pen/Strep) under standard culture conditions (37°C, 5% CO_2). For passaging, cells were washed once with sterile PBS to remove residual serum proteins and then incubated with TrypLE for ~5 min at 37°C to detach adherent cells. The enzymatic reaction was stopped by adding complete growth medium, and the cell suspension was collected and centrifuged at 300 x g for 5 min. The pellet was resuspended in fresh medium, and cells were either reseeded at the desired density or split for further expansion.

4.3.2 Primary neuronal cell culture

Primary hippocampal and cortical neurons were prepared from neonatal mouse pups (P0-P3). Before plating, coverslips were coated with a 200ul droplet of poly-L-lysine (0.0015% in sterile water) and dried under sterile conditions. For dissection, brains were rapidly isolated in ice-cold HBSS (Hank's balanced salt solution) supplemented with 20% FBS and 1% Pen/Strep. Under a stereomicroscope, hippocampi were carefully dissected from cortical tissue and collected in HBSS containing 20% FBS and 1% Pen/Strep. Tissue fragments were transferred into 15 ml tubes and washed twice with HBSS containing FBS (20% FBS, 1% Pen/Strep) and twice with HBSS alone (1% Pen/Strep). Washes were carried out by adding wash solution, letting the tissue pieces settle due to gravity, and then aspirating the solution. Following the wash steps, enzymatic dissociation was carried out using a 1 mg/ml trypsin digestion solution (137 mM NaCl, 5 mM KCl, 7 mM Na_2PO_4, 25 mM HEPES, pH 7.2) containing DNase (600 U/ml) for 15-20 min at 37°C. After digestion, the tissue was washed with HBSS as before to inactivate trypsin and subsequently resuspended in dissociation buffer (12 mM $MgSO_4$ in HBSS) containing DNase. Cells were dissociated mechanically triturated by gentle pipetting (approximately 10 times) until a homogenous suspension was obtained. The suspension was then centrifuged at 800 x g for 10 min at 4°C and resuspended in plating medium (MEM supplemented with 5 g/l glucose, 200 mg/l $NaHCO_3$, 100 mg/l transferrin, 10% FBS, 2 µg/ml insulin, 1x GlutaMax, 1x Pen/Strep). Viable cells were counted using Trypan Blue exclusion. Neurons were plated at the desired density ($1x10^5$ cells per 12 wel-plate and $1x10^6$ cells per 6 well-plate) on PLL-coated coverslips and allowed to attach for 30-60 min before addition of pre-warmed plating medium. On DIV1, half of the medium was replaced with growth medium (MEM supplemented with 5 g/l glucose, 200 mg/l $NaHCO_3$, 100 mg/l transferrin, 10% FBS, 2% B27 supplement, 1x GlutaMax, 1x Pen/Strep)

containing 2 µM cytosine β-D-arabinofuranoside (AraC) to inhibit glial proliferation, followed by supplementation with AraC to a final concentration of 4 µM on DIV2. Cultures were maintained at 37°C in a humidified incubator with 5% CO_2 and left undisturbed until DIV14, when neurons were considered mature and used for experiments.

4.3.3 Primary ependymal cell culture

Primary ependymal cell cultures were prepared from neonatal mouse telencephalon (P0-P4). Cortical tissue (excluding hippocampus) was dissected in ice-cold HBSS solution (HBSS, 10 mM HEPES, 0.0075% $NaHCO_3$, 1% Pen/Strep) and tissue fragments were collected into 15 ml tubes. The tissue fragments were pelleted at 100 x g for 1 min and subjected to digestion for 45-60 min at 37°C in an enzymatic solution (20 U/ml papain, 0.3 mg/ml L-cysteine, 1x GlutaMax, 1x Pen/Strep and 600 U/ml DNase in DMEM). Digestion was stopped by the addition of stop solution (1 mg/ml trypsin inhibitor/ovomucoid in Leibovitz L-15 medium), followed by rinsing in L-15 medium. The tissue was gently dissociated by pipetting (approximately 10 times) in the presence of DNase (600 U/ml), and the cell suspension was centrifuged at 110 x g for 7 min. Cells were resuspended in DMEM/GlutaMax containing 10% FBS and 1% Pen/Strep and plated into poly-L-lysine-coated T25 flasks. Culture medium was renewed on the following day, and cells were maintained until reaching confluence (typically 4-5 days).

Confluent cultures were subjected to orbital shaking (250 rpm) overnight at room temperature (22°C) in normal air, to eliminate weakly adherent and any differentiated cells, thereby enriching ependymal progenitors. The day after shaking, cultures were first rinsed with PBS and subsequently trypsinized with 0.05% trypsin-EDTA to detach the adherent cells. Harvested cells were resuspended in DMEM/Glutamax supplemented with 10% FBS and 1% Pen/Strep and seeded at desired density ($1.5x10^5$ cells per 12 well-plate and $1x10^6$ cells per 6 well-plate). Cell suspensions were carefully plated as droplets onto poly-L-lysine-coated glass coverslips and allowed to adhere for 1 h before addition of culture medium. On the following day (DIV0), cultures were switched to serum-free DMEM/GlutaMax containing 1% Pen/Strep, enabling progressive differentiation of progenitors into multiciliated ependymal cells, which were considered mature and ready for experiments by DIV14.

4.3.4 Transfection of cell lines with JetPrime

Transient transfections of cells (e.g. HeLa cells) were performed using the JetPrime reagent (Polyplus) according to the manufacturer's instructions. Cells were seeded at the desired density ($1x10^5$ cells per 12 well-plate) in the morning and transfected 4-5 h later to ensure optimal adherence. For transfection, plasmid DNA was diluted in JetPrime buffer and briefly vortexed.

Next JetPrime regent was added, and the mixture was vortexed again and incubated for 10 min at room temperature to allow complex formation. The exact DNA and reagent quantities used varied according to dish size (Table 4.12). After incubation the mixture was added dropwise to the cells and left overnight to facilitate transfection. The following day the culture medium was replaced with fresh medium, and cells were maintained under standard growth conditions. Transfected cells were used for experiment 24-48 h post-transfection.

Table 4.12 Reagent compositions for JetPrime transfection

Culture format	JetPrime buffer	Plasmid DNA	JetPrime reagent
12-well plate	100 µl	1 µg	2 µl
6-cm dish	200 µl	4 µg	8 µl
10-cm dish	400 µl	8 µg	16 µl

4.3.5 Calcium phosphate transfection of cells

Transient transfections of cells (e.g., HEK 293 cells) were also performed using the calcium phosphate method. Cells were seeded in the morning and transfected 4-5 h later, at a 50-60% confluency. For transfection plasmid DNA was first mixed with 0.1x TE buffer (1 mM Tris-HCl, 0.1 mM EDTA, pH 8), 2s M $CaCl_2$ and 2x HBS buffer (50 mM HEPES, 280 mM NaCl, 1.5 mM Na_2HPO_4, pH 7) under constant agitation and incubated for 15-20 min at room temperature. After incubation the DNA-calcium phosphate precipitate was added dropwise to the cells. The exact amount of DNA, $CaCl_2$, and buffers used varied according to dish size (Table 4.13). Cells were left with transfection mixture overnight. The following day the medium was replaced with fresh medium. Transfection efficiency was routinely verified by fluorescent reporter expression. Cells were used for experiments 48 h post-transfection.

Table 4.13 Reagent compositions for calcium phosphate transfection

Culture format	Plasmid DNA	0.1x TE buffer	2 M $CaCl_2$	2x HBS buffer
2.5-cm dish	1 – 1.5 µg	88 µl	12 µl	100 µl
6-cm dish	2.5 – 4 µg	220 µl	30 µl	250 µl
10-cm dish	5 – 8 µg	440 µl	60 µl	500 µl

4.3.6 Calcium phosphate transfection of primary neurons

Calcium phosphate transfection was employed to introduce plasmid DNA into primary hippocampal and cortical neurons using the commercial ProFection Mammalian Transfection Kit (Promega). Neurons were transfected at DIV 6-8, as per manufacturer's instructions. Prior to transfection, Hank's Balanced Salt Solution (HBSS) and Neurobasal-A (NBA) medium were equilibrated in the incubator for at least 1 h, and their osmolarities were measured along with that of the culture medium. To minimize osmotic stress, the osmolarity of HBSS and NBA was adjusted to match the culture medium using D-mannitol, allowing a tolerance of up to ±10 mOsm. Neurons grown on poly-L-lysine-coated coverslips were carefully transferred into wells containing NBA. The transfection mixture was freshly prepared by combining plasmid DNA, $CaCl_2$, and sterile water, which was then added dropwise into HEPES-buffered saline (HeBS) under gentle vortexing to promote calcium-phosphate DNA precipitate formation. The precise amount of each component varies depending on the culture format (Table 4.14). After 20 min of incubation in the dark, the precipitate was applied dropwise onto neuronal cultures and incubated for another 20 min at 37°C. After incubation the precipitate was rapidly removed, and neurons were gently washed three times with pre-warmed HBSS. Coverslips were returned to their original conditioned medium for continued culture. Transfected neurons were subsequently maintained under standard conditions and used for experiments at DIV14.

Table 4.14 Reagent compositions for calcium phosphate transfection of primary neurons

Culture format	Plasmid DNA	HeBS buffer	$CaCl_2$	Nuclease free H_2O
12- well plate	1 – 2 µg	50 µl	6.25 µl	40.75 µl
6-well plate	2 – 4 µg	100 µl	12.5 µl	81.5 µl

4.3.7 Immunocytochemistry

Cells grown on coverslips were washed twice with PBS at room temperature and fixed with ice-cold 4% paraformaldehyde (PFA) or 4% PFA containing sucrose (mainly primary cultures) for 10-15 min at room temperature. After fixation the cells were washed again three times with PBS and directly stained or stored at 4°C for a few days until processing. Immunostaining was continued by incubating the cells for blocking and permeabilization in GSDB (goat serum dilution buffer: 20% goat serum, 0.1% Triton X-100 in PBS) for 30 min. Primary antibodies were diluted in GSDB and pipetted as droplets onto Parafilm in a humidified chamber. Coverslips were placed with their cell-containing side down onto the droplets and incubated for 1-2 h at room temperature.

Coverslips were then washed three times in PBST (PBS, 0.1% Tween-20) and incubated again with GSDB-diluted secondary antibodies for 1 h at room temperature in the dark. Coverslips were washed as before and counterstained with DAPI (1 µg/ml) for 5-10 min, rinsed, and mounted in ImmuMount. The samples were stored in dry and dark conditions until imaging.

4.3.8 Sytox cell viability assay

To assess neuronal viability, hippocampal cultures were incubated in their growth medium with the membrane-impermeant DNA dye SYTOX™ Green reagent (0.1 µM), which only gains access to cells with compromised membrane integrity, and the membrane permeant dye Hoechst 33342 (0.5 µM), which stains the nuclei of all cells, for 30 min at 37°C. After staining, cells were washed once with warm HBSS and maintained in HBSS for live-cell imaging. SYTOX-positive nuclei were quantified as dead cells, and Hoechst served as a total nuclear counterstain.

4.3.9 Transferrin uptake

Transferrin endocytosis was assessed in hippocampal neurons at DIV14-16. Prior to ligand addition, cultures were starved for 1 h at 37°C in osmolarity-adjusted Neurobasal-A medium (NBA). For uptake experiments, Alexa-647 transferrin (25 µg/ml) was prepared in NBA and pipetted as droplets onto Parafilm in a humidified chamber. Coverslips were placed with their cell-containing side down onto the droplets and incubated for 30 min at 37°C to allow internalization, while control cells were incubated for 30 min at 4°C to inhibit endocytosis. Coverslips were then washed twice with ice-cold PBS containing 10 mM $MgCl_2$ and subjected to a quick 1 min acid wash (ice-cold 0.1 M sodium acetate, 0.2 M NaCl, pH 5.3) to remove surface-bound transferrin. The coverslips were washed again with PBS, and cells were fixed in ice-cold 4% PFA for 10 min at room temperature, rinsed in PBS, counterstained with DAPI for 5-10 min, and mounted for imaging. For quantification, images were analyzed using Fiji/ImageJ. ROIs (regions of interest) were drawn manually around dendritic segments of neurons with transferrin-positive puncta. Within these ROIs mean fluorescence intensity was measured.

4.3.10 pHluorin assay

pHluorin is a pH-sensitive GFP variant that is quenched in the acidic lumen of synaptic vesicles and becomes fluorescent upon exposure to the neutral extracellular space after vesicle fusion. This property of the probe enables quantitative tracking of exo- and endocytosis, with the reacidification-dependent fluorescence decay reflecting (in a delayed manner) the kinetics of vesicle endocytosis and recycling (Fig 2.9 A).

Hippocampal neurons were transfected with pHluorin-tagged plasmids on DIV 6-8, and live-imaging of these pHluorin-tagged proteins was performed between DIV12-14. Cover slips with neurons were mounted in an imaging chamber and perfused with TES-based physiological buffer (Table X9). Imaging was carried out on a Nikon epifluorescence microscope equipped with a 40x oil-immersion objective at 37°C. Images were acquired every 2 s with 100 ms exposure at 488 nm, using optimized parameters to minimize photobleaching while ensuring stable fluorescence over the recording period (>5 min). To determine the surface-to-total ratio of pHluorin-tagged proteins, neurons were first imaged in TES buffer to establish the baseline signal (steady state signal before quenching). The fluorescence of surface exposed pHluorin-tagged proteins (Fs) was quenched by replacing TES buffer with a MES-based acidic buffer to obtain the background fluorescence. The total fluorescence (Ft) was subsequently revealed by substituting the acidic buffer with a basic buffer (Table 4.15).

For quantification images were analyzed using Fiji/ImageJ and ROIs were selected manually, and dendritic segments were analyzed for GluA1 intensities, and the surface-to-total ratio was calculated as:

$$surface - to - total\ ratio = \frac{baseline - Fs}{(Ft - Fs)}$$

Table 4.15 Buffer composition for pHluorin live-cell imaging

Buffer	Composition	pH
Physiological buffer	170 mM NaCl, 3.5 mM KCl, 0.4 mM KH_2PO_4, 20 mM TES, 5 mM $NaHCO_3$, 5 mM Glucose, 1.2 mM Na_2SO_4, 1.2 mM $MgCl_2$, and 1.3 mM $CaCl_2$	7.4
Acidic buffer	Physiological buffer with TES replaced by MES	5.5
Basic buffer	Physiological buffer with 50 mM NaCl substituted by 50mM NH_4Cl	7.4

4.4 Histological methods

4.4.1 Perfusion of mice

Mice were deeply anesthetized with a lethal dosage of narcotics (10% Ketamine, 2% Xylazine), individually calculated based on body weight (Injection volume (in µl) = body weight (in g) x 3.4). After injection mice were observed until the absence of the pain reflex was verified. After thoracotomy, the rib cage was opened to reveal the pumping heart. A hypodermic needle linked to a peristaltic pump was placed into the left ventricle, and an incision was created in the right atrium to let blood flow out. To get rid of blood in the mice circulation, they were first perfused with lukewarm PBS at a flow rate of 3-4 ml/min, resulting in a paling of liver and limbs as a mark of blood loss. After that, the perfusion was continued with ice-cold 4% paraformaldehyde to fix the tissue. The perfusion lasted for 20 to 30 min. For the first 10 min the flow rate was set to 3-4 ml/min followed by a slower perfusion at 1-2 ml/min. Efficient tissue fixation was verified by checking stiffness of neck and tail. After perfusion was complete, the brain was dissected and briefly incubated for 1-2 h in fresh ice-cold 4% PFA, and subsequently post-fixed overnight in 4% PFA containing 30% sucrose at 4°C. The next day fixed brains were washed three times for 10 min each with 30% sucrose solution and incubated overnight in the same solution. The brains were maintained in sucrose solution at 4°C until further processing.

4.4.2 Cryosectioning of brain tissue

The mouse brains were sectioned into 40 µm coronal slices for Nissl and immunohistochemical staining using a microtome. The cutting platform was maintained at -22°C, and to ensure stable cutting a smooth surface layer was made using 30% sucrose (in PBS) on which the brain was mounted. The brain was trimmed by removing the brainstem and the majority of the olfactory bulb prior to mounting. After mounting on the platform, the brain was subsequently sectioned, and the slices were collected in a well plate (in a series of seven) containing 15% sucrose (in PBS). Following the complete brain dissection, the sections were washed twice for 10min each with 15% sucrose (in PBS), followed by a final wash with PBS alone. The slices were stored in PBS containing 0.02% Na-azide until further processing for Nissl staining, whereas the slices designated for immunohistochemical staining were stored in a cryoprotective solution (2% DMSO, 2% glycerol in 0.125 M phosphate buffer) at -20°C and thereafter transferred to -80°C for long-term storage until required.

4.4.3 Nissl staining

Nissl staining was performed with one series of sections (i.e. every first slice of the seven series). The sections were mounted on gelatin-coated slides at 41°C and allowed to dry. After drying, the

slices were incubated in chloroform-ethanol (1:1) solution overnight for degreasing, followed by dehydration in 100% ethanol for 1 h. Sections were then rehydrated by immersing them for 3 min each through a graded ethanol series (100%, 95%, 90%, 70%, 50%). The sections were briefly immersed in distilled water before subsequently immersing them in thionine-staining solution (0.125% thionine acetate, 50 mM acetic acid, 36 mM NaOH) for 3 min, followed by multiple rinses in distilled water to remove excess stain. Next, destaining and dehydration were performed by immersing the slices for 3 min in a series of solutions with increasing ethanol concentration (50%, 70%, 90%, 95%, 100%). Between the 90% ethanol and 95% ethanol stages, an additional step was incorporated to effectively destain the slices using 95% ethanol containing several drops of glacial acetic acid (10-15 drops) for a duration of 10-15 min. During the incubation time, the slices were examined under the binocular microscope for the proper level of destaining. Following dehydration, the slices were incubated in terpineol-xylol (1:1) solution for 3 min, followed by incubation in xylol twice for 3 min each. Upon completion of the staining procedure, the slides were mounted in Entellan.

4.4.4 Immunohistochemical staining

The slices for immunohistochemistry (IHC) staining were transferred from the -80°C storage and to -20°C for thawing one day prior to staining. The sections to be stained were collected in 0.125 M phosphate buffer (PB). This buffer was prepared by diluting stock solutions of 0.4 M NaH_2PO_4 (A) and 0.4 M Na_2HPO_4(B). For ca. 500 ml of 0.4 M PB, 387 ml solution B were taken, and solution A was added, until pH 7.4 was reached. All subsequent procedures were performed on a horizontal shaker. The slices were first thoroughly washed three times for 20 min each in 0.125 M PB for 1 h. The slices were then permeabilized by incubating them in 0.125 M PB containing 0.3% Triton X-100 for 2 h, with solution changes every 20 min. The slices were incubated in antigen retrieval buffer (10 mM sodium citrate, 0.05% Tween-20, pH 6) for 20 min at 90°C, followed by blocking in IHC blocking solution (5% goat serum, 0.125 M PB, 0.3% Triton X-100) for 1 h at room temperature. The sections were incubated with the primary antibodies diluted in IHC blocking solution for 2-3 days at 4°C. Sections were then washed in 0.125 M PB containing 0.3% Triton X-100 for 3 h (6 washes of 30 min each). The slices were incubated with the secondary antibody in IHC blocking solution for 2 h at 4°C followed by washes as before. Next the sections were stained with DAPI (1µg/ml) for 10 min and washed once for 15 min with 0.125 M PB. Stained slices were affixed onto Superfrost slides in gelatine mounting solution (0.2% gelatine in 50 mM Tris-HCl) at 41°C, subsequently dried, and mounted using Immumount.

4.5 Molecular Biology methods

4.5.1 Genotyping of mice

Tail biopsies (P0 – P4) or ear biopsies (from P5 onwards) were taken from mice by the animal caretakers for genotyping. Genomic DNA was isolated from mouse tissue to allow genotyping of transgenic mice before experiments. The tissue was lysed using 50 µl of alkaline lysis buffer (25 mM NaOH, 0.2 mM EDTA, pH 12) at 95°C for 60 min while shaking at 1000 rpm. Following lysis, 50 µl of neutralization buffer (40 mM Tris-HCl, 0.2 mM EDTA, pH 5) were used to inactivate the lysis process. Polymerase chain reaction (PCR) was employed to amplify specific DNA fragments for EPS15L1, EPS15, or CAG-Cre, to ascertain the distinct genotypes. The PCR reaction mixture was prepared (Table 4.16), and the corresponding cycling protocol was selected (Table 4.17).

Table 4.16 PCR reaction mixture for one sample

Components	Volume
Nuclease free water	7.9 µl
10x Orange dye	1.5 µl
$MgCl_2$ (25mM)	1.5 µl
Buffer B	1.5 µl
dNTPs (5 mM)	0.3 µl
Primer Mix (10 µM) (forward and reverse)	0.5 µl
Taq Polymerase (5 U/µl)	0.3 µl
Genomic DNA	1.5 µl

Table 4.17 Thermocycling programs for genotyping

	EPS15L1	EPS15	CAG Cre
Initial denaturation	94°C for 3 min	95°C for 2 min	95°C for 2 min
Number of cycles (Round1)	12x cycle	35x cycle	35x cycle
Denaturation	94°C for 30 s	95°C for 30 s	95°C for 30 s
Annealing	64°C for 30 s	62°C for 30 s	55°C for 30 s
Elongation	72°C for 30 s	72°C for 30 s	72°C for 30 s
Number of cycles (Round 2)	25x cycle	-not applicable-	-not applicable-
Denaturation	94°C for 20 s		
Annealing	58°C for 30 s		
Elongation	72°C for 45 s		
Final elongation	72°C for 2 min	72°C for 10 min	72°C for 2 min
Storage	8°C ∞	8°C ∞	8°C ∞

4.5.2 Molecular cloning

4.5.2.1 Design of cloning strategies

Cloning strategies were established using the SnapGene editing software. Primers intended for cloning were designed with an overlap of 15 to 18 base pairs (bp) between the primer and the target sequence along with the restriction site. Four extra nucleotides were usually added to the 5' terminus to facilitate effective cleavage by restriction enzymes. The entire plasmid was constructed in silico to eliminate potential errors, including frame shifts or incompatibility with restriction enzyme recognition sites.

4.5.2.2 Polymerase chain reaction

Polymerase chain reactions (PCRs) were employed to amplify specific DNA sequences from plasmid or genomic DNA. PCRs were typically conducted in a volume of 50 µl using different components (Table 4.18). The thermocycling program used was similar in most cases, except the annealing temperature (T_M) which was set to match the melting temperature of the respective primers (Table 4.19). PCR products were analyzed by agarose gel electrophoresis or purified using commercial PCR purification kit (Macherey-Nagel) as per manufacturer´s protocol.

Table 4.18 PCR reaction mixture for one sample

Components	Concentration
Genomic/plasmid DNA	50 ng
GC buffer	1x
dNTPs	200 µM
Forward primer	0.5 µM
Reverse primer	0.5 µM
Phusion polymerase	0.02 U/µl
Nuclease-free water	Fill up to 50 µl

Table 4.19 Thermocycling program for PCR

Phusion PCR	Condition
Initial denaturation	98°C for 30 s
Number of cycles	30x cycle
Denaturation	98°C for 10 s
Annealing	T_M °C for 20 s
Elongation	72°C for 90 s
Final elongation	72°C for 2 min
Storage	8°C ∞

4.5.2.3 Agarose gel electrophoresis

Agarose was solubilized in 1 x TAE buffer (40 mM Tris-acetate, 1mM EDTA) at a concentration ranging from 0.7% to 1.5% by heating in a microwave. Ethidium bromide was added to the gel at a final concentration of 100 ng/ml, to visualize the DNA. The gel was poured into casting trays and allowed to solidify. The DNA samples premixed with loading dye were loaded into the agarose gels and run in chambers containing 1x TAE buffer at 120V for 20-30 min. DNA bands were visualized by UV transillumination of agarose gels. If DNA was intended for further processing, the desired pieces were excised from the gel using sharp clean blades, while minimizing UV exposure.

4.5.2.4 DNA digestion

DNA digestion with restriction enzymes was conducted for analysis of DNA constructs or to produce DNA pieces for subcloning. Usually, 1-2 µg of plasmid DNA or the purified PCR product were incubated with FastDigest restriction enzymes and the other components listed (Table 4.20) and subjected to digestion for 1 h at 37°C. Digested fragments were confirmed using agarose gel electrophoresis and subsequently purified from the gel for cloning purposes using the NucleoSpin Clean-up kit (Macherey-Nagel).

Table 4.20 PCR reaction mixture for one sample

Components	Amounts
Genomic/plasmid DNA	1 µg
FastDigest buffer	1x
Restriction enzyme 1	1 µl
Restriction enzyme 1	1 µl
Nuclease-free water	Fill up to 20 µl

4.5.2.5 DNA ligation

Digested PCR products and plasmid backbones were subjected to ligation to obtain the desired plasmid. The ligation reaction was set up with an insert-to-vector molar ratio of 3:1. The ligation mixture was prepared by mixing the corresponding amounts of insert, vector, 1x T4 ligase buffer and 1 µl T4 DNA ligase, in a final volume of 20 µl. The ligation mix was incubated for 30 min at room temperature or overnight at 16°C. A reaction with only the plasmid was always included as control. 5 µl of the ligation mixture were used for transformation.

4.5.2.6 Transformation and plasmid DNA isolation

Chemically competent *E. coli* (Top10 or BL21) bacteria were thawed on ice, then 50 µl of thawed bacteria were incubated with 5 µl of ligation mix or 1 µg of plasmid DNA on ice for 30 min. Following incubation, the cells were heat-shocked at 42°C for 45 s and immediately transferred back to ice for 5 min. 500 µl of prewarmed LB medium without antibiotics was added to the bacteria mix and incubated at 37°C while shaking at 1000 rpm. The cells were then directly plated on pre-warmed LB agar plates supplemented with appropriate antibiotics at 37°C overnight, for selection of positive clones.

Positive individual colonies were picked for inoculating 5 ml LB medium supplemented with antibiotics and grown at 37°C overnight in a bacterial shaker at 180 rpm. The next day, 1 ml of starter culture was used to inoculate 250 ml of LB medium supplemented with antibiotics which were incubated overnight under the same conditions as before. Plasmid DNA was subsequently isolated from the bacterial cultures using the NucleoSpin Xtra Midi kit (Macherey-Nagel) according to the manufacturer´s protocol. The plasmid DNA was sent for sequencing to Eurofins Genomics (Eberberg, Germany) for Sanger sequencing. Sequencing results were analyzed using the NCBI nucleotide BLAST tool.

4.6 Statistical analysis

Statistical analyses were conducted using GraphPad Prism software. Data were first analyzed for normal distribution by normality tests mainly using the Shapiro-Wilk test. If not stated otherwise in the figure legends, for normally distributed data either unpaired student's t-tests were used to compare two groups (genotypes), or paired t-tests were performed in cases where matching control and dKO littermates were compared and n≥6. If the data were normally distributed but showed unequal variance, Welch's t-test was performed. For multiple comparisons for several groups of normally distributed data, one-way ANOVA tests were performed. In cases where control values were normalized to 100% or 1, one-sample t-tests were employed for comparisons. Unless stated otherwise, each data point represents an animal or the mean value of an individual experiment. Columns depict the mean value for all animals or experiments, with the error bars indicating the standard error of the mean (SEM). The number of animals, slices, cells or other samples is indicated in the figure legends. Significant differences were indicated as: * = $p < 0.05$, ** = $p < 0.01$, *** = $p < 0.001$, **** = $p < 0.0001$, $p > 0.05$ is indicated as not significant (ns).

Appendix

Supplementary figures and tables

S1

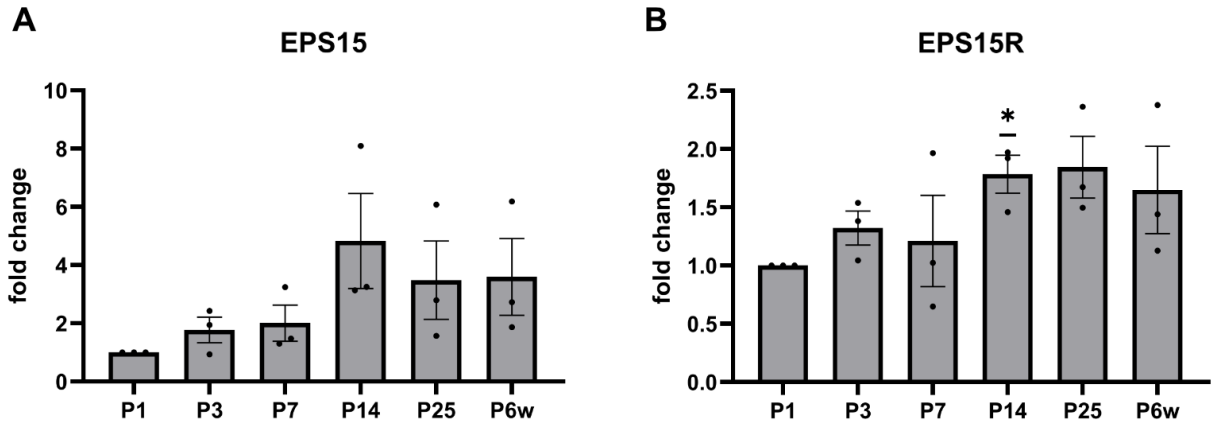

Figure S1 Developmental regulation of EPS15 and EPS15R expression in postnatal mouse brain. ***(A–B)*** *Quantification of EPS15 (A) and EPS15R (B) protein levels in whole-brain lysates from postnatal day 1 (P1) to 6-week-old (P6w) mice, normalized to P1. Both proteins show a gradual increase during postnatal development (n = 3 mice per age). (Data are shown as individual data points with mean ± SEM; significance level: *=p<0.05).*

S2

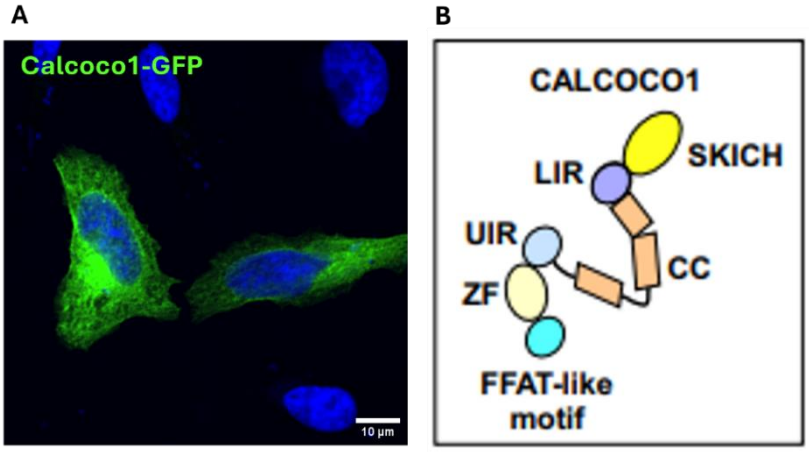

Figure S2 Expression pattern and domain architecture of CALCOCO1. ***(A)*** *Representative confocal image of HeLa cells transfected with CALCOCO1–GFP showing a predominantly diffuse cytoplasmic distribution. Nuclei are stained with DAPI (blue). Scale bar: 10 µm.* ***(B)*** *Domain architecture of CALCOCO1 illustrating the SKICH domain, a conserved LC3-interacting region (LIR), coiled-coil regions (CC), a ubiquitin-interacting region (UIR), a zinc finger domain (ZF), and a C-terminal FFAT-like motif. Adapted from (Nthiga et al., 2020a).*

S3

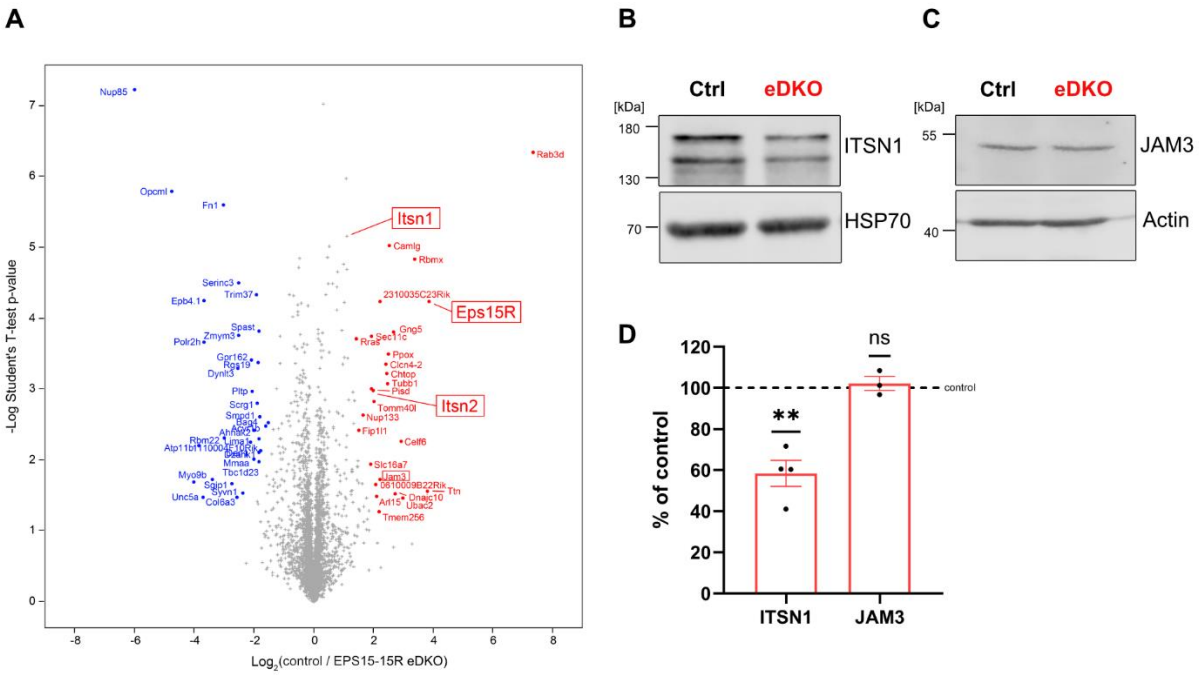

Figure S3 Proteomic analysis of EPS15/15R-deficient forebrains and validation of selected candidates. *(**A**) Volcano plot showing differential protein expression in forebrains of control and EPS15/15R eDKO mice. EPS15R and its known interactors ITSN1 and ITSN2 are highlighted (boxed), confirming efficient knockout and revealing reduced ITSN1/2 abundance in eDKO samples. (**B**) Western blot analysis of total forebrain lysates showing reduced ITSN1 protein levels in eDKO mice. (**C**) Western blot of forebrain synaptosome preparations showing comparable JAM3 levels between control and eDKO mice. (**D**) Quantification of ITSN1 and JAM3 protein levels expressed as percentage of control (n=3; one-sample t-test). (Data are shown as individual data points with mean ± SEM; significance levels: n.s.= non-significant, **=p<0.01).*

S4

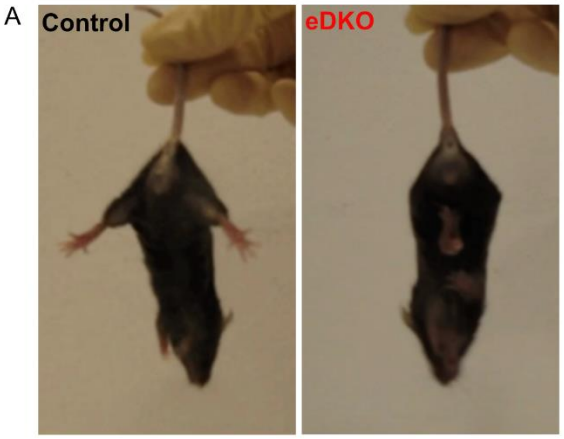

Figure S4 Hindlimb clasping phenotype in EPS15/15R eDKO mice. *(A) Representative images showing hindlimb clasping behavior in EPS15/15R eDKO mice compared to normal limb extension in control littermates, indicative of a neurological deficit.*

S5

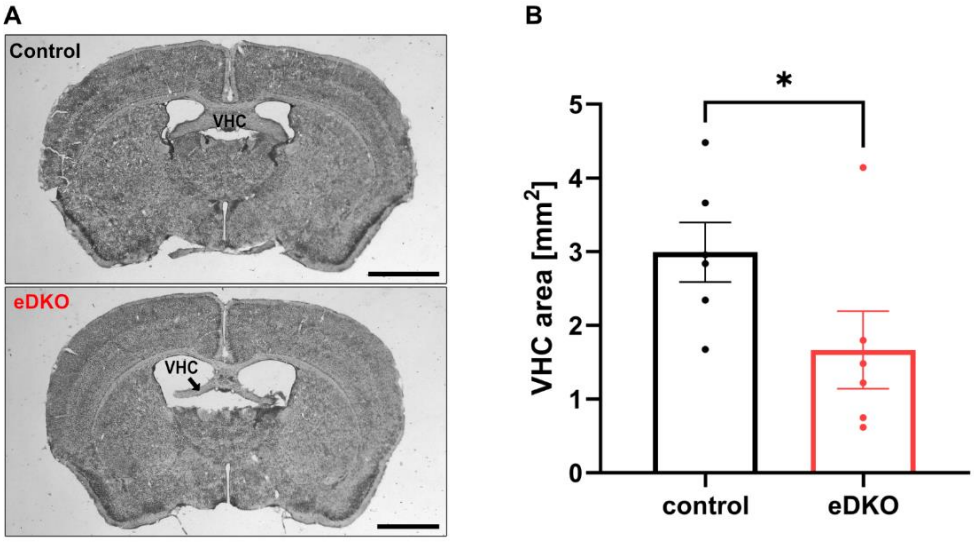

Figure S5 Reduced ventral hippocampal commissure (VHC) size in EPS15/15R eDKO mice. ***(A)*** *Representative Nissl-stained coronal brain sections showing the ventral hippocampal commissure (VHC) in control and EPS15/15R eDKO mice. The VHC appears visibly reduced in size in eDKO compared to control brains. Scale bar: 500 µm.* ***(B)*** *Quantification of VHC area measured across serial forebrain sections reveals a significant reduction in eDKO mice compared to controls (mean ± SEM; $p < 0.05$), indicating a partial loss of commissural projections ($n = 6$ per genotype; paired t-test). (Data are shown as individual data points with mean ± SEM; significance level: *=$p<0.05$).*

S6

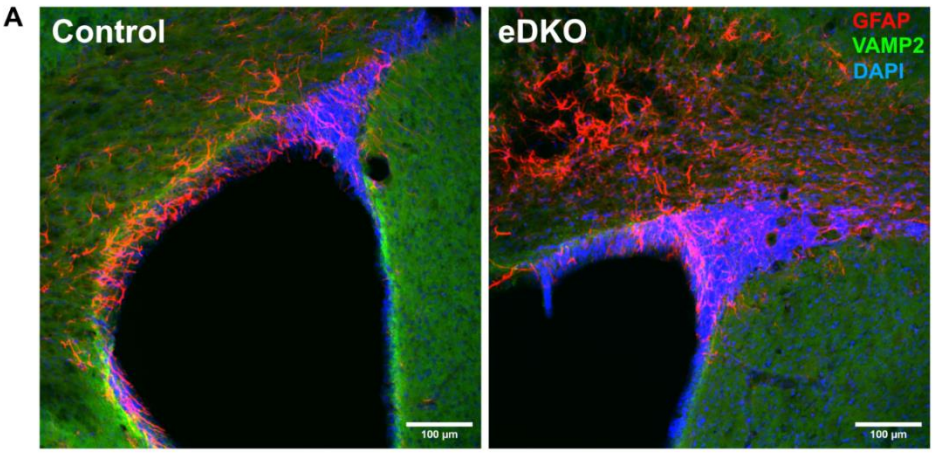

Figure S6 Localized astroglial enrichment along the SVZ and ventricular surface in EPS15/15R eDKO brains. ***(A)*** *Representative confocal images of coronal brain sections from control and EPS15/15R eDKO mice stained for GFAP (red), VAMP2 (green), and DAPI (blue). eDKO brains show locally increased GFAP immunoreactivity in the subventricular zone (SVZ) and ventricular lining compared to controls. This increase appeared in a regionally restricted manner and was variable across animals, suggesting localized astroglial activation. Scale bar: 100 µm.*

S7

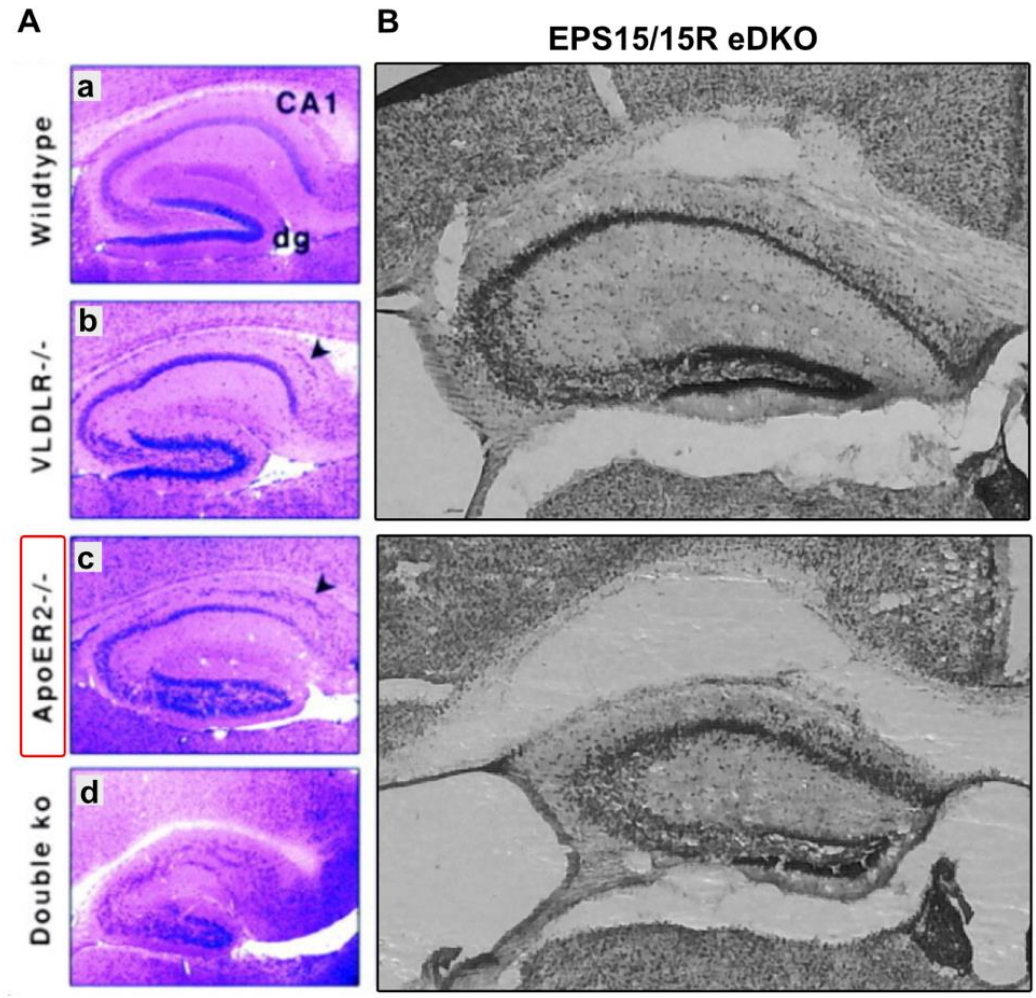

Figure S7 Hippocampal layering defects in EPS15/15R-deficient mice resemble those observed in ApoER2 knockout mutants. ***(A)*** *Representative Nissl-stained hippocampal sections from wild-type, VLDLR$^{-/-}$, ApoER2$^{-/-}$, and VLDLR/ApoER2 double knockout mice (adapted from (Trommsdorff et al., 1999a)) illustrating the characteristic neuronal disorganization in Reelin pathway mutants.* ***(B)*** *Corresponding Nissl-stained hippocampal sections from EPS15/15R eDKO mice (2 examples, top and bottom) showing disrupted lamination of the CA1–CA3 regions and an abnormal distribution of granule cells in the dentate gyrus, closely resembling the phenotype seen in ApoER2$^{-/-}$ mutants.*

Table S1 EPS15R co-IP mass-spectrometry candidates

Gene names	EPS15R	
	Fold change	-log 10 p-value
EPS15R	253.55	5.64
EPS15	3.250316303	2.04
Ap2a1	147.2783581	7.27
Clta	155.2124517	4.76
ITSN1	180.7914666	5.58
ITSN2	202.230568	5.82
Epsin3	9.587125944	3.80
FCHO2	17.72912993	3.80
Stonin2	34.61214356	5.07
Calcoco1	96.02030036	4.560587
Sec16a	91.33490609	4.41

The listed proteins were enriched in EPS15R IPs relative to IPs with control IgGs. For each hit, the **Fold change** indicates the magnitude of enrichment (higher = stronger association with EPS15R), and **–log10 *p*-value** indicates statistical support (higher = more significant). The dataset recovers known endocytic partners (e.g., AP2A1 (AP-2a), CLTA (clathrin light chain A), FCHO2, Stonin2, Epsin3, ITSN1/ITSN2), and highlights additional candidates such as CALCOCO1 and SEC16A.

List of abbreviations

Abbreviations	Fullforms
Aβ	Amyloid-beta
AMPAR	α-amino-3-hydroxy-5-methyl-4-isoxazolepropionic acid receptor
ApoER2	Apolipoprotein E receptor 2
Ara-C	Cytosine β-D-arabinofuranoside
BAR-domain	Bin/Amphiphysin/Rvs domain
BCA	Bicinchoninic acid
BrdU	5-Bromo-2'-deoxyuridine
BSA	Bovine serum albumin
CA	Cornu ammonis (hippocampal subfield)
CAG-Cre	Cytomegalovirus early enhancer/chicken β-actin promoter–driven Cre recombinase
CALM	Clathrin assembly lymphoid myeloid leukemia protein
CC	Corpus callosum
CHC	Clathrin heavy chain
CIE	Clathrin-independent endocytosis
CME	Clathrin-mediated endocytosis
co-IP	Co-immunoprecipitation
COPII	Coat protein complex II
CSF	Cerebrospinal fluid
CTIP2	COUP-TF-interacting protein 2
DAPI	4′,6-diamidino-2-phenylindole
DCX	Doublecortin
DG	Dentate Gyrus (hippocampus subfield)
DIV	Days in vitro
DKO	Double knockout
ECs	Ependymal cells
eDKO	EPS15/15R excitatory neuron-specific double knockout
EGFR	Epidermal growth factor receptor
EH	Eps15 homology domain
Emx-1-Cre	Empty spiracles homeobox 1 promoter–driven Cre recombinase
EPS15	Epidermal growth factor receptor pathway substrate 15
EPS15R	Epidermal growth factor receptor pathway substrate 15–related
EPS15L1	Epidermal growth factor receptor pathway substrate 15–like 1
EPSCs	Excitatory postsynaptic currents
ER	Endoplasmic reticulum
FCHo	F-BAR domain-only protein
FEME	Fast endophilin-mediated endocytosis
FOXJ1	Forkhead box J1
GCL	Granule cell layer
GFP	Green fluorescent protein
GluA1	Glutamate receptor subunit A1

GST	Glutathione S-transferase
HBSS	Hanks' balanced salt solution
HEPES	4-(2-hydroxyethyl)-1-piperazineethanesulfonic acid
iDKO	EPS15/15R inducible double knockout
IgG	Immunoglobulin G
IPSCs	Inhibitory postsynaptic currents
ITSN	Intersectin
JAM3	Junctional adhesion molecule 3
L1CAM	L1 cell adhesion molecule
LLPS	Liquid-liquid phase separation
LV	Lateral ventricle
ML	Molecular layer
MS	Mass spectrometry
MZ	Marginal zone
NeuN	Neuronal nuclei (RNA-binding protein Fox-3)
NICD	Notch intracellular domain
NMDAR	N-methyl-D-aspartate receptor
NPCs	Neuronal progenitor cells
NSCs	Neural stem cells
PBS	Phosphate-buffered saline
PBST	PBS containing Tween-20
PFA	Paraformaldehyde
PIC	Protease inhibitor cocktail
PMSF	Phenylmethylsulfonyl fluoride
RGC	Radial glial cell
RFP	Red fluorescent protein
ROI	Region of interest
SDS-PAGE	Sodium dodecyl sulfate–polyacrylamide gel electrophoresis
SEC16A	Protein transport protein Sec16A
SEM	Standard error mean
SGZ	Subgranular zone
SNAP25	Synaptosomal-associated protein 25
STED	Stimulated emission depletion (microscopy)
SVZ	Subventricular zone
SYP	Synaptophysin
TAE	Tris-acetate-EDTA buffer
TBR1	T-box brain transcription factor 1
TfR	Transferrin receptor
UFE	Ultra-fast endocytosis
UIM	Ubiquitin-interacting motif
VHC	Ventral hippocampal commissure
VLDLR	Very low-density lipoprotein receptor
VZ	Ventricular zone

List of figures

List of tables

References

Abdelhamed, Z., Vuong, S. M., Hill, L., Shula, C., Timms, A., Beier, D., Campbell, K., Mangano, F. T., Stottmann, R. W., & Goto, J. (2018). A mutation in Ccdc39 causes neonatal hydrocephalus with abnormal motile cilia development in mice. *Development (Cambridge, England)*, *145*(1), dev154500. https://doi.org/10.1242/dev.154500

Abdi, K., Neves, G., Pyun, J., Kiziltug, E., Ahrens, A., & Kuo, C. T. (2019). EGFR Signaling Termination via Numb Trafficking in Ependymal Progenitors Controls Postnatal Neurogenic Niche Differentiation. *Cell Reports*, *28*(8), 2012-2022.e4. https://doi.org/10.1016/j.celrep.2019.07.056

Aguilar, R. C., & Wendland, B. (2005). Endocytosis of membrane receptors: Two pathways are better than one. *Proceedings of the National Academy of Sciences*, *102*(8), 2679–2680. https://doi.org/10.1073/pnas.0500213102

Altman, J., & Bayer, S. A. (1990). Mosaic organization of the hippocampal neuroepithelium and the multiple germinal sources of dentate granule cells. *The Journal of Comparative Neurology*, *301*(3), 325–342. https://doi.org/10.1002/cne.903010302

Altman, J., & Das, G. D. (1965). Autoradiographic and histological evidence of postnatal hippocampal neurogenesis in rats. *The Journal of Comparative Neurology*, *124*(3), 319–335. https://doi.org/10.1002/cne.901240303

Alvarez-Buylla, A., & García-Verdugo, J. M. (2002). Neurogenesis in Adult Subventricular Zone. *The Journal of Neuroscience*, *22*(3), 629–634. https://doi.org/10.1523/JNEUROSCI.22-03-00629.2002

Arlotta, P., Molyneaux, B. J., Chen, J., Inoue, J., Kominami, R., & Macklis, J. D. (2005). Neuronal Subtype-Specific Genes that Control Corticospinal Motor Neuron Development In Vivo. *Neuron*, *45*(2), 207–221. https://doi.org/10.1016/j.neuron.2004.12.036

Azarnia Tehran, D., Kochlamazashvili, G., Pampaloni, N. P., Sposini, S., Shergill, J. K., Lehmann, M., Pashkova, N., Schmidt, C., Löwe, D., Napieczynska, H., Heuser, A., Plested, A. J. R., Perrais, D., Piper, R. C., Haucke, V., & Maritzen, T. (2022). Selective endocytosis of Ca2+-permeable AMPARs by the Alzheimer's disease risk factor CALM bidirectionally controls synaptic plasticity. *Science Advances*, *8*(21), eabl5032. https://doi.org/10.1126/sciadv.abl5032

Azarnia Tehran, D., López-Hernández, T., & Maritzen, T. (2019). Endocytic Adaptor Proteins in Health and Disease: Lessons from Model Organisms and Human Mutations. *Cells*, *8*(11), 1345. https://doi.org/10.3390/cells8111345

Bayer, S. A., & Altman, J. (1991). *Neocortical development*. Raven Press.

Beffert, U., Weeber, E. J., Durudas, A., Qiu, S., Masiulis, I., Sweatt, J. D., Li, W.-P., Adelmann, G., Frotscher, M., Hammer, R. E., & Herz, J. (2005). Modulation of synaptic plasticity and memory by Reelin involves differential splicing of the lipoprotein receptor Apoer2. *Neuron*, *47*(4), 567–579. https://doi.org/10.1016/j.neuron.2005.07.007

Benmerah, A., Lamaze, C., Bègue, B., Schmid, S. L., Dautry-Varsat, A., & Cerf-Bensussan, N. (1998). AP-2/Eps15 Interaction Is Required for Receptor-mediated Endocytosis. *The Journal of Cell Biology*, *140*(5), 1055–1062. https://doi.org/10.1083/jcb.140.5.1055

Bens, S., Haake, A., Tönnies, H., Vater, I., Stephani, U., Holterhus, P.-M., Siebert, R., & Caliebe, A. (2011). A *de novo* 1.1 Mb microdeletion of chromosome 19p13.11 provides indirect evidence for *EPS15L1* to be a strong candidate for split hand split foot malformation. *European Journal of Medical Genetics*, *54*(5), e501–e504. https://doi.org/10.1016/j.ejmg.2011.05.004

Berton, F., Iborra, C., Boudier, J.-A., Seagar, M. J., & Marquèze, B. (1997). Developmental Regulation of Synaptotagmin I, II, III, and IV mRNAs in the Rat CNS. *The Journal of Neuroscience*, *17*(4), 1206–1216. https://doi.org/10.1523/JNEUROSCI.17-04-01206.1997

Bitsikas, V., Corrêa, I. R., & Nichols, B. J. (2014). Clathrin-independent pathways do not contribute significantly to endocytic flux. *eLife*, *3*, e03970. https://doi.org/10.7554/eLife.03970

Boncompain, G., Divoux, S., Gareil, N., de Forges, H., Lescure, A., Latreche, L., Mercanti, V., Jollivet, F., Raposo, G., & Perez, F. (2012). Synchronization of secretory protein traffic in populations of cells. *Nature Methods*, *9*(5), 493–498. https://doi.org/10.1038/nmeth.1928

Borit, A., & Sidman, R. L. (1972). New mutant mouse with communicating hydrocephalus and secondary aqueductal stenosis. *Acta Neuropathologica*, *21*(4), 316–331. https://doi.org/10.1007/BF00685139

Bothwell, S. W., Janigro, D., & Patabendige, A. (2019). Cerebrospinal fluid dynamics and intracranial pressure elevation in neurological diseases. *Fluids and Barriers of the CNS*, *16*(1), 9. https://doi.org/10.1186/s12987-019-0129-6

Bouché, E., Romero-Ortega, M. I., Henkemeyer, M., Catchpole, T., Leemhuis, J., Frotscher, M., May, P., Herz, J., & Bock, H. H. (2013). Reelin induces EphB activation. *Cell Research*, *23*(4), 473–490. https://doi.org/10.1038/cr.2013.7

Boyken, J., Grønborg, M., Riedel, D., Urlaub, H., Jahn, R., & Chua, J. J. E. (2013). Molecular Profiling of Synaptic Vesicle Docking Sites Reveals Novel Proteins but Few Differences between Glutamatergic and GABAergic Synapses. *Neuron*, *78*(2), 285–297. https://doi.org/10.1016/j.neuron.2013.02.027

Bramall, A. N., Anton, E. S., Kahle, K. T., & Fecci, P. E. (2022). Navigating the ventricles: Novel insights into the pathogenesis of hydrocephalus. *EBioMedicine*, *78*, 103931. https://doi.org/10.1016/j.ebiom.2022.103931

Broekkamp, C. L., Rijk, H. W., Joly-Gelouin, D., & Lloyd, K. L. (1986). Major tranquillizers can be distinguished from minor tranquillizers on the basis of effects on marble burying and swim-induced grooming in mice. *European Journal of Pharmacology*, *126*(3), 223–229. https://doi.org/10.1016/0014-2999(86)90051-8

Brunger, A. T., Leitz, J., Zhou, Q., Choi, U. B., & Lai, Y. (2018). Ca2+-triggered synaptic vesicle fusion initiated by release of inhibition. *Trends in Cell Biology*, *28*(8), 631–645. https://doi.org/10.1016/j.tcb.2018.03.004

Brunne, B., Franco, S., Bouché, E., Herz, J., Howell, B. W., Pahle, J., Müller, U., May, P., Frotscher, M., & Bock, H. H. (2013). Role of the postnatal radial glial scaffold for the development of the dentate gyrus as revealed by Reelin signaling mutant mice. *Glia*, *61*(8), 1347–1363. https://doi.org/10.1002/glia.22519

Bucher, D., Mukenhirn, M., Sochacki, K. A., Saharuka, V., Huck, C., Zambarda, C., Taraska, J. W., Cavalcanti-Adam, E. A., & Boulant, S. (2018). *Focal adhesion-generated cues in extracellular matrix regulate cell migration by local induction of clathrin-coated plaques* (p. 493114). bioRxiv. https://doi.org/10.1101/493114

Cadwell, C. M., Su, W., & Kowalczyk, A. P. (2016). Cadherin tales: Regulation of cadherin function by endocytic membrane trafficking. *Traffic*, *17*(12), 1262–1271. https://doi.org/10.1111/tra.12448

Cai, J., Wu, Y., Mirua, T., Pierce, J. L., Lucero, M. T., Albertine, K. H., Spangrude, G. J., & Rao, M. S. (2002). Properties of a Fetal Multipotent Neural Stem Cell (NEP Cell). *Developmental Biology*, *251*(2), 221–240. https://doi.org/10.1006/dbio.2002.0828

Camblor-Perujo, S., & Kononenko, N. L. (2022). Brain-specific functions of the endocytic machinery. *The FEBS Journal*, *289*(8), 2219–2246. https://doi.org/10.1111/febs.15897

Cameron, H. A., Woolley, C. S., McEwen, B. S., & Gould, E. (1993a). Differentiation of newly born neurons and glia in the dentate gyrus of the adult rat. *Neuroscience*, *56*(2), 337–344. https://doi.org/10.1016/0306-4522(93)90335-D

Cameron, H. A., Woolley, C. S., McEwen, B. S., & Gould, E. (1993b). Differentiation of newly born neurons and glia in the dentate gyrus of the adult rat. *Neuroscience*, *56*(2), 337–344. https://doi.org/10.1016/0306-4522(93)90335-d

Campbell, K., & Götz, M. (2002). Radial glia: Multi-purpose cells for vertebrate brain development. *Trends in Neurosciences*, *25*(5), 235–238. https://doi.org/10.1016/S0166-2236(02)02156-2

Carbone, R., Fré, S., Iannolo, G., Belleudi, F., Mancini, P., Pelicci, P. G., Torrisi, M. R., & Di Fiore, P. P. (1997). Eps15 and eps15R Are Essential Components of the Endocytic Pathway1. *Cancer Research*, *57*(24), 5498–5504.

Cardano, M., Zasso, J., Ruggiero, L., Di Giacomo, G., Marcatili, M., Cremona, O., & Conti, L. (2019). Epsins Regulate Mouse Embryonic Stem Cell Exit from Pluripotency and Neural Commitment by Controlling Notch Activation. *Stem Cells International*, *2019*(1), 4084351. https://doi.org/10.1155/2019/4084351

Carroll, R. C., Beattie, E. C., von Zastrow, M., & Malenka, R. C. (2001). Role of ampa receptor endocytosis in synaptic plasticity. *Nature Reviews Neuroscience*, *2*(5), 315–324. https://doi.org/10.1038/35072500

Casamento, A., & Boucrot, E. (2020). Molecular mechanism of Fast Endophilin-Mediated Endocytosis. *Biochemical Journal*, *477*(12), 2327–2345. https://doi.org/10.1042/BCJ20190342

Cayouette, M., & Raff, M. (2002). Asymmetric segregation of Numb: A mechanism for neural specification from Drosophila to mammals. *Nature Neuroscience*, *5*(12), 1265–1269. https://doi.org/10.1038/nn1202-1265

Chai, X., & Frotscher, M. (2016). How does Reelin signaling regulate the neuronal cytoskeleton during migration? *Neurogenesis*, *3*(1), e1242455. https://doi.org/10.1080/23262133.2016.1242455

Chao, H.-T., Chen, H., Samaco, R. C., Xue, M., Chahrour, M., Yoo, J., Neul, J. L., Gong, S., Lu, H.-C., Heintz, N., Ekker, M., Rubenstein, J. L. R., Noebels, J. L., Rosenmund, C., & Zoghbi, H. Y. (2010). Dysfunction in GABA signalling mediates autism-like stereotypies and Rett syndrome phenotypes. *Nature*, *468*(7321), 263–269. https://doi.org/10.1038/nature09582

Chen, H., Fre, S., Slepnev, V. I., Capua, M. R., Takei, K., Butler, M. H., Di Fiore, P. P., & De Camilli, P. (1998). Epsin is an EH-domain-binding protein implicated in clathrin-mediated endocytosis. *Nature*, *394*(6695), 793–797. https://doi.org/10.1038/29555

Chen, H., Ko, G., Zatti, A., Di Giacomo, G., Liu, L., Raiteri, E., Perucco, E., Collesi, C., Min, W., Zeiss, C., De Camilli, P., & Cremona, O. (2009a). Embryonic arrest at midgestation and disruption of Notch signaling produced by the absence of both epsin 1 and epsin 2 in mice. *Proceedings of the National Academy of Sciences*, *106*(33), 13838–13843. https://doi.org/10.1073/pnas.0907008106

Chen, H., Ko, G., Zatti, A., Di Giacomo, G., Liu, L., Raiteri, E., Perucco, E., Collesi, C., Min, W., Zeiss, C., De Camilli, P., & Cremona, O. (2009b). Embryonic arrest at midgestation and disruption of Notch signaling produced by the absence of both epsin 1 and epsin 2 in mice. *Proceedings of the National Academy of Sciences*, *106*(33), 13838–13843. https://doi.org/10.1073/pnas.0907008106

Chen, W., Ouyang, X., Chen, L., & Li, L. (2022). Multiple functions of CALCOCO family proteins in selective autophagy. *Journal of Cellular Physiology*, *237*(9), 3505–3516. https://doi.org/10.1002/jcp.30836

Chi, S., Cao, H., Chen, J., & McNiven, M. A. (2008). Eps15 Mediates Vesicle Trafficking from the trans-Golgi Network via an Interaction with the Clathrin Adaptor AP-1. *Molecular Biology of the Cell*, *19*(8), 3564–3575. https://doi.org/10.1091/mbc.e07-10-0997

Coda, L., Salcini, A. E., Confalonieri, S., Pelicci, G., Sorkina, T., Sorkin, A., Pelicci, P. G., & Fiore, P. P. D. (1998). Eps15R Is a Tyrosine Kinase Substrate with Characteristics of a Docking Protein Possibly Involved in Coated Pits-mediated Internalization *. *Journal of Biological Chemistry*, *273*(5), 3003–3012. https://doi.org/10.1074/jbc.273.5.3003

Collins, B. M., McCoy, A. J., Kent, H. M., Evans, P. R., & Owen, D. J. (2002). Molecular architecture and functional model of the endocytic AP2 complex. *Cell*, *109*(4), 523–535. https://doi.org/10.1016/s0092-8674(02)00735-3

Confalonieri, S., & Di Fiore, P. P. (2002). The Eps15 homology (EH) domain. *FEBS Letters*, *513*(1), 24–29. https://doi.org/10.1016/S0014-5793(01)03241-0

Confalonieri, S., Salcini, A. E., Puri, C., Tacchetti, C., & Di Fiore, P. P. (2000). Tyrosine Phosphorylation of Eps15 Is Required for Ligand-Regulated, but Not Constitutive, Endocytosis. *Journal of Cell Biology*, *150*(4), 905–912. https://doi.org/10.1083/jcb.150.4.905

Connerly, P. L., Esaki, M., Montegna, E. A., Strongin, D. E., Levi, S., Soderholm, J., & Glick, B. S. (2005). Sec16 is a Determinant of Transitional ER Organization. *Current Biology*, *15*(16), 1439–1447. https://doi.org/10.1016/j.cub.2005.06.065

Curran, T., & D'Arcangelo, G. (1998). Role of reelin in the control of brain development1. *Brain Research Reviews*, *26*(2), 285–294. https://doi.org/10.1016/S0165-0173(97)00035-0

Cutler, R. W., Page, L., Galicich, J., & Watters, G. V. (1968). Formation and absorption of cerebrospinal fluid in man. *Brain: A Journal of Neurology*, *91*(4), 707–720. https://doi.org/10.1093/brain/91.4.707

Dahme, M., Bartsch, U., Martini, R., Anliker, B., Schachner, M., & Mantei, N. (1997). Disruption of the mouse L1 gene leads to malformations of the nervous system. *Nature Genetics*, *17*(3), 346–349. https://doi.org/10.1038/ng1197-346

D'Arcangelo, G. (2005). The reeler mouse: Anatomy of a mutant. *International Review of Neurobiology*, *71*, 383–417. https://doi.org/10.1016/s0074-7742(05)71016-3

D'Arcangelo, G., Homayouni, R., Keshvara, L., Rice, D. S., Sheldon, M., & Curran, T. (1999a). Reelin is a ligand for lipoprotein receptors. *Neuron*, *24*(2), 471–479. https://doi.org/10.1016/s0896-6273(00)80860-0

D'Arcangelo, G., Homayouni, R., Keshvara, L., Rice, D. S., Sheldon, M., & Curran, T. (1999b). Reelin Is a Ligand for Lipoprotein Receptors. *Neuron*, *24*(2), 471–479. https://doi.org/10.1016/S0896-6273(00)80860-0

D'Arcangelo, G., Miao, G. G., Chen, S. C., Soares, H. D., Morgan, J. I., & Curran, T. (1995a). A protein related to extracellular matrix proteins deleted in the mouse mutant reeler. *Nature*, *374*(6524), 719–723. https://doi.org/10.1038/374719a0

D'Arcangelo, G., Miao, G. G., Chen, S. C., Soares, H. D., Morgan, J. I., & Curran, T. (1995b). A protein related to extracellular matrix proteins deleted in the mouse mutant reeler. *Nature*, *374*(6524), 719–723. https://doi.org/10.1038/374719a0

Dautry-Varsat, A. (1986). Receptor-mediated endocytosis: The intracellular journey of transferrin and its receptor. *Biochimie*, *68*(3), 375–381. https://doi.org/10.1016/S0300-9084(86)80004-9

Day, K. J., Kago, G., Wang, L., Richter, J. B., Hayden, C. C., Lafer, E. M., & Stachowiak, J. C. (2021). Liquid-like protein interactions catalyse assembly of endocytic vesicles. *Nature Cell Biology*, *23*(4), 366–376. https://doi.org/10.1038/s41556-021-00646-5

de Brouwer, G., Fick, A., Harvey, B. H., & Wolmarans, D. W. (2019). A critical inquiry into marble-burying as a preclinical screening paradigm of relevance for anxiety and obsessive-compulsive disorder: Mapping the way forward. *Cognitive, Affective & Behavioral Neuroscience*, *19*(1), 1–39. https://doi.org/10.3758/s13415-018-00653-4

Delft, S. van, Govers, R., Strous, G. J., Verkleij, A. J., & Henegouwen, P. M. P. van B. en. (1997). Epidermal Growth Factor Induces Ubiquitination of Eps15 *. *Journal of Biological Chemistry*, *272*(22), 14013–14016. https://doi.org/10.1074/jbc.272.22.14013

Delgehyr, N., Meunier, A., Faucourt, M., Bosch Grau, M., Strehl, L., Janke, C., & Spassky, N. (2015). Ependymal cell differentiation, from monociliated to multiciliated cells. *Methods in Cell Biology*, *127*, 19–35. https://doi.org/10.1016/bs.mcb.2015.01.004

Demyanenko, G. P., Tsai, A. Y., & Maness, P. F. (1999). Abnormalities in neuronal process extension, hippocampal development, and the ventricular system of L1 knockout mice. *The Journal of Neuroscience: The Official Journal of the Society for Neuroscience*, *19*(12), 4907–4920. https://doi.org/10.1523/JNEUROSCI.19-12-04907.1999

Devenport, D. (2014). The cell biology of planar cell polarity. *The Journal of Cell Biology*, *207*(2), 171–179. https://doi.org/10.1083/jcb.201408039

Di Paolo, G., Sankaranarayanan, S., Wenk, M. R., Daniell, L., Perucco, E., Caldarone, B. J., Flavell, R., Picciotto, M. R., Ryan, T. A., Cremona, O., & De Camilli, P. (2002). Decreased synaptic vesicle recycling efficiency and cognitive deficits in amphiphysin 1 knockout mice. *Neuron*, *33*(5), 789–804. https://doi.org/10.1016/s0896-6273(02)00601-3

Diering, G. H., & Huganir, R. L. (2018). The AMPA Receptor Code of Synaptic Plasticity. *Neuron*, *100*(2), 314–329. https://doi.org/10.1016/j.neuron.2018.10.018

Doetsch, F., Caillé, I., Lim, D. A., García-Verdugo, J. M., & Alvarez-Buylla, A. (1999). Subventricular Zone Astrocytes Are Neural Stem Cells in the Adult Mammalian Brain. *Cell*, *97*(6), 703–716. https://doi.org/10.1016/S0092-8674(00)80783-7

Doetsch, F., García-Verdugo, J. M., & Alvarez-Buylla, A. (1997). Cellular composition and three-dimensional organization of the subventricular germinal zone in the adult mammalian brain. *The Journal of Neuroscience: The Official Journal of the Society for Neuroscience*, *17*(13), 5046–5061. https://doi.org/10.1523/JNEUROSCI.17-13-05046.1997

Donati, A., Schneider-Maunoury, S., & Vesque, C. (2024). Centriole Translational Planar Polarity in Monociliated Epithelia. *Cells*, *13*(17), 1403. https://doi.org/10.3390/cells13171403

Drakew, A., Deller, T., Heimrich, B., Gebhardt, C., Del Turco, D., Tielsch, A., Förster, E., Herz, J., & Frotscher, M. (2002). Dentate granule cells in reeler mutants and VLDLR and ApoER2 knockout mice. *Experimental Neurology*, *176*(1), 12–24. https://doi.org/10.1006/exnr.2002.7918

Dudek, B. C., Adams, N., Boice, R., & Abbott, M. E. (1983). Genetic influences on digging behaviors in mice (Mus musculus) in laboratory and seminatural settings. *Journal of Comparative Psychology (Washington, D.C.: 1983)*, *97*(3), 249–259.

Eichele, G., Bodenschatz, E., Ditte, Z., Günther, A.-K., Kapoor, S., Wang, Y., & Westendorf, C. (2019a). Cilia-driven flows in the brain third ventricle. *Philosophical Transactions of the Royal Society B: Biological Sciences*, *375*(1792), 20190154. https://doi.org/10.1098/rstb.2019.0154

Eichele, G., Bodenschatz, E., Ditte, Z., Günther, A.-K., Kapoor, S., Wang, Y., & Westendorf, C. (2019b). Cilia-driven flows in the brain third ventricle. *Philosophical Transactions of the Royal Society B: Biological Sciences*, *375*(1792), 20190154. https://doi.org/10.1098/rstb.2019.0154

Eisch, A. J., Cameron, H. A., Encinas, J. M., Meltzer, L. A., Ming, G.-L., & Overstreet-Wadiche, L. S. (2008). Adult Neurogenesis, Mental Health, and Mental Illness: Hope or Hype? *Journal of Neuroscience*, *28*(46), 11785–11791. https://doi.org/10.1523/JNEUROSCI.3798-08.2008

Evergren, E., Cobbe, N., & McMahon, H. T. (2018). Eps15R and clathrin regulate EphB2-mediated cell repulsion. *Traffic*, *19*(1), 44–57. https://doi.org/10.1111/tra.12531

Fazioli, F., Minichiello, L., Matoškovā, B., Wong, W. T., & Di Fiore, P. P. (1993). Eps15, A Novel Tyrosine Kinase Substrate, Exhibits Transforming Activity. *Molecular and Cellular Biology*, *13*(9), 5814–5828. https://doi.org/10.1128/mcb.13.9.5814-5828.1993

Feldner, A., Adam, M. G., Tetzlaff, F., Moll, I., Komljenovic, D., Sahm, F., Bäuerle, T., Ishikawa, H., Schroten, H., Korff, T., Hofmann, I., Wolburg, H., von Deimling, A., & Fischer, A. (2017a). Loss of Mpdz impairs ependymal cell integrity leading to perinatal-onset hydrocephalus in mice. *EMBO Molecular Medicine*, *9*(7), 890–905. https://doi.org/10.15252/emmm.201606430

Feldner, A., Adam, M. G., Tetzlaff, F., Moll, I., Komljenovic, D., Sahm, F., Bäuerle, T., Ishikawa, H., Schroten, H., Korff, T., Hofmann, I., Wolburg, H., von Deimling, A., & Fischer, A. (2017b). Loss of Mpdz impairs ependymal cell integrity leading to perinatal-onset hydrocephalus in mice. *EMBO Molecular Medicine*, *9*(7), 890–905. https://doi.org/10.15252/emmm.201606430

Ferguson, S., Raimondi, A., Paradise, S., Shen, H., Mesaki, K., Ferguson, A., Destaing, O., Ko, G., Takasaki, J., Cremona, O., O' Toole, E., & De Camilli, P. (2009). Coordinated Actions of Actin and BAR Proteins Upstream of Dynamin at Endocytic Clathrin-Coated Pits. *Developmental Cell*, *17*(6), 811–822. https://doi.org/10.1016/j.devcel.2009.11.005

Filippov, V., Kronenberg, G., Pivneva, T., Reuter, K., Steiner, B., Wang, L. P., Yamaguchi, M., Kettenmann, H., & Kempermann, G. (2003). Subpopulation of nestin-expressing progenitor cells in the adult murine hippocampus shows electrophysiological and morphological characteristics of astrocytes. *Molecular and Cellular Neurosciences*, *23*(3), 373–382. https://doi.org/10.1016/s1044-7431(03)00060-5

Fiuza, M., Rostosky, C. M., Parkinson, G. T., Bygrave, A. M., Halemani, N., Baptista, M., Milosevic, I., & Hanley, J. G. (2017). PICK1 regulates AMPA receptor endocytosis via direct interactions with AP2 α-appendage and dynamin. *The Journal of Cell Biology*, *216*(10), 3323–3338. https://doi.org/10.1083/jcb.201701034

Foerster, P., Daclin, M., Asm, S., Faucourt, M., Boletta, A., Genovesio, A., & Spassky, N. (2017). mTORC1 signaling and primary cilia are required for brain ventricle morphogenesis. *Development*, *144*(2), 201–210. https://doi.org/10.1242/dev.138271

Ford, M. G. J., Mills, I. G., Peter, B. J., Vallis, Y., Praefcke, G. J. K., Evans, P. R., & McMahon, H. T. (2002). Curvature of clathrin-coated pits driven by epsin. *Nature*, *419*(6905), 361–366. https://doi.org/10.1038/nature01020

Forrest, M. P., Parnell, E., & Penzes, P. (2018). Dendritic structural plasticity and neuropsychiatric disease. *Nature Reviews Neuroscience*, *19*(4), 215–234. https://doi.org/10.1038/nrn.2018.16

Förster, E., Tielsch, A., Saum, B., Weiss, K. H., Johanssen, C., Graus-Porta, D., Müller, U., & Frotscher, M. (2002). Reelin, Disabled 1, and β1 integrins are required for the formation of the radial glial scaffold in the hippocampus. *Proceedings of the National Academy of Sciences*, *99*(20), 13178–13183. https://doi.org/10.1073/pnas.202035899

Frotscher, M. (1998). Cajal-Retzius cells, Reelin, and the formation of layers. *Current Opinion in Neurobiology*, *8*(5), 570–575. https://doi.org/10.1016/s0959-4388(98)80082-2

Fukuda, S., Kato, F., Tozuka, Y., Yamaguchi, M., Miyamoto, Y., & Hisatsune, T. (2003). Two distinct subpopulations of nestin-positive cells in adult mouse dentate gyrus. *The Journal of Neuroscience: The Official Journal of the Society for Neuroscience*, *23*(28), 9357–9366. https://doi.org/10.1523/JNEUROSCI.23-28-09357.2003

Gemelli, T., Berton, O., Nelson, E. D., Perrotti, L. I., Jaenisch, R., & Monteggia, L. M. (2006). Postnatal Loss of Methyl-CpG Binding Protein 2 in the Forebrain is Sufficient to Mediate Behavioral Aspects of Rett Syndrome in Mice. *Biological Psychiatry*, *59*(5), 468–476. https://doi.org/10.1016/j.biopsych.2005.07.025

Gerth, F., Jäpel, M., Pechstein, A., Kochlamazashvili, G., Lehmann, M., Puchkov, D., Onofri, F., Benfenati, F., Nikonenko, A. G., Fredrich, K., Shupliakov, O., Maritzen, T., Freund, C., & Haucke, V. (2017).

Intersectin associates with synapsin and regulates its nanoscale localization and function. *Proceedings of the National Academy of Sciences of the United States of America*, *114*(45), 12057–12062. https://doi.org/10.1073/pnas.1715341114

Gheusi, G., Cremer, H., McLean, H., Chazal, G., Vincent, J.-D., & Lledo, P.-M. (2000). Importance of newly generated neurons in the adult olfactory bulb for odor discrimination. *Proceedings of the National Academy of Sciences*, *97*(4), 1823–1828. https://doi.org/10.1073/pnas.97.4.1823

Girão, H., Catarino, S., & Pereira, P. (2009). Eps15 interacts with ubiquitinated Cx43 and mediates its internalization. *Experimental Cell Research*, *315*(20), 3587–3597. https://doi.org/10.1016/j.yexcr.2009.10.003

Glodowski, D. R., Chen, C. C.-H., Schaefer, H., Grant, B. D., & Rongo, C. (2007). RAB-10 Regulates Glutamate Receptor Recycling in a Cholesterol-dependent Endocytosis Pathway. *Molecular Biology of the Cell*, *18*(11), 4387–4396. https://doi.org/10.1091/mbc.E07-05-0486

Götz, M., & Huttner, W. B. (2005). The cell biology of neurogenesis. *Nature Reviews Molecular Cell Biology*, *6*(10), 777–788. https://doi.org/10.1038/nrm1739

Grońska-Pęski, M., Schachner, M., & Hébert, J. M. (2020). L1cam curbs the differentiation of adult-born hippocampal neurons. *Stem Cell Research*, *48*, 101999. https://doi.org/10.1016/j.scr.2020.101999

Guerrini, R., & Dobyns, W. B. (2014). Malformations of cortical development: Clinical features and genetic causes. *The Lancet Neurology*, *13*(7), 710–726. https://doi.org/10.1016/S1474-4422(14)70040-7

Guipponi, M., Scott, H. S., Chen, H., Schebesta, A., Rossier, C., & Antonarakis, S. E. (1998). Two isoforms of a human intersectin (ITSN) protein are produced by brain-specific alternative splicing in a stop codon. *Genomics*, *53*(3), 369–376. https://doi.org/10.1006/geno.1998.5521

Guirao, B., Meunier, A., Mortaud, S., Aguilar, A., Corsi, J.-M., Strehl, L., Hirota, Y., Desoeuvre, A., Boutin, C., Han, Y.-G., Mirzadeh, Z., Cremer, H., Montcouquiol, M., Sawamoto, K., & Spassky, N. (2010). Coupling between hydrodynamic forces and planar cell polarity orients mammalian motile cilia. *Nature Cell Biology*, *12*(4), 341–350. https://doi.org/10.1038/ncb2040

Gulino, A., Di Marcotullio, L., & Screpanti, I. (2010). The multiple functions of Numb. *Experimental Cell Research*, *316*(6), 900–906. https://doi.org/10.1016/j.yexcr.2009.11.017

Guo, M., Jan, L. Y., & Jan, Y. N. (1996). Control of Daughter Cell Fates during Asymmetric Division: Interaction of Numb and Notch. *Neuron*, *17*(1), 27–41. https://doi.org/10.1016/S0896-6273(00)80278-0

Gupta, A., Tsai, L.-H., & Wynshaw-Boris, A. (2002). Life is a journey: A genetic look at neocortical development. *Nature Reviews Genetics*, *3*(5), 342–355. https://doi.org/10.1038/nrg799

Haffner, C., Takei, K., Chen, H., Ringstad, N., Hudson, A., Butler, M. H., Salcini, A. E., Di Fiore, P. P., & De Camilli, P. (1997). Synaptojanin 1: Localization on coated endocytic intermediates in nerve terminals and interaction of its 170 kDa isoform with Eps15. *FEBS Letters*, *419*(2–3), 175–180. https://doi.org/10.1016/S0014-5793(97)01451-8

Hamburgh, M. (1963). ANALYSIS OF THE POSTNATAL DEVELOPMENTAL EFFECTS OF "REELER," A NEUROLOGICAL MUTATION IN MICE. A STUDY IN DEVELOPMENTAL GENETICS. *Developmental Biology*, *8*, 165–185. https://doi.org/10.1016/0012-1606(63)90040-x

Hanley, J. G., & Henley, J. M. (2005). PICK1 is a calcium-sensor for NMDA-induced AMPA receptor trafficking. *The EMBO Journal*, *24*(18), 3266–3278. https://doi.org/10.1038/sj.emboj.7600801

Hartfuss, E., Förster, E., Bock, H. H., Hack, M. A., Leprince, P., Luque, J. M., Herz, J., Frotscher, M., & Götz, M. (2003). Reelin signaling directly affects radial glia morphology and biochemical maturation. *Development (Cambridge, England)*, *130*(19), 4597–4609. https://doi.org/10.1242/dev.00654

Hashimoto-Torii, K., Torii, M., Sarkisian, M. R., Bartley, C. M., Shen, J., Radtke, F., Gridley, T., Šestan, N., & Rakic, P. (2008). Interaction between Reelin and Notch signaling regulates neuronal migration in the cerebral cortex. *Neuron*, *60*(2), 273–284. https://doi.org/10.1016/j.neuron.2008.09.026

Haucke, V., & Kozlov, M. M. (2018). Membrane remodeling in clathrin-mediated endocytosis. *Journal of Cell Science*, *131*(17), jcs216812. https://doi.org/10.1242/jcs.216812

Hayashi, K., Kubo, K., Kitazawa, A., & Nakajima, K. (2015). Cellular dynamics of neuronal migration in the hippocampus. *Frontiers in Neuroscience*, *9*. https://doi.org/10.3389/fnins.2015.00135

Hayashi, S., & McMahon, A. P. (2002). Efficient Recombination in Diverse Tissues by a Tamoxifen-Inducible Form of Cre: A Tool for Temporally Regulated Gene Activation/Inactivation in the Mouse. *Developmental Biology*, *244*(2), 305–318. https://doi.org/10.1006/dbio.2002.0597

Helbig, I., Lopez-Hernandez, T., Shor, O., Galer, P., Ganesan, S., Pendziwiat, M., Rademacher, A., Ellis, C. A., Hümpfer, N., Schwarz, N., Seiffert, S., Peeden, J., Shen, J., Štěrbová, K., Hammer, T. B., Møller, R. S., Shinde, D. N., Tang, S., Smith, L., … Weber, Y. G. (2019). A Recurrent Missense Variant in AP2M1 Impairs Clathrin-Mediated Endocytosis and Causes Developmental and Epileptic Encephalopathy. *American Journal of Human Genetics*, *104*(6), 1060–1072. https://doi.org/10.1016/j.ajhg.2019.04.001

Helbig, I., Lopez-Hernandez, T., Shor, O., Galer, P., Ganesan, S., Pendziwiat, M., Rademacher, A., Ellis, C. A., Hümpfer, N., Schwarz, N., Seiffert, S., Peeden, J., Shen, J., Štěrbová, K., Hammer, T. B., Møller, R. S., Shinde, D. N., Tang, S., Smith, L., … White, P. (2019). A Recurrent Missense Variant in *AP2M1* Impairs Clathrin-Mediated Endocytosis and Causes Developmental and Epileptic Encephalopathy. *The American Journal of Human Genetics*, *104*(6), 1060–1072. https://doi.org/10.1016/j.ajhg.2019.04.001

Henne, W. M., Boucrot, E., Meinecke, M., Evergren, E., Vallis, Y., Mittal, R., & McMahon, H. T. (2010a). FCHo Proteins are Nucleators of Clathrin-Mediated Endocytosis. *Science (New York, N.Y.)*, *328*(5983), 1281–1284. https://doi.org/10.1126/science.1188462

Henne, W. M., Boucrot, E., Meinecke, M., Evergren, E., Vallis, Y., Mittal, R., & McMahon, H. T. (2010b). FCHo Proteins Are Nucleators of Clathrin-Mediated Endocytosis. *Science*, *328*(5983), 1281–1284. https://doi.org/10.1126/science.1188462

Henne, W. M., Kent, H. M., Ford, M. G. J., Hegde, B. G., Daumke, O., Butler, P. J. G., Mittal, R., Langen, R., Evans, P. R., & McMahon, H. T. (2007). Structure and Analysis of FCHo2 F-BAR Domain: A Dimerizing and Membrane Recruitment Module that Effects Membrane Curvature. *Structure*, *15*(7), 839–852. https://doi.org/10.1016/j.str.2007.05.002

Hevner, R. F., Shi, L., Justice, N., Hsueh, Y.-P., Sheng, M., Smiga, S., Bulfone, A., Goffinet, A. M., Campagnoni, A. T., & Rubenstein, J. L. R. (2001). Tbr1 Regulates Differentiation of the Preplate and Layer 6. *Neuron*, *29*(2), 353–366. https://doi.org/10.1016/S0896-6273(01)00211-2

Hiesberger, T., Trommsdorff, M., Howell, B. W., Goffinet, A., Mumby, M. C., Cooper, J. A., & Herz, J. (1999). Direct binding of Reelin to VLDL receptor and ApoE receptor 2 induces tyrosine phosphorylation of disabled-1 and modulates tau phosphorylation. *Neuron*, *24*(2), 481–489. https://doi.org/10.1016/s0896-6273(00)80861-2

Hirota, Y., Kubo, K., Katayama, K., Honda, T., Fujino, T., Yamamoto, T. T., & Nakajima, K. (2015). Reelin receptors ApoER2 and VLDLR are expressed in distinct spatiotemporal patterns in developing mouse cerebral cortex. *The Journal of Comparative Neurology*, *523*(3), 463–478. https://doi.org/10.1002/cne.23691

Hladky, S. B., & Barrand, M. A. (2014). Mechanisms of fluid movement into, through and out of the brain: Evaluation of the evidence. *Fluids and Barriers of the CNS*, *11*(1), 26. https://doi.org/10.1186/2045-8118-11-26

Hou, C. C., Li, D., Berry, B. C., Zheng, S., Carroll, R. S., Johnson, M. D., & Yang, H. W. (2023). Heterozygous FOXJ1 Mutations Cause Incomplete Ependymal Cell Differentiation and Communicating Hydrocephalus. *Cellular and Molecular Neurobiology*, *43*(8), 4103–4116. https://doi.org/10.1007/s10571-023-01398-6

Howell, B. W., Lanier, L. M., Frank, R., Gertler, F. B., & Cooper, J. A. (1999). The disabled 1 phosphotyrosine-binding domain binds to the internalization signals of transmembrane glycoproteins and to phospholipids. *Molecular and Cellular Biology*, *19*(7), 5179–5188. https://doi.org/10.1128/MCB.19.7.5179

Huang, F., Khvorova, A., Marshall, W., & Sorkin, A. (2004). Analysis of Clathrin-mediated Endocytosis of Epidermal Growth Factor Receptor by RNA Interference * [boxs]. *Journal of Biological Chemistry*, *279*(16), 16657–16661. https://doi.org/10.1074/jbc.C400046200

Huang, T.-N., & Hsueh, Y.-P. (2015). Brain-specific transcriptional regulator T-brain-1 controls brain wiring and neuronal activity in autism spectrum disorders. *Frontiers in Neuroscience*, *9*. https://doi.org/10.3389/fnins.2015.00406

Hussain, G., Akram, R., Anwar, H., Sajid, F., Iman, T., Han, H. S., Raza, C., & De Aguilar, J.-L. G. (2023). Adult neurogenesis: A real hope or a delusion? *Neural Regeneration Research*, *19*(1), 6–15. https://doi.org/10.4103/1673-5374.375317

Iannolo, G., Salcini, A. E., Gaidarov, I., Goodman, O. B., Jr., Baulida, J., Carpenter, G., Pelicci, P. G., Fiore, P. P. D., & Keen, J. H. (1997). Mapping of the Molecular Determinants Involved in the Interaction between eps15 and AP-21. *Cancer Research*, *57*(2), 240–245.

Ibañez-Tallon, I., Gorokhova, S., & Heintz, N. (2002). Loss of function of axonemal dynein Mdnah5 causes primary ciliary dyskinesia and hydrocephalus. *Human Molecular Genetics*, *11*(6), 715–721. https://doi.org/10.1093/hmg/11.6.715

Ibañez-Tallon, I., Pagenstecher, A., Fliegauf, M., Olbrich, H., Kispert, A., Ketelsen, U.-P., North, A., Heintz, N., & Omran, H. (2004). Dysfunction of axonemal dynein heavy chain Mdnah5 inhibits ependymal flow and reveals a novel mechanism for hydrocephalus formation. *Human Molecular Genetics*, *13*(18), 2133–2141. https://doi.org/10.1093/hmg/ddh219

Iwasato, T., Datwani, A., Wolf, A. M., Nishiyama, H., Taguchi, Y., Tonegawa, S., Knöpfel, T., Erzurumlu, R. S., & Itohara, S. (2000). Cortex-restricted disruption of NMDAR1 impairs neuronal patterns in the barrel cortex. *Nature*, *406*(6797), 726–731. https://doi.org/10.1038/35021059

Jacquet, B. V., Salinas-Mondragon, R., Liang, H., Therit, B., Buie, J. D., Dykstra, M., Campbell, K., Ostrowski, L. E., Brody, S. L., & Ghashghaei, H. T. (2009). FoxJ1-dependent gene expression is required for differentiation of radial glia into ependymal cells and a subset of astrocytes in the postnatal brain. *Development*, *136*(23), 4021–4031. https://doi.org/10.1242/dev.041129

Jakob, B., Kochlamazashvili, G., Jäpel, M., Gauhar, A., Bock, H. H., Maritzen, T., & Haucke, V. (2017a). Intersectin 1 is a component of the Reelin pathway to regulate neuronal migration and synaptic plasticity in the hippocampus. *Proceedings of the National Academy of Sciences of the United States of America*, *114*(21), 5533–5538. https://doi.org/10.1073/pnas.1704447114

Jakob, B., Kochlamazashvili, G., Jäpel, M., Gauhar, A., Bock, H. H., Maritzen, T., & Haucke, V. (2017b). Intersectin 1 is a component of the Reelin pathway to regulate neuronal migration and synaptic plasticity in the hippocampus. *Proceedings of the National Academy of Sciences*, *114*(21), 5533–5538. https://doi.org/10.1073/pnas.1704447114

Joo, J. H., Wang, B., Frankel, E., Ge, L., Xu, L., Iyengar, R., Li-Harms, X., Wright, C., Shaw, T. I., Lindsten, T., Green, D. R., Peng, J., Hendershot, L. M., Kilic, F., Sze, J. Y., Audhya, A., & Kundu, M. (2016). The Noncanonical Role of ULK/ATG1 in ER-to-Golgi Trafficking Is Essential for Cellular Homeostasis. *Molecular Cell*, *62*(4), 491–506. https://doi.org/10.1016/j.molcel.2016.04.020

Jouet, M., Rosenthal, A., Armstrong, G., MacFarlane, J., Stevenson, R., Paterson, J., Metzenberg, A., Ionasescu, V., Temple, K., & Kenwrick, S. (1994). X-linked spastic paraplegia (SPG1), MASA syndrome and X-linked hydrocephalus result from mutations in the L1 gene. *Nature Genetics*, *7*(3), 402–407. https://doi.org/10.1038/ng0794-402

Kaempf, N., & Maritzen, T. (2017). Safeguards of Neurotransmission: Endocytic Adaptors as Regulators of Synaptic Vesicle Composition and Function. *Frontiers in Cellular Neuroscience*, *11*. https://doi.org/10.3389/fncel.2017.00320

Kaksonen, M., & Roux, A. (2018). Mechanisms of clathrin-mediated endocytosis. *Nature Reviews Molecular Cell Biology*, *19*(5), 313–326. https://doi.org/10.1038/nrm.2017.132

Kamiguchi, H., Long, K. E., Pendergast, M., Schaefer, A. W., Rapoport, I., Kirchhausen, T., & Lemmon, V. (1998). The Neural Cell Adhesion Molecule L1 Interacts with the AP-2 Adaptor and Is Endocytosed via the Clathrin-Mediated Pathway. *Journal of Neuroscience*, *18*(14), 5311–5321. https://doi.org/10.1523/JNEUROSCI.18-14-05311.1998

Kaplan, M. S., & Hinds, J. W. (1977). Neurogenesis in the adult rat: Electron microscopic analysis of light radioautographs. *Science (New York, N.Y.)*, *197*(4308), 1092–1094. https://doi.org/10.1126/science.887941

Kastning, K., Kukhtina, V., Kittler, J. T., Chen, G., Pechstein, A., Enders, S., Lee, S. H., Sheng, M., Yan, Z., & Haucke, V. (2007). Molecular determinants for the interaction between AMPA receptors and the clathrin adaptor complex AP-2. *Proceedings of the National Academy of Sciences of the United States of America*, *104*(8), 2991–2996. https://doi.org/10.1073/pnas.0611170104

Kazazic, M., Bertelsen, V., Pedersen, K. W., Vuong, T. T., Grandal, M. V., Rødland, M. S., Traub, L. M., Stang, E., & Madshus, I. H. (2009). Epsin 1 is Involved in Recruitment of Ubiquitinated EGF Receptors into Clathrin-Coated Pits. *Traffic*, *10*(2), 235–245. https://doi.org/10.1111/j.1600-0854.2008.00858.x

Kempermann, G., Song, H., & Gage, F. H. (2015). Neurogenesis in the Adult Hippocampus. *Cold Spring Harbor Perspectives in Biology*, *7*(9), a018812. https://doi.org/10.1101/cshperspect.a018812

Kent, H. M., McMahon, H. T., Evans, P. R., Benmerah, A., & Owen, D. J. (2002). γ-Adaptin Appendage Domain: Structure and Binding Site for Eps15 and γ-Synergin. *Structure*, *10*(8), 1139–1148. https://doi.org/10.1016/S0969-2126(02)00801-8

Kiss, A. L., & Botos, E. (2009). Endocytosis via caveolae: Alternative pathway with distinct cellular compartments to avoid lysosomal degradation? *Journal of Cellular and Molecular Medicine*, *13*(7), 1228–1237. https://doi.org/10.1111/j.1582-4934.2009.00754.x

Knaus, P., Betz, H., & Rehm, H. (1986). Expression of synaptophysin during postnatal development of the mouse brain. *Journal of Neurochemistry*, *47*(4), 1302–1304. https://doi.org/10.1111/j.1471-4159.1986.tb00754.x

Koch, D., Spiwoks-Becker, I., Sabanov, V., Sinning, A., Dugladze, T., Stellmacher, A., Ahuja, R., Grimm, J., Schüler, S., Müller, A., Angenstein, F., Ahmed, T., Diesler, A., Moser, M., Tom Dieck, S., Spessert, R., Boeckers, T. M., Fässler, R., Hübner, C. A., … Qualmann, B. (2011). Proper synaptic vesicle formation and neuronal network activity critically rely on syndapin I. *The EMBO Journal*, *30*(24), 4955–4969. https://doi.org/10.1038/emboj.2011.339

Kochubey, O., Babai, N., & Schneggenburger, R. (2016). A Synaptotagmin Isoform Switch during the Development of an Identified CNS Synapse. *Neuron*, *90*(5), 984–999. https://doi.org/10.1016/j.neuron.2016.04.038

Koh, T.-W., Korolchuk, V. I., Wairkar, Y. P., Jiao, W., Evergren, E., Pan, H., Zhou, Y., Venken, K. J. T., Shupliakov, O., Robinson, I. M., O'Kane, C. J., & Bellen, H. J. (2007). Eps15 and Dap160 control synaptic vesicle membrane retrieval and synapse development. *Journal of Cell Biology*, *178*(2), 309–322. https://doi.org/10.1083/jcb.200701030

Koh, T.-W., Verstreken, P., & Bellen, H. J. (2004). Dap160/intersectin acts as a stabilizing scaffold required for synaptic development and vesicle endocytosis. *Neuron*, *43*(2), 193–205. https://doi.org/10.1016/j.neuron.2004.06.029

Koleva, M., & De Jesus, O. (2025). Hydrocephalus. In *StatPearls*. StatPearls Publishing. http://www.ncbi.nlm.nih.gov/books/NBK560875/

Komatsu, M., Waguri, S., Chiba, T., Murata, S., Iwata, J., Tanida, I., Ueno, T., Koike, M., Uchiyama, Y., Kominami, E., & Tanaka, K. (2006). Loss of autophagy in the central nervous system causes neurodegeneration in mice. *Nature*, *441*(7095), 880–884. https://doi.org/10.1038/nature04723

Kononenko, N. L., Claßen, G. A., Kuijpers, M., Puchkov, D., Maritzen, T., Tempes, A., Malik, A. R., Skalecka, A., Bera, S., Jaworski, J., & Haucke, V. (2017). Retrograde transport of TrkB-containing autophagosomes via the adaptor AP-2 mediates neuronal complexity and prevents neurodegeneration. *Nature Communications*, *8*(1), 14819. https://doi.org/10.1038/ncomms14819

Koo, S. J., Kochlamazashvili, G., Rost, B., Puchkov, D., Gimber, N., Lehmann, M., Tadeus, G., Schmoranzer, J., Rosenmund, C., Haucke, V., & Maritzen, T. (2015a). Vesicular Synaptobrevin/VAMP2 Levels Guarded by AP180 Control Efficient Neurotransmission. *Neuron*, *88*(2), 330–344. https://doi.org/10.1016/j.neuron.2015.08.034

Koo, S. J., Kochlamazashvili, G., Rost, B., Puchkov, D., Gimber, N., Lehmann, M., Tadeus, G., Schmoranzer, J., Rosenmund, C., Haucke, V., & Maritzen, T. (2015b). Vesicular Synaptobrevin/VAMP2 Levels Guarded by AP180 Control Efficient Neurotransmission. *Neuron*, *88*(2), 330–344. https://doi.org/10.1016/j.neuron.2015.08.034

Koscielny, A., Malik, A. R., Liszewska, E., Zmorzynska, J., Tempes, A., Tarkowski, B., & Jaworski, J. (2018). Adaptor Complex 2 Controls Dendrite Morphology via mTOR-Dependent Expression of GluA2. *Molecular Neurobiology*, *55*(2), 1590–1606. https://doi.org/10.1007/s12035-017-0436-3

Kozak, M., & Kaksonen, M. (2022a). Condensation of Ede1 promotes the initiation of endocytosis. *eLife*, *11*, e72865. https://doi.org/10.7554/eLife.72865

Kozak, M., & Kaksonen, M. (2022b). Condensation of Ede1 promotes the initiation of endocytosis. *eLife*, *11*, e72865. https://doi.org/10.7554/eLife.72865

Kriegstein, A. R., & Noctor, S. C. (2004). Patterns of neuronal migration in the embryonic cortex. *Trends in Neurosciences*, *27*(7), 392–399. https://doi.org/10.1016/j.tins.2004.05.001

Kuijpers, M., Kochlamazashvili, G., Stumpf, A., Puchkov, D., Swaminathan, A., Lucht, M. T., Krause, E., Maritzen, T., Schmitz, D., & Haucke, V. (2021). Neuronal Autophagy Regulates Presynaptic Neurotransmission by Controlling the Axonal Endoplasmic Reticulum. *Neuron*, *109*(2), 299-313.e9. https://doi.org/10.1016/j.neuron.2020.10.005

Kuo, C. T., Mirzadeh, Z., Soriano-Navarro, M., Rašin, M., Wang, D., Shen, J., Šestan, N., Garcia-Verdugo, J., Alvarez-Buylla, A., Jan, L. Y., & Jan, Y.-N. (2006). Postnatal Deletion of Numb/Numblike Reveals Repair and Remodeling Capacity in the Subventricular Neurogenic Niche. *Cell*, *127*(6), 1253–1264. https://doi.org/10.1016/j.cell.2006.10.041

Kyrousi, C., Arbi, M., Pilz, G.-A., Pefani, D.-E., Lalioti, M.-E., Ninkovic, J., Götz, M., Lygerou, Z., & Taraviras, S. (2015). Mcidas and GemC1 are key regulators for the generation of multiciliated ependymal cells in the adult neurogenic niche. *Development (Cambridge, England)*, *142*(21), 3661–3674. https://doi.org/10.1242/dev.126342

Lalonde, R., & Strazielle, C. (2011). Brain regions and genes affecting limb-clasping responses. *Brain Research Reviews*, *67*(1–2), 252–259. https://doi.org/10.1016/j.brainresrev.2011.02.005

Lampe, M., Vassilopoulos, S., & Merrifield, C. (2016). Clathrin coated pits, plaques and adhesion. *Journal of Structural Biology*, *196*(1), 48–56. https://doi.org/10.1016/j.jsb.2016.07.009

Langridge, P. D., & Struhl, G. (2017). Epsin-Dependent Ligand Endocytosis Activates Notch by Force. *Cell*, *171*(6), 1383-1396.e12. https://doi.org/10.1016/j.cell.2017.10.048

Latham, N., & Mason, G. (2004). From house mouse to mouse house: The behavioural biology of free-living *Mus musculus* and its implications in the laboratory. *Applied Animal Behaviour Science*, *86*(3), 261–289. https://doi.org/10.1016/j.applanim.2004.02.006

Lavado, A., & Oliver, G. (2011). Six3 is required for ependymal cell maturation. *Development (Cambridge, England)*, *138*(24), 5291–5300. https://doi.org/10.1242/dev.067470

Lee, S. H., Liu, L., Wang, Y. T., & Sheng, M. (2002). Clathrin adaptor AP2 and NSF interact with overlapping sites of GluR2 and play distinct roles in AMPA receptor trafficking and hippocampal LTD. *Neuron*, *36*(4), 661–674. https://doi.org/10.1016/s0896-6273(02)01024-3

Lemus, L., & Goder, V. (2016). A SNARE and specific COPII requirements define ER-derived vesicles for the biogenesis of autophagosomes. *Autophagy*, *12*(6), 1049–1050. https://doi.org/10.1080/15548627.2016.1164368

Li, J., Zhang, C., Meng, Y., Yang, S., Xia, J., Chen, H., & Liao, W. (2024). Morphometric brain organization across the human lifespan reveals increased dispersion linked to cognitive performance. *PLOS Biology*, *22*(6), e3002647. https://doi.org/10.1371/journal.pbio.3002647

Li, W., Puertollano, R., Bonifacino, J. S., Overbeek, P. A., & Everett, E. T. (2010). Disruption of the Murine Ap2β1 Gene Causes Nonsyndromic Cleft Palate. *The Cleft Palate Craniofacial Journal*, *47*(6), 566–573. https://doi.org/10.1597/09-145

Lim, D. A., & Alvarez-Buylla, A. (2016). The Adult Ventricular–Subventricular Zone (V-SVZ) and Olfactory Bulb (OB) Neurogenesis. *Cold Spring Harbor Perspectives in Biology*, *8*(5), a018820. https://doi.org/10.1101/cshperspect.a018820

Lin, A., & Man, H.-Y. (2014). Endocytic Adaptor Epidermal Growth Factor Receptor Substrate 15 (Eps15) Is Involved in the Trafficking of Ubiquitinated α-Amino-3-hydroxy-5-methyl-4-isoxazolepropionic Acid Receptors*. *Journal of Biological Chemistry*, *289*(35), 24652–24664. https://doi.org/10.1074/jbc.M114.582114

Lindwall, C., Fothergill, T., & Richards, L. J. (2007). Commissure formation in the mammalian forebrain. *Current Opinion in Neurobiology*, *17*(1), 3–14. https://doi.org/10.1016/j.conb.2007.01.008

Liu, K., Lei, R., Li, Q., Wang, X.-X., Wu, Q., An, P., Zhang, J., Zhu, M., Xu, Z., Hong, Y., Wang, F., Shen, Y., Li, H., & Li, H. (2016). Transferrin Receptor Controls AMPA Receptor Trafficking Efficiency and Synaptic Plasticity. *Scientific Reports*, *6*(1), 21019. https://doi.org/10.1038/srep21019

Liu, M., Guan, Z., Shen, Q., Lalor, P., Fitzgerald, U., O'Brien, T., Dockery, P., & Shen, S. (2016). Ulk4 Is Essential for Ciliogenesis and CSF Flow. *Journal of Neuroscience*, *36*(29), 7589–7600. https://doi.org/10.1523/JNEUROSCI.0621-16.2016

Lohmann, C., & Kessels, H. W. (2014). The developmental stages of synaptic plasticity. *The Journal of Physiology*, *592*(Pt 1), 13–31. https://doi.org/10.1113/jphysiol.2012.235119

Lois, C., & Alvarez-Buylla, A. (1994). Long-distance neuronal migration in the adult mammalian brain. *Science (New York, N.Y.)*, *264*(5162), 1145–1148. https://doi.org/10.1126/science.8178174

López-Hernández, T., Haucke, V., & Maritzen, T. (2020). Endocytosis in the adaptation to cellular stress. *Cell Stress*, *4*(10), 230–247. https://doi.org/10.15698/cst2020.10.232

Lowery, L. A., & Sive, H. (2009). Totally tubular: The mystery behind function and origin of the brain ventricular system. *BioEssays: News and Reviews in Molecular, Cellular and Developmental Biology*, *31*(4), 446–458. https://doi.org/10.1002/bies.200800207

Lu, H., Anujan, P., Zhou, F., Zhang, Y., Chong, Y. L., Bingle, C. D., & Roy, S. (2019). Mcidas mutant mice reveal a two-step process for the specification and differentiation of multiciliated cells in mammals. *Development*, *146*(6), dev172643. https://doi.org/10.1242/dev.172643

Luque, J. M., Morante-Oria, J., & Fairén, A. (2003). Localization of ApoER2, VLDLR and Dab1 in radial glia: Groundwork for a new model of reelin action during cortical development. *Brain Research. Developmental Brain Research*, *140*(2), 195–203. https://doi.org/10.1016/s0165-3806(02)00604-1

Macia, E., Ehrlich, M., Massol, R., Boucrot, E., Brunner, C., & Kirchhausen, T. (2006). Dynasore, a cell-permeable inhibitor of dynamin. *Developmental Cell*, *10*(6), 839–850. https://doi.org/10.1016/j.devcel.2006.04.002

Majumdar, A., Ramagiri, S., & Rikhy, R. (2006a). *Drosophila* homologue of Eps15 is essential for synaptic vesicle recycling. *Experimental Cell Research*, *312*(12), 2288–2298. https://doi.org/10.1016/j.yexcr.2006.03.030

Majumdar, A., Ramagiri, S., & Rikhy, R. (2006b). *Drosophila* homologue of Eps15 is essential for synaptic vesicle recycling. *Experimental Cell Research*, *312*(12), 2288–2298. https://doi.org/10.1016/j.yexcr.2006.03.030

Malatesta, P., Appolloni, I., & Calzolari, F. (2008). Radial glia and neural stem cells. *Cell and Tissue Research*, *331*(1), 165–178. https://doi.org/10.1007/s00441-007-0481-8

Maldonado-Báez, L., Williamson, C., & Donaldson, J. G. (2013). Clathrin-independent endocytosis: A cargo-centric view. *Experimental Cell Research*, *319*(18), 2759–2769. https://doi.org/10.1016/j.yexcr.2013.08.008

Martina, J. A., Bonangelino, C. J., Aguilar, R. C., & Bonifacino, J. S. (2001). Stonin 2: An Adaptor-like Protein That Interacts with Components of the Endocytic Machinery. *Journal of Cell Biology*, *153*(5), 1111–1120. https://doi.org/10.1083/jcb.153.5.1111

Mayle, K. M., Le, A. M., & Kamei, D. T. (2012). The Intracellular Trafficking Pathway of Transferrin. *Biochimica et Biophysica Acta*, *1820*(3), 264–281. https://doi.org/10.1016/j.bbagen.2011.09.009

Mayor, S., & Pagano, R. E. (2007). Pathways of clathrin-independent endocytosis. *Nature Reviews Molecular Cell Biology*, *8*(8), 603–612. https://doi.org/10.1038/nrm2216

Mayor, S., Parton, R. G., & Donaldson, J. G. (2014). Clathrin-Independent Pathways of Endocytosis. *Cold Spring Harbor Perspectives in Biology*, *6*(6), a016758. https://doi.org/10.1101/cshperspect.a016758

McEwan, F., Glazier, J. D., & Hager, R. (2023). The impact of maternal immune activation on embryonic brain development. *Frontiers in Neuroscience*, *17*. https://doi.org/10.3389/fnins.2023.1146710

McGill, M. A., Dho, S. E., Weinmaster, G., & McGlade, C. J. (2009). Numb Regulates Post-endocytic Trafficking and Degradation of Notch1*. *Journal of Biological Chemistry*, *284*(39), 26427–26438. https://doi.org/10.1074/jbc.M109.014845

McMahon, H. T., & Boucrot, E. (2011). Molecular mechanism and physiological functions of clathrin-mediated endocytosis. *Nature Reviews Molecular Cell Biology*, *12*(8), 517–533. https://doi.org/10.1038/nrm3151

Mendes, S. W., Henkemeyer, M., & Liebl, D. J. (2006). Multiple Eph receptors and B-class ephrins regulate midline crossing of corpus callosum fibers in the developing mouse forebrain. *The Journal of Neuroscience: The Official Journal of the Society for Neuroscience*, *26*(3), 882–892. https://doi.org/10.1523/JNEUROSCI.3162-05.2006

Merkle, F. T., Mirzadeh, Z., & Alvarez-Buylla, A. (2007). Mosaic Organization of Neural Stem Cells in the Adult Brain. *Science*, *317*(5836), 381–384. https://doi.org/10.1126/science.1144914

Merkle, F. T., Tramontin, A. D., García-Verdugo, J. M., & Alvarez-Buylla, A. (2004). Radial glia give rise to adult neural stem cells in the subventricular zone. *Proceedings of the National Academy of Sciences*, *101*(50), 17528–17532. https://doi.org/10.1073/pnas.0407893101

Messa, M., Fernández-Busnadiego, R., Sun, E. W., Chen, H., Czapla, H., Wrasman, K., Wu, Y., Ko, G., Ross, T., Wendland, B., & De Camilli, P. (2014). Epsin deficiency impairs endocytosis by stalling the actin-dependent invagination of endocytic clathrin-coated pits. *eLife*, *3*, e03311. https://doi.org/10.7554/eLife.03311

Milesi, C., Alberici, P., Pozzi, B., Oldani, A., Beznoussenko, G. V., Raimondi, A., Soppo, B. E., Amodio, S., Caldieri, G., Malabarba, M. G., Bertalot, G., Confalonieri, S., Parazzoli, D., Mironov, A. A., Tacchetti, C., Di Fiore, P. P., Sigismund, S., & Offenhäuser, N. (2019). Redundant and nonredundant organismal functions of EPS15 and EPS15L1. *Life Science Alliance*, *2*(1), e201800273. https://doi.org/10.26508/lsa.201800273

Mill, P., Christensen, S. T., & Pedersen, L. B. (2023). Primary cilia as dynamic and diverse signalling hubs in development and disease. *Nature Reviews Genetics*, *24*(7), 421–441. https://doi.org/10.1038/s41576-023-00587-9

Mirzadeh, Z., Han, Y.-G., Soriano-Navarro, M., García-Verdugo, J. M., & Alvarez-Buylla, A. (2010). Cilia Organize Ependymal Planar Polarity. *Journal of Neuroscience*, *30*(7), 2600–2610. https://doi.org/10.1523/JNEUROSCI.3744-09.2010

Mirzadeh, Z., Merkle, F. T., Soriano-Navarro, M., Garcia-Verdugo, J. M., & Alvarez-Buylla, A. (2008). Neural Stem Cells Confer Unique Pinwheel Architecture to the Ventricular Surface in Neurogenic Regions of the Adult Brain. *Cell Stem Cell*, *3*(3), 265–278. https://doi.org/10.1016/j.stem.2008.07.004

Mishra, S. K., Watkins, S. C., & Traub, L. M. (2002). The autosomal recessive hypercholesterolemia (ARH) protein interfaces directly with the clathrin-coat machinery. *Proceedings of the National Academy of Sciences*, *99*(25), 16099–16104. https://doi.org/10.1073/pnas.252630799

Mitsunari, T., Nakatsu, F., Shioda, N., Love, P. E., Grinberg, A., Bonifacino, J. S., & Ohno, H. (2005). Clathrin Adaptor AP-2 Is Essential for Early Embryonal Development. *Molecular and Cellular Biology*, *25*(21), 9318–9323. https://doi.org/10.1128/MCB.25.21.9318-9323.2005

Moldrich, R. X., Gobius, I., Pollak, T., Zhang, J., Ren, T., Brown, L., Mori, S., De Juan Romero, C., Britanova, O., Tarabykin, V., & Richards, L. J. (2010). Molecular regulation of the developing commissural plate. *The Journal of Comparative Neurology*, *518*(18), 3645–3661. https://doi.org/10.1002/cne.22445

Morgan, J. R., Prasad, K., Jin, S., Augustine, G. J., & Lafer, E. M. (2003). Eps15 homology domain-NPF motif interactions regulate clathrin coat assembly during synaptic vesicle recycling. *The Journal of Biological Chemistry*, *278*(35), 33583–33592. https://doi.org/10.1074/jbc.M304346200

Munch, T. N., Rostgaard, K., Rasmussen, M.-L. H., Wohlfahrt, J., Juhler, M., & Melbye, M. (2012). Familial aggregation of congenital hydrocephalus in a nationwide cohort. *Brain: A Journal of Neurology*, *135*(Pt 8), 2409–2415. https://doi.org/10.1093/brain/aws158

Neupane, S., Goto, J., Berardinelli, S. J., Ito, A., Haltiwanger, R. S., & Holdener, B. C. (2021). Hydrocephalus in mouse B3glct mutants is likely caused by defects in multiple B3GLCT substrates in ependymal cells and subcommissural organ. *Glycobiology*, *31*(8), 988–1004. https://doi.org/10.1093/glycob/cwab033

Nieuwenhuys, R., Ten Donkelaar, H. J., & Nicholson, C. (1998). *The Central Nervous System of Vertebrates*. Springer. https://doi.org/10.1007/978-3-642-18262-4

Nishimura, T., Yamaguchi, T., Tokunaga, A., Hara, A., Hamaguchi, T., Kato, K., Iwamatsu, A., Okano, H., & Kaibuchi, K. (2006). Role of numb in dendritic spine development with a Cdc42 GEF intersectin and EphB2. *Molecular Biology of the Cell*, *17*(3), 1273–1285. https://doi.org/10.1091/mbc.e05-07-0700

Nthiga, T. M., Kumar Shrestha, B., Sjøttem, E., Bruun, J., Bowitz Larsen, K., Bhujabal, Z., Lamark, T., & Johansen, T. (2020a). CALCOCO1 acts with VAMP-associated proteins to mediate ER-phagy. *The EMBO Journal*, *39*(15), e103649. https://doi.org/10.15252/embj.2019103649

Nthiga, T. M., Kumar Shrestha, B., Sjøttem, E., Bruun, J., Bowitz Larsen, K., Bhujabal, Z., Lamark, T., & Johansen, T. (2020b). CALCOCO1 acts with VAMP-associated proteins to mediate ER-phagy. *The EMBO Journal*, *39*(15), e103649. https://doi.org/10.15252/embj.2019103649

Nthiga, T. M., Shrestha, B. K., Bruun, J.-A., Larsen, K. B., Lamark, T., & Johansen, T. (2021). Regulation of Golgi turnover by CALCOCO1-mediated selective autophagy. *Journal of Cell Biology*, *220*(6), e202006128. https://doi.org/10.1083/jcb.202006128

Ohata, S., Nakatani, J., Herranz-Pérez, V., Cheng, J., Belinson, H., Inubushi, T., Snider, W. D., García-Verdugo, J. M., Wynshaw-Boris, A., & Álvarez-Buylla, A. (2014). Loss of Dishevelleds Disrupts Planar Polarity in Ependymal Motile Cilia and Results in Hydrocephalus. *Neuron*, *83*(3), 558–571. https://doi.org/10.1016/j.neuron.2014.06.022

Ohata, S., Nakatani, J., Herranz-Pérez, V., Cheng, J., Belinson, H., Inubushi, T., Snider, W. D., García-Verdugo, J. M., Wynshaw-Boris, A., & Alvarez-Buylla, A. (2014). Loss of Dishevelleds disrupts planar polarity in ependymal motile cilia and results in hydrocephalus. *Neuron*, *83*(3), 558–571. https://doi.org/10.1016/j.neuron.2014.06.022

Palmer, T. D., Takahashi, J., & Gage, F. H. (1997). The adult rat hippocampus contains primordial neural stem cells. *Molecular and Cellular Neurosciences*, *8*(6), 389–404. https://doi.org/10.1006/mcne.1996.0595

Pang, D., & Altschuler, E. (1994). Low-pressure hydrocephalic state and viscoelastic alterations in the brain. *Neurosurgery*, *35*(4), 643–655; discussion 655-656. https://doi.org/10.1227/00006123-199410000-00010

Patten, A. R., Yau, S. Y., Fontaine, C. J., Meconi, A., Wortman, R. C., & Christie, B. R. (2015). The Benefits of Exercise on Structural and Functional Plasticity in the Rodent Hippocampus of Different Disease Models. *Brain Plasticity (Amsterdam, Netherlands)*, *1*(1), 97–127. https://doi.org/10.3233/BPL-150016

Paul, N. R., Jacquemet, G., & Caswell, P. T. (2015). Endocytic Trafficking of Integrins in Cell Migration. *Current Biology*, *25*(22), R1092–R1105. https://doi.org/10.1016/j.cub.2015.09.049

Pechstein, A., Gerth, F., Milosevic, I., Jäpel, M., Eichhorn-Grünig, M., Vorontsova, O., Bacetic, J., Maritzen, T., Shupliakov, O., Freund, C., & Haucke, V. (2015). Vesicle uncoating regulated by SH3-SH3 domain-mediated complex formation between endophilin and intersectin at synapses. *EMBO Reports*, *16*(2), 232–239. https://doi.org/10.15252/embr.201439260

Piao, H., Kim, J., Noh, S. H., Kweon, H.-S., Kim, J. Y., & Lee, M. G. (2017). Sec16A is critical for both conventional and unconventional secretion of CFTR. *Scientific Reports*, *7*(1), 39887. https://doi.org/10.1038/srep39887

Pinto-Lord, M. C., Evrard, P., & Caviness, V. S. (1982). Obstructed neuronal migration along radial glial fibers in the neocortex of the reeler mouse: A Golgi-EM analysis. *Brain Research*, *256*(4), 379–393. https://doi.org/10.1016/0165-3806(82)90181-x

Polo, S., Confalonieri, S., Salcini, A. E., & Di Fiore, P. P. (2003). EH and UIM: Endocytosis and More. *Science's STKE*, *2003*(213), re17–re17. https://doi.org/10.1126/stke.2132003re17

Polo, S., Sigismund, S., Faretta, M., Guidi, M., Capua, M. R., Bossi, G., Chen, H., De Camilli, P., & Di Fiore, P. P. (2002). A single motif responsible for ubiquitin recognition and monoubiquitination in endocytic proteins. *Nature*, *416*(6879), 451–455. https://doi.org/10.1038/416451a

Pond, H. L., Heller, A. T., Gural, B. M., McKissick, O. P., Wilkinson, M. K., & Manzini, M. C. (2021). Digging behavior discrimination test to probe burrowing and exploratory digging in male and female mice. *Journal of Neuroscience Research*, *99*(9), 2046–2058. https://doi.org/10.1002/jnr.24857

Poupon, V., Polo, S., Vecchi, M., Martin, G., Dautry-Varsat, A., Cerf-Bensussan, N., Di Fiore, P. P., & Benmerah, A. (2002). Differential Nucleocytoplasmic Trafficking between the Related Endocytic Proteins Eps15 and Eps15R*. *Journal of Biological Chemistry*, *277*(11), 8941–8948. https://doi.org/10.1074/jbc.M108385200

Pozzi, B., Amodio, S., Lucano, C., Sciullo, A., Ronzoni, S., Castelletti, D., Adler, T., Treise, I., Betsholtz, I. H., Rathkolb, B., Busch, D. H., Wolf, E., Fuchs, H., Gailus-Durner, V., Angelis, M. H. de, Betsholtz, C., Casola, S., Fiore, P. P. D., & Offenhäuser, N. (2012a). The Endocytic Adaptor Eps15 Controls Marginal Zone B Cell Numbers. *PLOS ONE*, *7*(11), e50818. https://doi.org/10.1371/journal.pone.0050818

Pozzi, B., Amodio, S., Lucano, C., Sciullo, A., Ronzoni, S., Castelletti, D., Adler, T., Treise, I., Betsholtz, I. H., Rathkolb, B., Busch, D. H., Wolf, E., Fuchs, H., Gailus-Durner, V., Angelis, M. H. de, Betsholtz, C., Casola, S., Fiore, P. P. D., & Offenhäuser, N. (2012b). The Endocytic Adaptor Eps15 Controls Marginal Zone B Cell Numbers. *PLOS ONE*, *7*(11), e50818. https://doi.org/10.1371/journal.pone.0050818

Pozzi, B., Amodio, S., Lucano, C., Sciullo, A., Ronzoni, S., Castelletti, D., Adler, T., Treise, I., Betsholtz, I. H., Rathkolb, B., Busch, D. H., Wolf, E., Fuchs, H., Gailus-Durner, V., Angelis, M. H. de, Betsholtz, C., Casola, S., Fiore, P. P. D., & Offenhäuser, N. (2012c). The Endocytic Adaptor Eps15 Controls Marginal Zone B Cell Numbers. *PLOS ONE*, *7*(11), e50818. https://doi.org/10.1371/journal.pone.0050818

Pucharcos, C., Estivill, X., & de la Luna, S. (2000). Intersectin 2, a new multimodular protein involved in clathrin-mediated endocytosis. *FEBS Letters*, *478*(1–2), 43–51. https://doi.org/10.1016/s0014-5793(00)01793-2

Qian, W., Hong, Y., Zhu, M., Zhou, L., Li, H., & Li, H. (2017). Deletion of *Numb*/*Numblike* in glutamatergic neurons leads to anxiety-like behavior in mice. *Brain Research*, *1665*, 36–49. https://doi.org/10.1016/j.brainres.2017.02.025

Raj, T., Li, Y. I., Wong, G., Humphrey, J., Wang, M., Ramdhani, S., Wang, Y.-C., Ng, B., Gupta, I., Haroutunian, V., Schadt, E. E., Young-Pearse, T., Mostafavi, S., Zhang, B., Sklar, P., Bennett, D. A., & De Jager, P. L. (2018). Integrative transcriptome analyses of the aging brain implicate altered

splicing in Alzheimer's disease susceptibility. *Nature Genetics*, *50*(11), 1584–1592. https://doi.org/10.1038/s41588-018-0238-1

Rakic, P. (2009). Evolution of the neocortex: A perspective from developmental biology. *Nature Reviews Neuroscience*, *10*(10), 724–735. https://doi.org/10.1038/nrn2719

Redmond, S. A., Figueres-Oñate, M., Obernier, K., Nascimento, M. A., Parraguez, J. I., López-Mascaraque, L., Fuentealba, L. C., & Alvarez-Buylla, A. (2019). Development of Ependymal and Postnatal Neural Stem Cells and Their Origin from a Common Embryonic Progenitor. *Cell Reports*, *27*(2), 429-441.e3. https://doi.org/10.1016/j.celrep.2019.01.088

Rhyu, M. S., Jan, L. Y., & Jan, Y. N. (1994). Asymmetric distribution of numb protein during division of the sensory organ precursor cell confers distinct fates to daughter cells. *Cell*, *76*(3), 477–491. https://doi.org/10.1016/0092-8674(94)90112-0

Riva-Cambrin, J., Kulkarni, A. V., Burr, R., Rozzelle, C. J., Oakes, W. J., Drake, J. M., Alvey, J. S., Reeder, R. W., Holubkov, R., Browd, S. R., Cochrane, D. D., Limbrick, D. D., Naftel, R., Shannon, C. N., Simon, T. D., Tamber, M. S., McDonald, P. J., Wellons, J. C., Luerssen, T. G., … Kestle, J. R. W. (2022). Impact of ventricle size on neuropsychological outcomes in treated pediatric hydrocephalus: An HCRN prospective cohort study. *Journal of Neurosurgery. Pediatrics*, *29*(3), 245–256. https://doi.org/10.3171/2021.8.PEDS21146

Rogawski, M. A. (2013). AMPA receptors as a molecular target in epilepsy therapy. *Acta Neurologica Scandinavica*, *127*(s197), 9–18. https://doi.org/10.1111/ane.12099

Rosahl, T. W., Spillane, D., Missler, M., Herz, J., Selig, D. K., Wolff, J. R., Hammer, R. E., Malenka, R. C., & Südhof, T. C. (1995). Essential functions of synapsins I and II in synaptic vesicle regulation. *Nature*, *375*(6531), 488–493. https://doi.org/10.1038/375488a0

Rumpf, J., Simon, B., Jung, N., Maritzen, T., Haucke, V., Sattler, M., & Groemping, Y. (2008). Structure of the Eps15–stonin2 complex provides a molecular explanation for EH-domain ligand specificity. *The EMBO Journal*, *27*(3), 558–569. https://doi.org/10.1038/sj.emboj.7601980

Saigal, G., Ezuddin, N. S., & Vega, G. de la. (2018). Neurologic Emergencies in Pediatric Patients Including Accidental and Nonaccidental Trauma. *Neuroimaging Clinics of North America*, *28*(3), 453–470. https://doi.org/10.1016/j.nic.2018.03.007

Salcini, A. E., Chen, H., Iannolo, G., De Camilli, P., & Di Fiore, P. P. (1999). Epidermal growth factor pathway substrate 15, Eps15. *The International Journal of Biochemistry & Cell Biology*, *31*(8), 805–809. https://doi.org/10.1016/S1357-2725(99)00042-4

Salcini, A. E., Confalonieri, S., Doria, M., Santolini, E., Tassi, E., Minenkova, O., Cesareni, G., Pelicci, P. G., & Fiore, P. P. D. (1997a). Binding specificity and in vivo targets of the EH domain, a novel protein–protein interaction module. *Genes & Development*, *11*(17), 2239–2249. https://doi.org/10.1101/gad.11.17.2239

Salcini, A. E., Confalonieri, S., Doria, M., Santolini, E., Tassi, E., Minenkova, O., Cesareni, G., Pelicci, P. G., & Fiore, P. P. D. (1997b). Binding specificity and in vivo targets of the EH domain, a novel protein–protein interaction module. *Genes & Development*, *11*(17), 2239–2249. https://doi.org/10.1101/gad.11.17.2239

Salcini, A. E., Hilliard, M. A., Croce, A., Arbucci, S., Luzzi, P., Tacchetti, C., Daniell, L., De Camilli, P., Pelicci, P. G., Di Fiore, P. P., & Bazzicalupo, P. (2001a). The Eps15 C. elegans homologue EHS-1 is implicated in synaptic vesicle recycling. *Nature Cell Biology*, *3*(8), 755–760. https://doi.org/10.1038/35087075

Salcini, A. E., Hilliard, M. A., Croce, A., Arbucci, S., Luzzi, P., Tacchetti, C., Daniell, L., De Camilli, P., Pelicci, P. G., Di Fiore, P. P., & Bazzicalupo, P. (2001b). The Eps15 C. elegans homologue EHS-1 is implicated in synaptic vesicle recycling. *Nature Cell Biology*, *3*(8), 755–760. https://doi.org/10.1038/35087075

Savio, M. G., Wollscheid, N., Cavallaro, E., Algisi, V., Di Fiore, P. P., Sigismund, S., Maspero, E., & Polo, S. (2016). USP9X Controls EGFR Fate by Deubiquitinating the Endocytic Adaptor Eps15. *Current Biology: CB*, *26*(2), 173–183. https://doi.org/10.1016/j.cub.2015.11.050

Schiffmann, S. N., Bernier, B., & Goffinet, A. M. (1997). Reelin mRNA Expression During Mouse Brain Development. *European Journal of Neuroscience*, *9*(5), 1055–1071. https://doi.org/10.1111/j.1460-9568.1997.tb01456.x

Schlossman, D. M., Schmid, S. L., Braell, W. A., & Rothman, J. E. (1984). An enzyme that removes clathrin coats: Purification of an uncoating ATPase. *Journal of Cell Biology*, *99*(2), 723–733. https://doi.org/10.1083/jcb.99.2.723

Schmeisser, M. J., Ey, E., Wegener, S., Bockmann, J., Stempel, A. V., Kuebler, A., Janssen, A.-L., Udvardi, P. T., Shiban, E., Spilker, C., Balschun, D., Skryabin, B. V., Dieck, S. tom, Smalla, K.-H., Montag, D., Leblond, C. S., Faure, P., Torquet, N., Le Sourd, A.-M., … Boeckers, T. M. (2012). Autistic-like behaviours and hyperactivity in mice lacking ProSAP1/Shank2. *Nature*, *486*(7402), 256–260. https://doi.org/10.1038/nature11015

Schmid, R. S., & Maness, P. F. (2008). L1 and NCAM ADHESION MOLECULES AS SIGNALING CO-RECEPTORS IN NEURONAL MIGRATION AND PROCESS OUTGROWTH. *Current Opinion in Neurobiology*, *18*(3), 245–250. https://doi.org/10.1016/j.conb.2008.07.015

Schumacher, C., Knudsen, B. S., Ohuchi, T., Fiore, P. P. D., Glassman, R. H., & Hanafusa, H. (1995). The SH3 Domain of Crk Binds Specifically to a Conserved Proline-rich Motif in Eps15 and Eps15R (∗). *Journal of Biological Chemistry*, *270*(25), 15341–15347. https://doi.org/10.1074/jbc.270.25.15341

Schwarz, L. A., Hall, B. J., & Patrick, G. N. (2010). Activity-Dependent Ubiquitination of GluA1 Mediates a Distinct AMPA Receptor Endocytosis and Sorting Pathway. *The Journal of Neuroscience*, *30*(49), 16718–16729. https://doi.org/10.1523/JNEUROSCI.3686-10.2010

Sengar, A. S., Ellegood, J., Yiu, A. P., Wang, H., Wang, W., Juneja, S. C., Lerch, J. P., Josselyn, S. A., Henkelman, R. M., Salter, M. W., & Egan, S. E. (2013). Vertebrate intersectin1 is repurposed to facilitate cortical midline connectivity and higher order cognition. *The Journal of Neuroscience: The Official Journal of the Society for Neuroscience*, *33*(9), 4055–4065. https://doi.org/10.1523/JNEUROSCI.4428-12.2013

Sengar, A. S., Wang, W., Bishay, J., Cohen, S., & Egan, S. E. (1999a). The EH and SH3 domain Ese proteins regulate endocytosis by linking to dynamin and Eps15. *The EMBO Journal*, *18*(5), 1159–1171. https://doi.org/10.1093/emboj/18.5.1159

Sengar, A. S., Wang, W., Bishay, J., Cohen, S., & Egan, S. E. (1999b). The EH and SH3 domain Ese proteins regulate endocytosis by linking to dynamin and Eps15. *The EMBO Journal*, *18*(5), 1159–1171. https://doi.org/10.1093/emboj/18.5.1159

Sentürk, A., Pfennig, S., Weiss, A., Burk, K., & Acker-Palmer, A. (2011). Ephrin Bs are essential components of the Reelin pathway to regulate neuronal migration. *Nature*, *472*(7343), 356–360. https://doi.org/10.1038/nature09874

Seri, B., García-Verdugo, J. M., Collado-Morente, L., McEwen, B. S., & Alvarez-Buylla, A. (2004). Cell types, lineage, and architecture of the germinal zone in the adult dentate gyrus. *The Journal of Comparative Neurology*, *478*(4), 359–378. https://doi.org/10.1002/cne.20288

Seri, B., García-Verdugo, J. M., McEwen, B. S., & Alvarez-Buylla, A. (2001). Astrocytes give rise to new neurons in the adult mammalian hippocampus. *The Journal of Neuroscience: The Official Journal of the Society for Neuroscience*, *21*(18), 7153–7160. https://doi.org/10.1523/JNEUROSCI.21-18-07153.2001

Shao, X., Ding, Z., Zhao, M., Liu, K., Sun, H., Chen, J., Liu, X., Zhang, Y., Hong, Y., Li, H., & Li, H. (2017). Mammalian Numb protein antagonizes Notch by controlling postendocytic trafficking of the Notch ligand Delta-like 4. *Journal of Biological Chemistry*, *292*(50), 20628–20643. https://doi.org/10.1074/jbc.M117.800946

Shergill, J. K., & Tehran, D. A. (2025). Mouse-derived Synaptosomes Trypsin Cleavage Assay to Characterize Synaptic Protein Sub-localization. *Bio-Protocol*, *15*(2), e5164. https://doi.org/10.21769/BioProtoc.5164

Shih, S. C., Katzmann, D. J., Schnell, J. D., Sutanto, M., Emr, S. D., & Hicke, L. (2002). Epsins and Vps27p/Hrs contain ubiquitin-binding domains that function in receptor endocytosis. *Nature Cell Biology*, *4*(5), 389–393. https://doi.org/10.1038/ncb790

Sigismund, S., Woelk, T., Puri, C., Maspero, E., Tacchetti, C., Transidico, P., Di Fiore, P. P., & Polo, S. (2005). Clathrin-independent endocytosis of ubiquitinated cargos. *Proceedings of the National Academy of Sciences of the United States of America*, *102*(8), 2760–2765. https://doi.org/10.1073/pnas.0409817102

Simon, R., Baumann, L., Fischer, J., Seigfried, F. A., De Bruyckere, E., Liu, P., Jenkins, N. A., Copeland, N. G., Schwegler, H., & Britsch, S. (2016). Structure-function integrity of the adult hippocampus depends on the transcription factor Bcl11b/Ctip2. *Genes, Brain, and Behavior*, *15*(4), 405–419. https://doi.org/10.1111/gbb.12287

Spassky, N., Merkle, F. T., Flames, N., Tramontin, A. D., García-Verdugo, J. M., & Alvarez-Buylla, A. (2005). Adult Ependymal Cells Are Postmitotic and Are Derived from Radial Glial Cells during

Embryogenesis. *Journal of Neuroscience*, *25*(1), 10–18. https://doi.org/10.1523/JNEUROSCI.1108-04.2005

Spassky, N., & Meunier, A. (2017). The development and functions of multiciliated epithelia. *Nature Reviews Molecular Cell Biology*, *18*(7), 423–436. https://doi.org/10.1038/nrm.2017.21

Sporns, O., Chialvo, D. R., Kaiser, M., & Hilgetag, C. C. (2004). Organization, development and function of complex brain networks. *Trends in Cognitive Sciences*, *8*(9), 418–425. https://doi.org/10.1016/j.tics.2004.07.008

Stanfield, B. B., & Cowan, W. M. (1979). The morphology of the hippocampus and dentate gyrus in normal and reeler mice. *Journal of Comparative Neurology*, *185*(3), 393–422. https://doi.org/10.1002/cne.901850302

Steiner, B., Klempin, F., Wang, L., Kott, M., Kettenmann, H., & Kempermann, G. (2006). Type-2 cells as link between glial and neuronal lineage in adult hippocampal neurogenesis. *Glia*, *54*(8), 805–814. https://doi.org/10.1002/glia.20407

Suzuki, M., Tanaka, H., Tanimura, A., Tanabe, K., Oe, N., Rai, S., Kon, S., Fukumoto, M., Takei, K., Abe, T., Matsumura, I., Kanakura, Y., & Watanabe, T. (2012). The Clathrin Assembly Protein PICALM Is Required for Erythroid Maturation and Transferrin Internalization in Mice. *PLOS ONE*, *7*(2), e31854. https://doi.org/10.1371/journal.pone.0031854

Suzuki, N., Oota-Ishigaki, A., Kaizuka, T., Itoh, M., Yamazaki, M., Natsume, R., Abe, M., Sakimura, K., Mishina, M., & Hayashi, T. (2024). Limb-Clasping Response in NMDA Receptor Palmitoylation-Deficient Mice. *Molecular Neurobiology*, *61*(11), 9125–9135. https://doi.org/10.1007/s12035-024-04166-9

Sweitzer, S. M., & Hinshaw, J. E. (1998). Dynamin undergoes a GTP-dependent conformational change causing vesiculation. *Cell*, *93*(6), 1021–1029. https://doi.org/10.1016/s0092-8674(00)81207-6

Takagishi, M., Yue, Y., Gray, R. S., Verhey, K. J., & Wallingford, J. B. (2024). Motor protein Kif6 regulates cilia motility and polarity in brain ependymal cells. *Disease Models & Mechanisms*, *17*(2), dmm050137. https://doi.org/10.1242/dmm.050137

Tarsa, L., & Goda, Y. (2002). Synaptophysin regulates activity-dependent synapse formation in cultured hippocampal neurons. *Proceedings of the National Academy of Sciences of the United States of America*, *99*(2), 1012–1016. https://doi.org/10.1073/pnas.022575999

Tebar, F., Confalonieri, S., Carter, R. E., Di Fiore, P. P., & Sorkin, A. (1997). Eps15 Is Constitutively Oligomerized Due to Homophilic Interaction of Its Coiled-coil Region*. *Journal of Biological Chemistry*, *272*(24), 15413–15418. https://doi.org/10.1074/jbc.272.24.15413

Teixeira, C. M., Kron, M. M., Masachs, N., Zhang, H., Lagace, D. C., Martinez, A., Reillo, I., Duan, X., Bosch, C., Pujadas, L., Brunso, L., Song, H., Eisch, A. J., Borrell, V., Howell, B. W., Parent, J. M., & Soriano, E. (2012). Cell-Autonomous Inactivation of the Reelin Pathway Impairs Adult Neurogenesis in the Hippocampus. *The Journal of Neuroscience*, *32*(35), 12051–12065. https://doi.org/10.1523/JNEUROSCI.1857-12.2012

Terré, B., Piergiovanni, G., Segura-Bayona, S., Gil-Gómez, G., Youssef, S. A., Attolini, C. S., Wilsch-Bräuninger, M., Jung, C., Rojas, A. M., Marjanović, M., Knobel, P. A., Palenzuela, L., López-Rovira, T., Forrow, S., Huttner, W. B., Valverde, M. A., de Bruin, A., Costanzo, V., & Stracker, T. H. (2016). GEMC1 is a critical regulator of multiciliated cell differentiation. *The EMBO Journal*, *35*(9), 942–960. https://doi.org/10.15252/embj.201592821

Thomas, A., Burant, A., Bui, N., Graham, D., Yuva-Paylor, L. A., & Paylor, R. (2009). Marble burying reflects a repetitive and perseverative behavior more than novelty-induced anxiety. *Psychopharmacology*, *204*(2), 361–373. https://doi.org/10.1007/s00213-009-1466-y

Thomas, S., Ritter, B., Verbich, D., Sanson, C., Bourbonnière, L., McKinney, R. A., & McPherson, P. S. (2009). Intersectin Regulates Dendritic Spine Development and Somatodendritic Endocytosis but Not Synaptic Vesicle Recycling in Hippocampal Neurons. *The Journal of Biological Chemistry*, *284*(18), 12410–12419. https://doi.org/10.1074/jbc.M809746200

Tissir, F., Qu, Y., Montcouquiol, M., Zhou, L., Komatsu, K., Shi, D., Fujimori, T., Labeau, J., Tyteca, D., Courtoy, P., Poumay, Y., Uemura, T., & Goffinet, A. M. (2010). Lack of cadherins Celsr2 and Celsr3 impairs ependymal ciliogenesis, leading to fatal hydrocephalus. *Nature Neuroscience*, *13*(6), 700–707. https://doi.org/10.1038/nn.2555

Tomas, A., Futter, C. E., & Eden, E. R. (2014). EGF receptor trafficking: Consequences for signaling and cancer. *Trends in Cell Biology*, *24*(1), 26–34. https://doi.org/10.1016/j.tcb.2013.11.002

Toni, N., & Schinder, A. F. (2016). Maturation and Functional Integration of New Granule Cells into the Adult Hippocampus. *Cold Spring Harbor Perspectives in Biology*, *8*(1), a018903. https://doi.org/10.1101/cshperspect.a018903

Town, T., Breunig, J. J., Sarkisian, M. R., Spilianakis, C., Ayoub, A. E., Liu, X., Ferrandino, A. F., Gallagher, A. R., Li, M. O., Rakic, P., & Flavell, R. A. (2008). The stumpy gene is required for mammalian ciliogenesis. *Proceedings of the National Academy of Sciences*, *105*(8), 2853–2858. https://doi.org/10.1073/pnas.0712385105

Tramontin, A. D., García-Verdugo, J. M., Lim, D. A., & Alvarez-Buylla, A. (2003). Postnatal Development of Radial Glia and the Ventricular Zone (VZ): A Continuum of the Neural Stem Cell Compartment. *Cerebral Cortex*, *13*(6), 580–587. https://doi.org/10.1093/cercor/13.6.580

Trommsdorff, M., Gotthardt, M., Hiesberger, T., Shelton, J., Stockinger, W., Nimpf, J., Hammer, R. E., Richardson, J. A., & Herz, J. (1999a). Reeler/Disabled-like disruption of neuronal migration in knockout mice lacking the VLDL receptor and ApoE receptor 2. *Cell*, *97*(6), 689–701. https://doi.org/10.1016/s0092-8674(00)80782-5

Trommsdorff, M., Gotthardt, M., Hiesberger, T., Shelton, J., Stockinger, W., Nimpf, J., Hammer, R. E., Richardson, J. A., & Herz, J. (1999b). Reeler/Disabled-like disruption of neuronal migration in knockout mice lacking the VLDL receptor and ApoE receptor 2. *Cell*, *97*(6), 689–701. https://doi.org/10.1016/s0092-8674(00)80782-5

Trommsdorff, M., Gotthardt, M., Hiesberger, T., Shelton, J., Stockinger, W., Nimpf, J., Hammer, R. E., Richardson, J. A., & Herz, J. (1999c). Reeler/Disabled-like disruption of neuronal migration in knockout mice lacking the VLDL receptor and ApoE receptor 2. *Cell*, *97*(6), 689–701. https://doi.org/10.1016/s0092-8674(00)80782-5

Tully, H. M., & Dobyns, W. B. (2014). Infantile hydrocephalus: A review of epidemiology, classification and causes. *European Journal of Medical Genetics*, *57*(8), 359–368. https://doi.org/10.1016/j.ejmg.2014.06.002

Umair, M., Ullah, A., Abbas, S., Ahmad, F., Basit, S., & Ahmad, W. (2018). First direct evidence of involvement of a homozygous loss-of-function variant in the EPS15L1 gene underlying split-hand/split-foot malformation. *Clinical Genetics*, *93*(3), 699–702. https://doi.org/10.1111/cge.13152

Ungewickell, E., Ungewickell, H., Holstein, S. E. H., Lindner, R., Prasad, K., Barouch, W., Martini, B., Greene, L. E., & Eisenberg, E. (1995). Role of auxilin in uncoating clathrin-coated vesicles. *Nature*, *378*(6557), 632–635. https://doi.org/10.1038/378632a0

van Bergen en Henegouwen, P. M. (2009). Eps15: A multifunctional adaptor protein regulating intracellular trafficking. *Cell Communication and Signaling*, *7*(1), 24. https://doi.org/10.1186/1478-811X-7-24

Vieira, A. V., Lamaze, C., & Schmid, S. L. (1996). Control of EGF Receptor Signaling by Clathrin-Mediated Endocytosis. *Science*, *274*(5295), 2086–2089. https://doi.org/10.1126/science.274.5295.2086

Vollweiter, D., Shergill, J. K., Hilse, A., Kochlamazashvili, G., Koch, S. P., Mueller, S., Boehm-Sturm, P., Haucke, V., & Maritzen, T. (2023a). Intersectin deficiency impairs cortico-striatal neurotransmission and causes obsessive–compulsive behaviors in mice. *Proceedings of the National Academy of Sciences*, *120*(35), e2304323120. https://doi.org/10.1073/pnas.2304323120

Vollweiter, D., Shergill, J. K., Hilse, A., Kochlamazashvili, G., Koch, S. P., Mueller, S., Boehm-Sturm, P., Haucke, V., & Maritzen, T. (2023b). Intersectin deficiency impairs cortico-striatal neurotransmission and causes obsessive–compulsive behaviors in mice. *Proceedings of the National Academy of Sciences*, *120*(35), e2304323120. https://doi.org/10.1073/pnas.2304323120

von Kleist, L., Stahlschmidt, W., Bulut, H., Gromova, K., Puchkov, D., Robertson, M. J., MacGregor, K. A., Tomilin, N., Pechstein, A., Chau, N., Chircop, M., Sakoff, J., von Kries, J. P., Saenger, W., Kräusslich, H.-G., Shupliakov, O., Robinson, P. J., McCluskey, A., & Haucke, V. (2011). Role of the clathrin terminal domain in regulating coated pit dynamics revealed by small molecule inhibition. *Cell*, *146*(3), 471–484. https://doi.org/10.1016/j.cell.2011.06.025

Wang, W., Bouhours, M., Gracheva, E. O., Liao, E. H., Xu, K., Sengar, A. S., Xin, X., Roder, J., Boone, C., Richmond, J. E., Zhen, M., & Egan, S. E. (2008). ITSN-1 Controls Vesicle Recycling at the Neuromuscular Junction and Functions in Parallel with DAB-1. *Traffic (Copenhagen, Denmark)*, *9*(5), 742–754. https://doi.org/10.1111/j.1600-0854.2008.00712.x

Wang, X., Zhou, Y., Wang, J., Tseng, I.-C., Huang, T., Zhao, Y., Zheng, Q., Gao, Y., Luo, H., Zhang, X., Bu, G., Hong, W., & Xu, H. (2016). SNX27 Deletion Causes Hydrocephalus by Impairing Ependymal Cell Differentiation and Ciliogenesis. *The Journal of Neuroscience: The Official Journal of the Society for Neuroscience*, *36*(50), 12586–12597. https://doi.org/10.1523/JNEUROSCI.1620-16.2016

Ware, M. L., Fox, J. W., González, J. L., Davis, N. M., Rouvroit, C. L. de, Russo, C. J., Chua, S. C., Goffinet, A. M., & Walsh, C. A. (1997). Aberrant Splicing of a Mouse disabled Homolog, mdab1, in the scrambler Mouse. *Neuron*, *19*(2), 239–249. https://doi.org/10.1016/S0896-6273(00)80936-8

Watanabe, S., & Boucrot, E. (2017). Fast and ultrafast endocytosis. *Current Opinion in Cell Biology*, *47*, 64–71. https://doi.org/10.1016/j.ceb.2017.02.013

Watanabe, S., Liu, Q., Davis, M. W., Hollopeter, G., Thomas, N., Jorgensen, N. B., & Jorgensen, E. M. (2013). Ultrafast endocytosis at Caenorhabditis elegans neuromuscular junctions. *eLife*, *2*, e00723. https://doi.org/10.7554/eLife.00723

Watanabe, S., Rost, B. R., Camacho-Pérez, M., Davis, M. W., Söhl-Kielczynski, B., Rosenmund, C., & Jorgensen, E. M. (2013). Ultrafast endocytosis at mouse hippocampal synapses. *Nature*, *504*(7479), 242–247. https://doi.org/10.1038/nature12809

Watanabe, S., Trimbuch, T., Camacho-Pérez, M., Rost, B. R., Brokowski, B., Söhl-Kielczynski, B., Felies, A., Davis, M. W., Rosenmund, C., & Jorgensen, E. M. (2014). Clathrin regenerates synaptic vesicles from endosomes. *Nature*, *515*(7526), 228–233. https://doi.org/10.1038/nature13846

Watson, P., Townley, A. K., Koka, P., Palmer, K. J., & Stephens, D. J. (2006). Sec16 defines endoplasmic reticulum exit sites and is required for secretory cargo export in mammalian cells. *Traffic (Copenhagen, Denmark)*, *7*(12), 1678–1687. https://doi.org/10.1111/j.1600-0854.2006.00493.x

Weeber, E. J., Beffert, U., Jones, C., Christian, J. M., Forster, E., Sweatt, J. D., & Herz, J. (2002). Reelin and ApoE receptors cooperate to enhance hippocampal synaptic plasticity and learning. *The Journal of Biological Chemistry*, *277*(42), 39944–39952. https://doi.org/10.1074/jbc.M205147200

Weiss, K. H., Johanssen, C., Tielsch, A., Herz, J., Deller, T., Frotscher, M., & Förster, E. (2003a). Malformation of the radial glial scaffold in the dentate gyrus of reeler mice, scrambler mice, and ApoER2/VLDLR-deficient mice. *The Journal of Comparative Neurology*, *460*(1), 56–65. https://doi.org/10.1002/cne.10644

Weiss, K. H., Johanssen, C., Tielsch, A., Herz, J., Deller, T., Frotscher, M., & Förster, E. (2003b). Malformation of the radial glial scaffold in the dentate gyrus of reeler mice, scrambler mice, and ApoER2/VLDLR-deficient mice. *Journal of Comparative Neurology*, *460*(1), 56–65. https://doi.org/10.1002/cne.10644

Wilfling, F., Lee, C.-W., Erdmann, P. S., Zheng, Y., Sherpa, D., Jentsch, S., Pfander, B., Schulman, B. A., & Baumeister, W. (2020a). A Selective Autophagy Pathway for Phase-Separated Endocytic Protein Deposits. *Molecular Cell*, *80*(5), 764-778.e7. https://doi.org/10.1016/j.molcel.2020.10.030

Wilfling, F., Lee, C.-W., Erdmann, P. S., Zheng, Y., Sherpa, D., Jentsch, S., Pfander, B., Schulman, B. A., & Baumeister, W. (2020b). A Selective Autophagy Pathway for Phase-Separated Endocytic Protein Deposits. *Molecular Cell*, *80*(5), 764-778.e7. https://doi.org/10.1016/j.molcel.2020.10.030

Willems, J., Jong, A. P. H. de, Scheefhals, N., Mertens, E., Catsburg, L. A. E., Poorthuis, R. B., Winter, F. de, Verhaagen, J., Meye, F. J., & MacGillavry, H. D. (2020). ORANGE: A CRISPR/Cas9-based genome editing toolbox for epitope tagging of endogenous proteins in neurons. *PLOS Biology*, *18*(4), e3000665. https://doi.org/10.1371/journal.pbio.3000665

Witkowska, A., & Haucke, V. (2021). Liquid-like protein assemblies initiate endocytosis. *Nature Cell Biology*, *23*(4), 301–302. https://doi.org/10.1038/s41556-021-00665-2

Woelk, T., Oldrini, B., Maspero, E., Confalonieri, S., Cavallaro, E., Di Fiore, P. P., & Polo, S. (2006). Molecular mechanisms of coupled monoubiquitination. *Nature Cell Biology*, *8*(11), 1246–1254. https://doi.org/10.1038/ncb1484

Wong, W. T., Schumacher, C., Salcini, A. E., Romano, A., Castagnino, P., Pelicci, P. G., & Di Fiore, P. (1995). A protein-binding domain, EH, identified in the receptor tyrosine kinase substrate Eps15 and conserved in evolution. *Proceedings of the National Academy of Sciences*, *92*(21), 9530–9534. https://doi.org/10.1073/pnas.92.21.9530

Wyss, L., Schäfer, J., Liebner, S., Mittelbronn, M., Deutsch, U., Enzmann, G., Adams, R. H., Aurrand-Lions, M., Plate, K. H., Imhof, B. A., & Engelhardt, B. (2012). Junctional Adhesion Molecule (JAM)-C Deficient C57BL/6 Mice Develop a Severe Hydrocephalus. *PLOS ONE*, *7*(9), e45619. https://doi.org/10.1371/journal.pone.0045619

Yao, P. J., Petralia, R. S., Bushlin, I., Wang, Y., & Furukawa, K. (2005). Synaptic distribution of the endocytic accessory proteins AP180 and CALM. *Journal of Comparative Neurology*, *481*(1), 58–69. https://doi.org/10.1002/cne.20362

Youn, Y. H., & Han, Y.-G. (2018). Primary Cilia in Brain Development and Diseases. *The American Journal of Pathology*, *188*(1), 11–22. https://doi.org/10.1016/j.ajpath.2017.08.031

Yu, X., Ng, C. P., Habacher, H., & Roy, S. (2008). Foxj1 transcription factors are master regulators of the motile ciliogenic program. *Nature Genetics*, *40*(12), 1445–1453. https://doi.org/10.1038/ng.263

Zhang, X., Medow, J. E., Iskandar, B. J., Wang, F., Shokoueinejad, M., Koueik, J., & Webster, J. G. (2017). Invasive and noninvasive means of measuring intracranial pressure: A review. *Physiological Measurement*, *38*(8), R143–R182. https://doi.org/10.1088/1361-6579/aa7256

Zhao, Z., Sagare, A. P., Ma, Q., Halliday, M. R., Kong, P., Kisler, K., Winkler, E. A., Ramanathan, A., Kanekiyo, T., Bu, G., Owens, N. C., Rege, S. V., Si, G., Ahuja, A., Zhu, D., Miller, C. A., Schneider, J. A., Maeda, M., Maeda, T., … Zlokovic, B. V. (2015). Central role for PICALM in amyloid-β blood-brain barrier transcytosis and clearance. *Nature Neuroscience*, *18*(7), 978–987. https://doi.org/10.1038/nn.4025

Zou, W., Lv, Y., Liu, Z. I., Xia, P., Li, H., & Jiao, J. (2020). Loss of Rsph9 causes neonatal hydrocephalus with abnormal development of motile cilia in mice. *Scientific Reports*, *10*(1), 12435. https://doi.org/10.1038/s41598-020-69447-4

Acknowledgement

First and foremost, I would like to express my sincere gratitude to my supervisor, **Prof. Dr. Tanja Maritzen**, for giving me the opportunity to work on such an interesting and challenging project and for her constant support throughout this journey. Your door was always open for me to walk in and ask any kind of question, from the smallest to the most complex ones. Moving from Berlin to Kaiserslautern was not the most exciting change at first, but it was your warmth and encouragement that made me stay and continue in the lab with confidence. You showed trust in me even when I doubted myself, and that has meant a lot. I am deeply thankful for your guidance and support, which have been invaluable at every stage of my PhD.

I would also like to thank my thesis committee members, **Prof. Dr. Stefan Kins** and **Prof. Dr. Jan Pielage**, for readily agreeing to be part of my committee. Your time, support, and commitment have been essential to my efforts in completing this degree.

I would like to thank **Dr. Markus Räschle** for sharing his mass spectrometry expertise, which has greatly contributed to my project and its progress, and **Dr. Nathalie Spassky** for kindly allowing me to learn ependymal culture techniques in her lab.

A special mention goes to the wonderful professors and mentors I have had the privilege to learn from throughout my studies. I am deeply grateful to **Prof. Dr. Santanu Palchaudhuri** for seeing potential in me and making me believe that research was something I could truly pursue. My heartfelt thanks also to **Prof. Dr. Srikanth Vadali** for his unwavering support and mentorship, without his guidance, I would not be here today, earning my PhD in Germany.

A special thanks to **Dr. Domenico A. Tehran** for being my personal mentor during my initial PhD days and now in life. You were my first friend in this new country and have always been my support system throughout this journey. I am so grateful to have met such a wonderful person. Thank you for teaching me so much, for always believing in me, and for lifting my spirits whenever I felt lost during my PhD. You were always just one phone call away. We make a great team, and I will never say no to any chance I get to work with you again.

Next, I would like to thank the entire **AG Maritzen group**. Thank you for being such a fun and wonderful bunch of people and making the lab always feel like a comfortable and welcoming space. A special thanks to **Fabian**, for always being patient and helping me out whenever I was stuck. We have shared a unique journey, from working together in a small room with a few instruments to helping shape the lab into what it is today. Thank you to **Alex** for bringing color to

my rather monotonous lab and social life in Kaiserslautern. We have a *mice-bond* for life. **Fiorella**, my reality-TV partner, thank you for always making me laugh with your quick wit and jokes. **Marlen**, thank you for being my chatter buddy and for all our tea-filled chats that made the days so much more fun. And, to **Gina**, **Ben**, and all the students I have met during this journey, thank you for supporting me in one way or another. A special thanks to our best TA, **Ralph**, for always helping out with a smile, no matter how lost we were in translation, and to our Hiwi, **Nicolas**, for all his help and support in the lab. I will always cherish my PhD days thanks to everyone in the group. *Go Nanoballzzz!!*

I would also like to express my heartfelt thanks to my loved ones outside the lab who made this journey brighter and more enjoyable. Thank you to **David** and **Anne** for being the best roommates; moving to a new place in a new country was not easy, but you both made it feel like home. Thank you to **Adit** for always being a friend who's the best listener, my life would not be half as fun without you. **Nikita**, thank you for being you — my saviour and my soul sister for life. I have survived my PhD and KL because of you. And a special thanks to **Tanish Tara** for being the *sun to my sunflower* and for filling my life with love, laughter, and sunshine. You made my stressful PhD writing days easier by keeping my spirits high, my stomach full, and my caffeine levels perfectly maintained.

And finally, a big thank you to my family for believing in me and supporting my ambitions, even when it meant being 6000 kilometers away from everyone. **Gagan**, you have been the most supportive brother and thank you for always being my biggest cheerleader. Thank you, **Chanda** bhabhi, for supporting the family and bringing so much joy into our lives with **Manveer**, my tiny nephew, who has been my constant source of happiness. Thank you, **Maa**, for your endless love and support — I am forever indebted to you for everything. I would not be the person I am today without you. Lastly, thank you, **Papa**, for all the love you showered on me during our time together. Losing you during this journey was one of the hardest things I have faced. I miss you every day and hope you are watching over me and will be proud of me for becoming *Dr. Shergill*. You always sang this to me as a kid, *"Papa kehte hain bada naam karega...beta humara aisa kaam karega..."*, and I hope I've somehow lived up to these words. I dedicate this work and my PhD degree to you!

Curriculum vitae

JASMEET KAUR SHERGILL

Logenstrasse 18, 67655 Kaiserslautern, Germany
shergill@rptu.de

EDUCATION

Doctor of Philosophy 2021–Present
Neurobiology
RPTU Kaiserslautern-Landau, Germany
Thesis: *Dissecting the role of EPS15 and EPS15R in the mammalian brain*

Master of Science 2018–2020
Animal Biology and Biotechnology
University of Hyderabad, India
Thesis: *Role and regulation of EBF1 in B-cell development*

Bachelor of Science 2018–2020
Biotechnology
Amity University, India
Thesis: *In-silico characterization of neurodegenerative disease-associated proteins*

INTERNSHIPS

Summer Research Fellowship 2019
Indian Academy of Sciences
Topic: *Cellular copper homeostasis in glial and neuronal cells*

Research Internship 2017
Novozymes, India
Topic: *Assessing and optimizing the efficiency of enzymes in bio-detergents*

ADDITIONAL EXPERIENCE

Subject matter expert in Biology *(Freelance)* 2020
Chegg Inc., India

Scientific Curator *(Freelance)* 2020
Excelra, India

PUBLICATIONS

Shergill, J.K. & Azarnia Tehran, D. Mouse-derived Synaptosomes Trypsin Cleavage Assay to Characterize Synaptic Protein Sub-localization. Bio-protocol **(2025)**

Vollweiter, D., **Shergill, J.K.**, et al. Intersectin deficiency impairs cortico-striatal neurotransmission and causes obsessive–compulsive behaviors in mice. PNAS **(2023)**

Azarnia Tehran, D., Kochlamazashvili, G., **Shergill, J.K.**, et al. Selective endocytosis of Ca^{2+}-permeable AMPARs by the Alzheimer's disease risk factor CALM bidirectionally controls synaptic plasticity. Science Advances **(2022)**

CERTIFICATIONS

Animal Care Certificate
TARC Mainz, 2023

Lab Animal Science Course (Mouse)
MDC Berlin ,2021

ACHIEVEMENTS

Gold Medal - First in Academics 2020
(Department of Animal Biology, University of Hyderabad)

Women Topper Academics Medal 2020
(Department of Animal Biology, University of Hyderabad)

All Round Best Student Award 2018
(Department of Biotechnology, Amity University Kolkata)

Silver Medal - Second in Academics 2018
(Department of Biotechnology, Amity University Kolkata)

Best in Interpersonal Skills and Team Spirit Award 2018
(Department of Biotechnology, Amity University Kolkata)

Academic Scholarship for BSc degree 2015-2018
(Department of Biotechnology, Amity University Kolkata)

Darlegung des Eigenanteils

Alle in dieser Dissertation dargestellten Experimente und Analysen wurden von mir konzipiert und überwiegend eigenständig durchgeführt, sofern im Folgenden nicht anders angegeben. Die Probenvorbereitung für die Massenspektrometrie erfolgte mit Unterstützung von Dr. Markus Räschle (Abteilung Molekulare Genetik, RPTU), der auch die Messungen und die Datenauswertung durchführte (Fig. 2.5, S3 A). Der pHluorin Assay wurde von Dr. Domenico A. Tehran (FMP, Berlin) durchgeführt und ausgewertet (Fig. 2.9). Unter meiner Betreuung leisteten mehrere Studierende im Rahmen ihrer Abschlussarbeiten oder Praktika Beiträge: Celine Schuster führte im Rahmen ihrer Masterarbeit mehrere Co-Immunpräzipitationen (Fig. 2.3, 2.6B) durch, klonierte das Eps15R-mRFP Plasmid und führte die entsprechenden Transfektionen durch (Fig. 2.6C, Fig. S2). Im Rahmen ihrer Master- bzw. Bachelorarbeiten fertigten Stefanie Heinrichs, Michelle Kölsch und Julia Sledge Nissl-Färbungen und entsprechende Quantifizierungen an (Fig. 2.12, 2.13, 2.21, S3, S5) sowie verschiedene immunhistochemische Färbungen (Fig. 2.14–2.16, 2.18, 2.19, S6). Der GST-Pulldown (Fig. 2.20) wurde von Michelle Kölsch im Rahmen ihrer Masterarbeit durchgeführt. Der neuronale Viabilitätsassay (Fig. 2.8A,B) wurde von Stefanie Heinrichs während ihrer Masterarbeit und von Marina Polozova während ihres Forschungspraktikums mit meiner Unterstützung durchgeführt. Die Färbungen primärer Zilien wurden gemeinschaftlich von Stefanie Heinrichs im Rahmen ihrer Masterarbeit und von Anne Rosskopf und Jonas Frey im Rahmen ihres Vertiefungspraktikums angefertigt und ausgewertet (Fig. 2.21 B,C). Andrei Gordeev trug im Rahmen seines Forschungspraktikums zur Erhöhung der biologischen Replikate für das Experiment zur Modifikation der Ependymzellkultur bei (Fig. 2.25), und Marina Polozova half in ihrem Forschungspraktikum bei der Erhöhung der biologischen Replikate für die Analyse der Altersreihe der Mäuse (Fig. S1). Julia Sledge führte in ihrer Bachelorararbeit die Immunfluoreszenzfärbung der Ependymzellkulturen sowie die Analyse der entsprechenden Bilder durch (Fig. 2.24). Die Verhaltensbeobachtungen wurden von mir durchgeführt, und die zugehörigen Auswertungen wurden von Anne Rosskopf und Jonas Frey in ihrem Vertiefungspraktikum vorgenommen (Fig. 2.11C,D). Obwohl die oben genannten Experimente Beiträge anderer Personen beinhalten, wurden sämtliche primären neuronalen und ependymalen Zellkulturen sowie alle Gewebepräparationen und Perfusionen, die diesen Experimenten zugrunde liegen, eigenständig von mir etabliert und durchgeführt. Die Versuchstiere wurden vom Personal des Tierhauses betreut und gewogen.

Jasmeet Kaur Shergill	**Prof. Dr. Tanja Maritzen**
Kaiserslautern, den 17.10.2025	Kaiserslautern, den17.10.2025

Darlegung aller benutzten Hilfsmittel und Hilfestellungen

Zur Erstellung der Arbeit wurde das Microsoft Office 365 Software Paket genutzt. Das Literaturverzeichnis und die Literaturverweise wurden mit Zotero erstellt. Die statistischen Analysen und Auswertungen wurden mit Graph Pad Prism durchgeführt. Biorender wurde für die Erstellung von Illustrationen verwendet. Die Abbildungen wurden mit Affinity Designer erstellt. Die Analyse des massenspektrometrischen Datensatzes wurde mit MaxQuant Perseus durchgeführt. Die Genanreicherungsanalyse der Massenspektrometriedaten wurde mit dem Online-Tool WebGestalt durchgeführt. Mikroskopische Aufnahmen wurden mit NIS Elements aufgenommen und mit Fiji oder Cellpose analysiert. Western Blots wurden mit der Licor Acquisition Software aufgenommen und mit Image Studio ausgewertet. Quillbot und ChatGPT wurden für die Paraphrasierung und Grammatikprüfung verwendet. DeepL wurde für die Übersetzung der Zusammenfassung vom Englischen ins Deutsche verwendet. Eine detailiertere Auflistung der verwendeten Programme findet sich im Kapitel zu den Materialien.

Jasmeet Kaur Shergill

Kaiserslautern, den 17.10.2025

Eidesstattliche Erklärung

Hiermit erkläre ich wahrheitsgemäß, dass ich die hier vorliegende Dissertation selbstständig und ohne unzulässige Hilfe Dritter verfasst habe sowie keine anderen als die angegebenen Quellen und Hilfsmittel verwendet habe. Die aus anderen Quellen übernommenen Daten und Konzepte sind unter Angabe der Quelle gekennzeichnet.

Zur Erstellung der vorliegenden Arbeit habe ich keine entgeltliche Hilfe von Vermittlungs- und Beratungsdiensten in Anspruch genommen.

Diese Arbeit und auch keine Teile hiervon wurden weder im In- noch im Ausland bereits als Prüfungsarbeit für eine wissenschaftliche Prüfung eingereicht, und ich habe mich zuvor noch keiner Doktorprüfung unterzogen. Ich erkläre, dass ich weder die gleiche noch eine andere Abhandlung bei einem anderen Fachbereich oder einer anderen Universität als Dissertation eingereicht habe.

Die Bestimmungen der Promotionsordnung des Fachbereiches Biologie der Rheinland-Pfälzischen Technischen Universität Kaiserslautern-Landau sind mir bekannt. Im Besonderen weiß ich, dass ich vor Vollzug der Promotion zur Führung des Doktortitels nicht berechtigt bin.

Jasmeet Kaur Shergill

Kaiserslautern, 17.10.2025